The University Of Sheffield.

Early visual encoding of *Musca domestica*

Neveen Mansour

A thesis submitted in partial fulfilment of the requirements for the degree of Doctor of Philosophy

The University of Sheffield
Faculty of Science
Department of Biomedical Science

February 2021

Acknowledgements

First and foremost, I want to thank my houseflies. Not only did they breed continuously throughout my four years of research but they were there to keep me company during those late evenings spent in the lab alone.

Moving on to humans, I want to thank my supervisor, Prof Mikko Juusola, for giving me the opportunity to study the exciting field of fly vision. I would also like to say thank you to my advisors, Dr Andrew Lin, Dr Natalia Bulgakova and Dr Ivana Barbaric for their helpful guidance and scientific discussions. A special thanks is reserved for Andrew for hosting the lab meetings and journal clubs - not only did I learn about fly vision, but olfaction and many other research areas.

I want to show my appreciation to everyone in my lab and the people I shared the office with: Keivan, James, Joni, Ben, Jouni, Anthi, Katie, Daniel, Hoger and Alice. They all helped make each and every day something I looked forward to. Whether it was our conversions, pranks, football sessions or occasional tea/lunch breaks, I regularly had an amazing time with you and a truly well-rounded PhD experience. I also met two people outside my lab who I want to say a special thank you to, Emily and Ingrid who started their PhDs with me and we became close friends. I very much hope that we will remain in contact no matter where our lives take us.

I could not possibly ignore how important my family has been throughout this entire experience. Despite living in a different country, they have provided me with constant love and support, something I will always be grateful for. Kiitos isä, äiti, Nevon, Marven ja varsinkin Nipsu, olette aivan mahtavia! Kiitos Kirsille iltakävelyistä. I would also like to express a sincere thanks to Andy for bringing so much joy into my life throughout this time. Although I learned so much about fly vision, you opened the door to so many other experiences.

Finally, I would like to thank Sheffield for providing me with such a welcoming and wholesome experience. It was a great pleasure to live in such a lovely city and to be able to call this place home.

Abstract

Fly vision has often been considered to be quite poor, both temporally and spatially, as it is limited by numerous different factors (i.e. number of sampling units, lens dimensions, photoreceptors' slow integration time, ambient light level as well as flies' own speed when in motion) (Mallock, 1894; Fermi and Richardt, 1963; Srinivasan and Bernard, 1975; Warrant and McIntyre, 1992; Land, 1997; Warrant, 1999).

Some studies have challenged these views and found that flies have evolved to partially overcome these constraints (i.e. via acute zones, head/thorax and body movements) (van Hateren and Schilstra, 1999; Hornstein et al., 2000; Burton, Tatler and Laughlin, 2001; Burton and Laughlin, 2003). One recent example from Juusola et al. (2017) showed that *Drosophila* photoreceptors contract to light and these photomechanical contractions coupled with refractory sampling enable the fly to overcome motion blur even to objects smaller than their optical limit.

Following on from this work, my aim was to test whether different aspects of a fast-flying housefly (*Musca domestica*) would also have enhanced spatial and temporal vision beyond our current understanding. If slow-flying *Drosophila* with its optically poorer vision has evolved to compensate for its limitations, then in theory we should see similar, or better, improvements in a faster flying fly such as *Musca*. Additionally, working with *Musca* created the opportunity to investigate any presence of sexual dimorphism, as males have "love spots", which *Drosophila* males lack (Gonzalez-Bellido, Wardill and Juusola, 2011; Perry and Desplan, 2016).

My work focussed on examining via *in vivo* intracellular recordings visual encoding of *Musca* photoreceptors (R1-R6) and what happens to that information when passed downstream to large monopolar cells (LMCs, L1-L3). In total, this examination resulted in three separate studies: (i) early temporal encoding during body saccades, (ii) R1-R6 and L1-L3 cells' response properties during light adaptation and its impact on underlying quantum bumps (QBs) and (iii) hyperacuity of photoreceptors and LMCs.

I found that temporal encoding of *Musca* early vision was better than previously thought, especially in male flies. Additionally, both photoreceptors' and LMCs' signalling performance to different stimulus statistics improved when brightening mean light levels. However, when looking at spatial encoding, both male and female photoreceptors were in general not able to resolve details finer than their optical limit i.e. they were not hyperacute. LMCs may have this ability but further investigations are required.

Contents

List of abbreviations

Am	Amacrine cell
A/D	Analog-to-digital
att	Attenuation
BG	Background
C2,C3	Centrifugal neurons
DC	Direct current
DRA	Dorsal rim area
Drp	Dark resting potential
EM	Electron microscopy
EMD	Elementary motion detection
ERG	Electroretinogram
FFT	Fast Fourier transform
G_q	G-protein
GDP	Guanosine diphosphate
GFP	Green fluorescent protein
GTP	Guanosine triphosphate
GWN	Gaussian white-noise
HR	Hassenstein-Reichardt
HS	Horizontal system (in the lobula plate)
KCl	Potassium chloride
Lat	Lamina tangential neuron
Lawf	Lamina wide-field neuron
LED	Light-emitting diode
LIC	Light-induced current
LMC	Large monopolar cell

LPi	Lobula plate intrinsic cell
LPTC	Lobula plate tangential cell
Mi	Medulla intrinsic cell
ND	Null direction
PD	Preferred direction
PDF	Probability density function
PIP_2	Phosphatidylinositol 4,5-bisphosphate
PLC	Phospholipase C
QB	Quantum bump
R1-R6	A major class of fly photoreceptors (outer photoreceptors)
R7-R8	A minor class of fly photoreceptors (inner photoreceptors)
RF	Receptive field
Rh	Rhodopsin
SEM	Scanning electron microscopy
SNR	Signal-to-noise ratio
SRA	Smallest resolvable angle
SD	Standard deviation
TEM	Transmission electron microscopy
Tm	Transmedullary neuron
TRP	Light-sensitive channel (encoded by the transient receptor potential gene, *trp*)
TRPL	Light-sensitive channel (encoded by the *trp*-like gene)
UV	Ultraviolet
VS	Vertical system (in the lobula plate)
WN	White noise

List of Symbols

$\Delta\rho$	Acceptance angle
P or P_{max}	Amplitude of the larger peak
P_{min}	Amplitude of the smaller peak
c	Contrast
f	Focal distance
$T_V(f)$	Frequency response
$\Gamma_V(t; n, \tau)$	Gamma distribution
$K_1(t)$	Impulse response (first-order Wiener kernel)
t_p	Impulse response time-to-peak
∞	Infinity
R	Information transfer rate or resolvability (depending on the context)
$\left\|N_V^{instrumental}(f)\right\|^2$	Instrumental noise power spectrum
I	Intensity
$\Delta\varphi$	Interommatidial angle
$\Delta\varphi_h$	Horizontal interommatidial angle
$\Delta\varphi_v$	Vertical interommatidial angle
F^{-1}	Inverse FFT
$l(t)$	Latency distribution
D	Lens diameter or duration of the stimulus (depending on the context)
λ	Light wavelength
$\gamma_{lin}^2(f)$	Linear coherence
μ	Mean
θ	Motion direction
$\|\langle N_V(f)\rangle\|^2$	Noise power spectrum

n and τ	Parameters for gamma distribution
α	QB amplitude
T	QB duration or through (when estimating the SRA)
$\lvert B_V(f)\rvert^2$	QB noise
$b_V(t)$	QB waveform
d	Rhabdomere diameter or diffraction or dip between two peaks in the voltage response (depending on the context)
s	Speed
σ^2	Variance
$n_v(t)$	Voltage noise in the time domain
$s_v(t)$	Voltage signal in the time domain
$\lvert\langle S_V(f)\rangle\rvert^2$	Signal power spectrum
$SNR_V(f)$	Signal-to-noise ratio in the frequency domain
$SNR_V(t)$	Signal-to-noise ratio in the time domain
a	Width factor

General note on notations

||	Absolute value
≅	Approximate equality
⟨⟩	Average
*	Complex conjugate
⊗	Convolution
~	Fourier transform
∝	Proportional

List of Tables

List of Figures

1 General introduction

1.1 The fly visual system

In this section, I will discuss the fly visual system, with the main focus on early information processing. Incoming light is sampled by two separate photoreceptive organs: mainly by two compound eyes and three simple lens eyes (ocelli) at the vertex of the head. The compound eye is composed of hundreds to thousands of discrete visual units, called the ommatidia (~750 units in *Drosophila*, ~3,500 in *Musca* and ~5,600 in *Calliphora*) (**Figure 1-1**) (Franceschini and Kirschfeld, 1971a; Hardie, 1985; Sukontason et al., 2008; Wada, 1974). The fly visual system consists of four distinct retinotopically organised optic ganglia: the retina, lamina, medulla, and the lobula complex, composed of the lobula and lobula plate. The modularity begins in the retina (**Figure 1-2**).

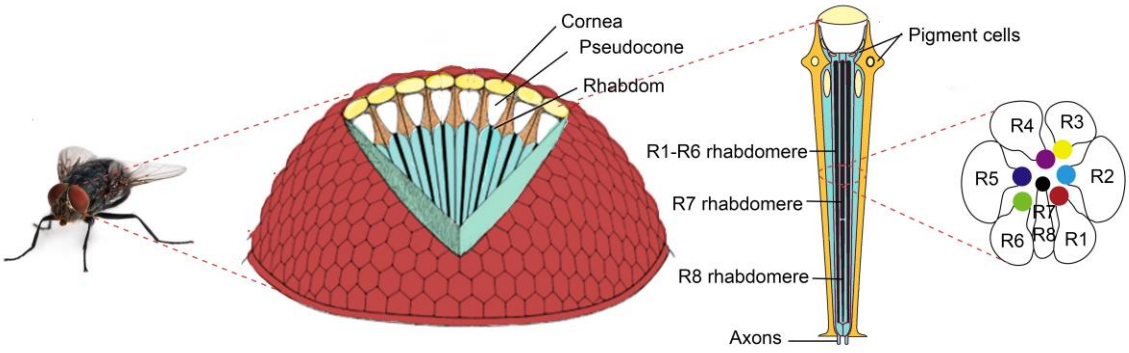

Figure 1-1. The fly compound eye. The compound eye is composed of single visual units, called the ommatidia (~750 units in *Drosophila*, ~3,500 in *Musca* and ~5,600 in *Calliphora*) (Franceschini and Kirschfeld, 1971a; Hardie, 1985; Sukontason et al., 2008; Wada, 1974). Each ommatidium has a dioptric apparatus consisting of a hexagonal facet (forms the cornea) and a fluid-filled pseudocone. In addition, each ommatidium contains eight photoreceptor cells (R1–R8), which can be divided into two classes: the outer (R1-R6) and the inner (R7-R8) photoreceptors, which are stacked on top of each other (Dietrich, 1909). Pigment cells absorb and scatter incoming light to shield the photoreceptors from getting scattered light (Stavenga, 1989) (modified from Horridge, 1977; Wolff and Ready, 1993; Sato, Suzuki and Nakai, 2013).

Each ommatidium consists of an optical structure of two lenses: first, a hexagonal facet lens forming the cornea that is followed by a cone-shaped optical material (fluid-filled pseudocone). They also contain eight photoreceptor cells (R1–R8) surrounded by pigment cells, which shield the photoreceptors from getting scattered light from adjacent photoreceptors (called cross-talk) (Stavenga, 1989).

Photoreceptors are arranged in an asymmetrical trapezoidal pattern and can be divided into two classes: the outer (R1-R6) and the inner (R7-R8) photoreceptors (Dietrich, 1909). The optical waveguides (rhabdomeres) in the photoreceptors are the most essential components because they contain the photopigments and the phototransduction machinery (Hardie and Raghu, 2001). All the outer photoreceptors have a separate rhabdomere, unlike the R7 and R8, which are stacked on top of each other, with their rhabdomeres vertically aligned. In advanced flies (suborder: *Brachycera*), all the rhabdomeres in an ommatidium are physically spaced out, forming an open rhabdom (Dietrich, 1909; Osorio, 2007). In most insect eyes (e.g. bees, butterflies, beetles, and numerous mosquitoes), the rhabdomeres are fused, forming a single waveguide (fused rhabdom) and thus, presumably looking at the same point in space (Snyder, Menzel and Laughlin, 1973).

The six outer photoreceptors (R1-R6) from neighbouring ommatidia broadly collect light information from the same point in visual space (Pick, 1977; Kirschfeld and Franceschini, 1969) and their axons terminate in a predetermined lamina cartridge, pooling their signals (the neural superposition principle) (Braitenberg, 1967; Kirschfeld, 1967). In true flies (Diptera), this is thought to increase the absolute sensitivity without sacrificing much acuity (Pick, 1977). All R1-R6 express a single blue-sensitive opsin (Rh1) (O'Tousa et al., 1985) with sensitising UV-pigment (Kirschfeld, Franceschini and Minke, 1977), detect achromatic contrast and predominantly mediate motion vision (Heisenberg and Buchner, 1977).

The inner photoreceptors (R7-R8), apart from their potent gap-junctions to R1 and R6 axons (Shaw, Fröhlich and Meinertzhagen, 1989; Wardill et al., 2012), bypass the lamina and project directly to two separate layers in the medulla (Cajal and Sanchez, 1915; Melamed and Trujillo-Cenóz, 1967). Unlike the outer photoreceptors, R7 and R8 are chromatically heterogeneous and stochastically paired, resulting in three

different subtypes of ommatidia: named as pale, yellow and DRA (dorsal rim area) (Wernet et al., 2006). These are thought to be primarily involved in colour vision and detection of polarised light (Hardie, 1985; Gao et al., 2008; Wernet et al., 2012).

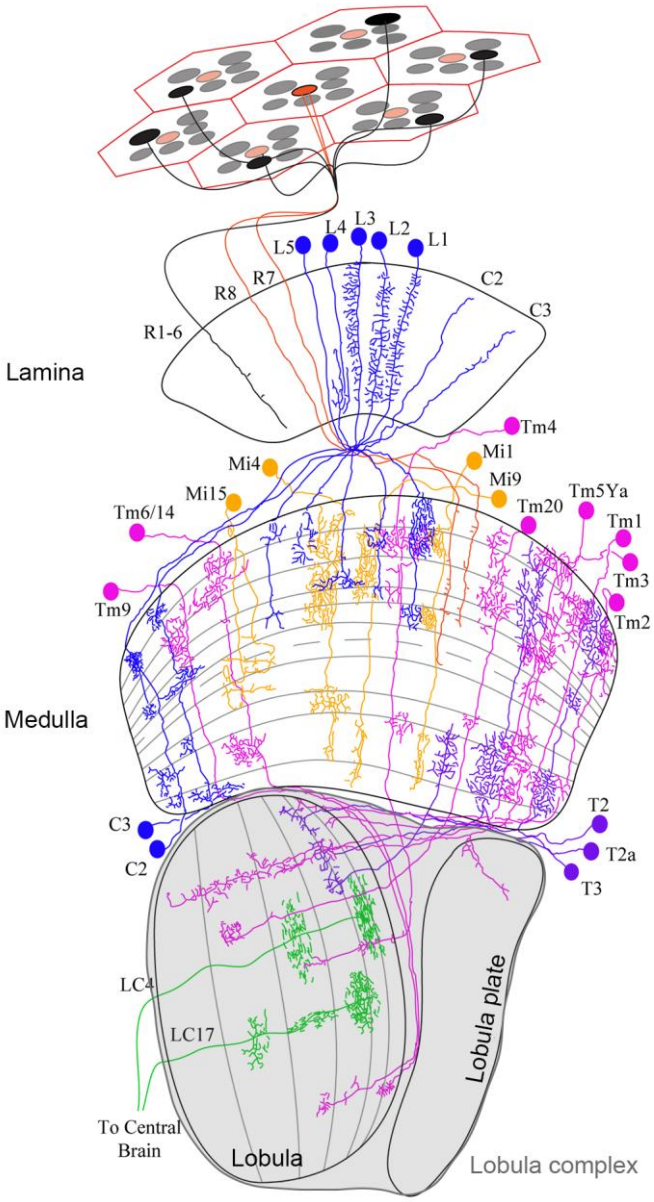

Figure 1-2. Neural superposition and the retinotopic organisation of the fly visual system. The fly visual system is retinotopically organised into four optic ganglia: the retina, lamina, medulla, and the lobula complex, composed of the lobula and lobula plate. Some Diptera such as fruitfly (*Drosophila)*, housefly (*Musca)* and blowfly (*Calliphora)* have a neural superposition eye. R1-R6 from the same ommatidium look at neighbouring points in the visual scene and send their axons to different cartridges in the lamina, whereas R1-R6 from the six neighbouring ommatidia have the same visual axis and terminate in the same lamina cartridge (Braitenberg, 1967; Kirschfeld, 1967). Unlike the outer photoreceptors, R7 and R8 bypass the lamina, apart from their gap-junctions with R1/R6 axons (Shaw,

Fröhlich and Meinertzhagen, 1989; Wardill et al., 2012), and project directly to two separate layers in the medulla (modified from Fischbach and Dittrich, 1989; Schneider et al., 2018).

1.1.1 Lamina – The first optic neuropil

The anatomy and connectivity of lamina neurons have been studied thoroughly by Golgi studies and electron microscopy (EM) reconstructions in flies, especially in fruitfly (*Drosophila)* (Fischbach and Dittrich, 1989; Meinertzhagen and O'Neil, 1991; Rivera-Alba et al., 2011) and in housefly (*Musca)* (Strausfeld, 1970; Braitenberg, 1967; Burkhardt and Braitenberg, 1976; Strausfeld, 1976; Shaw, 1981; Nicol and Meinertzhagen, 1982).

Lamina is an array of repeated retinotopically organised cylindrical cartridges (Cajal and Sanchez, 1915), which are surrounded and isolated by different glial cells (Rivera-Alba et al., 2011; Edwards et al., 2012). There is one cartridge for each ommatidium. In addition to R1-R6 photoreceptor axons, which are electrically coupled by gap-junctions (Ribi, 1978; Shaw and Stowe, 1982; van Hateren, 1986), lamina has 12 other neuronal cell types: 5 lamina output neurons, 6 putative feedback neurons and one lamina intrinsic cell (Fischbach and Dittrich, 1989; Tuthill et al., 2013). Lamina neurons can be divided into two classes: eight columnar (one cell per cartridge) and four multi-columnar (less than one cell per cartridge). The feedforward lamina monopolar cells (LMC: L1-L5) and three putative feedback neurons (T1, C2 and C3) are columnar and all these cells connect lamina with medulla. The lamina intrinsic (amacrine) neurons (Am), two wide-field neurons (Lawf1, Lawf2) and lamina tangential neurons (Lat) are multi-columnar.

As mentioned earlier, photoreceptors (R1-R6) form synapses with L1-L3 monopolar cells, the amacrine cell, and the epithelial glia with most of these connections to L1, L2, and the amacrine cell (**Figure 1-3**) (Meinertzhagen and O'Neil, 1991; Rivera-Alba et al., 2011). This feedforward pathway is histaminergic (Hardie, 1987; Hardie, 1989; Sarthy, 1991; Pantazis et al., 2008). Interestingly, L1 and L2 appear electrically coupled by gap-junctions (Chi and Carlson, 1980; Joesch et al., 2010) possibly to reduce the noise by synaptic R1-R6 signal summation. L1, L3 and L5 are the only purely postsynaptic cells in the lamina, as they form no synaptic feedback to photoreceptor axons (Rivera-Alba et al., 2011).

Besides their output synapses, R1-R6 photoreceptors form small numbers of feedback synapses with several lamina neurons, L2, L4 (including $L4_{+x}$ and $L4_{-y}$), C3, and the amacrine cell (Rivera-Alba et al., 2011), presumably enhancing temporal contrast detection (Zheng et al., 2006). This feedback is excitatory: glutamatergic and cholinergic (Meinertzhagen and O'Neil, 1991; Raghu and Borst, 2011; Takemura et al., 2011). L2 is mainly postsynaptic, but it also receives feedback from L4: L2 has reciprocal connections with L4 and with the two neighbouring collaterals ($L4_{+x}$ and $L4_{-y}$). (Strausfeld and Campos-Ortega, 1973; Meinertzhagen and O'Neil, 1991; Rivera-Alba et al., 2011).

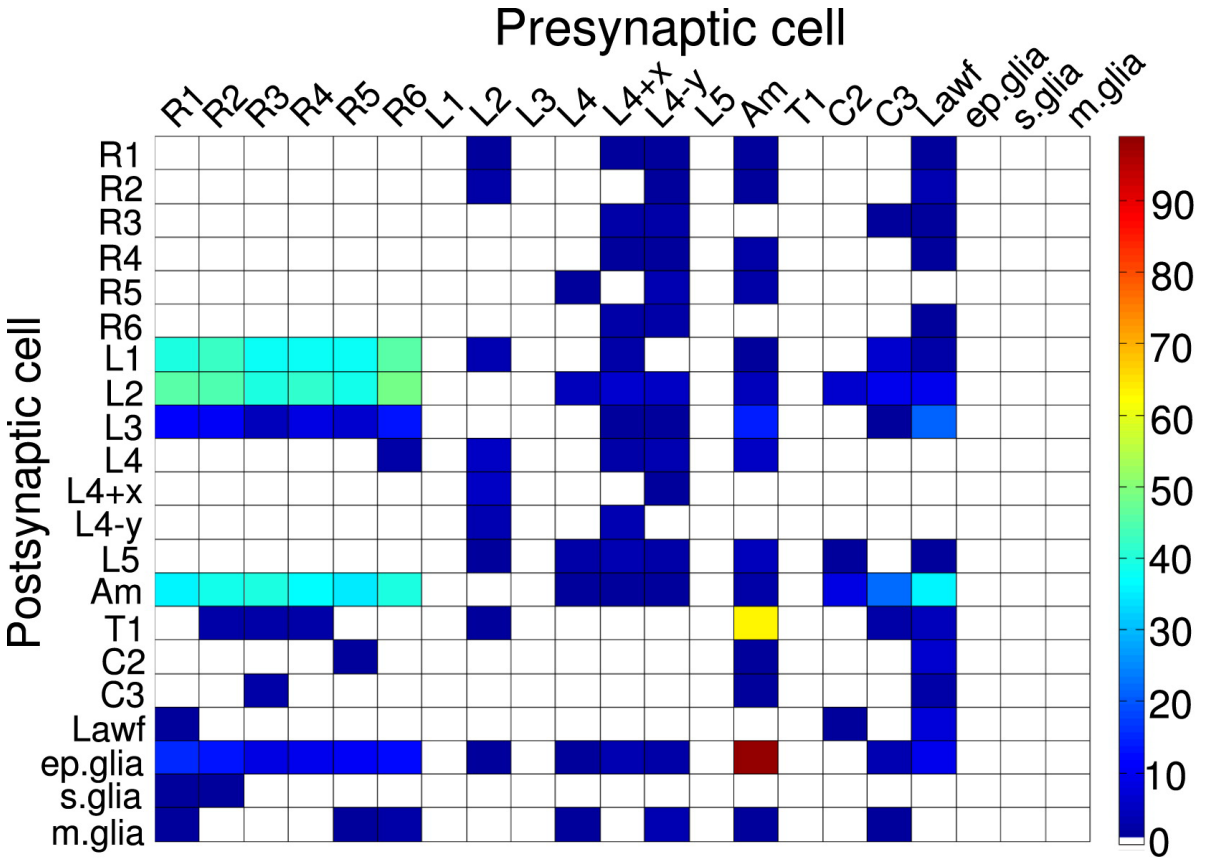

Figure 1-3. Synaptic connectivity between presynaptic and postsynaptic cells in the lamina cartridge. R1-R6 photoreceptors form synapses with L1-L3 monopolar cells, the amacrine cell (Am), and the epithelial glia with most of these connections to L1, L2, and the amacrine cell. In addition, several lamina neurons, L2, L4 (including $L4_{+x}$ and $L4_{-y}$), C3, and the amacrine cell send feedback input to R1-R6. L1, L3 and L5 are purely postsynaptic in the lamina. L2 has reciprocal connections with L4 and with the two neighbouring collaterals ($L4_{+x}$ and $L4_{-y}$). The colour scale indicates the number of synapses between the presynaptic and the postsynaptic cell (Rivera-Alba et al., 2011).

It is possible that every lamina neuron in *Musca* would have its counterpart in *Drosophila* (Strausfeld, 1976; Fischbach and Dittrich, 1989). However, perhaps due to neuroethological adaptations, not every connection that occurs in *Drosophila* exists in *Musca*. There is some evidence from older studies that find instances of this. First, the feedback synapse from Am to R1-R6 present in *Drosophila* and *Calliphora* (blowfly) is absent in *Musca domestica* (Trujillo-Cenóz, 1965; Strausfeld and Campos-Ortega, 1973; Shaw, 1984; Shaw, 1988). Second, there are possibly some differences in the L4 synaptic connections. Shown in both species, L4 forms reciprocal connections with two neighbouring collaterals ($L4_{+x}$ and $L4_{-y}$) and L2, and is presynaptic to L1. Interestingly, the distal dendrites postsynaptic to amacrine cells are absent in *Drosophila* (Strausfeld and Campos-Ortega, 1973; Fischbach and Dittrich, 1989).

1.2 Fly photoreceptor and LMC responses to light

Light is a flux of photons. Vision starts when these photons are absorbed by the light-sensitive pigment (rhodopsin) and converted into electrical signals through a G-protein-coupled signalling cascade. The *Drosophila* phototransduction is one of the fastest known G-protein-coupled signalling cascades (Montell, 1989; Ranganathan, Malicki and Zuker, 1995; Hardie and Raghu, 2001; Hardie and Postma, 2008) and a widely used model to explain invertebrate and microvillar visual transduction.

In the animal kingdom, two major classes of photoreceptors have evolved: ciliary photoreceptors (vertebrate rods and cones) and microvillar (also called rhabdomeric) photoreceptors, which are found in many invertebrates (Arendt, 2003). In microvillar photoreceptors (**Figure 1-4A**), each microvillus contains all the phototransduction reactions and therefore, it is called a photon sampling unit (**Figure 1-4B**) (Smith, Stamnes and Zuker, 1991; Hardie and Raghu, 2001). These transduction units (~30,000 microvilli in *Drosophila*, ~60,000 in *Musca* and ~90,000 in *Calliphora*) form the rhabdomere (Hardie, 1985; Song et al., 2012).

Every microvillus can generate a quantum bump (QB) from a single photon that photoisomerises one of its rhodopsin molecules (**Figure 1-4C**) (Fuortes and Yeandle, 1964; Kirschfeld, 1966; Lillywhite, 1977; Wu and Pak, 1975; Hardie and Juusola, 2015). Due to refractoriness (50-300 ms in *Drosophila*), a microvillus can only produce

one QB at a time and during that time window, it cannot respond to another incoming photon. QBs (single-photon responses) are then summed to produce photoreceptor's graded macroscopic voltage response (**Figure 1-4D**) (Wu and Pak, 1975; Dubs, 1981; Hochstrate and Hamdorf, 1990; Henderson, Reuss and Hardie, 2000; Song et al., 2012). Even though the summation appears linear (at dim intensities), the bumps are nonlinear events having different waveform and latency distributions.

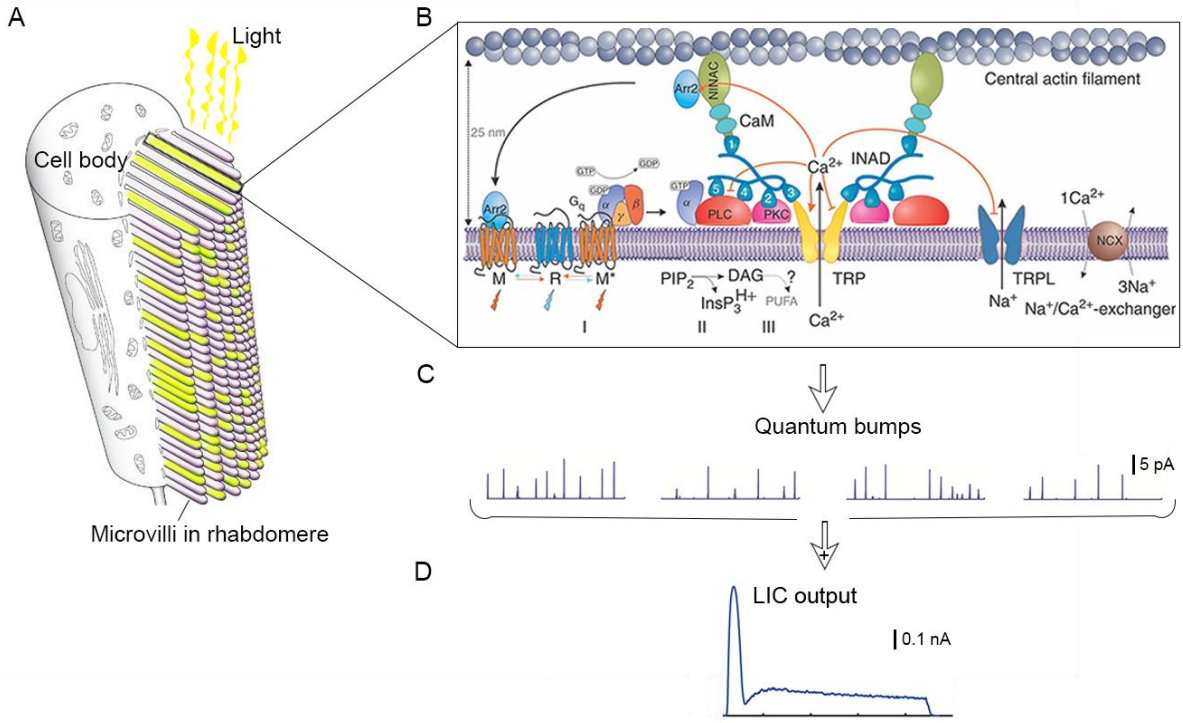

Figure 1-4. Quantal light information sampling by *Drosophila* R1-R6 photoreceptors. (A) A longitudinal view of a photoreceptor shows that a rhabdomere is composed of microvilli (~30,000 microvilli in *Drosophila*, ~60,000 in *Musca* and ~90,000 in *Calliphora*). Yellow microvilli are the ones that have absorbed a photon (modified from Montell, 2012). **(B)** These single photon energies are converted into electrical signals (quantum bumps, QBs) through a G-protein-coupled signalling cascade. *Drosophila* phototransduction is one of the fastest known G-protein-coupled signalling cascades (Hardie, 2011). **(C)** Example of QB distributions in time from different microvilli. QBs have different waveform and latency distributions (modified from Song, Zhou and Juusola, 2016). **(D)** All the QBs from all the microvilli are summed to produce the macroscopic light-induced current (LIC) and eventually the graded macroscopic voltage response (modified from Song, Zhou and Juusola, 2016).

1.2.1 Photoreceptors depolarise to light increments

Microvillar photoreceptors depolarise to light increments, unlike ciliary photoreceptors (Fain, Hardie and Laughlin, 2010). The macroscopic response is shaped not only by the phototransduction cascade but also by the passive (lipid membrane capacitance and resistance) and active membrane properties: the voltage- and Ca^{2+} -gated channels and two electrogenic transporters (Na^+/K^+ ATPase and Na^+/Ca^{2+} exchanger). The main potassium channels (*Shaker*, slowly activating delayed rectifier and fast delayed rectifier) are very important in shaping the voltage response. Rapid inactivation of the *Shaker* (voltage-gated K^+ channel gene) helps to better allocate voltage responses within the cells' limited bandwidth in light-adapted conditions (Hardie et al., 1991; Niven et al., 2003; Juusola, Song and Hardie, 2015). In addition, the slowly activating delayed rectifier, which is encoded by the *Shab* gene, lowers the membrane time-constant, supporting fast signal conduction (Vähäsöyrinki et al., 2006; Juusola, Song and Hardie, 2015). The fast delayed rectifier is possibly encoded by the *Shal* gene and is likely to be fine-tuning the kinetics of the voltage response (Hardie, 1991; Vähäsöyrinki et al., 2006) while two different Ca^{2+}-activated K^+ channels (*Sk* and *Slo*) seem to regulate the dynamics of the peak-to-plateau transition (Li et al., 2019). The Na^+/K^+ ATPase generates an afterhyperpolarisation under bright illumination (Jansonius, 1990; Uusitalo et al., 1995), whereas the Na^+/Ca^{2+} exchanger (*calx*) regulates the cytosolic Ca^{2+} in the microvilli (Liu et al., 2020). In concordance, the *calx* mutants show reduced sensitivity to light and rapid hyperadaptation (Wang et al., 2005).

As introduced earlier, fly photoreceptors have a high single-photon sensitivity and a fast temporal resolution. But to encode vast intensity changes (>10^6 photons/s) in their natural environment, they need a large dynamic range (~70 mV) to respond. This is done mostly through refractoriness, which can reduce the sensitivity to bright light by >99% (Song et al., 2012; Juusola et al., 2017) and by the intracellular Ca^{2+}-dependent pupil mechanism (Kirschfeld and Vogt, 1980; Howard, Blakeslee and Laughlin, 1987), which together can effectively prevent saturation. Additional cellular mechanisms that help the adaptation are the ion channels and the electrogenic transporters (Juusola and Hardie, 2001a; Wang et al., 2005; Hardie and Juusola, 2015). Photoreceptors are surrounded by pigment granules and during light adaptation, these granules migrate

towards the rhabdomere to absorb and reflect the incoming photons, whereas when dark-adapted they move radially away. This way the eye is able to control the light flux in the rhabdomere, acting as a pupil (Kirschfeld and Franceschini, 1969; Franceschini, 1972; Stavenga, 1975; Howard, Blakeslee and Laughlin, 1987; Roebroek and Stavenga, 1990). Pigment migration has been studied to decrease the photon flux through the rhabdomere by up to a factor of 100 (Franceschini, 1972) and, therefore, it extends the photoreceptors dynamic intensity range (Howard, Blakeslee and Laughlin, 1987; Song and Juusola, 2014).

The most important factor that gives the foundations for a large dynamic range is the contrast invariance of the physical world to which animal vision has adapted. This comes from the invariance of object reflectance (Carpenter and Reddi, 2012). The photoreceptor's sensitivity decreases to small intensity changes, while the response amplitude increases. By Weber's law, the contrast is defined as:

$$c = \frac{\Delta I}{I}, \tag{1-1}$$

where ΔI is change in the intensity divided by the mean intensity (i.e. the background) I (Shapley and Enroth-Cugell, 1984).

Fly photoreceptors code the contrast over all natural light background intensities. The photoreceptor's response amplitude to constant contrast increases with the background, until saturation. At a given background, brief negative and positive contrast changes produce similar-looking responses (Juusola, 1993; Juusola, Uusitalo and Weckström, 1995). This is not true for steady-state adapted peak responses to long-lasting contrast stimuli (Zettler, 1969; Juusola, 1993). Effectively, background adaptation causes a logarithmic shift in the photoreceptor's sensitivity (Laughlin and Hardie, 1978). Contrast coding is highly advantageous for a fly moving between different environments with diverse light levels, enabling it to scale light input proportional to mean light intensity without losing the ability to detect behaviourally important light changes (Laughlin, 1989; Juusola, 1993).

1.2.2 LMCs hyperpolarise to light increments

Although lamina is the first optic neuropil and contains about 12 anatomically identified neurons (Rivera-Alba et al., 2011), only a few of them have been characterised via electrophysiological recordings. The lamina interneurons are notoriously small and difficult to record from, but by L1-L3 being the largest ones, they are more accessible for intracellular recordings (Scholes, 1969; Autrum, Zettler and Järvilehto, 1970; Järvilehto and Zettler, 1971; Laughlin and Hardie, 1978; Guy and Srinivasan, 1988; van Hateren, 1992b; Uusitalo et al., 1995; Juusola et al., 2016). As more is known about them, this chapter will mainly focus on their response properties.

Like R1-R8 photoreceptors, LMCs respond with graded potentials to light changes. However, in the LMCs, the signal from the outer photoreceptors (adjacent R1-R6) goes through three transformations: inversion, amplification and adaptive response waveform changes to intensifying light inputs (Järvilehto and Zettler, 1971; Laughlin, 1973; Laughlin and Hardie, 1978). Unlike photoreceptors, which depolarise to light increments, an LMC responds with a transient hyperpolarisation (ON-transient) followed by a light-off response, a depolarising OFF-transient. The inversion is caused by the photoreceptors' inhibitory neurotransmitter (histamine). Histamine binds to the chloride channels in the LMC membrane, causing them to open (Hardie, 1989) with the resulting inward Cl^--flux hyperpolarising the cell. Histamine release is tonic even in darkness (Uusitalo et al., 1995). The depolarising OFF-transient is most prominent in response to bright light flashes. However, in dim light conditions, the LMC response becomes monophasic having only the hyperpolarising light ON-peak. Furthermore, the light OFF-transient seems more obvious when recording in chiasma or near medulla and thus, it is thought to be generated in the medulla terminal (Järvilehto and Zettler, 1971; Laughlin and Hardie, 1978; Guy and Srinivasan, 1988).

Amplification and generation of light ON- and OFF-transients are thought to be important for efficient information coding of the natural environment. Both photoreceptors and LMCs respond with increasing amplitudes (depolarisation vs hyperpolarisation) to increasing light contrasts. Pooling six presynaptic photoreceptor terminals amplifies the transmitted signals and reduces noise (Laughlin and Hardie, 1978; Laughlin, 1989). While synaptic adaptation, through dynamic synaptic

feedforward-feedback interactions and membrane conductances, reallocates the responses within the LMC amplitude and frequency ranges (~60 mV) (Hardie and Weckström, 1990; Zheng et al., 2006; Zheng et al., 2009; Nikolaev et al., 2009; Li et al., 2019).

Two early static models, predictive coding (Srinivasan, Laughlin and Dubs, 1982) and matched amplification (Laughlin, 1981a), were constructed to explain how LMCs, respectively, subtract and amplify stationary signals to maximise the information transfer from the incoming signal. The key components in predictive coding were spatial and temporal inhibition. In the schemes, these were both used to remove the redundant (or predictable) component from the input signal to increase the sensitivity and to reduce the intrinsic noise (Srinivasan, Laughlin and Dubs, 1982). Thus, within these simplified concepts, LMCs were considered to be adaptive spatiotemporal filters enhancing the contrast coding by background subtraction.

In space, the adjacent pixel intensities correlate strongly (van Hateren, 1997) and, therefore, to combat redundancy, the local weighted average can be calculated and then subtracted from the signal (Srinivasan, Laughlin and Dubs, 1982). The weighting function presumably depends on the signal-to-noise ratio (SNR) of the input signal and can relate to lateral inhibition (Hartline, 1949; Barlow, 1953). In the fly eye, lateral inhibition is thought to reflect the centre-surround structure of the LMC receptive field (Zettler and Järvilehto, 1972; Dubs, 1982). Subsequently, the net LMC response has been approximated as the difference between the response generated in the centre of its receptive field and the response of the surround generated by the mean light intensity (the background). At bright intensities, the SNR of the light input is high and thus, the local average can be calculated using only a few neighbouring photoreceptors. This would make the antagonistic surround of the LMC receptive field strong but narrow, causing spatiotemporal differentiation. Whereas, at dim light intensities, the photon noise is high, reducing the SNR, so more photoreceptors would be needed to generate the local average. Therefore, the inhibition would be weaker and wider, causing spatiotemporal integration.

The temporal inhibition (feedback self-inhibition) contributes clearly to adaptation. The net LMC response can be thought as the difference between the current signal and the weighted average of the earlier inputs. The temporal weighting function is intensity-dependent similar to the spatial weighting function. It generates the biphasic response – the depolarising light OFF transient to bright light increments, which is not evident in dim illumination. This depolarisation is the temporal counterpart to lateral inhibition. Interestingly, the shape and the amplitude of the saturated LMC transients change in response to the background intensity levels. With a brightening background, a +1-contrast pulse evokes about equal amplitude but faster hyperpolarising responses, whilst a -1-contrast pulse generates larger and faster depolarising responses (Juusola, Uusitalo and Weckström, 1995). In conclusion, when the light intensity changes from dim to bright, both the spatial and temporal inhibition gets stronger causing the LMCs to shift from low-pass filters to band- or high-pass filters.

To make the contrast coding efficient after the presumed subtraction, the remaining signal is, nevertheless, amplified. Crucially, the dynamic range of LMCs (~70-100 mV, peak-to-peak, Juusola, Uusitalo and Weckström, 1995; Zheng et al., 2009) is biophysically limited. Therefore, to combat the saturation, the response amplification and frequency distribution should continuously adapt to the statistical distribution of contrasts the fly encounters in its natural environment (van Hateren, 1992a; van Hateren, 1992b; Zheng et al., 2009). This minimises information loss (Shannon and Weaver, 1949; Laughlin, 1981a; van Hateren, 1992a; van Hateren, 1992b; Zheng et al., 2009).

Barlow (1961) hypothesised that the goal of early vision is to remove the redundancy from the signal. The predictive coding by Srinivasan et al. (1982) explained how redundancy can be minimised through spatial and temporal inhibition. In contrast, van Hateren (1992a) presented a theory where removing redundancy would not necessarily be optimal in every situation, suggesting the goal of the early sensory processing is to maximise the information, instead of removing the predictable components from the signal. His theoretical model explains how LMCs maximise the information transfer by changing their filtering properties - in low light backgrounds (dusk/dawn, low-SNR) the response is low-pass-filtered where redundancy will be increased. Whereas at bright light backgrounds (daylight, high SNR), the response is

band- or high-pass-filtered and thus, redundancy will reduce. To summarise, the theory stated that redundancy would be beneficial for the system in low light conditions. Later, van Hateren (1992b) tested his computational theory by carrying out experiments (*in vivo* intracellular recordings) at steady-state conditions using blowfly (*Calliphora vicina*) LMCs. The predictions matched reasonably well with the experimental results, showing that LMCs shift their "neural" filters according to the mean light intensity to maximise the information transfer rate.

A further experimental study from blowfly LMCs (Juusola, Uusitalo and Weckström, 1995) using a Gaussian white noise (GWN) stimulation, was consistent with the previous theory and findings from van Hateren (1992a, 1992b). It should be noted that both of the studies by van Hateren and Juusola et al. investigated the information processing in LMCs by using either a point source/wide-field or a GWN stimulation, respectively, neither of which excite the photoreceptors' full dynamic range. Subsequently, such stimuli would underestimate response information transfer rate in respect to naturalistic or bursty stimuli (Juusola et al., 1994; van Hateren, 1997; Juusola and Song, 2017; Juusola et al., 2017). Therefore, it is important to excite the full dynamic range to any sampling nonlinearities, such as refractoriness or saccadic photoreceptor photomechanics, by using a stimulus with more complex naturalistic and behavioural statistics (Juusola et al., 2017).

1.2.3 Different response properties of L1-L3

Although I have referred to LMCs as a homogeneous group, detailed anatomical, electrophysiological and two-photon imaging research have revealed subtle differences between them. Here, I will discuss mainly the electrophysiological findings on L1-L3 (**Table 1-1**).

Like photoreceptors, L1-L3 are non-spiking neurons as opposed to the two remaining LMCs (L4 and L5), which are probably spiking neurons (Shaw, 1981; van Hateren and Laughlin, 1990). All the L1-L3 get inhibitory feedforward histaminergic input from the outer photoreceptors (L1: ~250 synapses, L2: ~250 synapses and L3: ~51 synapses) but L2, as well as L4 (including $L4_{+x}$ and $L4_{-y}$) and amacrine cells, provide excitatory feedback to R1-R6 (~6 synapses) (Rivera-Alba et al., 2011). L2 possibly shows

stronger lateral inhibition than L1 and L3 (Laughlin and Osorio, 1989). All LMCs presumably receive opposing polarity push-pull inputs from the neighbouring cartridges (Zettler and Järvilehto, 1972; Strausfeld and Campos-Ortega, 1973; Meinertzhagen and O'Neil, 1991; Rivera-Alba et al., 2011), which potentially enhances the centre-surround-antagonism.

L1-L3 have different membrane properties (Hardie and Weckström, 1990). Hence their voltage responses to light differ from each other. LMCs can be divided into two subclasses (L1/L2 and L3) based on their electrical properties. With respect to the *Calliphora* R1-R6's -60 to -75 mV resting potentials and ~20-35 MΩ input resistance in darkness, L1 and L2 are more depolarised (~-40 mV) and leakier (10-20 MΩ). However, L3 resting potential is -60 mV and it has a higher input resistance (30-40 MΩ) than L1 and L2 (Hardie and Weckström, 1990; van Hateren and Laughlin, 1990). Hardie and Weckström (1990) further performed intracellular recordings from L1-L3 to examine, which potassium channels contribute to shaping the voltage response to light. They found that L1 and L2 mainly express a rapidly inactivating current (an A-current, K_a), whereas L3 mainly expresses a slowly inactivating current (a delayed rectifier current, K_d). Unlike the A-current, the delayed rectifier current is most likely activated under normal physiological conditions, potentially shaping the signal by sharpening the light OFF depolarisation.

Hardie and Weckström (1990) discovered that L3 has a positive transient superimposed on the depolarising light OFF response (**Figure 1-5A**). This was further studied by Uusitalo, Juusola and Weckström (1995) who observed a similar but smaller spike-like event in L1 after a brief hyperpolarisation of the resting potential. L2, on the other hand, did not show any spike-like events in any conditions tested (**Figure 1-5B**). They suggested that the spikes are mediated by the voltage-gated sodium channels in the LMC axons. However, none of the LMCs produced spikes in response to small contrasts or white noise (WN) stimulation.

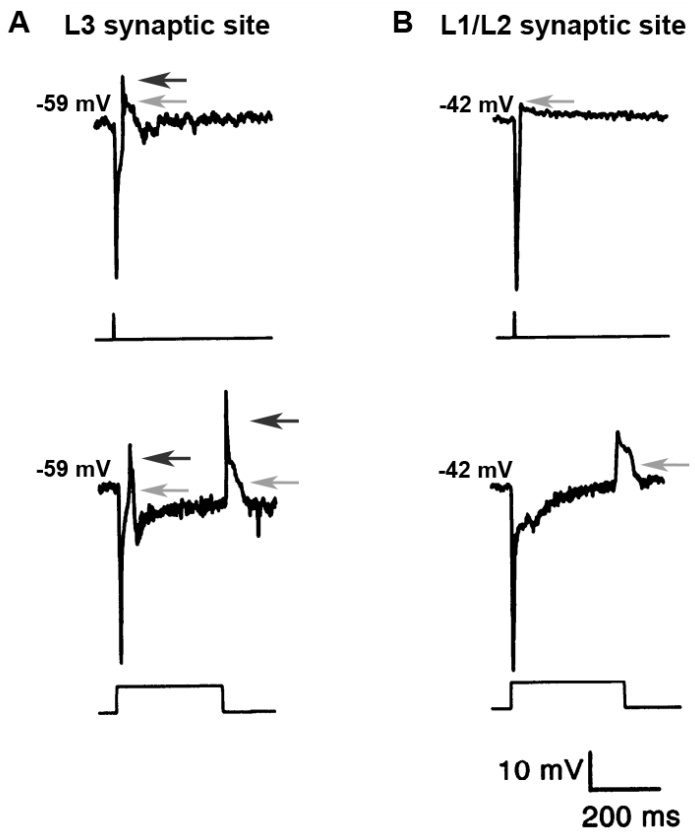

Figure 1-5: Intracellular responses of *Calliphora* LMC subtypes (L1/L2 and L3) to light in the synaptic site. (A) Top: L3 responds with a brief hyperpolarisation followed by a depolarising light OFF response (light grey arrow) to a short 2-ms light pulse. There was a positive OFF spike (dark grey arrow) superimposed on the light OFF response. Bottom: L3 response to a long 300-ms light pulse. Longer light stimulation produced an additional OFF spike (first dark grey arrow) after the light ON response (first light grey arrow). L3 has a resting potential of about -59 mV. **(B)** L1/L2 has a higher resting potential (about -42 mV) and did not produce OFF spikes to either of the light stimuli (top: 2-ms light pulse, bottom: 300-ms light pulse). Moreover, the L1/L2 had a much smaller OFF response (light grey arrow) to the short light pulse (modified from Uusitalo, Juusola and Weckström, 1995).

In the past, the electrophysiological differences between L1-L3 have been generally attributed to their different sizes, synaptic terminal locations (Strausfeld, 1976) and axon lengths (van Hateren and Laughlin, 1990), as L1-L3 each feeds to different medulla layers; likely contributing to different visual pathways. In the next chapter (1.3), I will further discuss their function in the motion pathway, how they feed the two parallel ON and OFF motion pathways, and their role in direction selectivity.

	Photoreceptors	LMCs		
	R1-R6	L1	L2	L3
Feedforward from R1-R6 (number of synapses)	No	Yes (~250)	Yes (~250)	Yes (~51)
Feedback to R1-R6 (number of synapses)	No	No	Yes (~6)	No
Signal propagation	Graded	Graded	Graded	Graded
Spiking properties	No	Yes*	No	Yes
Lateral inhibition	No	Yes	Strong	Yes
Resting potential (mV)	-60 to -75	-40	-40	-60
Input resistance (MΩ)	20-35	10-20	10-20	30-40
Motion/Colour pathway	Motion	Motion	Motion	Both
ON/OFF motion pathway	-	ON	OFF	OFF(Both)
Direction selectivity	No	No	No	No

Table 1-1. Different response properties of fly photoreceptors (R1-R6) and LMCs (L1-L3). All of the L1-L3 receive feedforward histaminergic input from R1-R6 (Hardie, 1987; Hardie, 1989; Sarthy, 1991; Pantazis et al., 2008). Only L2 sends feedback to R1-R6 and has a stronger lateral inhibition than L1 and L3 (Laughlin and Osorio, 1989; Rivera-Alba et al., 2011). Note that the number of synapses are in *Drosophila* (larger flies have about four times more synapses) (Rivera-Alba et al., 2011). Although being graded neurons, L1 (*only after a brief hyperpolarisation of the resting potential) and L3 exhibit a spiking OFF response (Hardie and Weckström, 1990; Uusitalo, Juusola and Weckström, 1995). L1 and L2 have very similar membrane properties: expressing mainly a K_a current, -40 mV resting potential and 10-20 MΩ input resistance (Hardie and Weckström, 1990; van Hateren and Laughlin, 1990). L3 differs from these two LMCs by expressing mainly a K_d current, having a more negative resting potential and a higher input resistance. R1-R6, L1, and L2 are in the motion pathway while L3 feeds both the parallel ON and OFF motion pathways (stronger input to OFF pathway) (Joesch et al., 2010; Clark et al., 2011; Eichner et al., 2011; Joesch et al., 2013; Silies et al., 2013; Shinomiya et al., 2014; Takemura et al., 2017; Shinomiya et al., 2019). Motion is divided into two pathways in the lamina, L1 being the major input for ON motion pathway and L2 for the OFF motion pathway. Direction selectivity has been shown to arise in the dendrites of the T4 and T5 neurons and thus, photoreceptors nor LMCs are considered to be direction-selective (Bausenwein, Dittrich and Fischbach, 1992; Joesch et al., 2010; Maisak et al., 2013).

1.3 Motion detection – From ON and OFF pathways to direction selectivity

Seeing is very rarely just gazing at a static image – either flies move themselves (flying, walking or head-body movements) or something in the scene moves. Therefore, it is vital for flies (and animals in general) to distinguish between the background and an object moving against it. Furthermore, a key aspect of vision is to extract essential image/object properties such as contrast, size, orientation differences, direction and velocity. Motion detection, from parallel ON and OFF pathways to direction selectivity, have been studied extensively over the past decades, especially in the fruitfly (*Drosophila melanogaster*).

The classical elementary motion detector (EMD), established by Hassenstein and Reichardt (1956), remains the most studied local motion detection model in insects. The Hassenstein-Reichardt (HR) detector is a generalised model, which computes the direction of motion by correlating the temporal luminance changes between two adjacent photoreceptors. It does this by multiplying the directional responses (to a moving stimulus) of the two neighbouring photoreceptors after one of them has been temporally delayed (**Figure 1-6A top**). The output signals from both photoreceptors are then subtracted, enhancing the direction-selectivity: a positive response to motion in the preferred direction (PD) and an opposite, negative response to motion in the null direction (ND) (**Figure 1-6A bottom**) (Reichardt, 1961). These direction-selective responses have been characterised by physiological recordings of giant lobula plate tangential cells (LPTCs), which are considered the output neurons of the EMD model (Schnell et al., 2012).

Photoreceptors (R1-R6) are classically thought to only detect luminance changes without being able to separate whether those fluctuations are moving or stationary. As a result, they have been considered motion insensitive and direction unselective. They do, however, provide input to L1 and L2, which are both required for motion detection (Rister et al., 2007). In the lamina, motion detection is divided into two parallel motion pathways, ON and OFF pathways (**Figure 1-6B**). Both behavioural and functional studies have indicated that L1 is the primary input for ON pathway encoding moving light (ON) edges, whereas L2 feeds into the OFF pathway and, accordingly, encodes

dark (OFF) edges (Joesch et al., 2010; Clark et al., 2011; Eichner et al., 2011; Joesch et al., 2013; Silies et al., 2013). Although both L1 and L2 are inputs for these two separate pathways, they seem not directly encode motion nor be direction selective.

Direction selectivity arises in the dendrites of T4 (dendrites in the medulla) and T5 (dendrites in the lobula) cells, which are the outputs for ON and OFF motion pathways, respectively (**Figure 1-6C**) (Bausenwein, Dittrich and Fischbach, 1992; Joesch et al., 2010; Maisak et al., 2013). These neurons are considered the local motion detection outputs and they respond to one of the four cardinal directions (front-to-back, back-to-front, upward and downward) according to which one of the four layers in the lobula plate they terminate (Buchner, Buchner and Buelthoff, 1984; Fischbach and Dittrich, 1989; Maisak et al., 2013). In the lobula plate, both of these neurons synapse with LPTCs, which process wide-field motion in either front-and-back horizontal (HS cells) or up-and-down vertical (VS cells) direction (Scott, Raabe and Luo, 2002; Joesch et al., 2008; Schnell et al., 2010). In addition to the direct excitation from T4 and T5 cells, to enhance the motion opponency, LPTCs receive indirect inhibition from the bistratified lobula plate intrinsic (LPi) cells located in the oppositely tuned, neighbouring layer (Mauss et al., 2015). LPi cells receive their input from the T4 and T5 cells that terminate in the neighbouring layer. LPTCs further receive collateral inputs from the contralateral eye (Farrow, Haag and Borst, 2003).

The medulla columnar neurons that connect LMCs to T4 and T5 cells have been identified by extensive EM reconstructions (Takemura et al., 2011; Takemura et al., 2013; Shinomiya et al., 2014; Takemura et al., 2017; Shinomiya et al., 2019). In the ON pathway, medulla intrinsic 1 (Mi1) and transmedullary 3 (Tm3) neurons in downstream of L1 are the major inputs to T4. T4 gets additional input from C3, CT1, Mi4, Mi9 and from itself (T4) (Takemura et al., 2013; Takemura et al., 2017). Out of all the inputs, Mi1, Mi4, Mi9 and Tm3 predominantly shape the direction selectivity of the T4 neurons. Mi4 receives indirect input from L1 and L3 through L5 and Mi9. In addition to the main input from L3, Mi9 has strong reciprocal connections with Mi4 (Arenz et al., 2017; Takemura et al., 2017).

In the OFF pathway, the synaptic inputs to T5 neurons are four transmedullary neurons: Tm1, Tm2, Tm4 and Tm9 (Shinomiya et al., 2014). L2 synapses with Tm1, Tm2 and Tm4 while forming reciprocal connections with L4, which also sends input to Tm2 (Takemura et al., 2011). In addition, Tm2 is presynaptic to L5 (Takemura et al., 2011; Takemura et al., 2013). Even though L3 receives input from R1-R6 much like L1 and L2, it was thought to contribute to orientation behaviour and colour pathway, rather than having any sort of function in motion detection (Rister et al., 2007; Gao et al., 2008). It was later revealed that L3 not only has a substantial role in motion detection but, surprisingly, it also feeds into both of the motion pathways: ON pathway through Mi9 and OFF pathway via Tm9 (Silies et al., 2013; Shinomiya et al., 2014; Takemura et al., 2017; Shinomiya et al., 2019). Out of these two pathways, L3 is considered to have a more significant input to the OFF pathway alongside L2.

Because direction selectivity emerges in the dendrites of T4 and T5 cells (Bausenwein, Dittrich and Fischbach, 1992; Joesch et al., 2010; Maisak et al., 2013), neither the upstream neurons nor photoreceptors are considered to be direction selective. However, a recent study (Juusola et al., 2017) found that *Drosophila* photoreceptors contract (front-to-back) to light to enhance the visual acuity and to maximise the information capture. In addition, this study found an interesting correlation between the photoreceptor contractions and possible direction selectivity. Intracellular recordings from *Drosophila* photoreceptors (R1-R6) revealed a slight difference in the voltage response time to rise and decay when responding to a dot moving in opposing directions (front-to-back vs back-to-front). The photoreceptor voltage response showed faster rising and decaying to back-to-front direction although the time-to-peak remained unchanged. The study suggested that this is evidence of direction-selective encoding at the level of photoreceptors, which probably reflected their rapid front-to-back sweeping photomechanical contractions. Further research is required to elucidate whether such direction selectivity is indeed present in photoreceptors and what impact it has.

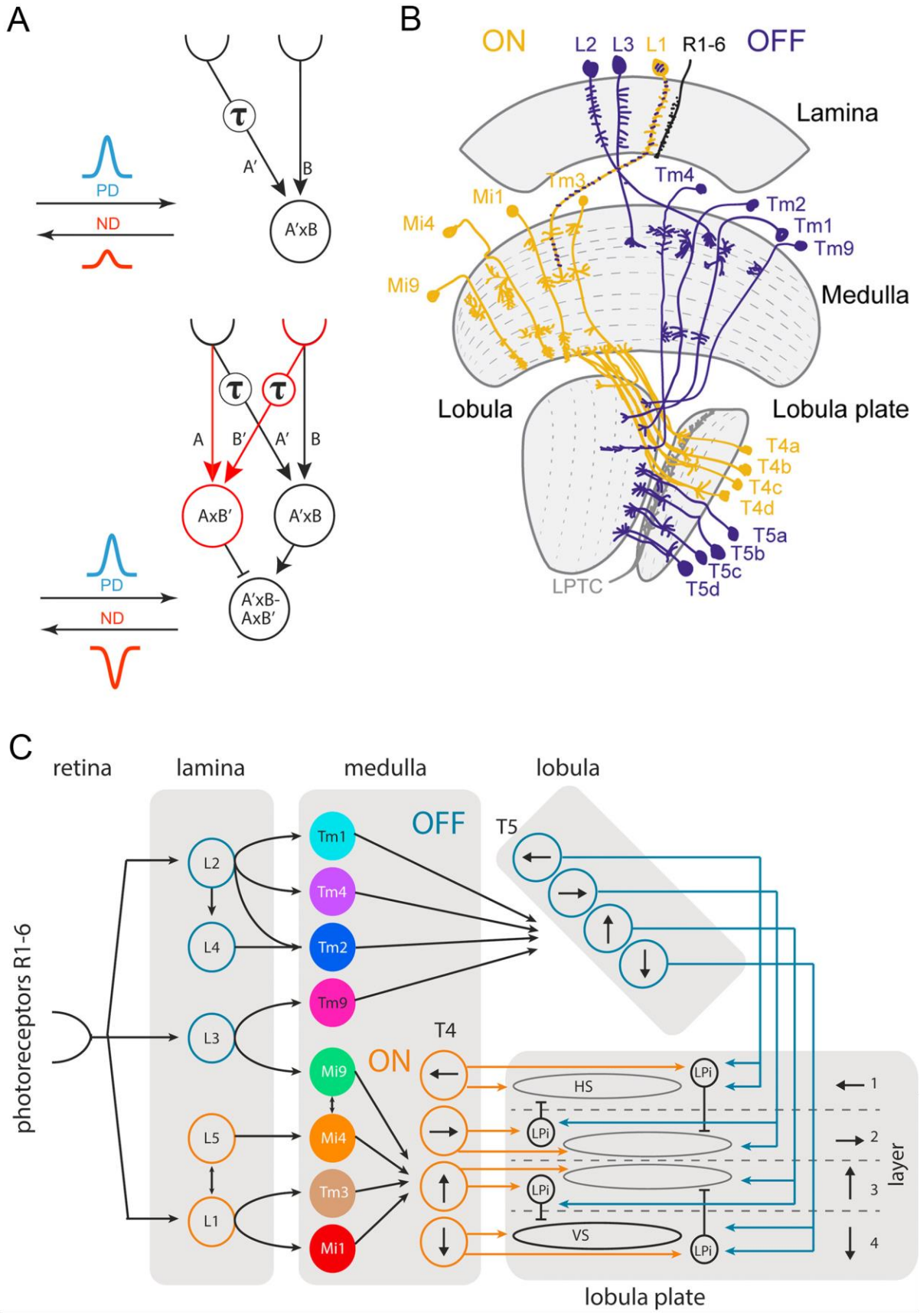
A
PD
ND
A′
B
A′xB
A
B′
A′
B
AxB′
A′xB
A′xB-
AxB′
B
ON
L2
L3
L1
R1-6
OFF
Lamina
Tm3
Tm4
Mi1
Tm2
Mi4
Tm1
Tm9
Mi9
Medulla
Lobula
Lobula plate
T4a
T4b
T4c
T4d
T5a
T5b
T5c
T5d
LPTC
C
retina
lamina
medulla
lobula
photoreceptors R1-6
L2
L4
L3
L5
L1
Tm1
Tm4
Tm2
Tm9
Mi9
Mi4
Tm3
Mi1
OFF
ON
T5
T4
HS
VS
LPi
1
2
3
4
layer
lobula plate

Figure 1-6. Motion detection in the fly visual system. (A) The Hassenstein-Reichardt (HR) detector is the most commonly used elementary motion detection (EMD) model to explain the local motion detection in insects. The HR detector is a correlation-type detector, which computes the direction of motion by correlating the temporal luminance changes between two adjacent photoreceptors. Top: Showing only a half-HR detector in which the signals of the two neighbouring photoreceptors are multiplied after one of them has been temporally delayed. Therefore, the response to the motion in a preferred direction is larger than to null direction although both produce a positive response. Bottom: The full-HR detector is a combination of two mirror-symmetric subunits (half detectors). In the full detector after multiplication, the outputs are then subtracted, enhancing the direction-selectivity: a positive response to motion in the preferred direction (PD) and an opposite, negative response to motion in the null direction (ND). These direction-selective responses have been characterised by physiological recordings of giant lobula plate tangential cells (LPTCs), which are considered the output neurons of the EMD model (modified from Arenz et al., 2017) **(B)** Motion detection is divided in the lamina into two parallel motion pathways, ON and OFF pathways. L1 is the primary input for ON pathway encoding moving light (ON) edges, whereas L2 feeds into the OFF pathway and, accordingly, encodes dark (OFF) edges (Ramos-Traslosheros, Henning and Silies, 2018). **(C)** Direction selectivity arises in the dendrites of T4 (dendrites in the medulla) and T5 (dendrites in the lobula) cells, which are the outputs for ON and OFF motion pathways, respectively. These neurons are considered the outputs for the local motion detection and they respond to one of the four cardinal directions (front-to-back, back-to-front, upward and downward) according to which one of the four layers in the lobula plate they terminate. In the lobula plate, both of these neurons synapse with LPTCs, which process wide-field motion in either front-and-back horizontal (HS cells) or up-and-down vertical (VS cells) direction. LPTCs also receive indirect inhibition from the bistratified LPi cells located in the oppositely tuned, neighbouring layer. In addition, the medulla columnar neurons in the ON pathway are Mi1, Mi4, Mi9 and Tm3 and in the OFF pathway, the synaptic inputs to T5 neurons are Tm1, Tm2, Tm4 and Tm9 (from Arenz et al., 2017).

1.4 Visual acuity and optics of the compound eye

Visual acuity defines the finest detail an animal can see. In my thesis, visual acuity (maximum spatial resolution) is defined as the minimum neurally resolvable angle between two equally sized objects. It is limited by the optical image quality (diffraction) and the image sampling pixel density, which relate to rhabdomere (or rhabdom in fused rhabdom eye) and lens dimensions/interommatidial pixel distance ($\Delta\varphi$), respectively, and the speed of phototransduction reactions (a photoreceptor's integration time) (Land, 1997). Additionally, the ambient light level and the eye movement/object speed impact visual acuity.

1.4.1 Diffraction and rhabdomere dimensions

Mallock (1894) is believed to be the first to consider the optical limitations of compound eyes and proposing that it would project a poor quality image. The compound eye is composed of hundreds to thousands of ommatidia, with each of them having its own lens. These lens-capped facets are very small and, therefore, they are limited by diffraction (**Figure 1-7**). Due to the wave-particle duality, light does not only have properties of a particle (photon), but it also behaves like a wave (Broglie, 1924). Hence, the incoming light will spread (i.e. diffract) when passing through a lens:

$$d = \frac{\lambda}{D}\,. \tag{1-2}$$

When this occurs, a point object in the receptive field will not be seen as a point but as a blurred spot (an Airy disc) (Kuiper, 1966). The two ways to reduce diffraction are: to increase the size of the lens (*D*) or to reduce wavelength (λ) (Land, 1997).

Another important factor is the rhabdomere dimensions. The narrower the rhabdomere, the better the resolvability, because it collects light from a narrower receptive field in the visual space. How rhabdomere dimensions impact the spatial resolution was studied in *Drosophila* and *Coenosia* (killerfly) compound eyes (Gonzalez-Bellido, Wardill and Juusola, 2011). These similar-sized flies have different habitats and lifestyles: *Coenosia* is a fast-flying diurnal predator, whereas *Drosophila* is a slow-flying crepuscular fructivore. Based on its demanding visual ecology, it is especially beneficial for a predatory killerfly to rapidly and accurately detect small prey. Intracellular recordings from both of these species implied that *Coenosia* photoreceptors have three-to-four-times better resolvability compared to *Drosophila*. High visual acuity was not a result of diffraction because although *Coenosia* has two to three times more lenses than *Drosophila,* the lens sizes are similar. Interestingly, TEM (transmission electron microscopy) cross-sections of ommatidia showed that *Coenosia* has much smaller (narrower) rhabdomeres. This improved the spatial resolution by narrowing their receptive fields and reducing blur and cross-talk between neighbouring photoreceptors.

However, even the narrowest rhabdomeres (<2 µm) suffer from interference leading to waveguide modes. Rhabdomere is a waveguide in which the light propagates by internal modes. In narrow rhabdomeres, some of the light propagates outside the rhabdomere and is then absorbed by the pigment granules (see pupil mechanism) (Snyder, 1975; van Hateren, 1989; Land, 1997). This leakage can potentially lower spatial resolution.

Pupil closure reduces these higher-order modes and affects both the angular and spectral sensitivity (Hardie, 1979; Vogt, Kirschfeld and Stavenga, 1982; Smakman, van Hateren and Stavenga, 1984; Stavenga, 2004). Light adaptation induces pupil closure in which the surrounding pigment granules migrate towards the rhabdomere to reduce the incoming light flux (Kirschfeld and Franceschini, 1969). The pupil closure improves spatial resolution by narrowing the receptive field (its acceptance angle) for short wavelengths, causing a blue shift in spectral sensitivity (Stavenga, 2004). By contrast, during dark adaptation, the pigment granules move radially away, which widens the acceptance angle, reducing the spatial acuity.

1.4.2 Interommatidial angle ($\Delta\varphi$) and acceptance angle ($\Delta\rho$)

Eyes in general, not only insect compound eyes, should thrive to achieve high sensitivity to light and a good spatial resolution. Unfortunately, the eye needs to compromise one to maximise the other. Due to this trade-off, the spatial resolution is highest in bright light conditions where the acuity is classically thought to reduce to the interommatidial angle ($\Delta\varphi$), the eye's believed pixel density limit. On the contrary, in low light or dark conditions, the eye needs to compromise resolution to maximise sensitivity and thus, the limit of acuity is set by the photon catch, which may be neurally integrated over multiple ommatidia (Fermi and Richardt, 1963; Warrant and McIntyre, 1992; Warrant, 1999).

Interommatidial angle ($\Delta\varphi$) is the angular separation between two neighbouring sampling units, ommatidia (**Figure 1-7**). Hence, this angle has been thought to define the minimum separable angle or the smallest feature that the eye can resolve. In other words, the interommatidial angle sets the limit for spatial resolution (Land, 1997). It should be noted that some researchers use partial interommatidial angles ($\Delta\varphi_h$ and

$\Delta\varphi_v$) to divide the horizontal and vertical interommatidial angles to match the hexagonal shape of the mosaic (Burkhardt, de la Motte and Seitz, 1966; Beersma, Stavenga and Kuiper, 1975).

In diffraction-limited eyes, the acceptance angle ($\Delta\rho$) is the half-width of a photoreceptor's angular sensitivity (receptive field), which has a Gaussian distribution (**Figure 1-7**) (Snyder, 1977). It can also be calculated using the following equation:

$$\Delta\rho = \sqrt{\left(\frac{\lambda}{D}\right)^2 + \left(\frac{d}{f}\right)^2}\,, \tag{1-3}$$

where
λ = light wavelength
D = lens diameter
d = rhabdomere diameter
f = focal distance.

This equation is not reliable, however, for narrow rhabdomeres (<2 μm) because it overestimates the value for acceptance angle due to the waveguide modes.

As seen from **Table 1-2**, the interommatidial and acceptance angles can vary throughout the eye. The region where the highest resolution is achieved due to bigger facets and smaller interommatidial angles is called the acute zone. Acute zones are quite often sex-specific, occurring generally in males; especially, when it is for sexual pursuit (**Figure 1-8A-B**). But in predatory flies, acute zones can be found in both sexes (Dietrich, 1909). Interestingly, anatomical differences were found in the male housefly (*Musca domestica*) frontal-dorsal acute zone, usually referred to as the "love spot" (Land and Eckert, 1985; Perry and Desplan, 2016). There R7 does not bypass lamina and terminate in medulla like in the rest of the eye. Instead, it terminates in the lamina, increasing the sensitivity in the acute zone (Hardie et al., 1981).

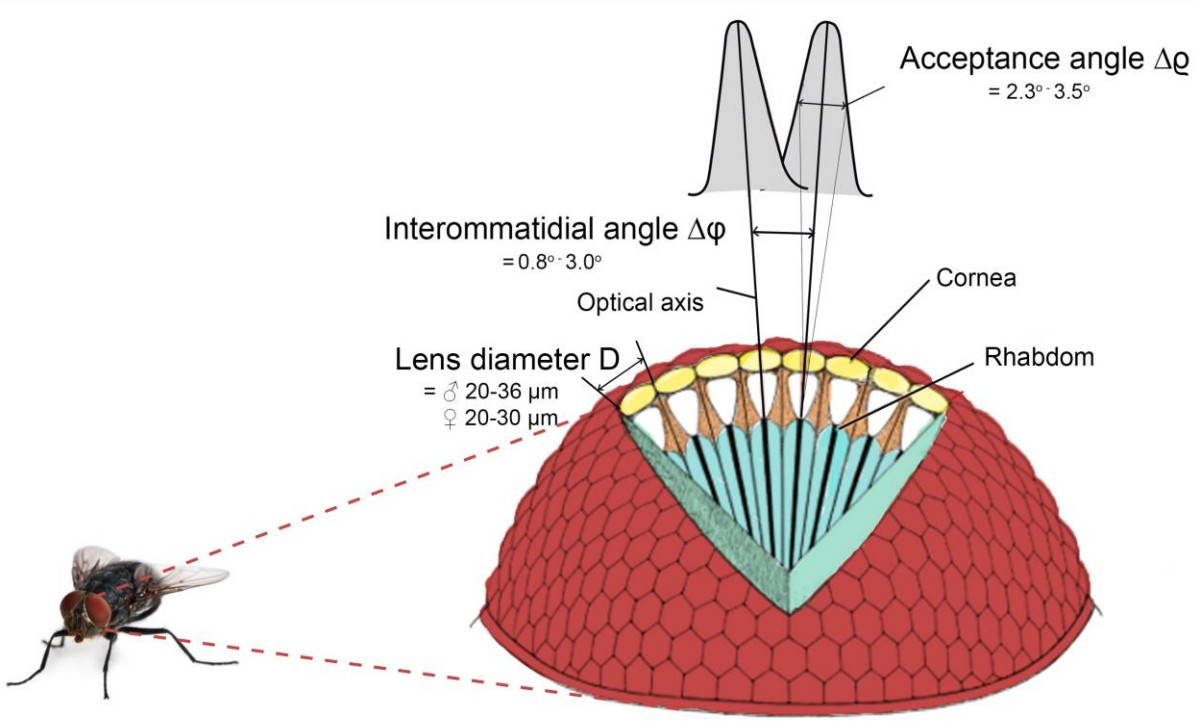

Figure 1-7. Optical parameters that define visual acuity of the compound eye. *Musca* compound eye is composed of about 3,500 small lenses. Due to the small diameter of the lens (D), the eye is limited by diffraction. In addition, visual acuity is limited by the interommatidial angle (Δ*φ*) and the acceptance angle (Δ*ρ*). Interommatidial angle is the angular separation between two neighbouring ommatidia and it defines the minimum angle the eye can resolve. In diffraction-limited eyes, the acceptance angle is the half-width of a photoreceptor's angular sensitivity (values from **Table 1-2**) (modified from Horridge, 1977).

Most acute zones are frontal-dorsal and coherently the interommatidial angles are smallest in these regions and increases when moving towards lateral regions in *Musca* (Beersma, Stavenga and Kuiper, 1975) and *Calliphora* (Franceschini, Münster and Heurkens, 1979) (**Figure 1-8C-D**). In the frontal regions the rhabdomeres are longer, lens diameters larger and acceptance angle smaller in *Musca* (Hauser-Holschuh, 1975; Hardie, 1979; Hardie, 1985) and *Calliphora* (Washizu, Burkhardt and Streck, 1964; Hardie, 1979; Hardie, 1985; Stavenga, Kruizinga and Leertouwer, 1990). By contrast, in *Drosophila* these parameters do not have a similar gradient throughout the eye, instead, they remain almost the same (Hauser-Holschuh, 1975; Gonzalez-Bellido, Wardill and Juusola, 2011; Juusola et al., 2017).

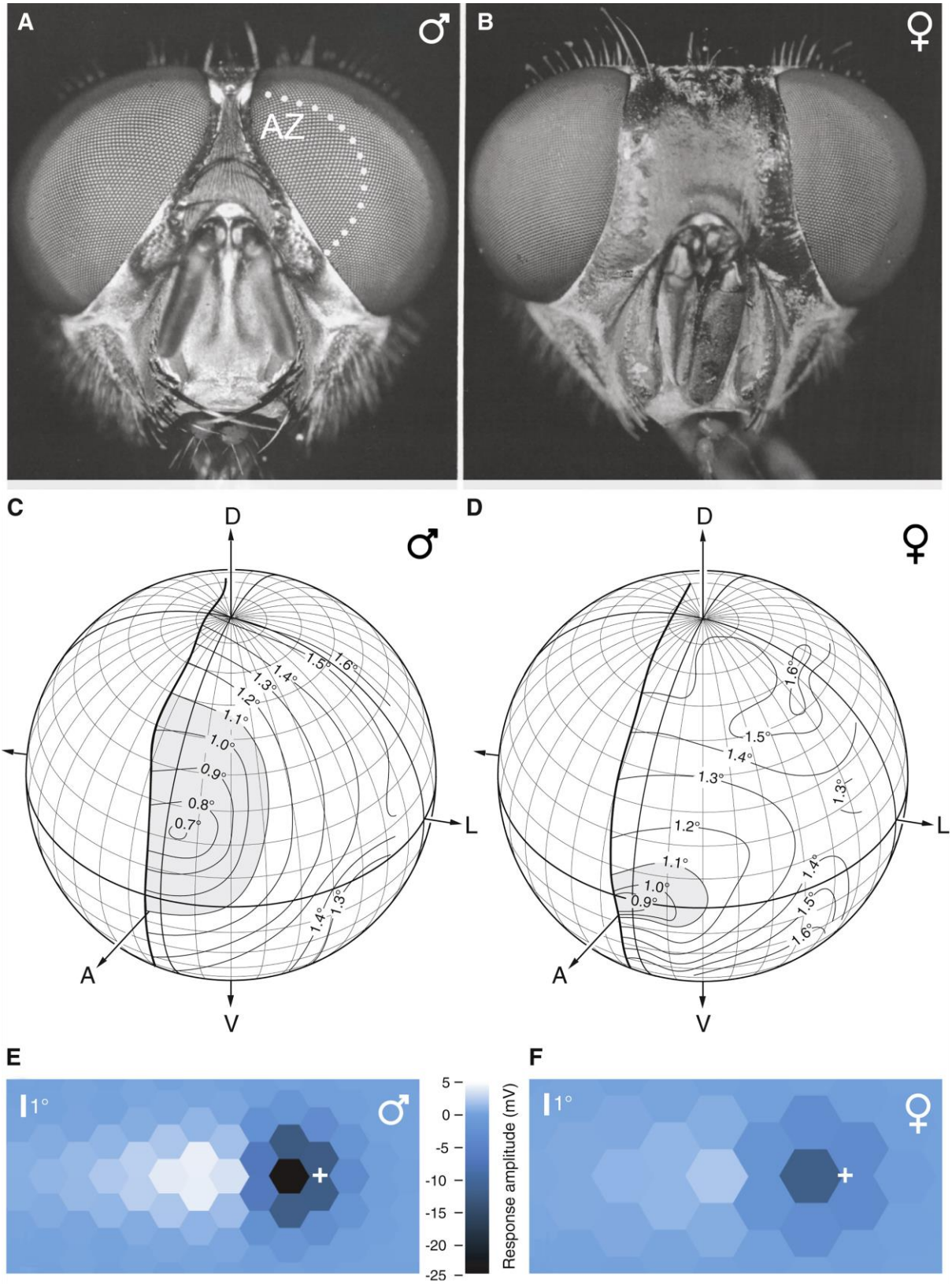

Figure 1-8. The sex-specific acute zone "love spot" in flies. Frontal view of **(A)** male and **(B)** female blowfly (*Calliphora erythrocephala*) head. Male eyes are bigger and almost merge on the dorsal part of the head. This part of the eye is called the "love spot", which is a male-specific acute zone (AZ) for female detection (modified from Strausfeld, 1991). Maps of **(C)** male and **(D)** female hoverfly (*Volucella*

pellucens) visual fields and interommatidial angles (see isolines) of the left eye. Male hoverflies have a larger acute zone with small interommatidial angles (compare the grey region). D=dorsal, V=ventral, A=anterior and L=lateral (modified from Warrant, 2001). Neural images of **(E)** male and **(F)** female housefly (*Musca domestica)* acute zones reconstructed from photoreceptor voltage responses to a dark target (angular width 3.44º) moving at 180 º/s. The colouring of each hexagon indicates the amplitude of each photoreceptor's immediate voltage response and the cross shows the current position of the target. Males have a higher sampling density – photoreceptors are separated about 1.6º in male and about 2.5º in female frontal eye regions, which enables males to have a better spatial resolution (modified from Burton and Laughlin, 2003). Figure structure taken from (Warrant, 2016).

	Lens diameter *D* (µm)	Rhabdomere dimensions (µm)		Interommatidial angle $\Delta\varphi$ (º)		Acceptance angle $\Delta\rho$ (º)
		R1-R6		Horizontal $\Delta\varphi_h$	Vertical $\Delta\varphi_v$	R1-R6
		Length	Diameter			
Fruitfly (*Drosophila*)	16-17♀	83♂♀	1.7 ± 0.15♀	4.4-7.5♀	3-9♀	~9.5♀
Housefly (*Musca*)	20-36♂ 20-30♀	140-250♂ 180-230♀	1-2♀	0.8-1.7♂	1.6-3♂	2.3-3.5♀
Blowfly (*Calliphora*)	20-40♂	230-340♂ 220-280♀	1.7-1.9	0.6-1.3♂	1-2♂	1.5-3♀

Table 1-2. Eye parameters in fruitfly (*Drosophila*), housefly (*Musca*) and blowfly (*Calliphora*). In *Musca* and *Calliphora* frontal-dorsal part of the eye, the lens diameter is the largest, R1-R6 rhabdomeres longest, the interommatidial angle and the acceptance angle smallest. In contrast, *Drosophila* does not have a similar gradient over the eye except for the interommatidial angle. Rhabdomere diameter is the widest at distal parts of the eye and gets narrower proximally, which can be seen in all the flies above. Note that the horizontal interommatidial angle ($\Delta\varphi_h$) is smallest in the front and increases towards the lateral part of the eye. The vertical interommatidial angle ($\Delta\varphi_v$) is the smallest around the equator and increases towards the dorsal and ventral part of the eye. For *Drosophila:* lens diameter (SEM; Gonzalez-Bellido, Wardill and Juusola, 2011), R1-R6 rhabdomere length (EM; Hauser-Holschuh, 1975), R1-R6 rhabdomere diameter (TEM; Juusola et al., 2017), interommatidial angle (SEM; Gonzalez-Bellido, Wardill and Juusola, 2011) and R1-R6 acceptance angle (intracellular recordings; Juusola et al., 2017). For *Musca:* lens diameter (EM; Hauser-Holschuh, 1975), R1-R6 rhabdomere length (theoretical; Hardie, 1985), R1-R6 rhabdomere diameter (EM; Boschek, 1971), interommatidial angle (deep pseudopupil method; Beersma, Stavenga and Kuiper, 1975) and R1-R6 acceptance angle (intracellular recordings, latter value estimated from optical data; Hardie, 1979). For *Calliphora* lens diameter (microreflectometry; Stavenga, Kruizinga and Leertouwer,

1990), R1-R6 rhabdomere length (theoretical; Hardie, 1985), R1-R6 rhabdomere diameter (EM; Horridge, Mimura and Hardie, 1976), interommatidial angle (behaviour; Franceschini, Münster and Heurkens, 1979) and R1-R6 acceptance angle (intracellular recordings; Hardie, 1979). Table updated from Hardie (1985).

An important optical requirement for neural superposition is that the interommatidial angle and the angle between neighbouring rhabdomeres should be equal (Kirschfeld, 1967; Pick, 1977). In the neural superposition eye, R1-R6 from the same ommatidium look at adjacent points in the visual field and send their axons to different cartridges in the lamina. The outer photoreceptors from six neighbouring ommatidia, conversely, have the same visual axis resulting in a “perfectly” overlapped image that is projected to the same lamina cartridge (Braitenberg, 1967; Kirschfeld, 1967). However, Pick (1977) showed in *Musca* that these visual axes are not parallel but they converge about 4mm in front of the eye, causing a slightly misaligned (shortsighted) image of the same point in space. Due to the overlapping receptive fields, the acceptance angle is slightly increased, leading to impaired visual acuity.

Recently, it was shown (Juusola et al., 2017) that photoreceptors possibly overcome this limitation by contracting to light, which by dynamically moving and narrowing their receptive fields generates a stream of neural snapshots. Moreover, through *in vivo* intracellular recordings and modelling, the study showed how these snapshots may enable *Drosophila* to have hyperacute vision (spatial acuity beyond the eyes’ optical limits).

1.4.3 Motion blur

Previously, I have only discussed how a stationary eye may sample an image of a stationary object. However, motion is something that needs to be taken into account. Most of the time the animal, its eyes or an object/scene is moving and, therefore, motion blur becomes a limiting factor for the spatial resolution. Therefore, a “neural” image of a moving point-object should not be a point but rather a horizontal streak. This blurring depends on the angular velocity of the object (or the animal itself) and photoreceptors’ integration time (Srinivasan and Bernard, 1975).

Juusola and French (1997) theoretically simulated how photoreceptors and LMCs resolve moving two-point objects with different angular distances in different light conditions. All of the data used in this paper was collected from blowflies (*Calliphora vicina*), at rather cool room temperatures (16-18 ^{o}C), which slows down vision (Juusola et al., 1995). Unexpectedly, photoreceptors and LMCs responded similarly: both were able to resolve points with separation below 2^{o} at velocities up to ~200 ^{o}/s with LMCs responding faster at higher velocities to increasing background illumination. Above this threshold, the "neural" image began to blur although flies exhibit different behaviours beyond this velocity. Note that this study was based upon Gaussian white-noise stimuli, which does not fully test encoding (Song and Juusola, 2014; Juusola et al., 2017). And, it did not take into account lateral inhibition in LMCs, which would narrow the acceptance angle. Moreover, it used an unrealistic value for the acceptance angle (0.2^{o}) arguing that at high velocities (>200 ^{o}/s) the receptor spacing should not limit the resolution.

However, vision has evolved to overcome this motion blur limitation through different measures (acute zones, head/thorax and body movements and the combination of refractory sampling and photomechanical contractions). Interestingly, the optics have developed to minimise the effect of motion blur by having a specific acute zone where the optics and phototransduction are enhanced (**Figure 1-8E-F**) (Hornstein et al., 2000; Burton, Tatler and Laughlin, 2001; Burton and Laughlin, 2003). Therefore, to achieve sharper "neural" images, flies aim to view moving objects in their frontal part of the eye.

In addition, flies exhibit saccadic and fixation behaviour: gaze is held still during fixation, whilst during saccades flies rapidly shift their gaze predominantly through head and body movements (also called body saccades) (Collett and Land, 1975; van Hateren and Schilstra, 1999; Schilstra and van Hateren, 1999). Through the head saccades, flies (and other flying insects) counter the body movement by moving the head and thorax to stabilise the visual scene, reducing the motion blur.

Furthermore, Juusola et al. (2017) were first to show that although flies' eyes have a rigid position in the head, they exhibit rapid photomechanical contractions (microsaccades) to light, somewhat comparable to human eye microsaccades. They

revealed in *Drosophila* how refractory sampling and photomechanical contractions together enable the fly to overcome the motion blur limit (even at high velocities to objects smaller than the optical limit). They also clarified through modelling, *in vivo* intracellular recordings (**Figure 1-9A-C**) and behavioural (optomotor flight) experiments (**Figure 1-9D-F**) how previous studies (Srinivasan and Bernard, 1975; Juusola and French, 1997) overestimate the motion blur and underestimate the spatial resolution of the fly eye. In other words, the study showed that *Drosophila* (and most likely flies and other insects) have a hyperacute vision – not only do they see fine spatial details but they can resolve them as well.

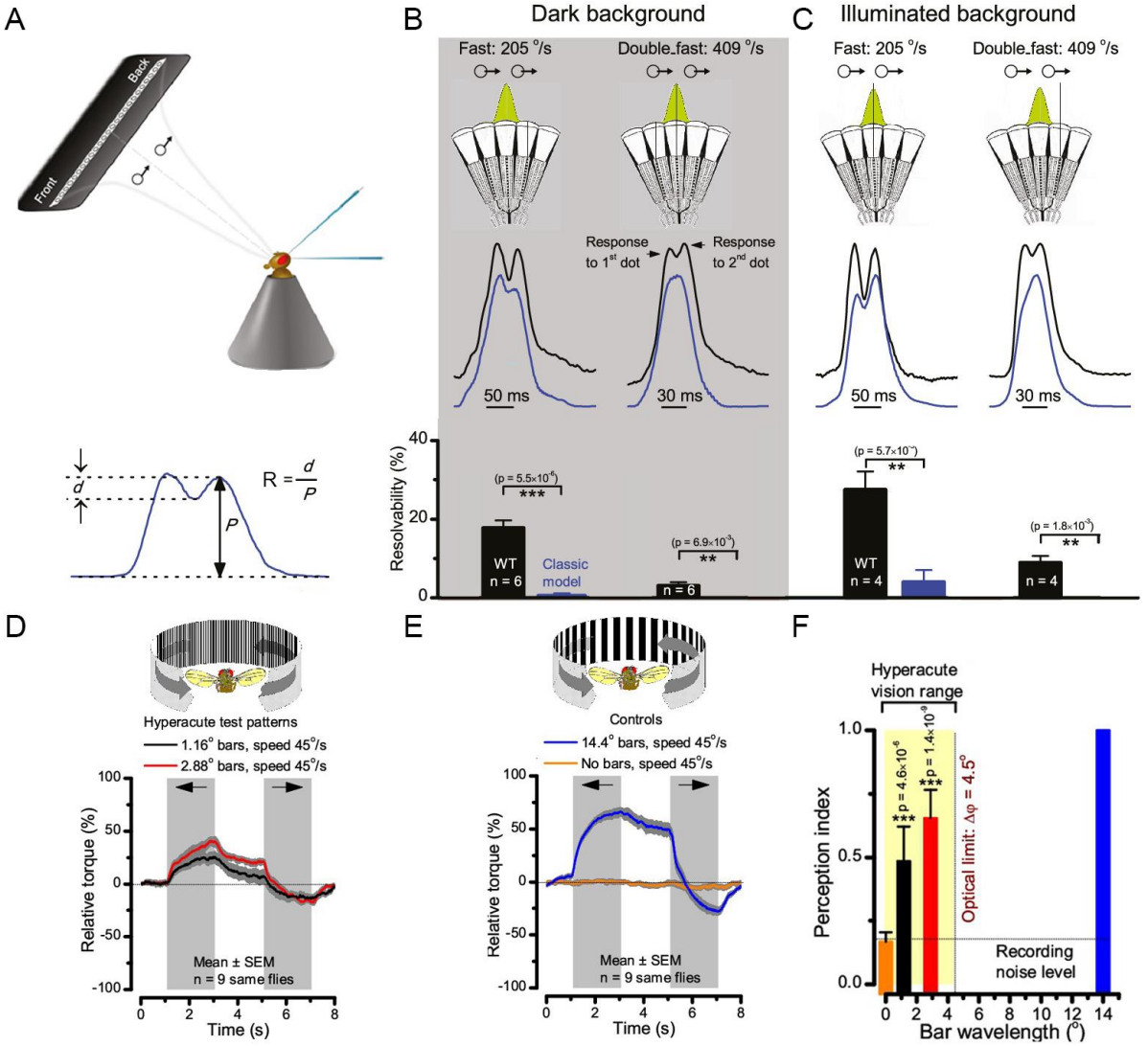

Figure 1-9. *Drosophila* hyperacute vision. (A) Top: A schematic illustrating the intracellular setup and the 25-point LED array for the light stimulation for *Drosophila* used in the experiments in **(B and C).** Two bright dots (angular separation 6.8°, which is smaller than the acceptance angle $\Delta\rho$ = 8.2°) cross photoreceptor's (R1-R6) receptive field in front-to-back direction at high saccadic speeds (205 °/s

or 409 °/s (compare to Juusola and French, 1997). Bottom: The resolvability (*R*) was calculated by using the Rayleigh criterion. R1-R6 intracellular response (black trace) compared to the simulated response (blue trace) under **(B)** dark adaptation and **(C)** light adaptation. The simulated response is based on the classic model predictions (convolving photoreceptor's impulse response with its angular sensitivity function). In both conditions, photoreceptor's real response gave better resolvability (two separate peaks in the voltage response for the two moving dots) than the expected response based on the simulation. **(D**, **E** and **F)** Open-loop optomotor flight experiments to show visual hyperacuity. Setup is composed of a torque meter measuring the tethered fly optomotor responses to a 360° hyperacute black-and-white bar panorama rotating counterclockwise and clockwise (grey, arrows) around the fly. **(D)** Using bars with 1.16° or 2.88° wavelengths (0.58° and 1.44° inter-bar-distances), which are smaller than the optical limit (interommatidial angle $\Delta\varphi$ = 2.5°-7°) moving at 45 °/s. **(E)** Control experiments with the same flies to either a white panorama with no bars or to a panorama with wide bars (wavelength 14.4°, inter-bar-distance 7.2°), which are larger than *Drosophila*'s interommatidial angle. **(F)** All the tested flies responded to bars that were separated with an angle smaller than their interommatidial angle (in theory they could not resolve these bars). 2-tailed t-tested was used (modified from Juusola et al., 2017).

1.5 Focus of the thesis

While much is already known about fly vision, some gaps remain in our current understanding. As it is valuable to find answers to open questions, I wanted to investigate several less charted territories, seek answers to three specific questions, and provide novel data to aid further research. In all cases, I used housefly (*Musca domestica*) in the experiments.

1) How much visual information can *Musca* photoreceptors and LMCs sample from the environment? Is the male's early visual encoding better?

   This question was studied in Chapter 2. Using *in vivo* intracellular recordings, I examined *Musca* R1-R6 photoreceptors' encoding capacity to high and mid-contrast bursty "saccadic" stimuli, which resemble the light input a fly encounters when performing head and body saccades. Additionally, I studied what happened to that information when passed downstream to L1-L3 LMCs. My results indicated that *Musca* early vision performs well during fast saccadic behaviours. Furthermore, male photoreceptors and LMCs seem to better encode "saccadic" stimuli, suggesting that this might be more relevant for their visual behaviour.

2) How does light adaptation impact *Musca* R1-R6 photoreceptors' and L1-L3 LMCs' response properties and signalling performance? Additionally, how is *Musca* quantum bump (QB) shape and latency distribution affected?

   These questions were addressed in Chapter 3. *In vivo* intracellular recordings from photoreceptors and LMCs showed that their signalling performance improved with brightening the mean light. Applying shot-noise analysis revealed that photoreceptors' enhanced signalling performance resulted from the integration of more and smaller QBs with faster and tighter latency distributions.

3) Do *Musca* photoreceptors and LMCs resolve hyperacute features? If so, is this impacted by the location of the eye, sexual dimorphism and direction selectivity?

In Chapter 4, using *in vivo* intracellular recordings, I attempted to look at how R1-R6 and L1-L3 cells resolved two separate visual objects (dots or bars) moving across their receptive field. These experiments were done using many different angular separations, including the hyperacute range, with four different directions and various velocities. Additionally, the impact of light adaptation to resolvability was addressed by using a moving narrowing bar-grating stimulus. The experiments were performed by using either a 25-point LED array or a digital light projector. Although there was some indication of photoreceptors resolving within the hyperacute range when using the 25-point LED array, this was not replicated when testing on a larger scale with a projector system. The projector data ultimately undermines the case for hyperacuity or direction selectivity being present within photoreceptors. For LMCs however, it does appear from my findings that hyperacuity and direction selectivity could be present but further research would be needed to make a convincing case for this.

2 Transformation of information encoding at the first synapse

2.1 Introduction

Like humans, flies are visual animals. Vision is vital for their survival: finding food, mates and shelter, and avoiding predators. Therefore, it is essential that flies can detect movement relative to their spatiotemporal self-position. Failure to do so would be evolutionary highly disadvantageous and, thus, their vision must have evolved to match their ecological needs.

Nevertheless, many scientists considered that fly vision has a severely limited capacity to resolve details in rapidly changing scenery despite the selective pressures. Flies exhibit fast body saccades when changing direction while flying or walking (Geurten et al., 2014; Mongeau and Frye, 2017). Such behaviours generate fast angular velocity changes, which - together with photoreceptors' slow integration time - should blur vision (Srinivasan and Bernard, 1975; Juusola and French, 1997). Although counter head and thorax movements might compensate for the motion blur (Collett and Land, 1975; van Hateren and Schilstra, 1999; Schilstra and van Hateren, 1999; Blaj and van Hateren, 2004) with the fly eyes showing acute-zones of improved vision (Burton and Laughlin, 2003), it was argued that flies would effectively be blind during saccadic behaviour (Land, 1999).

Juusola et al. (2017) challenged this viewpoint by exploring if, and how, refractory sampling and photoreceptor contractions could help flies encode information more efficiently. Their work showed that *Drosophila* photoreceptors contract to light and that these photomechanics, combined with refractory photon sampling, enable *Drosophila* to overcome motion blur even during fast saccades. These results were obtained through *in vivo* intracellular recordings, examining how *Drosophila* R1-R6 photoreceptors sample information from fast temporal light intensity changes that resemble the flies' saccadic viewing. The results were further tested against biophysically-realistic photoreceptor model simulations.

Although *Drosophila* is a widely used model organism, it cannot fully predict vision or visual behaviour of other insects, or even other flies, because of their different lifestyles and habitats. In this thesis work, the central aim was to test whether Juusola et al. (2017) findings were also valid for a different fly species, using the housefly (*Musca domestica*) as the test case. *Drosophila* is a slow-flying crepuscular fructivore, whereas *Musca* is a bigger fast-flying diurnal carnivore. Hence, *Musca* has better vision; higher temporal resolution (faster phototransduction, which leads to faster response dynamics and shorter integration time) (Laughlin and Weckström, 1993; Skingsley, Laughlin and Hardie, 1995; Weckström and Laughlin, 1995) and higher spatial resolution (bigger lenses and smaller interommatidial angles) (Beersma, Stavenga and Kuiper, 1975; Hardie, 1979; Hardie, 1985).

To check whether houseflies are “effectively blind” while performing body saccades, I tested if they could respond to behaviourally relevant stimuli that resemble the fast temporal changes they encounter while manoeuvring (i.e. during body saccades). These experiments were done by recording *in vivo* intracellular responses from houseflies’ R1-R6 photoreceptors while simultaneously presenting them with different visual “saccadic” stimuli: mid and high-contrast bursty light-intensity-time-series from a point light source. High-contrast “saccadic” stimuli (c ~1.29) had periods of fast light changes followed by dark periods while mid-contrast saccadic stimuli (c ~0.61) contained less dark periods. The responses to “saccadic” bursts were then compared to the ones evoked by low-contrast Gaussian white-noise (GWN) stimuli (c ~0.33), which has been regularly used for characterising visual neuron’s maximal information capacity. GWN lacks relevant non-linearities, present in natural scenes, which improve the visual coding (van Hateren, 1997; van Hateren and Snippe, 2001; Song and Juusola, 2014; Juusola and Song, 2017). Moreover, I tested what happens to photoreceptor information when transmitted to LMCs (L1-L3) as this has not previously been examined with this kind of stimuli.

My investigation indicates that houseflies are likely to see the world in finer temporal resolution than previously thought. Not only can *Musca* R1-R6s encode “saccadic” stimuli, but my results show that their information capture is maximised for such contrast bursts. This information is further accentuated in LMCs during parallel quantal neurotransmitter (histamine) sampling from six photoreceptors in the lamina.

2.2 Materials and methods

2.2.1 Fly stocks

Adult, wild-type houseflies (*Musca domestica*) were used in the experiments. The housefly larvae/pupae were ordered from a commercial provider (Blades Biological Ltd, Cowden, Kent, UK). The houseflies, cultured in a standard laboratory incubator (60% humidity) at the Department of Biomedical Science, were fed with liver, and sugar water. The flies were kept at ~22 ^{o}C in a 12:12 h light:dark cycle.

2.2.2 *In vivo* intracellular recordings

Preparations for *in vivo* intracellular recordings were done as described before (Juusola et al., 2016). In brief, a housefly was first anaesthetised with ice, and once immobilised, its legs and wings were cut off. It was fixed from the thorax, proboscis and right eye in a conical fly holder (made out of copper and ceramic) with beeswax to minimise recording artefacts caused by head or body movements. A small hole (size of 6-10 ommatidia) was cut in the left eye's dorsal cornea for the recording microelectrode, and it was sealed with Vaseline to prevent the eye from drying. Both R1-R6 photoreceptors' and L1-L3 LMCs' voltage responses were recorded using sharp filamented fire-polished borosilicate microelectrodes (Sutter instruments; outer diameter: 1.0 mm, inner diameter 0.5 mm) with a 100-250 MΩ resistance, pulled by a horizontal laser micropipette puller (P-2000, Sutter instruments). The reference electrode was pulled using a different pipette puller program to make the tip blunt.

Recordings from photoreceptors and LMCs were performed separately. Just before the experiments, both the recording and the reference electrode were filled from the back: the recording electrode with 3 M KCl solution for photoreceptors and 3 M potassium acetate with 0.5 mM KCl for LMCs, to maintain the chloride battery. Similarly, the reference electrode for photoreceptor and LMC recordings was filled with fly Ringer solution (120 mM NaCl, 5 mM KCl, 5 mM TES, 1.5 mM $CaCl_2$, 4 mM $MgCl_2$ and 30 mM sucrose) (Juusola and Hardie, 2001a). The blunt reference electrode was then gently inserted into the ocelli, and the recording electrode was carefully driven to the small hole (made earlier) by using a remote-controlled micromanipulator (PM10, Mertzhauser) under a stereomicroscope (Nikon SMZ645).

The temperature of the fly was kept at 25 ±1 C° by a feedback-controlled Peltier device. Only stable, high-quality recordings were used. In the dark, R1-R6 photoreceptors' resting potentials were < -60 mV, and maximum responses to saturating bright pulses (100 ms) were ≥ 45 mV. For L1-L3, the resting potentials in darkness were < -30 mV and maximum responses ≥ 20 mV. The recorded LMCs cannot be reliably identified because they were blindly penetrated and not stained. However, most of the recordings were probably from L1 and L2 cells because they are the lamina's largest cells. The data collected from LMCs were analysed together owing to their similar response properties such as the dark resting potential, hyperpolarisation to light increments and the response amplitude.

2.2.3 Visual stimuli

A high-intensity "white" LED (Seoul Z-Power P4 star, white, 100 Lumens) was used for the light stimulation by centring it in the middle of the cell's receptive field through a randomised quartz fibre optic bundle (transmission range: 180-1,200 nm) fixed on a rotatable Cardan-arm system, subtending a 3° homogeneous light field seen by the fly. The output was controlled by an OptoLED driver (Cairn Research Ltd, UK).

The temporal encoding capacity was measured over different bandwidth and contrast distributions. The stimuli consisted of 5 different (20, 50, 100, 200 and 500 Hz) 2-s-long Gaussian white noise (GWN) light-intensity-time-series patterns (generated by using MATLAB's *randn* function) with a flat power spectrum and a same peak-to-peak modulation (two units), low-pass filtered in MATLAB's filter toolbox. These bandwidths were tested over three different contrast backgrounds: high-contrast BG0 (0 units, dark), mid-contrast BG1 (1 unit) and low-contrast BG2 (2 units, bright) on a linear intensity scale. The light contrast was defined by using Weber's law:

$$c = \frac{\Delta I}{I} \qquad (2\text{-}1)$$

where ΔI is the intensity change, and I the mean background intensity (Shapley and Enroth-Cugell, 1984). For the white noise (WN) contrast modulation, ΔI is the standard deviation (SD) of the stimulation, and I is the mean light intensity of the stimulation. The contrast value for high-contrast "saccadic" bursts was c(BG0) = 1.29 ± 0.13, for

mid-contrast bursts *c*(BG1) = 0.61 ± 0.10 and for low-contrast GWN *c*(BG2) = 0.33 ± 0.05. Experiments were performed from the lowest to the highest adapting backgrounds, and before every stimulation, cells were dark-adapted. Only cells with stable electrophysiological recording conditions throughout the entire stimulation (all 15 different stimulus patterns) were further analysed. In all these experiments, each stimulus was repeated 30 times for every recording.

The stimuli and responses were low-pass filtered at 500 Hz (KEMO VBF/23 low-pass elliptic filter, UK), and sampled at 1–2 kHz using a 12-bit A/D converter (National Instruments, USA). For the information loss calculations (**Figure 2-7**) the stimuli and responses were low-pass filtered either at 500 Hz or 1 kHz (KEMO VBF/23 low-pass elliptic filter, UK). A custom-written software system controlled both the stimulus generation and data acquisition, Biosyst in MATLAB (MathWorks, USA) (Juusola and Hardie, 2001a; Juusola and de Polavieja, 2003), with an interface package for National Instruments (Austin, TX) boards (MATDAQ: H. P. C. Robinson, 1997-2005).

2.2.4 Data analysis

Only the steady-state adapted responses were analysed and, therefore, the first 5-10 responses to the repeated stimulation (n = 30) were discarded. The signal is the mean of all the repetitions, and the noise is the difference between individual traces and the mean (Juusola and Hardie, 2001a). Therefore, n repetitions (n = 30) gave one signal and 30 noise traces. Both the signal $s_v(t)$ and noise $n_v(t)$ traces were segmented into 50% overlapping stretches and windowed with a Blackman-Harris 4-term window, each giving three 500-point-long samples. A fast Fourier transform (FFT) algorithm was used to calculate the signal and noise spectra in the frequency domain, $S_V(f)$ and $N_V(f)$, respectively. The signal-to-noise ratio in the frequency domain $SNR_V(f)$ is:

$$SNR_V(f) = \frac{|\langle S_V(f)\rangle|^2}{|\langle N_V(f)\rangle|^2} \ , \qquad (2\text{-}2)$$

where $|\langle S_V(f)\rangle|^2$ and $|\langle N_V(f)\rangle|^2$ are the signal and noise power spectra, respectively. *v* stands for voltage, || denotes the absolute value and ⟨⟩ denotes the average over different stretches of the signal and the noise (Juusola and Hardie, 2001a).

Information transfer rate (R) was calculated from the $SNR_V(f)$ using Shannon information theory (Shannon, 1948), which has been widely applied for these types of signals (Juusola and de Polavieja, 2003; Song and Juusola, 2014; Juusola et al., 2017). The information transfer rate estimations for photoreceptors and LMCs was calculated from steady-state recordings as follows:

$$R = \int_0^\infty (log_2[SNR_V(f) + 1])df \text{ (bits/s)}, \quad (2\text{-}3)$$

The data was sampled at 1 kHz and windowed with 500-point Blackman-Harris window. Therefore, the integral's upper and lower bounds are 2 Hz and 500 Hz; not 0 and infinity (∞). I tested whether the limited bandwidth affects the information transfer estimates by recording from photoreceptors and LMCs with 2 kHz sampling rate and windowing the responses using 1,000-point data chunks (**Figure 2-7**). The SNR and R were calculated as described earlier, but now having 1,000-point-long samples and the range for the integral was from 2 Hz to 1 kHz.

2.2.5 Statistics

Statistical analyses were carried out in Prism 9 (Graphpad) and MATLAB. Maximum information rates between male and female photoreceptors as well as between the whole population of photoreceptors and LMCs were compared by using unpaired two-tailed t-test with Welch's correction as the raw data passed the Kolmogorov-Smirnov normality test. Additionally, a power analysis was performed to confirm that the sample sizes were sufficient for the used statistical test.

2.3 Results

2.3.1 Photoreceptors respond maximally to “saccadic” stimuli

To test how well *Musca* can encode visual information, which mimics light inputs during head and body saccades, I first measured *in vivo* its R1-R6 photoreceptors’ intracellular responses to different “saccadic” visual stimuli. The "saccadic" stimuli ranged from high-contrast bursts (*c* ~1.29) to mid-contrast bursts (*c* ~0.61). These responses were then compared to the same cell’s responses to low-contrast GWN (*c* ~0.33), often used to determine the maximal information capacity. All the stimuli were generated by superimposing a specific (preselected) GWN time-series light-intensity pattern on different light levels (BG0, BG1 and BG2); BG0 is darkness and BG2 full bright light. The GWN pattern was pre-filtered to different bandwidths (20, 50, 100, 200 and 500 Hz); the larger the cut-off frequency, the more the light stimulus carries information.

Similar to *Drosophila* (Juusola et al., 2017), intracellular recordings (**Figure 2-1A** and **2-2A**) from *Musca* R1-R6 photoreceptors showed that these cells respond maximally (largest peak-to-peak responses) to high-contrast “saccadic” bursts, generating significantly larger responses than to GWN stimuli (**Figure 2-1B** and **2-2B**). Increasing the stimulus contrast increased the responses (**Figure 2-1B** and **2-2B**, **rows**), whereas increasing the stimulus bandwidth reduced the responses (**Figure 2-1B** and **2-2B**, **columns**) because the stimulus became too fast to follow. Thus, the signal-to-noise ratio was highest for high-contrast bursty 20 Hz stimulus and decreased with the increasing stimulus bandwidth (**Figure 2-3A**).

Characteristically, the cell population responses (**Figure 2-2**; 14 photoreceptors) varied more than individual cells’ responses (**Figure 2-1**; representative cell). This difference comes from a combination of factors: variable recording locations (responses vary slightly across the eye) (Hornstein et al., 2000), differences between sexes (Burton, Tatler and Laughlin, 2001) and differences between R1, R2, R3, R4, R5 and R6 response properties (Juusola et al., 2017). Despite these variations, they all responded in a highly consistent manner to the tested stimuli.

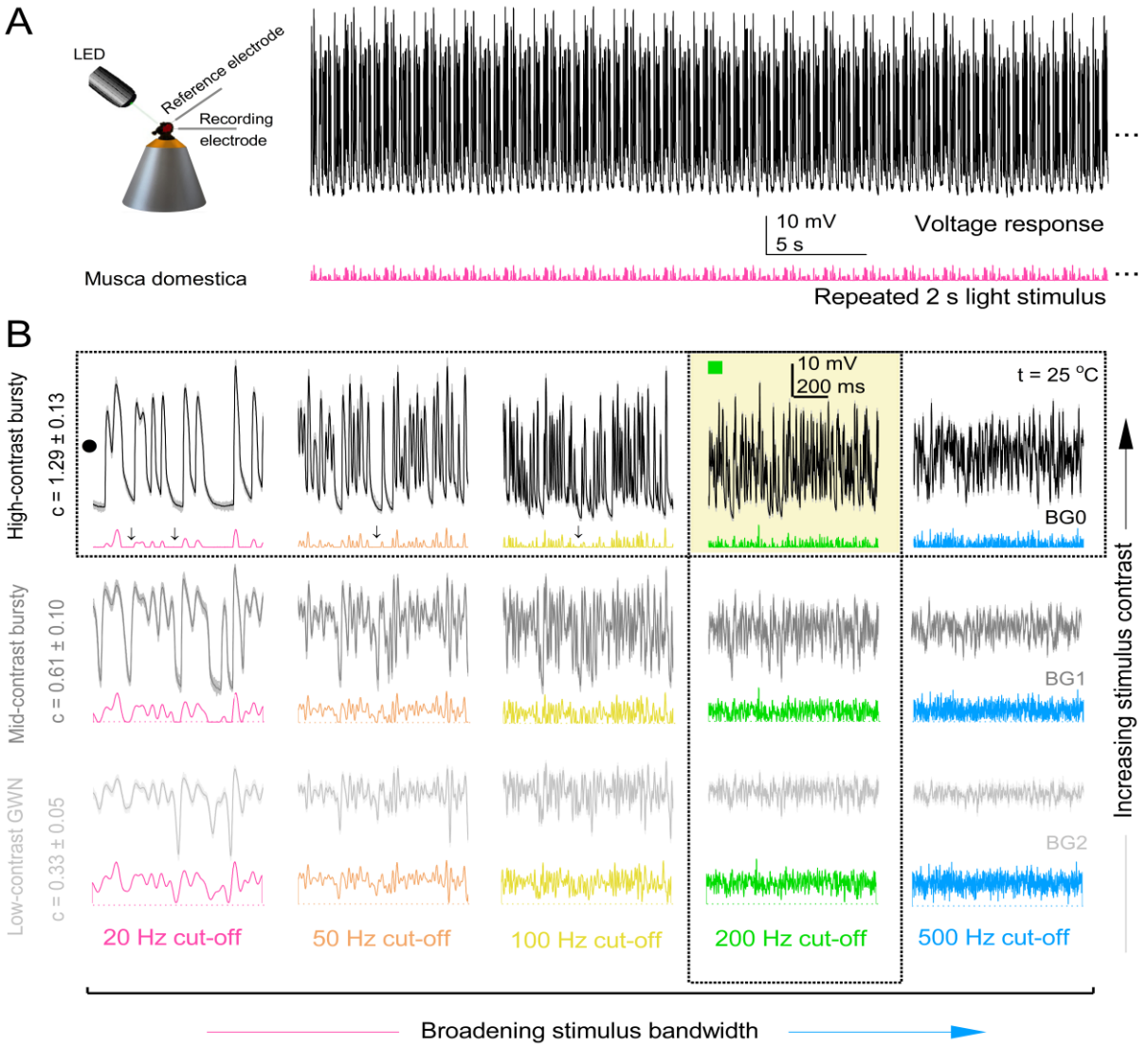

Figure 2-1. High-contrast "saccadic" bursts maximise photoreceptor's response. (A) Left: A schematic of *in vivo* intracellular recording from *Musca* eye. Right: An example of a repeated high-contrast bursty stimulus (pink trace) and a response (black trace) at 20 Hz bandwidth. **(B)** An R1-R6 response ranging from high-contrast "saccadic" bursts (BG0) to low-contrast GWN stimuli (BG2) in different cut-off frequencies, i.e. bandwidth patterns (20, 50, 100, 200 and 500 Hz). Mean (thick black and grey traces) and individual responses (thin, lightly coloured) to 15 different stimuli (colourful traces beneath the responses). Yellow box: maximum information responses (at 200 Hz bandwidth). Arrows: dark intervals in saccadic stimuli. Vertical dotted rectangle and a horizontal rectangle: responses for increasing bandwidth and contrast used in **Figures 2-3A-D** and **2-3E-H**, respectively. These recordings are from the same photoreceptor.

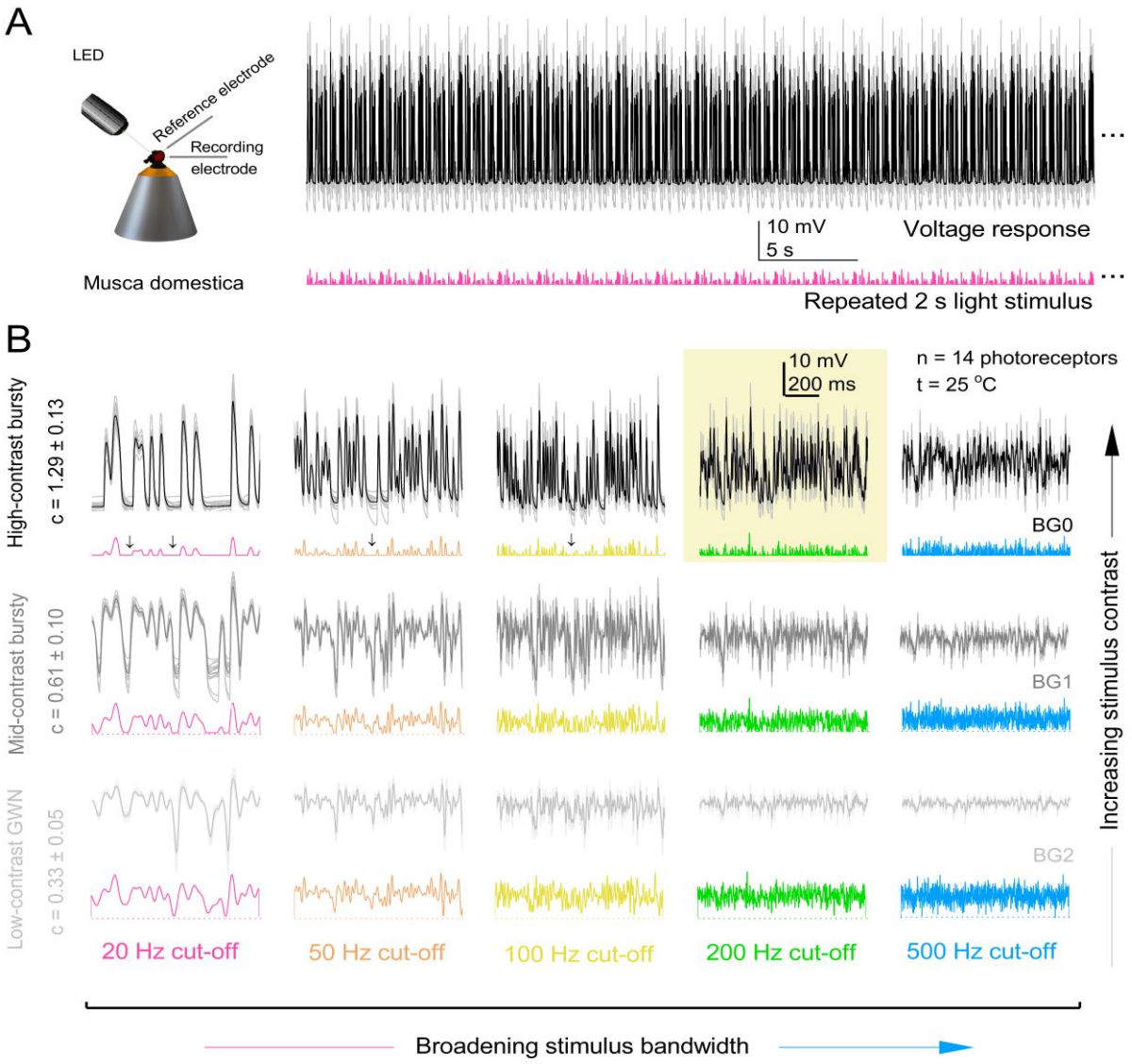

Figure 2-2. All the R1-R6s respond best to high-contrast saccadic stimuli. (A) Left: A schematic of *in vivo* intracellular recording from *Musca* eye. Right: An example of a repeated high-contrast bursty stimulus (pink trace) and responses of all the recorded photoreceptors (n = 14, black trace) at 20 Hz bandwidth. **(B)** R1-R6 responses (n = 14) ranging from high-contrast "saccadic" bursts (BG0) to low-contrast GWN stimuli (BG2) in different cut-off frequencies i.e. bandwidth patterns (20, 50, 100, 200 and 500 Hz). Mean of all the recorded photoreceptor responses (thick black and grey traces) and individual photoreceptor responses (thin, lightly coloured) to 15 different stimuli (colourful traces beneath the responses). Yellow box: maximum information responses of all the photoreceptors (at 200 Hz bandwidth). Arrows: dark intervals in saccadic stimuli.

2.3.2 Photoreceptors encode maximally high-contrast 200 Hz "saccadic" bursts

Figures 2-1 and **2-2** show that housefly R1-R6 photoreceptors respond vigorously to fast "saccadic" light input. To estimate these voltage responses' information transfer rates (*R*), I used the Shannon formula (Shannon, 1948) (**Figure 2-3**). To perform these estimations, I first calculated the responses' *SNR*(*f*) for all the tested contrast stimuli. **Figure 2-3A-D** shows the results for increasing the stimulus bandwidth, and **Figure 2-3E-H** shows the results for increasing the stimulus contrast.

For accurate information transfer estimation, the Shannon formula requires that the signal and noise are additive and Gaussian. Favourably, the voltage signals' probability density functions (PDFs; **Figure 2-3B**, **top**) to different high-contrast bursts (c ~1.29) are Gaussian (500 Hz) or nearly Gaussian (100 Hz and 200 Hz), bar 20 Hz and 50 Hz, although all the stimulus intensity distributions were skewed (**Figure 2-3B**, **bottom**). Previously, it was shown by comparing the information estimates calculated using Shannon formula and the triple extrapolation method (Juusola and de Polavieja, 2003) that the Shannon formula provides reasonably reliable information estimates for this kind of stimuli (Juusola and de Polavieja, 2003; Juusola et al., 2017).

Increasing the stimulus contrast resulted in higher SNRs, being the highest to high-contrast bursty "saccadic" stimuli and the lowest to GWN stimuli (**Figure 2-3E**). For mid-contrast bursty and low-contrast Gaussian stimuli, the Shannon information estimates were presumably more accurate because the voltage signals were Gaussian (**Figure 2-3F**).

In line with Juusola et al. (2017) findings, high-contrast "saccadic" bursty stimuli drove the photoreceptor's maximal information transfer, and it was about 2-to-3-times larger than GWN stimuli (**Figure 2-3C** and **2-3G**), being consistent for all the tested photoreceptors (n = 14) (**Figure 2-3D** and **2-3H**). Moreover, the information capture peaked at 200 Hz in which the photoreceptors had the broadest frequency and Gaussian voltage distributions (**Figure 2-3A** and **2-3B**, **yellow area**).

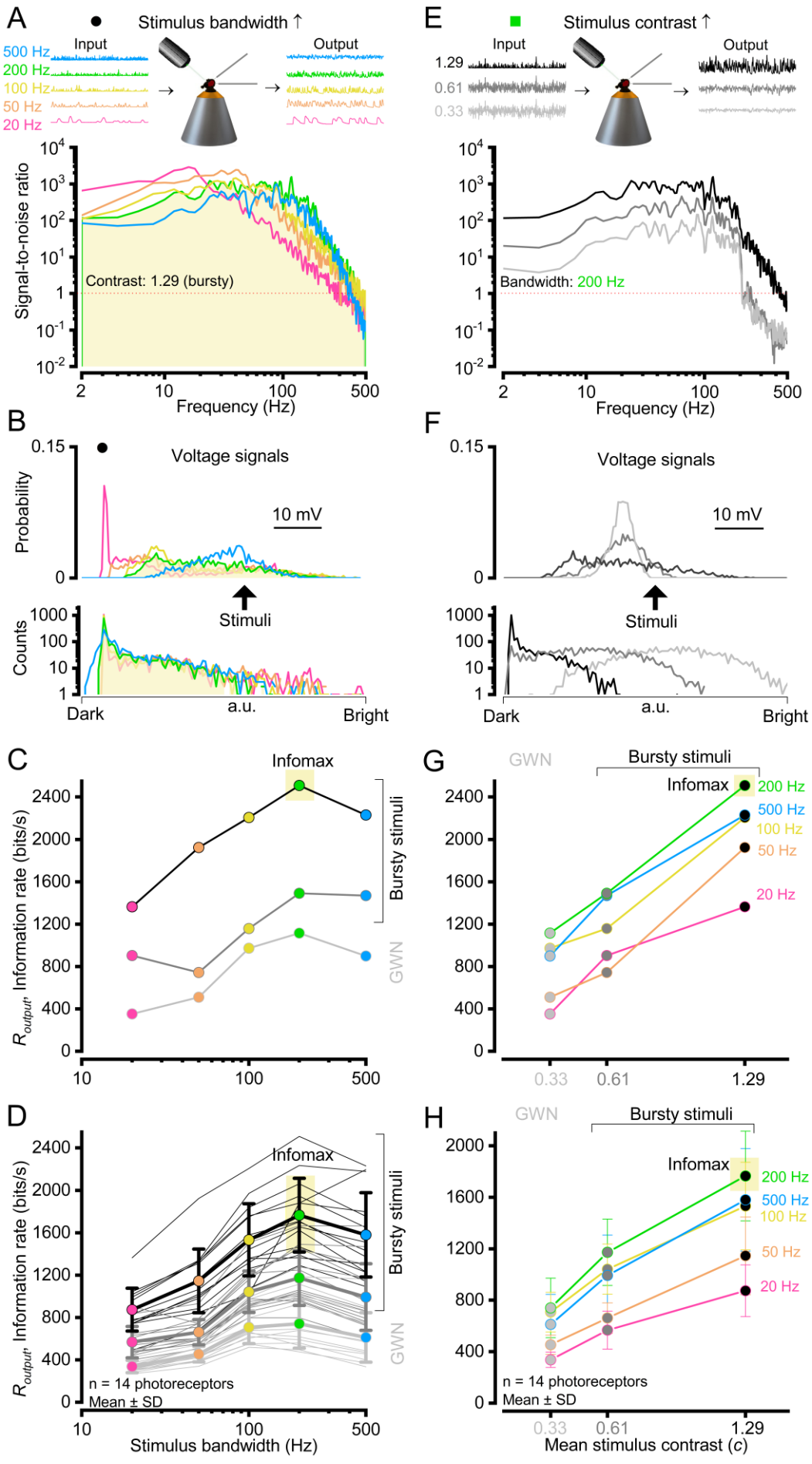
A
Stimulus bandwidth ↑
Input
Output
500 Hz
200 Hz
100 Hz
50 Hz
20 Hz
Signal-to-noise ratio
Contrast: 1.29 (bursty)
Frequency (Hz)
E
Stimulus contrast ↑
1.29
0.61
0.33
Bandwidth: 200 Hz
B
Voltage signals
Probability
10 mV
Stimuli
Counts
Dark
a.u.
Bright
F
C
Infomax
Information rate (bits/s)
Bursty stimuli
GWN
G
D
n = 14 photoreceptors
Mean ± SD
Stimulus bandwidth (Hz)
H
Mean stimulus contrast (c)

Figure 2-3. Photoreceptors' (R1-R6) information transfer peaks at 200 Hz and is 2-to-3-times larger for high-contrast bursty stimuli than for GWN stimuli. (A) Response signal-to-noise ratio (SNR) when increasing the bandwidth from 20 Hz to 500 Hz. **(B)** Top: Response PDFs are all nearly Gaussian except for 20 Hz and 50 Hz. Bottom: Stimulus intensity distributions are skewed Gaussian. At 200 Hz the photoreceptor had the widest frequency and Gaussian voltage distribution. **(C)** The information transfer rates (from a representative photoreceptor in **Figure 2-1**) were best for high-contrast "saccadic" stimuli, and it peaked at 200 Hz bandwidth (marked with a yellow box). The information transfer rates were calculated using the Shannon formula (Shannon, 1948). **(D)** Information transfer calculated for all the photoreceptors measured (n = 14) to all the bandwidths. Bursty "saccadic" stimuli drove the maximal information transfer, which peaked at 200 Hz. **(E)** Response signal-to-noise ratio (SNR) at 200 Hz stimulus bandwidth when increasing the contrast from c ~0.33 to c ~1.29. SNR is the best for high-contrast bursty stimulus. **(F)** Top: Response PDFs are Gaussian for low and mid-contrast stimulus but slightly skewed for high-contrast bursty stimulus. Bottom: Stimulus intensity distribution is Gaussian for low-contrast stimulus but slightly skewed for mid and high-contrast stimuli. **(G)** Same as in **C** but comparing against different contrast levels. **(H)** Same as in **D** but comparing against different contrast levels. Data in **A-C** and **E-G** are from the same photoreceptor (presented in **Figure 2-1**), whereas **D** and **H** show the results for all the photoreceptors (presented in **Figure 2-2**).

2.3.3 LMCs respond best to "saccadic" stimuli

Earlier, I demonstrated that "saccadic" stimuli do not blind housefly R1-R6 photoreceptors. Not only do the photoreceptors respond most vigorously to the "saccadic" stimulations, but it also produced these cells' maximal information transfer rates. My next aim was to study what happens downstream, specifically in the lamina: what kind of stimulus patterns are most amplified and carry most information from photoreceptors to LMCs (L1-L3).

I performed similar recordings as from the photoreceptors but now targeting LMCs (L1-L3) (**Figure 2-4A** and **2-5A**). Histaminergic transmitter release from photoreceptors hyperpolarises LMCs to light increments and depolarises them to light decrements (compare **Figure 2-1A** and **2-4A**) (Hardie, 1989). In LMCs, similar to photoreceptors, increasing the stimulus contrast evoked larger responses (**Figure 2-4B** and **2-5B**, **rows**). However, these changes were less conspicuous (or significant) than in photoreceptors. Furthermore, increasing the stimulus bandwidth somewhat decreased the peak-to-peak responses (**Figure 2-4B** and **2-5B**, **columns**). But again, this change was less than what we saw in photoreceptors. Interestingly, LMCs

responded maximally and almost equally to both mid and high-contrast "saccadic" bursty stimuli and less so to GWN (**Figure 2-4B** and **2-5B**, **yellow area**).

At the population level, the voltage responses of all LMCs varied more than the responses of an individual LMC (n = 3, **Figure 2-5**) compared to responses measured from one representative LMC (**Figure 2-4**); similar to what we saw with the photoreceptor output. This variation is most likely caused by differences between L1, L2 and L3 (Uusitalo et al., 1995).

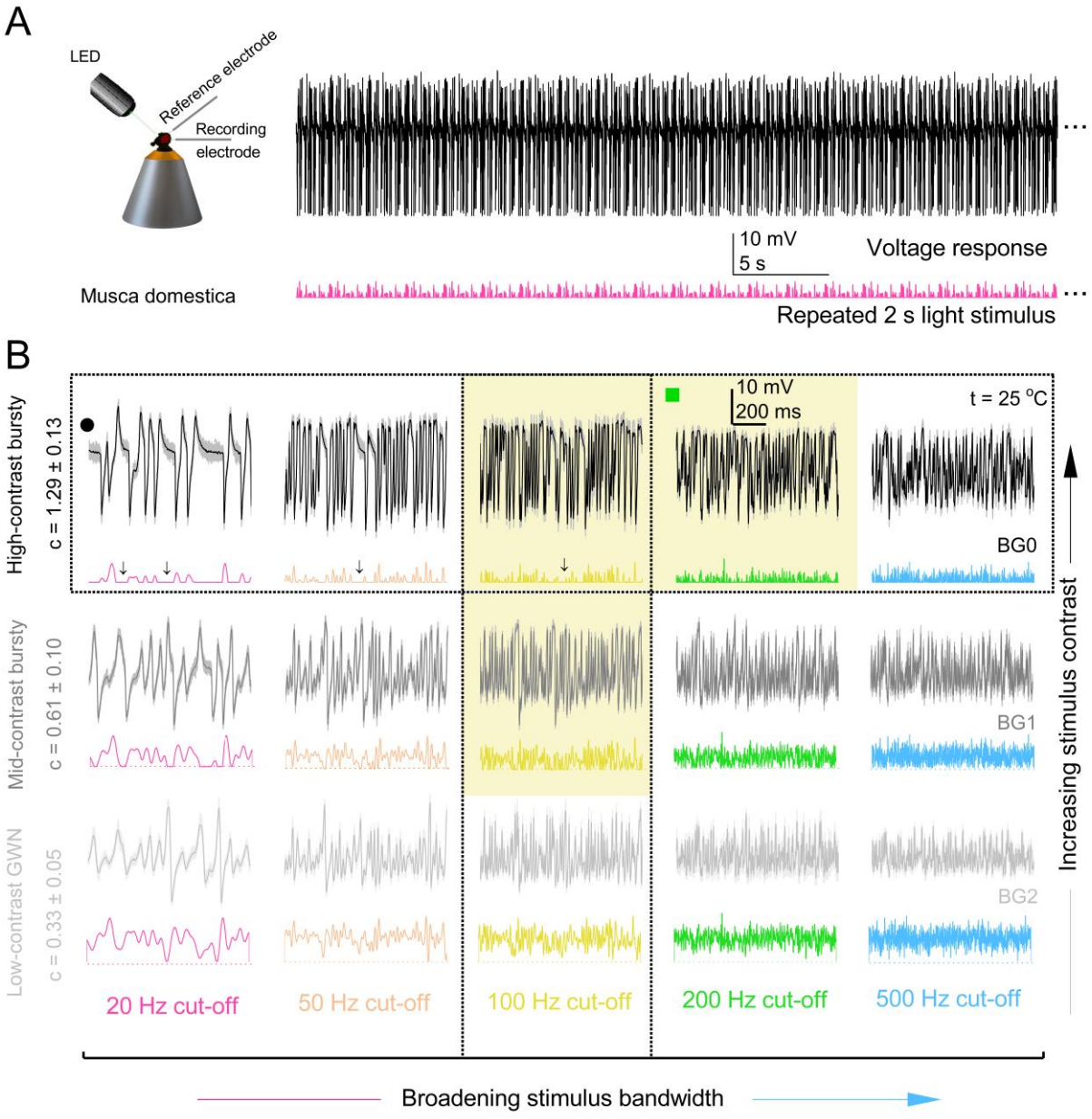

Figure 2-4. Both mid and high-contrast "saccadic" bursts maximise LMC's response. (A) Left: A schematic of *in vivo* intracellular recording from *Musca* eye. Right: An example of a repeated high-

contrast bursty stimulus (pink trace) and a response (black trace) at 20 Hz bandwidth. **(B)** An L1-L3 response ranging from high-contrast "saccadic" bursts (BG0) to low-contrast GWN stimuli (BG2) in different cut-off frequencies, i.e. bandwidth patterns (20, 50, 100, 200 and 500 Hz). Mean (thick black and grey traces) and individual responses (thin, lightly coloured) to 15 different stimuli (colourful traces beneath the responses). Yellow box: maximum information responses. Arrows: dark intervals in saccadic stimuli. Vertical dotted rectangle and a horizontal rectangle: responses for bandwidth and contrast used in **Figure 2-6A-E** and **2-6E-H**, respectively. The recordings are from the same LMC.

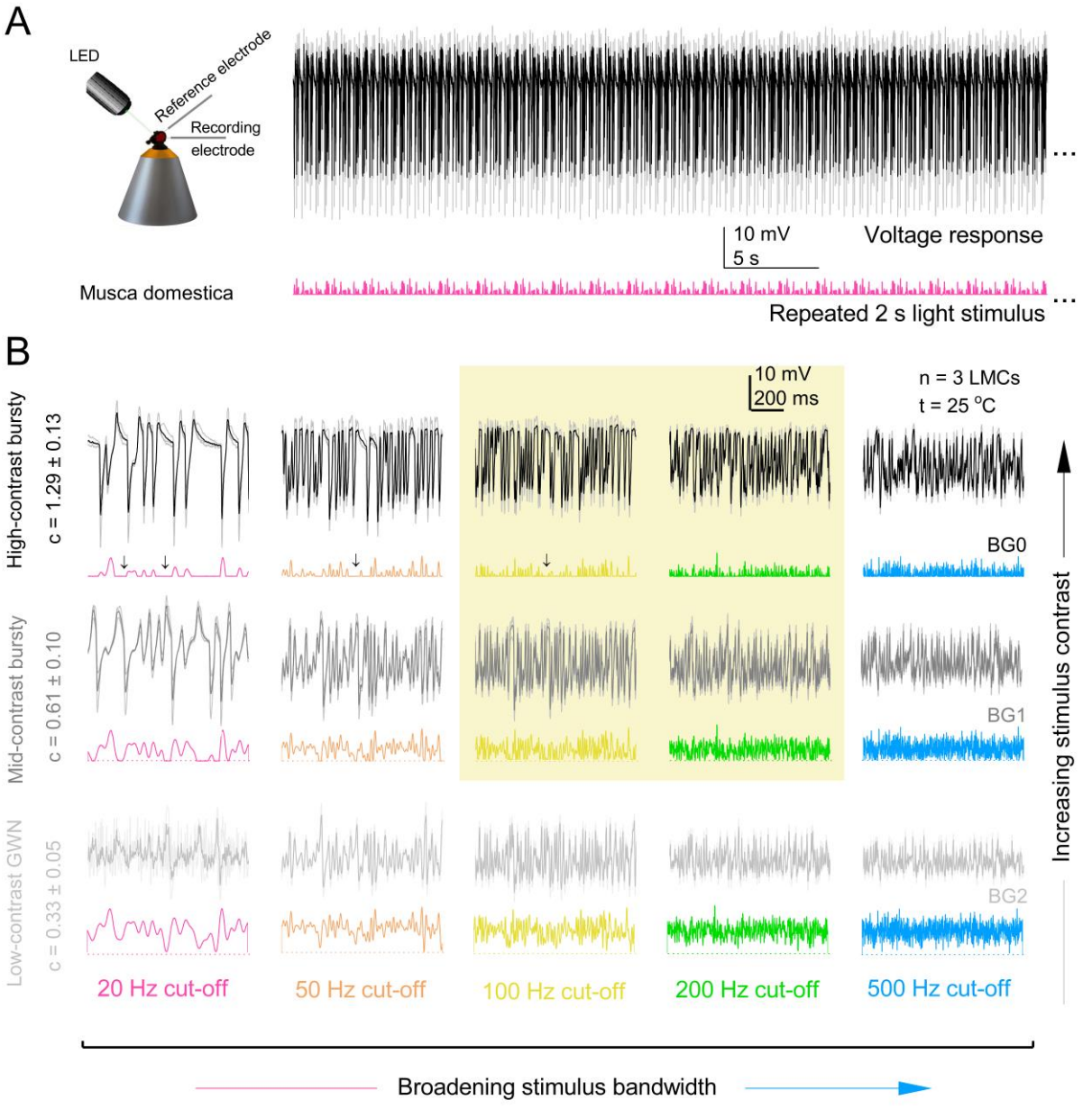

Figure 2-5. All the LMCs respond best to mid and high-contrast saccadic stimuli. (A) Left: A schematic of *in vivo* intracellular recording from *Musca* eye. Right: An example of a repeated high-contrast bursty stimulus (pink trace) and responses of all the recorded LMCs (n = 3, black trace) at 20 Hz bandwidth. **(B)** L1-L3 responses (n = 3) ranging from high-contrast "saccadic" bursts (BG0) to low-

contrast GWN stimuli (BG2) in different cut-off frequencies i.e. bandwidth patterns (20, 50, 100, 200 and 500 Hz). Mean of all the recorded LMC responses (thick black and grey traces) and individual LMC responses (thin, lightly coloured) to 15 different stimuli (colourful traces beneath the responses). Yellow box: maximum information responses of all the LMCs. Arrows: dark intervals in saccadic stimuli.

2.3.4 LMCs' information capacity peaks at 100 Hz and 200 Hz "saccadic" bursts

LMCs' information capacity was calculated similarly to photoreceptors. **Figure 2-6A-D** shows the increasing stimulus bandwidth results, and **Figure 2-6E-H** shows the increasing stimulus contrast results. Unlike when measuring from photoreceptors, the data sampling rate used (1 kHz with 500-point window size) was not sufficient to utilise the full encoding capacity of LMCs (except for 20 Hz) because high-frequency response components have SNR > 1 and, thus contain signal (compare **Figure 2-3A** to **2-6A**). Due to the information loss caused by the limited bandwidth, the calculated information transfer rates were underestimates of the real information capacity (further discussed in the next chapter). This underestimation only applied to the mid and high-contrast "saccadic" stimuli and not to the low-contrast Gaussian stimuli (**Figure 2-6E**).

Moreover, the information capacity estimates at high-contrast were not as accurate as for photoreceptors because the voltage signals were not Gaussian (except for 500 Hz) (**Figure 2-6B**). Here, Shannon information estimates were likely more accurate for mid-contrast and low-contrast stimuli as both generate voltage signal dynamics with Gaussian distributions (**Figure 2-6F**).

The "saccadic" stimuli drove the LMCs' (n = 3) maximal information capture (**Figure 2-6C-D** and **2-6G-H**); similar to photoreceptors. However, in contrast to photoreceptors, LMC's information capacity peaked for both high-contrast and mid-contrast bursty stimuli. Expectedly, as the LMC noise changes were less prominent, the cells' information capacity peaked to 100 Hz and 200 Hz mid-contrast and high-contrast bursty "saccadic" stimuli for which the LMC signals showed the broadest frequency and voltage distribution (**Figure 2-6A** and **2-6B**, **yellow area**).

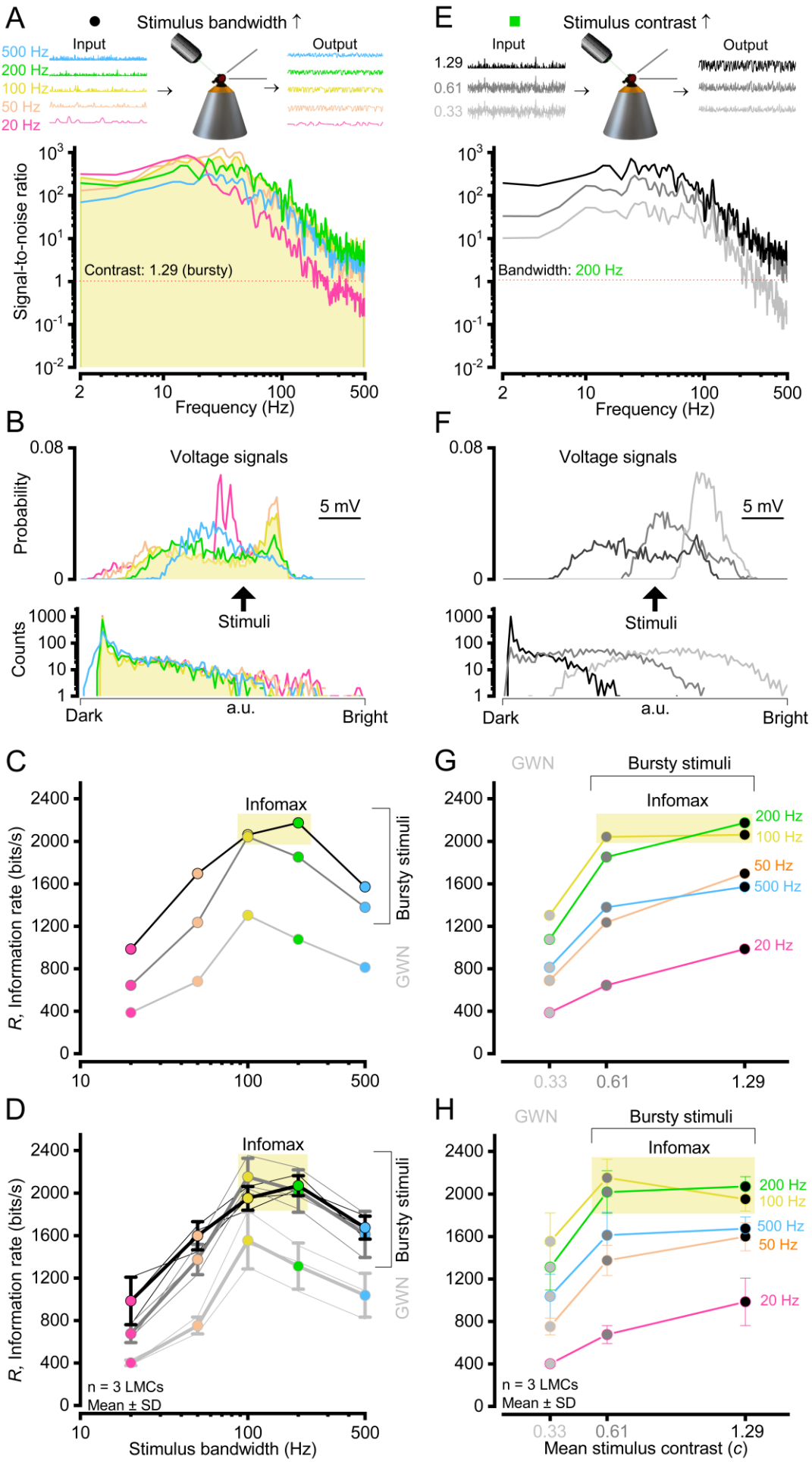
A
Stimulus bandwidth ↑
Input
Output
500 Hz
200 Hz
100 Hz
50 Hz
20 Hz
Signal-to-noise ratio
Contrast: 1.29 (bursty)
Frequency (Hz)
E
Stimulus contrast ↑
1.29
0.61
0.33
Bandwidth: 200 Hz
B
Voltage signals
5 mV
Probability
Stimuli
Counts
Dark
a.u.
Bright
F
C
Infomax
Bursty stimuli
GWN
R, Information rate (bits/s)
G
Bursty stimuli
200 Hz
100 Hz
50 Hz
500 Hz
20 Hz
D
n = 3 LMCs
Mean ± SD
Stimulus bandwidth (Hz)
H
Mean stimulus contrast (c)

Figure 2-6. LMCs' information capacity is maximally driven by 100 Hz and 200 Hz "saccadic" stimuli (both mid and high-contrast). (A) Response signal-to-noise ratio (SNR) to high-contrast bursty stimuli when increasing the bandwidth from 20 Hz to 500 Hz. **(B)** Top: Response PDFs to high-contrast bursty stimuli are not Gaussian except for 500 Hz. Bottom: Stimulus intensity distributions are skewed Gaussian. At 100 Hz and 200 Hz, the photoreceptor had the widest frequency and Gaussian voltage distributions. **(C)** The information transfer rates (from a representative LMC in **Figure 2-4**) were best for mid-contrast and high-contrast "saccadic" stimuli, and it peaked at 100 Hz and 200 Hz (marked with a yellow box). The information transfer rates were calculated using the Shannon formula (Shannon, 1948). **(D)** Information transfer rates calculated for all the LMCs measured (n = 3) to all the bandwidths. Mid and high-contrast bursty "saccadic" stimuli drove the maximal information transfer, peaked at 100 Hz and 200 Hz. **(E)** Response signal-to-noise ratio (SNR) at 200 Hz stimulus bandwidth when increasing the contrast from c ~0.33 to c ~1.29. SNR is the best for high-contrast bursty stimulus. **(F)** Top: Response PDFs are Gaussian for low and mid-contrast stimulus but skewed for high-contrast bursty stimulus. Bottom: Stimulus intensity distribution is Gaussian for low-contrast stimulus but slightly skewed for mid and high-contrast stimuli. **(G)** Same as in **C** but now comparing against different contrast levels. **(H)** Same as in **D** but now comparing against different contrast levels. Data in **A-C** and **E-G** show results from the same LMC (**Figure 2-4**), while **D** and **H** pool all LMC results.

2.3.5 Limited sampling rate causing information loss in LMCs

All LMC data was sampled at 1 kHz and windowed with 500-point Blackman-Harris window. The data (**Figure 2-6A** and **E**) suggested that the chosen data sampling rate did not drive the LMCs maximally at mid and high-contrasts, leading to underestimating the information capacity. Therefore, I tested how much the stimulus bandwidth and sampling-rate limited both photoreceptors' and LMCs' encoding by recording their responses to similar stimuli (20, 50, 100, 200, 300, 500, 600, 750 and 1,000 Hz cut-off frequencies) when sampled at 2 kHz and windowed with 1,000-point window (**Figure 2-7**).

Recordings from photoreceptors (**Figure 2-7A**) show no signal (SNR < 1) beyond 500 Hz for the test stimulus bandwidths shown (200 Hz and 1 kHz) (**Figure 2-7B-C**). The SNR for the stimuli is presented in **Figure 2-7G-H**. However, LMCs (**Figure 2-7D**), show signal (SNR > 1) beyond 500 Hz (**Figure 2-7E-F**). Thus, I estimated the information loss by calculating the information capacity for the same 2 kHz data by down-sampling with 1 kHz; thus, having a 1,000-point window and then comparing that value when using a 500-point window. Photoreceptors' (n = 2) information loss was about 5% whereas LMCs (n = 2) was significantly larger, varying between 5-23%

depending on the stimulus bandwidth (maximum information loss at 200 Hz) (**Figure 2-7I**). Here, photoreceptors' information loss was very consistent between the tested cells, whereas LMCs' information loss varied substantially between them.

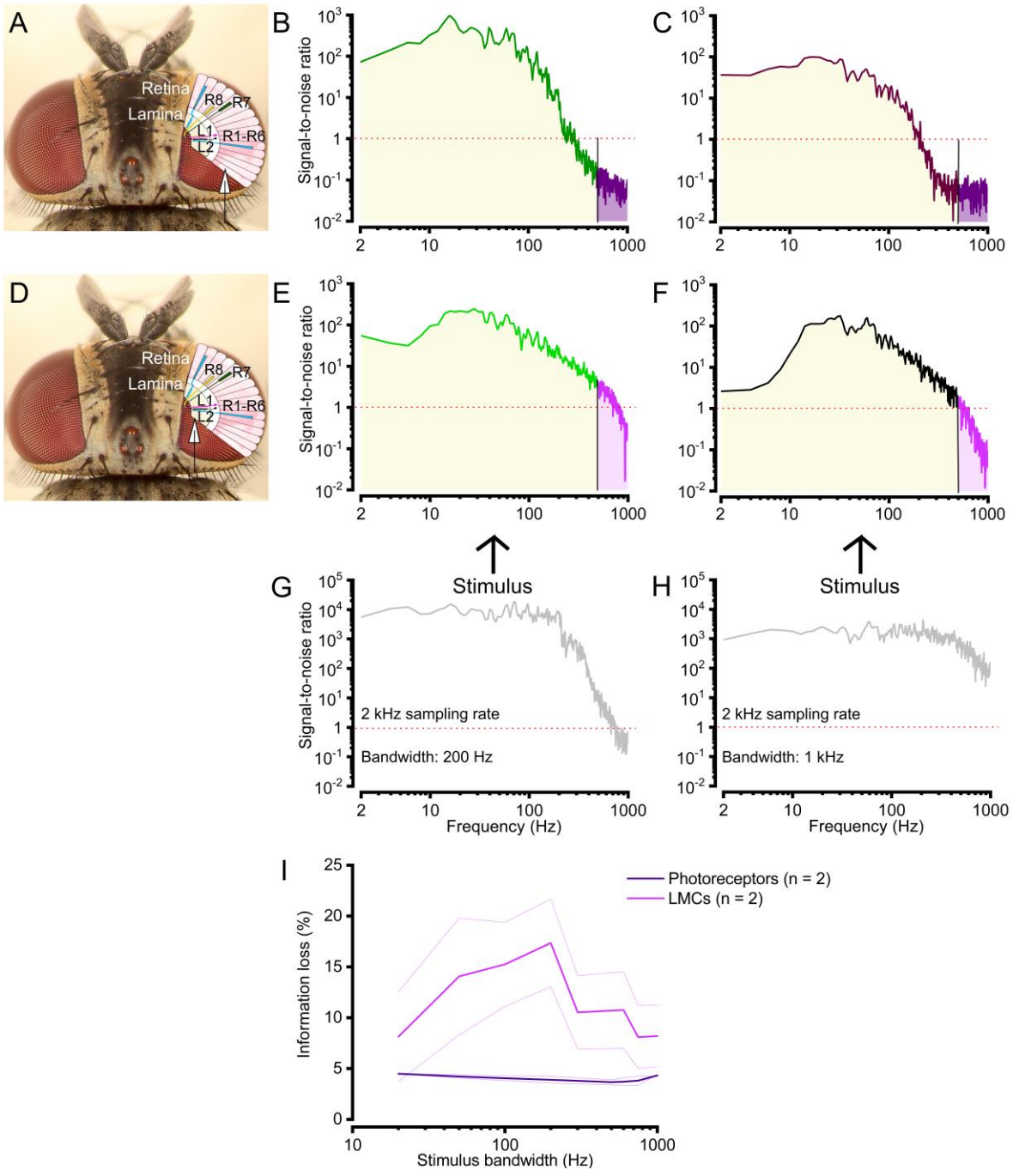

Figure 2-7. Information loss in photoreceptors and LMCs resulting from the limited bandwidth. **(A)** A schematic of *in vivo* intracellular recording from *Musca* retina. Photoreceptor's *SNR(f)* to **(B)** 200 Hz bursty stimulus (stimulus in **G**) and to **(C)** 1 kHz bursty stimulus (stimulus in **H**). **(D)** A schematic of *in vivo* intracellular recording from *Musca* lamina. LMCs *SNR(f)* to **(E)** 200 Hz bursty stimulus and to **(F)** 1 kHz bursty stimulus. **(I)** Information loss calculated for photoreceptors and LMCs. Mean (thick purple

for photoreceptors and thick magenta for LMCs) and individual responses (thin, lightly coloured). The information loss is relatively small for photoreceptors (~5%) but significantly larger for LMCs, reaching 23%.

2.3.6 "Saccadic" information is amplified at the first synapse

In line with Juusola et al. (2017) findings, both photoreceptors and LMCs responded best to the fast "saccadic" stimuli. I calculated the maximum information transfer rates for all the photoreceptors (n = 20) and LMCs (n = 6) measured. LMCs' information transfer rates were significantly higher (**Figure 2-8A**). As stated previously, these values were underestimates due to the limited bandwidth and, thus, I proposed a way to correct the information loss calculated earlier (**Figure 2-7**). When corrected, LMCs' had even larger *R* values compared to photoreceptors (**Figure 2-8B**).

Interestingly, male housefly photoreceptors' maximum information rates were higher than females (**Figure 2-8A-B**). The recording electrode locations should not bias these findings, as I did not specifically target the acute-zone photoreceptors (Dietrich, 1909; Land and Eckert, 1985; Perry and Desplan, 2016). While LMC information rates were accentuated, I did not collect enough recordings to compare the differences between the sexes. However, it seems feasible that this could be the case in LMCs as well.

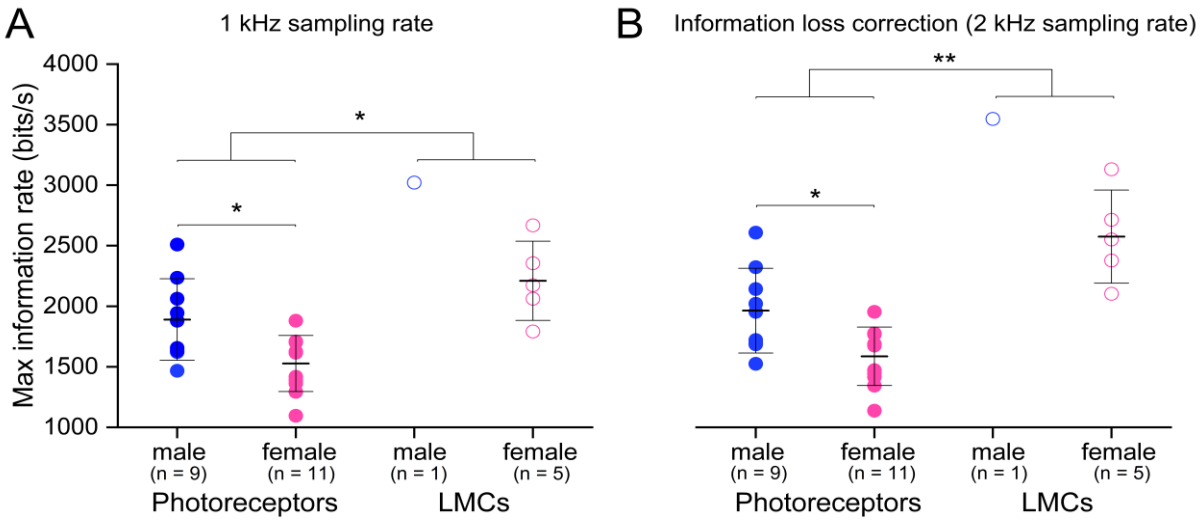

Figure 2-8. Information amplification at the photoreceptor-LMC synapse and the difference between sexes. (A) LMCs (n = 6) have significantly higher (p = 0.0127) information rates than photoreceptors (n = 20). In addition, male photoreceptors have higher information rates than females (p = 0.0160). **(B)** When correcting the values for information loss, LMCs' R values are significantly larger than photoreceptors (p = 0.0044) and the sex-specific difference remained significant after the correction (p = 0.0160), mean ± SD, unpaired two-tailed t-test with Welch's correction.

2.4 Discussion

2.4.1 Photoreceptors encode fast “saccadic” light changes

My main aim was to unravel whether houseflies are effectively blind during saccadic behaviour – first at the level of photoreceptors (R1-R6) as shown in *Drosophila* (Juusola et al., 2017) and then in their direct outputs (LMCs, L1-L3). *In vivo* intracellular recordings from housefly photoreceptors (R1-R6) showed that not only can they encode fast “saccadic” light changes but they encode more information from “saccadic” stimuli than GWN stimuli (**Figure 2-3D** and **2-3H**), similar to *Drosophila* (Juusola et al., 2017). Moreover, because *Musca* is a fast-flying diurnal species, its photoreceptors can code more information from the same natural scene, or in this case, from the given light stimuli– *Musca* photoreceptors’ information transfer rate peaked at 2,510 bits/s. In contrast, *Drosophila* photoreceptors reached their maximum at 850 bits/s for high-contrast “saccadic stimuli (*Musca*: **Figure 2-3D** and *Drosophila*: Juusola et al., 2017). Moreover, *Musca* can encode better fast rate changes and higher temporal frequencies, and therefore, its information capacity peaked at 200 Hz, in contrast to *Drosophila*’s 100 Hz (*Musca*: **Figure 2-3D** and *Drosophila*: Juusola et al., 2017).

Visual blurring during body saccades can be reduced by countering head and thorax movements, enhanced acute-zone processing, and the combination of photoreceptors’ refractory photon sampling and photomechanical contractions in response to light. It is important to note that the houseflies were fixed into a conical holder during the experiments, cancelling the head/thorax and body movements. Moreover, the acute zones were not purposefully targeted when recording from photoreceptors, so the recording electrode location should not bias these results. Hence, the enhanced sampling to “saccadic” stimuli likely results from the photoreceptors’ refractory sampling and photomechanical contractions. High-contrast “saccadic” bursts contain bright periods, which should maximally activate the microvilli (photon sampling units) and darker periods in which the photoreceptor should recover from refractoriness (**Figure 2-9**). Although GWN stimuli contain more photons, it lacks these darker events causing the microvilli to become refractory, preventing them from capturing the incoming photons (Song and Juusola, 2014; Juusola et al., 2017).

Like *Drosophila* (Juusola et al., 2017), *Musca* photoreceptors also contract photomechanically (unpublished data), but these dynamics are even faster. *In vivo* high-speed videos revealed that photoreceptor rhabdomeres shift rapidly away from the focal point when illuminated with light. This movement might accentuate refractory photon sampling – to reduce saturation and maximise encoding capacity. We aim to examine these results against biophysically-realistic model simulations, using a stochastic model of *Musca* photoreceptors (akin to the *Drosophila* R1-R6 model, see Juusola et al., 2017).

2.4.2 LMCs amplify “saccadic” light information

L1-L3s responded maximally to “saccadic” bursty stimuli and less so to low-contrast GWN stimuli (**Figure 2-9**), somewhat comparable to R1-R6 photoreceptors. The LMC information capacity estimates for mid and high-contrast “saccadic” stimuli might be slightly inaccurate because all the criteria for using Shannon formula were not fully met (signal and noise were not perfectly Gaussian) (Shannon, 1948).

LMCs maximum information capacity was to mid and high-contrast bursts at 100 Hz and 200 Hz (compare **Figure 2-3D** and **2-3H** to **2-6D** and **2-6H**), whereas photoreceptors’ information capacity peaked to high-contrast 200 Hz bursts. Note that the limited bandwidth affected the information capacity estimation, particularly in LMCs, because some information from the high-frequency components was lost by using a bit too low sampling rate (1 kHz instead of 2 kHz). Information loss was the highest for high-contrast bursty stimuli, and it peaked at 200 Hz (**Figure 2-7I**). This finding suggests that LMCs’ maximal information capacity might be to high-contrast stimuli at 200 Hz, similar to photoreceptors.

Not only did the “saccadic” stimuli drive maximal encoding, but it amplified LMC voltage responses (**Figure 2-8**) significantly. Therefore, flies are far from being blind during body saccades (Land, 1999) and the visual information collected during these manoeuvres is not redundant for the visual system. Instead, the resulting bursty stimuli contain important features amplified and efficiently passed to the neurons, downstream.

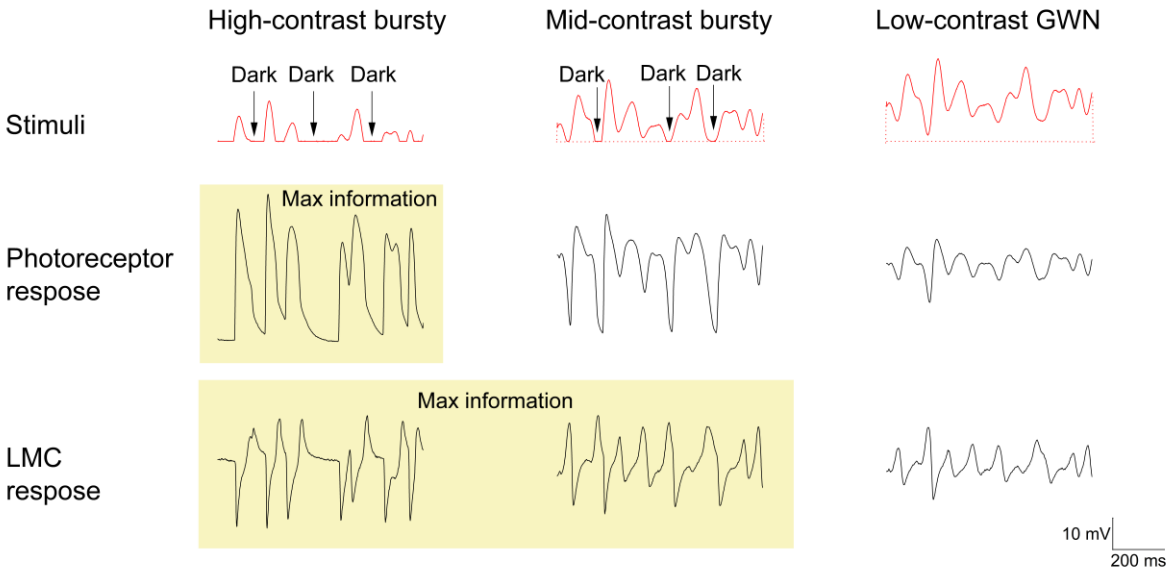

Figure 2-9. Houseflies' visual system is adapted to encode fast temporal changes in its environment. Both photoreceptors and LMCs respond best to bursty "saccadic" stimuli. Interestingly, LMC output is less contrast-specific, suggesting dynamic synaptic contrast normalisation of signals routed towards the brain.

2.4.3 Males encode better "saccadic" stimuli

Both male and female flies responded best to "saccadic" stimuli. Interestingly, male photoreceptors (and possibly LMCs) showed significantly higher information transfer rates (**Figure 2-8**). Previously, it has been shown that males have a better temporal and spatial resolution in their acute zones (Hornstein et al., 2000; Burton and Laughlin, 2003), which could contribute to these results. However, I did not purposefully target the frontal-dorsal acute zone. Instead, the recording location was quite randomly selected by the stable, high-quality microelectrode cell penetrations.

An interesting question arises from this finding: why is it more beneficial for male flies to see better during body saccades? One feasible explanation for this sexual dimorphism is related to male-specific sexual pursuit behaviour. While chasing flying females for mating, males exhibit fast body saccades to change their course, using mainly their frontal-dorsal acute zones ("love spots") (Land and Collett, 1974; Wehrhahn, 1979; Wehrhahn, Poggio and Bülthoff, 1982; Wagner, 1986; Burton and Laughlin, 2003). By contrast, female houseflies do not have a "love spot", and their ability to track is both infrequent and possibly less well controlled.

In future, it would be interesting to stain LMCs (L1-L3) electrophoretically and to test whether significant differences are present among them when responding to “saccadic” stimuli. For example, we know that L3 is the largest in the male “love spot” (Braitenberg, 1972), which can be beneficial during body saccades.

3 Visual coding under light adaptation in *Musca* photoreceptors and LMCs

3.1 Introduction

Flies perceive contrast changes in their natural environment in which illumination ranges from dim conditions to bright daylight, covering >10^6 intensity range. This visual performance depends upon the fly photoreceptors' rapid adaption, providing high single-photon sensitivity in dim conditions and low sensitivity in bright conditions, preventing saturation while maximising contrast information capture (Fain, Hardie and Laughlin, 2010). Adaptive contrast coding (Juusola, 1993; Juusola et al., 2017) results from multiple interconnecting factors affecting phototransduction. These include refractoriness (Song et al., 2012; Juusola et al., 2017), intracellular Ca^{2+}-dependent pupil mechanism (Kirschfeld and Vogt, 1980; Howard, Blakeslee and Laughlin, 1987), ion channels (especially voltage-gated K^+ channels) and electrogenic transporters (Weckström, Hardie and Laughlin, 1991; Juusola and Hardie, 2001a; Wang et al., 2005; Hardie and Juusola, 2015).

The fly photoreceptors must rapidly adapt to the natural environment's ambient light to maintain a perceptual contrast constancy of the world (Shapley and Enroth-Cugell, 1984; Laughlin, 1989; Juusola, 1993). Efficient light adaptation is vital for seeing animals, living and moving in an environment with vastly changing light intensities. Hence, it is not a surprise that light adaptation is evident already at the fundamental photon sampling level in elementary responses, so-called quantum bumps (QBs), evoked by the absorption of single photons (Wong and Knight, 1980; Juusola and Hardie, 2001a; Hardie and Juusola, 2015).

How light adaptation impacts a photoreceptor's QBs, their summed macroscopic voltage response and coding/signalling have been studied extensively in *Drosophila* (Wu and Pak, 1978; Johnson and Pak, 1986; Hardie et al., 1993; Henderson, Reuss and Hardie, 2000; Juusola and Hardie, 2001a; Juusola and Hardie, 2001b; Gu et al., 2005) and *Calliphora* (Weckström, Hardie and Laughlin, 1991; Juusola et al., 1994; de Ruyter van Steveninck and Laughlin, 1996). There have also been comparative

adaptation studies, including both species (Energy consumption: Niven, Anderson and Laughlin, 2007. Adaptive, stochastic sampling: Song et al., 2012; Juusola and Song, 2017). However, much of the early work on adaptive QBs was performed on the horseshoe crab (*Limulus*) (Dodge, Knight and Toyoda, 1968; Wong and Knight, 1980; Wong, Knight and Dodge, 1980).

Although these studies suggest that many aspects of light-adaptation can be generalised to other species with microvillar photoreceptors, species-specific studies still have their importance. There has been limited research exploring *Musca* photoreceptor light adaptation, with only a few notable examples. The study by Burton (2002) investigated long-term light adaptation in the photoreceptors' impulse responses and some aspects of their signalling performance. Another Burton (2006) article examined how QB waveform change in response to different light background intensities, and concluded that increasing the mean light (i.e. higher input SNR) made QBs smaller and faster, similar to findings in other Diptera (*Drosophila:* Juusola and Hardie, 2001a *Calliphora:* Juusola et al., 1994; de Ruyter van Steveninck and Laughlin, 1996) and *Limulus* (Wong and Knight, 1980; Wong, Knight and Dodge, 1980). However, this study's primary focus was showing the benefits of bispectrum estimate (and not the conventional power spectrum estimate) in reconstructing the QB shape in dim light levels, which skews voltage response distributions.

Unlike in the species mentioned above, there has been no prior experimental research on how *Musca* QB latency distribution (the time from photon absorption to a QB) adapts to vast mean light intensity changes. Hence, I aimed to conduct a detailed study exploring *Musca* R1-R6 photoreceptor response properties (including QB shape and latency distribution) and their signalling performance when adapted to different light intensity levels, using linear signal and noise analysis. In this *in vivo* investigation, photoreceptors' intracellular voltage responses to contrast stimuli at different light levels were recorded at 25 ^{o}C. The photoreceptors' coding performance was tested by comparing two different contrast series: a high-contrast bursty "saccadic" stimulus and a low-contrast GWN stimulus (both introduced in Chapter 2). A shot-noise analysis was then used (for responses to low-contrast GWN stimulus) to characterise how QB shape and latency distribution adapt at different light levels.

Furthermore, after quantifying photoreceptors' adaptive response properties and signalling performance, I aimed to reveal how *Musca* L1-L3 LMC voltage responses adapt to the changing mean light levels, using the same methodology. Analysis of the LMC (histamine) QB shape or latency distribution at different adapting backgrounds, however, were not performed due to LMCs' nonlinear nature of responding (Laughlin, Howard and Blakeslee, 1987; Juusola et al., 1994; Juusola et al., 1995; Juusola, Uusitalo and Weckström, 1995).

For LMCs, the main aim was to quantify how contrast coding differs between two different contrast series (high-contrast bursty "saccadic" stimulus and low-contrast GWN stimulus) at different adapting backgrounds. The high-contrast bursty stimulus has not been tested on LMCs before.

Both photoreceptors' and LMCs' signalling performance (SNR and information transfer rates) improved when increasing the mean light levels. Expectedly, their responses to contrast stimuli at the lowest light intensities were dominated by photon shot-noise, whilst brightening massively improved visual coding (information transfer rate), especially for the bursty contrasts. Thus, when adapting to brightening stimuli, the high-contrast bursts utilised better the photoreceptors' and LMCs' full dynamic range than low-contrast GWN stimuli. Shot-noise analysis of the underlying adaptation dynamics revealed that the enhanced macroscopic voltage responses resulted from more and smaller QBs being integrated during shorter and tighter latency distributions. Somewhat comparable QB dynamics have previously been shown to govern *Drosophila* and *Limulus* photoreceptors' light-adaptation (Wong and Knight, 1980; Wong, Knight and Dodge, 1980; Juusola and Hardie, 2001a). However, these dynamics in *Musca* occur in a much briefer time scale, consistent with its faster visual lifestyle. As such, my new results from *Musca* provide more evidence about how QBs adapt.

3.2 Materials and methods

3.2.1 Fly stocks

Adult, wild-type houseflies (*Musca domestica*) were used in the experiments. The housefly larvae/pupae were ordered from a commercial provider (Blades Biological Ltd, Cowden, Kent, UK). The houseflies, cultured in a standard laboratory incubator (60% humidity) at the Department of Biomedical Science, were fed with liver, and sugar water. The flies were kept at ~22 ^{o}C in a 12:12 h light:dark cycle.

3.2.2 *In vivo* intracellular recordings

In vivo intracellular recordings were performed from R1-R6 photoreceptors L1-L3 and LMCs as described in Chapter 2. All the experiments were done at 25 ^{o}C, *Drosophila*'s preferred temperature (Sayeed and Benzer, 1996; Juusola and Hardie, 2001b). This choice enabled direct comparisons of the early visual neurons' signalling performance between these two Diptera.

3.2.3 Visual stimuli

A high-intensity "white" LED (Seoul Z-Power P4 star, white, 100 Lumens) was used for light stimulation. Its light output was fed through a randomised quartz fibre optic bundle (transmission range: 180-1,200 nm) fixed on a rotatable Cardan-arm system, subtending a 3^{o} homogeneous light field seen by the fly. The LED output was controlled by an OptoLED driver (Cairn Research Ltd, UK) and monitored with a pin diode circuit.

Recordings from R1-R6 photoreceptors and L1-L3 LMCs were done in the dark and under different adapting light backgrounds. Neutral density (ND) filters (Thorlabs) were used to attenuate the LED light output in 1-log unit steps providing six different adapting backgrounds (BG0, BG-1, BG-2, BG-3, BG-4, BG-5). These light intensity levels (as effective photons) were determined by counting photoreceptors' single-photon responses (QBs) to dim illumination (attenuated by ND filters) after a prolonged dark-adaptation of at least 30 minutes. The effective photon rate (effective photons/s) for each adapting background was then determined by extrapolating the QB rate and multiplying it with the ND filter attenuation. Consequently, each adapting background's

estimated intensities from the lowest (BG-5) to the highest (BG0, no filter) were 70, 700, 7,000, …, 7x10^6 effective photons/s. This method assumes that the number of QBs reduces linearly in response to ND filter attenuation. It does not take into consideration, the intracellular pupil mechanism (Kirschfeld and Franceschini, 1969; Franceschini, 1972; Stavenga, 1975; Howard, Blakeslee and Laughlin, 1987; Roebroek and Stavenga, 1990; Song and Juusola, 2014), the refractoriness (Hochstrate and Hamdorf, 1990; Song et al., 2012; Song and Juusola, 2014) nor the photomechanical photoreceptor contractions (Juusola et al., 2017), which reduce quantum efficiency in bright light conditions. As a result, the effective photon rates at the highest adapting backgrounds are overestimated.

Light adaptation in photoreceptors and LMCs were tested with two different contrast distributions - bursty "saccadic" stimulus and GWN stimulus (see Chapter 2 for more details). Photoreceptors were tested with 2-s-long contrast modulations with a 500 Hz cut-off frequency whereas LMCs were tested with a 200 Hz cut-off frequency because it evoked the maximal information capacity (see Chapter 2).

The light contrast was defined by using Weber's law:

$$c = \frac{\Delta I}{I}, \tag{3-1}$$

where ΔI is the change in the intensity and I the mean background intensity (Shapley and Enroth-Cugell, 1984). For the Gaussian white noise (GWN) contrast modulation, ΔI is the standard deviation (SD) of the stimulation and I the mean light intensity. The contrast (c) for bursty "saccadic" stimulus was ~1.29 and for GWN stimulus ~0.33. Experiments were performed from the lowest to the highest adapting backgrounds. Only cells that remained stable throughout the entire stimulation protocol were further analysed. In all these experiments, each stimulus was repeated 30 times. The stimuli and responses were low-pass filtered at 500 Hz (KEMO VBF/23 low-pass elliptic filter, UK), and sampled at 1 kHz using a 12-bit A/D converter (National Instruments, USA). A custom-written software system controlled both the stimulus generation and data acquisition, Biosyst in MATLAB (MathWorks, USA) (Juusola and Hardie, 2001a;

Juusola and de Polavieja, 2003), with an interface package for National Instruments (Austin, TX) boards (MATDAQ: H. P. C. Robinson, 1997-2005).

3.2.4 Data analysis

Only the steady-state adapted responses were analysed and, therefore, the first 1-5 responses to the repeated stimulation (n = 30) were discarded. The analysis in this chapter was much performed as described in (Juusola and Hardie, 2001a).

3.2.4.1 Signal, Noise, SNR and Information transfer rate

The signal $s_v(t)$ and $S_V(f)$ and noise $n_v(t)$ and $N_V(f)$, and signal-to-noise ratio $SNR_V(f)$ and information transfer rates (*R*) were calculated as described in Chapter 2. The data was sampled at 1 kHz, and a 500-point Blackman-Harris window was used in the analyses.

3.2.4.2 Coherence

Coherence is the measure of how linear the system is, and is calculated from the $SNR_V(f)$ (Bendat and Piersol, 1971):

$$\gamma_{lin}^2(f) = \frac{SNR_V(f)}{SNR_V(f)+1}. \quad (3\text{-}2)$$

The system is purely linear and noise-free when $\gamma_{lin}^2(f) = 1$. Thus, the coherence function estimates both the system's linearity and signal-to-noise ratio (Bendat and Piersol, 1971).

3.2.4.3 Frequency and Impulse responses

Here the autospectrum of the contrast input is $\langle C(f) \cdot C^*(f) \rangle$ and the autospectrum of the output (photoreceptor signal) is $\langle S_V(f) \cdot S_V^*(f) \rangle$ resulting in their cross-spectrum to be $\langle S_V(f) \cdot C^*(f) \rangle$. Thus, the frequency response, $T_V(f)$, was calculated:

$$T_V(f) = \frac{\langle S_V(f) \cdot C^*(f) \rangle}{\langle C(f) \cdot C^*(f) \rangle}, \quad (3\text{-}3)$$

where the asterisk (*) denotes the complex conjugate and ⟨⟩ denotes the average over different stretches of the signal and the noise.

The impulse response $K_1(t)$, (or first-order Wiener kernel) is used to characterise the linear filtering properties of a photoreceptor in the time domain and is calculated by taking the inverse FFT of its frequency response:

$$K_1(t) = F^{-1}T_V(f)\ . \tag{3-4}$$

3.3 Results

3.3.1 R1-R6 Photoreceptors' signalling efficiency improves with brightening adapting background

I wanted to explore the impact of light adaptation to *Musca* R1-R6 photoreceptors' QB and macroscopic response properties and signalling performance using *in vivo* intracellular recordings. Briefly, in Chapter 2, I studied how well *Musca* photoreceptors and LMCs responded to contrast stimulus that resembles the fast temporal changes the fly encounters during body saccades by using two different bursty stimuli and GWN stimuli. The results showed that both R1-R6 photoreceptors and L1-L3 LMCs responded best to bursty "saccadic" contrast stimulation.

Here, I aimed to compare *Musca* photoreceptors' signalling performance to two of these contrast series (high-contrast bursty "saccadic" stimulus, c ~1.29 and low-contrast GWN stimulus, c ~0.33) at different adapting backgrounds. Unlike bursty "saccadic" stimulation, GWN does not have complex naturalistic nor behavioural statistics, subsequently linearising photoreceptors' voltage response (Marmarelis and Marmarelis, 1978; van Hateren, 1997). Therefore, for analysing the QB shape and latency distribution (Chapter 3.3.3 and 3.3.4) GWN stimulation ensures a better estimation when using linear signal and noise analysis methods.

Figure 3-1A-B shows an R1-R6 photoreceptor's intracellular voltage responses to repeated presentations (n = 30) of two different 2-s-long contrast stimuli at six adapting backgrounds (BG0, BG-1, BG-2, BG-3, BG-4 and BG-5). BG0 (no filter) is the brightest and BG-5 (attenuated 10^5 times) the dimmest background. **Figure 3-1C-D** shows the corresponding signal and noise traces (extracted from the voltage responses) and their corresponding probability density functions (PDFs) to the contrast stimuli; the signal is the mean of the repetitions, and the noise is the difference between individual traces and the signal. The instrumental noise (recorded outside the cell in the extracellular space in darkness) and the dark noise (noise inside the cell in darkness) are shown in **Figure 3-1C-D**.

Noise is the major limitation at the lower light levels (input contains few photons) and it includes photon shot-noise, intrinsic transducer noise (from the phototransduction), dark noise (stochastic channel openings, synaptic feedback from downstream) and instrumental noise (mainly from the high resistance electrodes) (Lillywhite and Laughlin, 1979; Laughlin and Lillywhite, 1982). The light-induced photoreceptor voltage noise at different mean light intensities was estimated by subtracting the instrumental noise - using the corresponding power spectra - by assuming that the noise sources are independent and additive. Many previous studies have used the estimated dark noise power spectrum for subtraction (Dodge, Knight and Toyoda, 1968; Roebroek, van Tjonger and Stavenga, 1990; Suss-Toby, Selinger and Minke, 1991; Juusola and Hardie, 2001a; Burton, 2006; Faivre and Juusola, 2008), but this was not done here. Juusola and Hardie (2001a) noted that the photoreceptor membrane impedance is not constant under dark adaption and different light adaptation levels. As a result, dark noise subtraction is suboptimal when estimating the QB waveform and latency distribution from the noise power spectrum. That said, Burton (2006) showed that using dark noise for the subtraction can still produce reasonable QB estimates, as demonstrated by comparing them to the ones extracted from the bispectrum estimate.

The photoreceptor (n = 15 photoreceptors) response properties improved with brightening stimulation (**Figure 3-1** and **3-2**). In the time domain, when increasing the mean light intensity, the photoreceptor voltage signal $s_v(t)$ variance increased, more so to the high-contrast bursty stimulus (from ~0.2 mV at BG-5 to ~12 mV at BG0) than to low-contrast GWN stimulus (from ~0.2 mV at BG-5 to ~3 mV at BG0) (**Figure 3-1C-D** and **Figure 3-2A-B**). Correspondingly, the frequency domain representation of the signal power spectrum $|\langle S_V(f)\rangle|^2$ amplified and extended to higher frequencies (**Figure 3-2A-B**), carrying more information. The growing signal power was evident for both of the contrast series, although the voltage signals to bursty stimulation were larger than GWN stimulation.

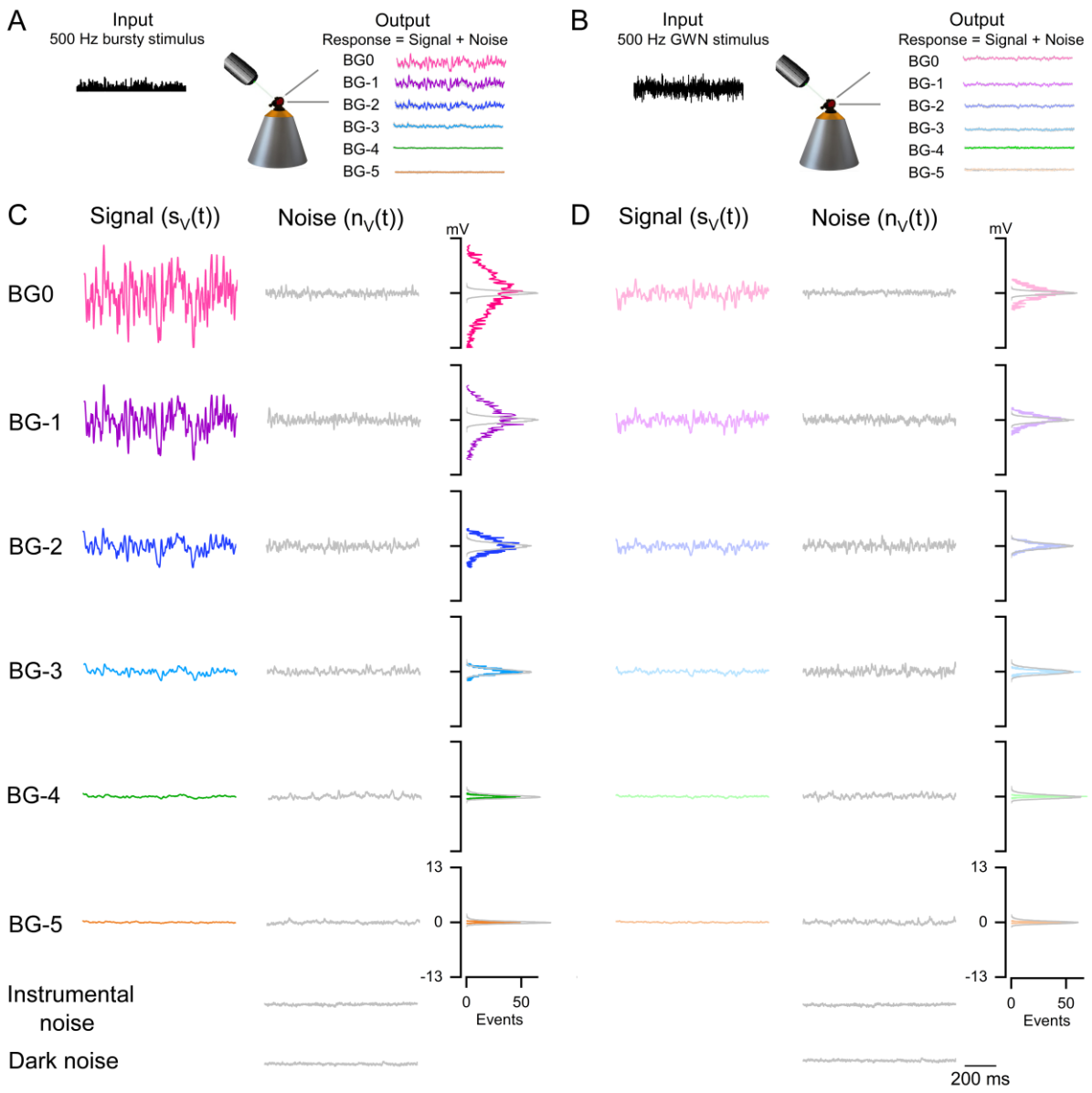

Figure 3-1. Time-domain representation of the photoreceptor responses (signal and noise) to two different contrast series (high-contrast bursty "saccadic" and low-contrast GWN) at different adapting backgrounds. (A) A schematic showing *in vivo* intracellular voltage responses (showing 1-s-long samples) from *Musca* photoreceptors (R1-R6) when using a 2-s-long high-contrast bursty stimulus (500 Hz cut-off frequency) at six different adapting backgrounds (BG0, BG-1, BG-2, BG-3, BG-4 and BG-5). **(B)** Same as in **A** but for low-contrast GWN stimulation. **(C)** Photoreceptor voltage signal $s_v(t)$ and noise $n_v(t)$ traces, as well as their corresponding probability density functions (PDFs) to high-contrast bursty stimulus at six different adapting backgrounds. **(D)** The same as in **C** but for low-contrast GWN stimulation. In both **C** and **D**, the instrumental noise (measured in the extracellular space in darkness) and the dark noise (measured in the cell in darkness) are shown. These recordings are from the same photoreceptor.

Unlike photoreceptor voltage signal variance, the voltage noise $n_v(t)$ variance increased only up to around BG-2 (with some variation between the 15 recorded photoreceptors) and then slightly decreased. These adapting dynamics occurred similarly during high and low-contrast stimulations (**Figure 3-1C-D** and **Figure 3-2C-D**), with the photoreceptor noise variance at each adapting background being similar for both the stimuli, even though the high-contrast bursts evoked larger voltage signals. The frequency-domain representation showed that the photoreceptor noise power $|\langle N_V(f)\rangle|^2$ shifted to higher frequencies for brightening bursts and GWN stimulation (**Figure 3-2C-D**). Noise dynamics for the GWN stimulation is consistent with other findings from *Drosophila* (Juusola and Hardie, 2001a), *Musca* (Burton, 2006) and *Calliphora* (Juusola et al., 1994). However, the noise power behaved somewhat differently during bright contrast bursts, which most likely reflected additional nonlinearities. These noise estimates were affected by the instrumental noise. Instrumental noise was subtracted when estimating the QB noise ($|B_V(f)|^2$ in Chapter 3.3.3.

In the time domain, the signal-to-noise ratio $SNR_V(t)$ was calculated by dividing the photoreceptor signal variance by its noise variance. Whereas, in the frequency domain, the signal-to-noise ratio $SNR_V(f)$ was calculated by dividing the photoreceptor signal power spectrum by its noise power spectrum. Signal-to-noise ratio is a good measure of photoreceptor's signalling performance; if $SNR_V < 1$, the photoreceptor output contains more noise than signal and, thus, is not reliable. In the time domain, the maximum $SNR_V(t)$ increased with brightening stimulation; bursty stimulation: from ~0.2 at BG-5 to ~400 at BG0, GWN stimulation: from ~0.2 at BG-5 to ~40 at BG0 (**Figure 3-2E-F**). The two dimmest adapting backgrounds (BG-4 and BG-5) contained more noise than signal ($SNR_V < 1$), while at the brightest adapting background, the SNR_V curve tails off slightly, presumably reflecting the cells' saturation prevention mechanisms (i.e. the intracellular Ca^{2+}-dependent pupil) (Kirschfeld and Vogt, 1980; Howard, Blakeslee and Laughlin, 1987). In the frequency domain, the $SNR_V(f)$ became amplified with increasing the mean light intensity, shifting to higher frequencies.

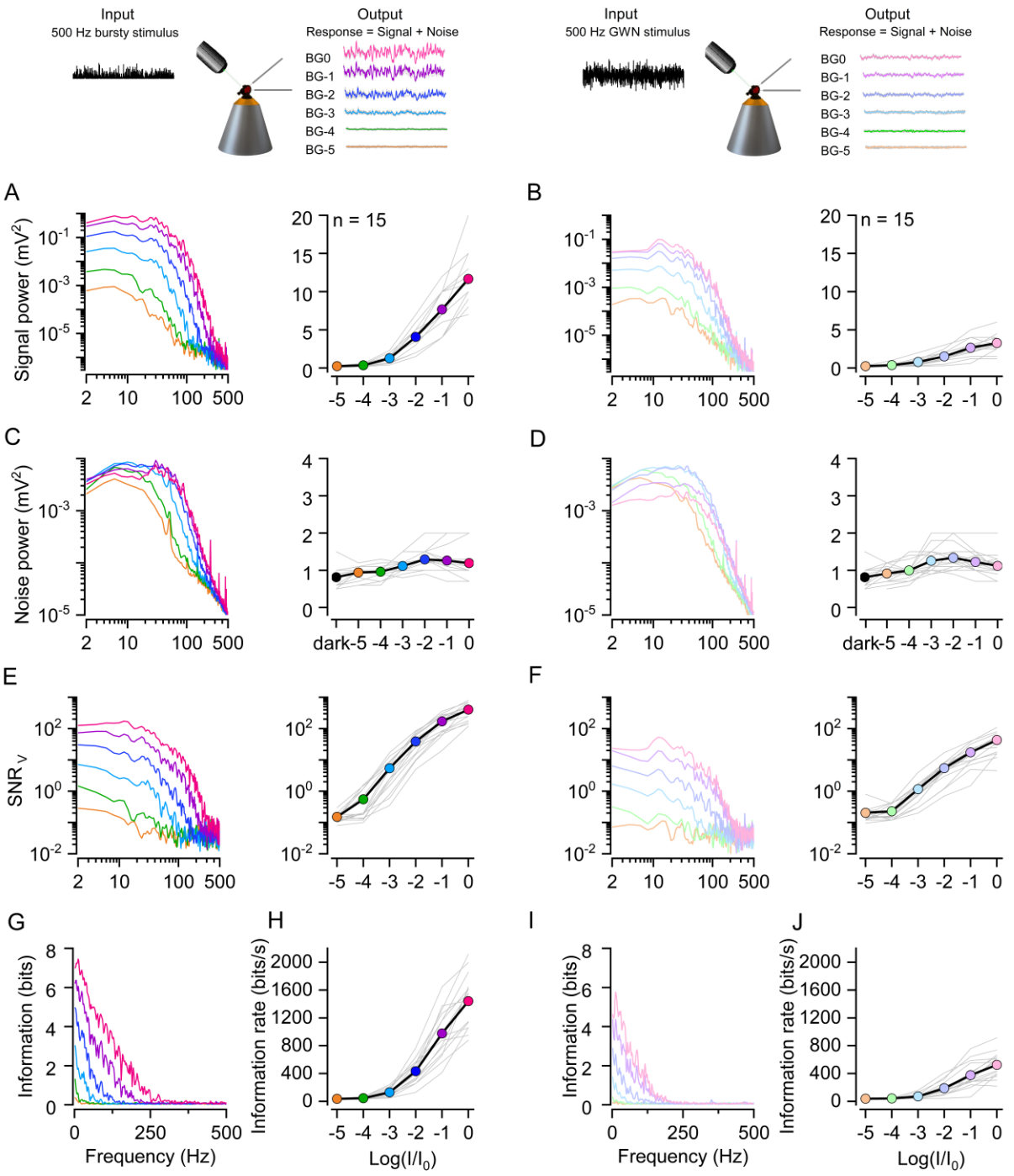

Figure 3-2. Brighter light adaptation improves photoreceptors' coding performance to both tested contrast series. Response properties to bursty stimulation are shown on the left panel and GWN stimulation on the right panel. When increasing the mean light intensity from BG-5 to BG0 **(A)** the photoreceptor signal power spectrum $|\langle S_V(f)\rangle|^2$ for bursty stimulus amplified (amplification highest at the lowest frequencies) and extended to higher frequencies. Additionally, the photoreceptor (n = 15 photoreceptors) voltage signal $s_v(t)$ variance increased. **(B)** The same happened when using GWN contrast modulation. **(C)** For bursty stimulus, the photoreceptor noise power spectrum $|\langle N_V(f)\rangle|^2$ shifted to higher frequencies, and the lower frequency end was slightly amplified up to around BG-3, slightly

attenuating after. Increasing the mean light intensity, the voltage noise $n_v(t)$ variance increased up to about BG-2 (some variation between the 15 recorded photoreceptors) before slightly decreasing. **(D)** The voltage noise variance was similar to GWN stimulus. Otherwise, the noise dynamics were consistent with previous research from other Diptera (Juusola et al., 1994, Juusola and Hardie, 2001a; Burton, 2002). When increasing the mean light intensity for both **(E)** bursty stimulus and **(F)** GWN stimulus, the $SNR_V(f)$ was amplified and shifted to higher frequencies. Moreover, information and information capacity (R) increased for **(G-H)** the bursty stimulus (more so) and for **(I-J)** the GWN stimulus when brightening the adapting background.

The resulting adaptive signal and noise dynamics, and subsequently, the SNR (**Figure 3-2G** and **I**), meant that photoreceptors sampled more information (bits) and distributed it over a broader frequency bandwidth with brightening stimulation (**Figure 3-2H** and **J**). The photoreceptors' information transfer rate *R* (bits/s) was calculated from $SNR_V(f)$ (Shannon information theory: Shannon, 1948), ranging from ~40 bits/s at BG-5 to ~1,440 bits/s at BG0 (bursts) and from ~40 bits/s at BG-5 to ~520 bits/s at BG0 (GWN). Both of the contrast series showed a similar enhancement in their coding performance, although information transfer rates were 2-to-3-times higher for bursts. Chapter 2 explained in detail why the high-contrast bursty stimulus drove photoreceptors' encoding better.

3.3.2 Photoreceptor's coherence function and linear impulse response at different adapting backgrounds

I tested whether *Musca* photoreceptors operate linearly to the two different contrast stimuli under different adapting backgrounds (from BG-5 to BG0). The high-contrast bursty stimulus excites photoreceptors' full dynamic range better than the low-contrast GWN stimulus, which linearises photoreceptor output (Juusola et al., 1994). This observation was apparent when comparing the photoreceptor signal and noise PDFs to bursty and GWN stimuli. For the bursty stimulus, photoreceptor signal PDFs were Gaussian at lower adapting backgrounds but became slightly skewed (towards depolarisation) with brightening (**Figure 3-1C**), indicative of nonlinear (refractory) QB summation (Song et al., 2013). However, the noise PDFs were Gaussian for all the tested adapting backgrounds. For the GWN stimulus, both the signal and the noise were Gaussian, suggesting that the photoreceptor responded linearly to this type of light stimulation (**Figure 3-1D**).

Furthermore, the coherence function $\gamma_{lin}^2(f)$ was used to estimate how linear the photoreceptor responses were for both contrast stimulations under different adapting backgrounds. The system is entirely linear and noise-free when $\gamma_{lin}^2(f) = 1$ (Bendat and Piersol, 1971). For both of the contrast stimuli, the two brightest adapting backgrounds (BG0 and BG-1) had $\gamma_{lin}^2(f) \approx 1$ over almost the full bandwidth (broader for bursty stimulus), suggesting that photoreceptors operated approximately linearly at these mean light intensities (**Figure 3-3A** and **3-3C**). However, the signal probability distributions at the brightest backgrounds were skewed for the contrast bursts, suggesting that the unity of coherence function might result from high signal-to-noise ratios, rather than the system's linearity (**Figure 3-1C** and **3-2E**). The dimmer intensities produced low coherence values, most likely due to low SNR. GWN contrast stimulus at different adapting backgrounds was used for further analysis (QB shapes and latency distributions) because a photoreceptor can be treated as a linear system.

Photoreceptor's linear impulse response $K_1(t)$, was calculated for both of the contrast series at six different adapting backgrounds, although for the bursty contrasts these estimates could be less accurate (due to nonlinearities) (**Figure 3-3B** and **3-3D**). These first-order Wiener kernels approximate a photoreceptor's voltage response to a brief contrast pulse at different adapting backgrounds. Increasing the mean light intensity (i.e. increasing photons) increased the impulse response amplitude (bursty contrasts: from ~0.2 mV at BG-5 to ~27 mV at BG0, GWN stimulus: from ~0.1 mV at BG-5 to ~4 mV at BG0), showing little saturation at the brightest backgrounds. Besides, the impulse response latency and the total duration reduced with brightening; its time-to-peak (t_p) shortened from 30 ms at BG-5 to ~10 ms at BG0 for both contrast stimuli. The responses were 8-times larger for contrast bursts predominantly because such stimulation enables more microvilli to participate in photon sampling, accentuating fast contrast changes, rather than keeping most microvilli refractory during GWN stimulation (Juusola et al., 2017).

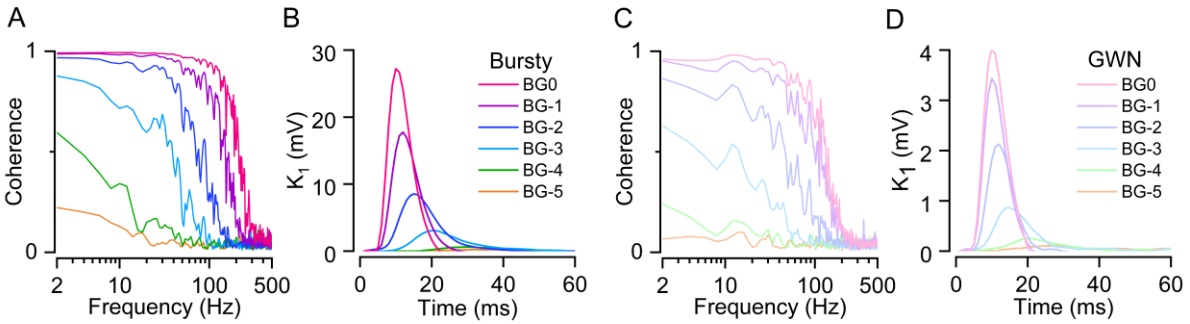

Figure 3-3. Photoreceptor's coherence function and linear impulse responses at six different adapting backgrounds. (A) Photoreceptor's coherence function to high-contrast bursty stimulus and **(B)** its linear impulse response (i.e. first-order Wiener kernel estimates). **(C)** Photoreceptor's coherence function to low-contrast GWN stimulus and **(D)** its linear impulse response at BG-5 to BG0. These recordings were from the same photoreceptor.

3.3.3 QB shape analysis at different adapting backgrounds

Here, I aimed to quantify how the average light-induced QB shape adapts to different levels. Single-photon absorptions evoke QBs in microvilli (~60,000 in *Musca*) (Fuortes and Yeandle, 1964; Kirschfeld, 1966; Lillywhite, 1977; Wu and Pak, 1975; Hardie and Juusola, 2015). QBs can be visible in photoreceptor voltage recordings at very dim light conditions. However, at brighter illumination, they sum up to produce the macroscopic voltage response, becoming less distinguishable. Shot-noise analysis was used to characterise the photoreceptors' QB shape (QB amplitude, waveform and duration) at different mean light intensities from dim to very bright, as done previously (Wong and Knight, 1980; Juusola et al., 1994; Juusola and Hardie, 2001a).

To accurately estimate the light-induced noise (QB noise) at different mean light levels, other noise sources (intrinsic transducer noise, dark noise and instrumental noise) needed to be removed, if possible, assuming they are additive and independent. I subtracted only the instrumental noise power spectrum from the photoreceptor noise power spectrum at different adapting backgrounds (**Figure 3-4A**):

$$|B_V(f)|^2 \cong |\langle N_V(f)\rangle|^2 - \left|N_V^{instrumental}(f)\right|^2. \quad (3\text{-}5)$$

This approach is suboptimal because different intrinsic noise sources, such as noise from the feedback synapses (Zheng et al., 2006), could further contaminate the QB

noise power spectrum in an activity-dependent manner (the feedback is most active in darkness).

Another factor to consider when using the noise power spectrum for estimating the QB shape, is that the noise power spectrum does not contain any information about the phase, and so, QBs are considered to be minimum-phase (i.e. QBs have the smallest possible phase lag at all frequency bandwidths) (Wong and Knight, 1980; de Ruyter van Steveninck and Laughlin, 1996). Crucially, however, while photoreceptors do not operate as minimum-phase systems (French, 1980), the underlying QBs seem to be minimum-phase (Burton, 2006).

Here I assumed that the QB shape function $(b_V(t))$ follows the Γ-distribution (gamma distribution):

$$b_V(t) \propto \Gamma_V(t; n, \tau) = \frac{1}{n!\tau}\left(\frac{1}{\tau}\right)^n e^{-t/\tau}, \tag{3-6}$$

where two parameters (n and τ) were attained by fitting a single Lorentzian to the calculated QB noise power spectrum (**Figure 3-4B**):

$$|B_V(f)|^2 \propto \left|\tilde{\Gamma}_V(f; n, \tau)\right|^2 = [1 + (2\pi\tau f)^2]^{-(n+1)}, \tag{3-7}$$

where $\tilde{\Gamma}_V$ is the Fourier transform of the gamma distribution.

To better understand QB-shape-adaptation, I first estimated the effective duration (*T*) and the mean QB amplitude (α). The effective QB duration (*T*) was calculated by using the two parameters obtained earlier from the fitted single Lorentzian:

$$T = \tau \frac{(n!)^2 2^{2n+1}}{(2n)!}. \tag{3-8}$$

The mean QB amplitude (α) estimation, follows Campbell's theorem (Rice, 1944), which states that QB amplitude and rate can be extracted from Poisson shot noise

(composed of superimposed QBs) (Wong and Knight, 1980; Juusola and Hardie, 2001a). The mean QB amplitude (α) for all the different mean light intensities was calculated as shown by Wong and Knight (1980):

$$\alpha = \frac{\sigma^2}{\mu}, \tag{3-9}$$

where σ^2 and μ are the variance and the mean of the photoreceptor voltage noise, respectively. The estimated QBs became smaller and briefer (shorter effective duration) with brightening (**Figure 3-4C**).

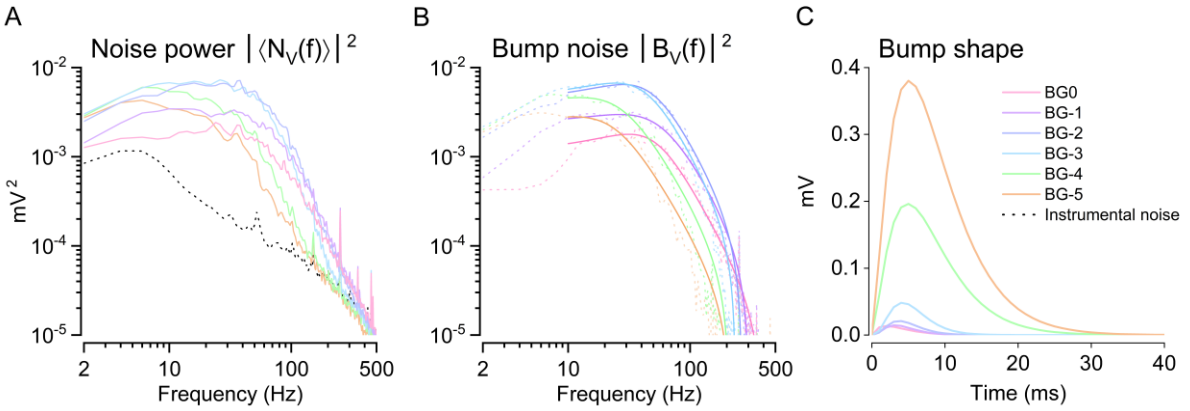

Figure 3-4. QB shape analysis at different adapting backgrounds. (A) Instrumental noise power spectrum (dotted line) was subtracted from the photoreceptor noise power spectrum $|\langle N_V(f)\rangle|^2$ at six different adapting backgrounds (coloured lines, BG-5 to BG0) to get the QB noise $|B_V(f)|^2$. The higher frequency range is contaminated by the instrumental noise (50 Hz harmonics). **(B)** QB noise power spectrum shown as dotted lines with a single Lorentzian fitted on them (coloured lines). **(C)** QB shape was estimated from the QB noise and by assuming that it follows the Γ-distribution. The estimated QBs got smaller and faster with brightening. These recordings are from the same photoreceptor.

3.3.4 QB latency distribution at different adapting backgrounds

Microvillar absorption of single photons and phototransduction reactions are stochastic; thus, the resulting QBs show variable waveform and latency distributions (time from photon absorption to a QB) (Song et al., 2012). This variability over time limits the temporal resolution of a photoreceptor's macroscopic (voltage) response.

How to estimate the QB latency distribution to increasing light adaptation? Using Juusola and Hardie (2001a) method, the QB latency distribution at different adapting backgrounds was estimated by deconvolving the QB waveform from the photoreceptor's impulse responses at the different mean light intensities; assuming the system operates linearly (tested in Chapter 3.3.2, thus low-contrast GWN stimulus was used for the analysis). Linear impulse response $K_1(t)$ can be considered a convolution of the QB waveform $(b_V(t))$ and its corresponding latency distribution $(l(t))$ at the same mean light intensity:

$$K_1(t) = b_V(t) \otimes l(t), \tag{3-10}$$

where ⊗ denotes convolution. To minimise the noise in the latency distribution estimation at different adapting backgrounds, normalised photoreceptor impulse response $K_{1;norm}(t)$ was fitted with a lognormal function at different adapting backgrounds (**Figure 3-5A**) and QB shape with a Γ-distribution (normalised after) (**Figure 3-5B**). The fitting of the photoreceptor impulse response was done as follows:

$$K_{1;norm}(t) \cong e^{\left\{\frac{-[\ln(t/t_p)]^2}{2a^2}\right\}}, \tag{3-11}$$

where (t_p) is the impulse response time-to-peak, and *a* is the width factor.

Figure 3-5C shows the deconvoluted latency distributions at six different adapting backgrounds, and **Figure 3-5D** shows the normalised latency distributions at the corresponding adapting backgrounds. At the brightest mean intensities (BG0, BG-1 and BG-2), the QB latency distributions were very similar to each other. However, when dimming the adapting backgrounds, the latency distributions became slower (t_p occurred later) and wider. The dimmest adapted background (BG-5) features an imprecise estimate, contaminated by recording noise.

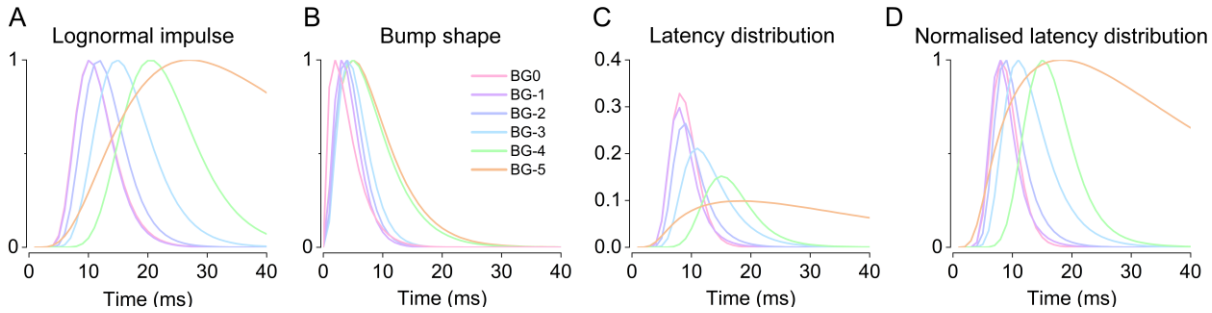

Figure 3-5. Deconvolving the latency distribution from the linear impulse response and the QB shape. (A) Linear impulse response was fitted with a lognormal function at different adapting backgrounds. **(B)** Normalised QB shape at corresponding backgrounds. **(C)** Latency distribution was attained by deconvolving the QB waveforms from the photoreceptor's impulse responses at different mean light intensities. **(D)** Normalised latency distributions. These recordings were from the same photoreceptor.

3.3.5 L1-L3 signalling improves with brightening stimulation

After quantifying the *Musca* photoreceptors' (R1-R6) response properties and coding performance to changing light backgrounds, I aimed to study how light adaptation impacted *Musca* LMC (L1-L3) signalling. Earlier I had shown that *Musca* photoreceptors and LMCs encode better bursty temporal light changes than GWN stimuli. This section's focus is to explore light-adapted L1-L3 LMCs' signalling performance, using the same stimuli. The LMCs were tested similarly as the photoreceptors but now using "saccadic" high-contrast bursts (c ~1.29) and low-contrast GWN stimulus (c ~0.33) with 200 Hz cut-off frequency (see Chapter 2: this stimulus bandwidth generated the highest information transfer). LMC response properties were studied at six different adapting backgrounds (BG0, BG-1, BG-2, BG-3, BG-4 and BG-5) (**Figure 3-6A-B**). **Figure 3-6C-D** shows the signal and noise traces (extracted from the voltage responses) and their corresponding PDFs to bursty and GWN contrast series at different adapting backgrounds. Additionally, the instrumental noise and the dark noise were recorded, as shown in the figure.

The LMC (n = 3 LMCs) response properties improved when brightening the adapting background (**Figure 3-6** and **3-7**) (also shown in *Calliphora*: Juusola et al., 1995), similar to photoreceptor signalling. Increasing mean light intensity amplified the LMC voltage signal $s_v(t)$ variance; more so for the high-contrast bursty stimulus (from ~0.7 mV at BG-5 to ~13 mV at BG0) than for low-contrast GWN stimulus (from ~0.7 mV at BG-5 to ~7 mV at BG0) (**Figure 3-6C-D** and **Figure 3-7A-B**). The LMC signal variance

remained unchanged for the two brightest adapting backgrounds (BG-1 and BG0) when using GWN, evident in the signal power spectrum $|\langle S_V(f)\rangle|^2$ (**Figure 3-7B**). Furthermore, the signal amplification (especially at the lowest frequencies) for both of the contrast series was not as clear as in photoreceptors, most likely due to some nonlinearities at the three brightest adapting backgrounds (BG-2, BG-1 and BG0) (see PDFs in **Figure 3-6C-D**).

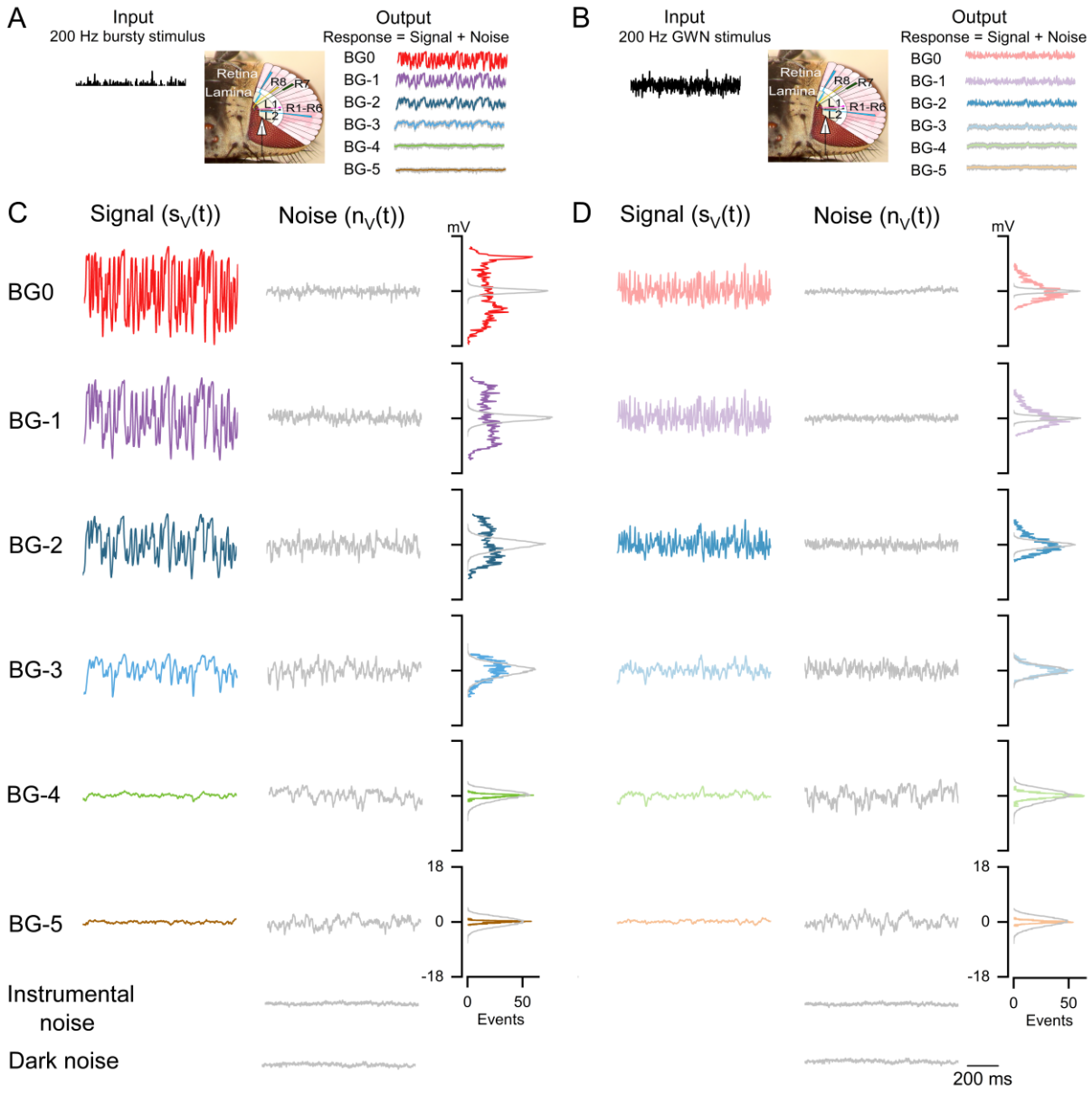

Figure 3-6. Time-domain representation of the LMC responses (signal and noise) to two different contrast series (high-contrast bursty "saccadic" and low-contrast GWN) at different adapting backgrounds. (A) A schematic showing *in vivo* intracellular recordings from *Musca* LMCs (L1-L3) when using 2-s-long (only showing 1-s-long samples) high-contrast bursty stimulus (200 Hz cut-off frequency) at six different adapting backgrounds (BG0, BG-1, BG-2, BG-3, BG-4 and BG-5) to measure the impact

of light adaptation in LMCs' voltage responses. **(B)** Same as in **A** but for low-contrast GWN stimulus. **(C)** LMC voltage signal $s_v(t)$ and noise $n_v(t)$ traces and corresponding PDFs to the high-contrast bursty stimulus at six different adapting backgrounds attenuating 1-log unit steps from BG0 (no filter) to BG-5 (attenuated 10^5-fold). The noise probability distribution was Gaussian at all the tested adapting backgrounds. On the other hand, the signal distribution was Gaussian only at the lowest adapting backgrounds (BG-5, BG-4 and BG-3) but then became non-Gaussian. **(D)** The same as in **C** but for low-contrast GWN stimulus. The noise probability distribution was Gaussian to all the tested adapting backgrounds. The signal distribution was Gaussian at the lowest mean light intensities (BG-5, BG-4 and BG-3) but skewed to hyperpolarising values with brightening. In both **C** and **D**, the instrumental noise (noise measured in the extracellular space in darkness) and the dark noise (noise measured in the cell when in darkness) are shown. These recordings were from the same LMC.

The LMC voltage noise variance at different adapting backgrounds was more extensive than LMC dark voltage noise variance (maximum difference in photoreceptors ~1 mV and in LMCs ~3 mV) (compare **Figure 3-2C-D** and **Figure 3-7C-D**). The LMC noise variance differed between the two contrast series: for the bursts, the noise variance peaked at BG-2 and decreased with further brightening (**Figure 3-7C**). Conversely, for GWN stimulus, the LMC voltage noise variance peaked at BG-4 (**Figure 3-7D**). Furthermore, increasing the mean light intensity broadened and attenuated (especially the lower frequency end) the LMC noise power spectrum $|\langle N_V(f)\rangle|^2$. Note that these noise estimates included the instrumental noise as well as the dark noise.

$SNR_V(t)$ increased with brightening intensity for both contrast series; contrast bursts from ~0.1 (BG-5) to ~307 (BG0), and GWN from ~0.1 (BG-5) to ~97 (BG0) (**Figure 3-7E-F**). The LMC responses at the two dimmest adapting backgrounds (BG-4 and BG-5) contained more noise than signal $(SNR_V < 1)$, whereas at the brightest background, the SNR_V slightly flattened (especially to GWN stimulus), similar to photoreceptors. Concurrently, $SNR_V(f)$ increased and shifted to higher frequencies. Whereas, for the GWN, the SNR_V saturated at the two brightest backgrounds (see signal and noise variance at these backgrounds in **Figure 3-7B** and **D**). For the responses to bursty contrasts, the used sampling rate (1 kHz with 500-point window size) was not sufficient at the three brightest backgrounds, resulting in signal clipping, and subsequently, a loss of information. Such clipping did not occur when using GWN. More about this can be found in Chapter 2.3.5.

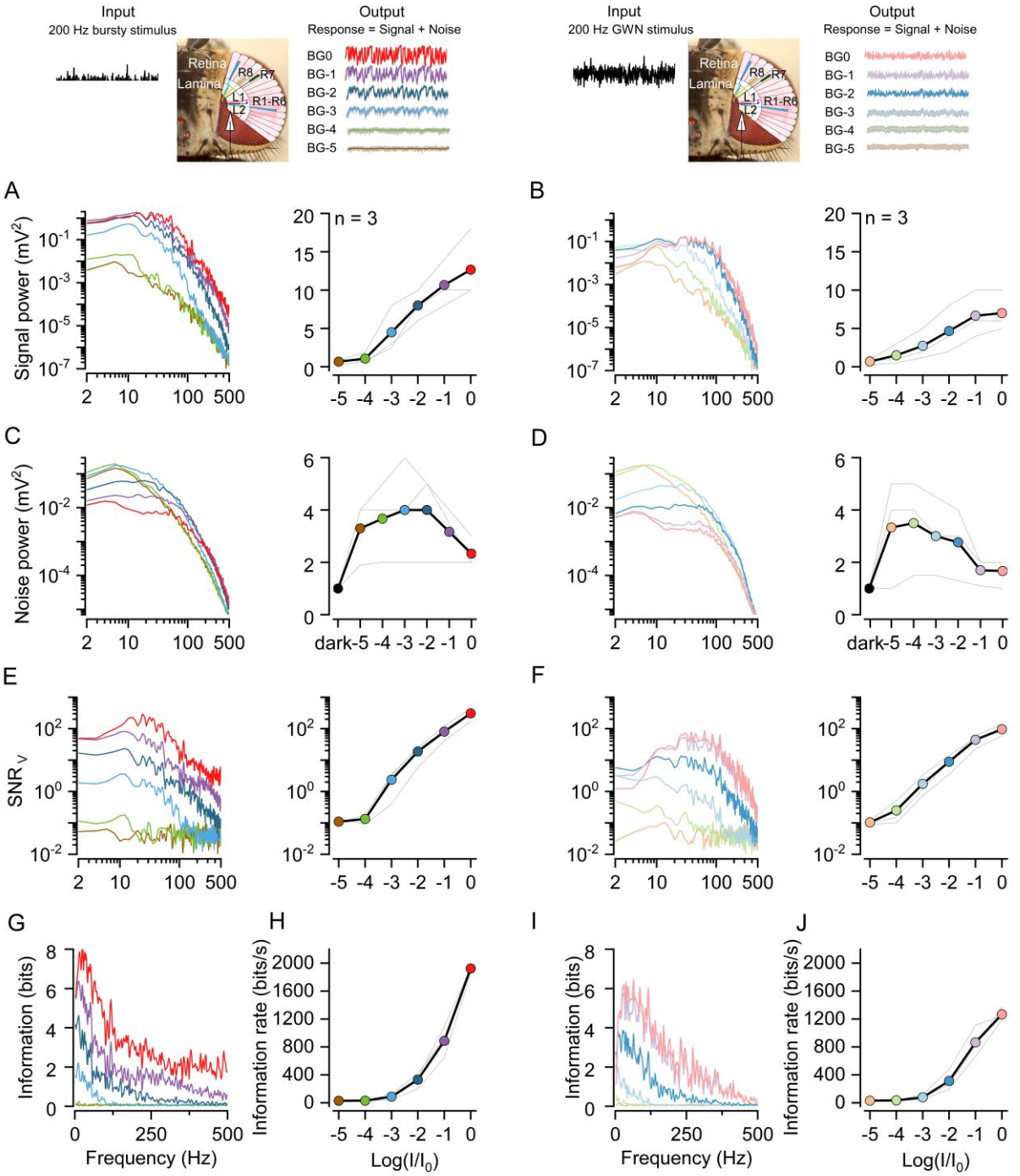

Figure 3-7. LMC signalling efficiency improved to the brightening adapting background to both of the tested contrast series. Response properties to the bursty stimulus are shown on the left panel and GWN stimulus on the right panel. Brightening from BG-5 to BG0 **(A)** amplified the LMC signal power spectrum $|\langle S_V(f)\rangle|^2$ for bursts (maxima at the lowest frequencies) and extended the bandwidth to higher frequencies. Concurrently, the LMC (n = 3) voltage signal $s_v(t)$ variance increased. **(B)** The same happened when using GWN contrast modulation, although, the signal variance saturated at two brightest adapting backgrounds. **(C)** For bursty stimulus, brightening broadened the LMC noise power spectrum $|\langle N_V(f)\rangle|^2$ while attenuating its low frequencies. The noise variance peaked at BG-2 and decreased slightly with further brightening. **(D)** For the GWN stimulus, brightening broadened the LMC

noise power and attenuated its low frequencies; its variance peaked at BG-4. With brightening **(E)** bursts and **(F)** GWN the LMC $SNR_V(f)$ increased and shifted to higher frequencies. Accordingly, LMC information transfer rate (*R*) increased **(G-H)** for bursts and **(I-J)** GWN.

Despite this information (bits) loss due to undersampling, the LMC frequency range broadened during brightening bursts (**Figure 3-7G**) and GWN (**Figure 3-7I**). Accordingly, information transfer rate (*R*) increased with brightening; burst from ~30 bits/s (BG-5) to ~1,930 bits/s (BG0), and GWN from ~30 bits/s (BG-5) to ~1,270 bits/s (BG0) (**Figure 3-7H** and **J**). Chapter 2 explained in detail why the high-contrast bursty stimulus drove LMCs' encoding better.

3.4 Discussion

3.4.1 Visual coding improved under light adaptation

My study provided new insight into how the signalling performance of *Musca* photoreceptors and LMCs adapt. Additionally, I presented the underlying adapting elementary response dynamics (QB waveform and latency distribution) to explain the improved performance.

The photoreceptor (n = 15) and LMC (n = 3) response properties improved with brightening the adapting background (**Figure 3-1** and **3-6**). The signal power increased and broadened to the higher frequencies, indicating that both photoreceptors and LMCs employ a larger voltage range to encode fast, high-frequency contrast changes with brightening adapting background (**Figure 3-2** and **3-7**). Concurrently, these adaptive signalling changes were accompanied by diminishing noise, which jointly increased visual information flow.

I further explored the impact of stimulus statistics on the photoreceptor and LMC signalling performance by comparing their responses to high-contrast bursty and low-contrast GWN stimuli at different light backgrounds. I showed how brightening bursty stimuli evoked larger responses with higher SNR than GWN in both cell types (**Figure 3-2A-F** and **3-7A-F**), boosting the cells' information transfer rates (**Figure 3-2G-J** and **3-7G-J**).

I also showed how 1 kHz sampling rate was not sufficient to fully drive LMCs at the three brightest backgrounds for bursty stimulus, which resulted in information loss (**Figure 3-7E**, **G** and **H**). Therefore, the information rates calculated for LMCs at these light intensities represent underestimates. Although the LMC noise variance surpassed photoreceptor noise, LMCs still transmitted more information (compare **Figure 3-2C-J** and **Figure 3-7C-J**). At bright adapted states, the LMC information transfer rates for bursts were just over 1.5-times higher than for GWN (**Figure 3-7G-J**). I will not further discuss the differences between photoreceptor and LMC coding, as covered in Chapter 2. Moreover, comparisons between photoreceptors and LMCs in different light-adaptational states will not be discussed because different stimulus bandwidths were used to test these cells (for photoreceptors: stimulus with a 500 Hz cut-off frequency and for LMCs: stimulus with a 200 Hz cut-off frequency).

I will, however, discuss why I used linear system analysis as voltage signals from the LMCs, especially to bursty stimuli, were not Gaussian (**Figure 3-6C**) and even in response to GWN, the voltage signals were very skewed (**Figure 3-6D**). This was also the case with photoreceptor voltage signals at the brightest mean light intensities but only to the bursty stimuli (**Figure 3-1C**). This shows that LMCs and to a lesser extent photoreceptors respond more or less nonlinearly to this type of stimulation, so the assumption would be that linear analysis (Shannon information theory: Shannon, 1948) would not provide a realistic representation of the information transfer rates.

As an alternative, one might opt to use the triple extrapolation method (Juusola and de Polavieja, 2003) as it is more suitable to use for calculating information transfer rates for nonlinear systems. The encoding performance using this method is not derived from the SNR, as when using the Shannon formula, but through dividing the continuous voltage response into time intervals and then performing extrapolation for the infinite data size, voltage levels and time intervals.

Juusola et al. (2017) used very similar light stimulation (bursty and GWN stimuli) on *Drosophila*, and calculated the information rates using both, Shannon formula and triple extrapolation method, to highly non-Gaussian responses (similar to mine). When comparing the results, the two methods gave similar estimates (maximally differing ~5-20%). Two other studies (Song and Juusola, 2014; Dau et al., 2016) found this to

be the case as well. As such, it is fair to assume that because similar stimuli were used as in Juusola et al. (2017), using the triple extrapolation method would have likely produced similar estimates to what I calculated using Shannon formula.

3.4.2 More, smaller and faster QBs increase the photoreceptor signalling performance in light adaption

In this section, I will discuss how light adaptation affects QB waveform and latency distribution, shaping photoreceptor's macroscopic voltage response and increasing information transfer. A well-established method, the shot-noise analysis (Wong and Knight, 1980; Juusola and Hardie, 2001a), was used to characterise the single-photon responses (QBs) that sum up the macroscopic voltage responses.

QBs are responses to single-photon absorptions, which follow Poisson statistics and take place in the microvillus (photoreceptor's photon sampling unit) (Fuortes and Yeandle, 1964; Kirschfeld, 1966; Lillywhite, 1977; Wu and Pak, 1975; Hardie and Juusola, 2015). QBs are nonlinear events having variable waveforms and latency distributions, mainly due to the stochastic phototransduction cascade (G-protein-coupled signalling cascade) (Song et al., 2012). However, the convolution of the variable QB waveforms and latency distributions smoothens macroscopic response, making the QB waveform and latency distribution the key limiting factors of a photoreceptor's temporal resolution. The latency distribution determines the photoreceptor’s upper signalling speed, constraining its bandwidth.

In adaptation, the phototransduction cascade can improve photoreceptor signalling by making QBs smaller and faster, and shortening their latency distribution (Wong and Knight, 1980; Wong, Knight and Dodge, 1980; Henderson, Reuss and Hardie, 2000; Juusola and Hardie, 2001a). However, ultimately, to improve information sampling, the microvilli need to convert more photons to QBs, as information increases with the number of synchronised samples. Such dynamics occurred in *Musca* photoreceptors with brightening stimulation (i.e. higher input SNR) as microvilli generated more QBs, which became smaller and faster with shorter latencies (**Figure 3-4C** and **3-5**); similar to *Drosophila* photoreceptors (Juusola and Hardie, 2001a). With the tighter latency distribution at the three brightest adapting backgrounds (BG-2, BG-1 and BG0), QBs

appeared sooner and were better synchronised (**Figure 3-5D**). Therefore, brightening increases QB numbers and broadens the photoreceptor bandwidth, resulting in enhanced information transfer to LMCs.

3.4.3 Phototransduction mechanisms underpinning light adaptation

Light adaptation ultimately results from the microvillar phototransduction reactions and the light-insensitive cell membrane working in synchrony in integrating QBs to macroscopic responses. However, due to lack of membrane impedance data, I will only discuss the former, considering explanations for the light-current QB and latency distribution changes. To do this, I will review the current understanding of the underlying molecular mechanisms. *Drosophila* phototransduction is the most studied G-protein-coupled signalling cascade and widely used model to explain invertebrate and microvillar visual transduction (Montell, 1989; Ranganathan, Malicki and Zuker, 1995; Hardie and Raghu, 2001; Hardie and Postma, 2008). Assuming these photochemical reactions also occur in *Musca* photoreceptors, I will consider the potential molecular mechanisms underpinning light adaptation.

Light is a flux of photons. Photoreceptors are considered (linear) photon counters up to moderately bright daylight intensities when microvillar refractoriness and intracellular Ca^{2+}-dependent pupil mechanisms kick in (Kirschfeld and Vogt, 1980; Howard, Blakeslee and Laughlin, 1987; Song et al., 2012; Juusola et al., 2017). Photon absorption photoisomerises the visual pigment, rhodopsin, to its active metarhodopsin state. Metarhodopsin then catalyses the activation of a heterotrimeric G-protein, causing the GDP/GTP exchange. The G-protein (G_q) activates phospholipase C (PLC), which hydrolyses phosphatidylinositol 4,5-bisphosphate (PIP_2), finally culminating in the opening of two classes of highly Ca^{2+}-permeable light-sensitive channels, TRP (encoded by the transient receptor potential gene, *trp*) and TRPL (encoded by the *trp*-like gene). The light-induced current (LIC) that depolarises the photoreceptor is a result of Ca^{2+} (calcium), Na^{+} (sodium) and Mg^{2+} (magnesium) influx, arising from the light-sensitive channel openings (Hardie and Raghu, 2001; Hardie and Postma, 2008).

Early genetic studies on *Drosophila* demonstrated that latency distribution is determined by the cascade components upstream of PLC (including PLC), whereas the QB amplitude is possibly regulated downstream of PLC (Pak et al., 1976; Bloomquist et al., 1988; Scott et al., 1995; Scott and Zuker, 1998). Both QB shape (amplitude and duration) and latency distribution are independently mediated by Ca^{2+}, with the QB shape being most dependent on it (Henderson, Reuss and Hardie, 2000). The QB amplitude and duration decreased to increasing mean light intensity due to the negative feedback mediated by Ca^{2+} - brightening increases calcium influx to the microvilli, which inhibit the TRP (and TRPL) channels, causing gain reduction (Juusola and Hardie, 2001a; Hardie and Postma, 2008; Hardie, 2011). Moreover, brightening depolarises the photoreceptor and, thus, the electromotive driving force (through TRP and TRPL channels) also impacts the QB size reduction (Song et al., 2012; Song and Juusola, 2017).

3.4.4 Ecological impact – *Musca* and *Drosophila* light adaptation

The project included unravelling different visual coding aspects (both temporal and spatial) in *Musca*. Although *Drosophila* is the go-to species for studying invertebrate vision, I felt *Musca* could provide new insights due to their different lifestyle and habitat. *Musca*'s data could then be compared with *Drosophila* to see where their visual differences lie; and if their unique ecologies would reflect these.

The *Musca* R1-R6 photoreceptor results of this chapter are broadly consistent with the knowledge about visual encoding from *Drosophila* (Juusola and Hardie, 2001a) and *Limulus* (Wong and Knight, 1980; Wong, Knight and Dodge, 1980). Although the tested mean light intensity range differed slightly from the *Drosophila* study (Juusola and Hardie, 2001a), *Musca* QBs were faster and smaller and had briefer latencies than *Drosophila* (*Musca*: **Figure 3-4C** and **3-5** *Drosophila:* Juusola and Hardie, 2001a). Two critical factors in their photoreceptor biophysics can explain these results: the number of microvilli and phototransduction speed. As *Musca* is a bigger fast-flying diurnal carnivore, it has about 2-times more microvilli (~60,000 in a *Musca* R1-R6 vs ~30,000 in a *Drosophila* R1-R6) and faster temporal resolution (faster phototransduction giving faster response dynamics and shorter integration time) (Laughlin and Weckström, 1993; Skingsley, Laughlin and Hardie, 1995; Weckström

and Laughlin, 1995). Thus, R1-R6 photoreceptors' information rates are consistently higher in *Musca* than *Drosophila* (*Musca*: **Figure 3-2** *Drosophila:* Juusola and Hardie, 2001a).

Another interesting discrepancy between the two species was seen in the QB latency distribution variation to different mean light levels. *Musca* QB latency distribution was more affected by the mean light intensity, getting briefer with brightening (**Figure 3-5D**), and staying constant only for the three brightest backgrounds. Whereas in *Drosophila*, the latency distributions remained more constant throughout the tested light backgrounds (apart from the dimmest, which was noisy) (Juusola and Hardie, 2001a). Whilst some of these differences may reflect the different light stimuli and setups used, it is more likely that the differences were physiological.

3.4.5 Constraints in analysing LMCs' adapting "histamine" QBs

Photoreceptor-interneuron synapses have been studied extensively in the past, providing insights into how the early insect vision functions (Scholes, 1969; Laughlin, 1973; Shaw, 1981; Dubs, 1982; van Hateren, 1992b; Juusola et al., 1995; Juusola, Uusitalo and Weckström, 1995; Uusitalo, Juusola and Weckström, 1995; Nikolaev et al., 2009; Zheng et al., 2009). Visual information from the optically superimposed R1-R6 photoreceptors from adjacent ommatidia is transmitted to L1-L3 LMCs and amacrine cell (Am) (Meinertzhagen and O'Neil, 1991; Rivera-Alba et al., 2011). This feedforward pathway is histaminergic, and thus, inhibitory (Hardie, 1987; Hardie, 1989; Sarthy, 1991; Pantazis et al., 2008). Presynaptic photoreceptor voltage fluctuations cause quantal histamine release, which is then sampled by Cl^--channels on the postsynaptic LMC membrane. These ligand-biding dynamics govern the channel opening probability, causing Cl^--influx that hyperpolarises the LMC (Hardie, 1989). Even in darkness, the synaptic release is tonic (Uusitalo et al., 1995).

This chapter's main focus was light-adaptational changes in photoreceptor and LMC response dynamics, thus I will discuss the first synapse from this perspective. LMCs are commonly considered adaptive spatiotemporal filters that maximise information transfer to downstream neurons (van Hateren, 1992a; van Hateren, 1992b; Juusola, Uusitalo and Weckström, 1995). In dim conditions (i.e. low SNR) the synaptic output

appears low-pass-filtered, yet at bright light (i.e. high SNR), the output appears band- or high-pass-filtered. However, no studies have revealed whether the synaptic (histamine) release adapts to the changing mean light intensities at a single postsynaptic (histamine) QB level, similar to photoreceptor QBs, apart from the theoretical suggestions (Juusola et al., 1995; Juusola et al., 1996).

This question was briefly touched in one doctoral thesis (Li, 2011) where *in vivo* intracellular recordings from *Calliphora* photoreceptors and LMCs were analysed to extrapolate quantal histaminergic transmission during light adaptation. Linear shot-noise analysis was used to extract the histamine QB shape in the same way as I have shown in Chapter 3.3.3. The results showed that the histaminergic QB waveform adapted to the mean light intensities, similar to photoreceptor QBs. More specifically, in dim light conditions, the mean histamine QBs were large and slow, whereas they were smaller and faster at bright light conditions. Although these results were consistent with the pre-existing theory of LMCs operating as adaptive spatiotemporal filters (van Hateren, 1992a; van Hateren, 1992b; Juusola, Uusitalo and Weckström, 1995), this work went deeper by suggesting that the synaptic filtering reflect the underlying adaptive quantal sampling process.

However, the extrapolation of LMC QB dynamics has analytical limitations. LMC output is more phasic than the corresponding photoreceptor output, showing additional nonlinearities (especially at bright light conditions), (Laughlin, Howard and Blakeslee, 1987; Juusola et al., 1994; Juusola et al., 1995; Juusola, Uusitalo and Weckström, 1995) that complicate linear analysis and can make it less reliable. The LMC responses' phasic nature was addressed (in the thesis) by assuming that QBs follow the gamma distribution's first derivative at bright light conditions and the gamma distribution at low light levels. Secondly, the QB amplitude and the rates were more loosely attained by using Campbell's theorem, normalising the QB by its noise variance for an approximate estimation. Finally, because stochastic postsynaptic sampling removes presynaptic noise, it was argued that the LMC noise predominantly reflected postsynaptic binding of the presynaptically released histamine boluses (quanta).

In my results, the LMC noise power spectrum followed a similar trend as photoreceptors. This finding suggests that the histamine QB waveform could change similarly to photoreceptor QBs to brightening mean light intensities (**Figure 3-7C-D**). However, due to the limitations of quantifying the underlying postsynaptic "histamine" QB waveforms and latency distributions, no further analysis was made.

4 Hyperacute resolvability of *Musca* photoreceptors and LMCs

4.1 Introduction

The previous scientific consensus was that flies have rigid, stationary eyes, with relatively low spatial resolution. It was thought their acuity would be limited by (i) their small lenses' diffraction; (ii) rhabdomere dimensions; (iii) interommatidial angle ($\Delta\varphi$) (the smallest separable angle the eye can resolve); (iv) their photoreceptors' slow integration time; (v) the low number of photons and motion blur attributable to their high-speed behaviours (Mallock, 1894; Fermi and Richardt, 1963; Srinivasan and Bernard, 1975; Warrant and McIntyre, 1992; Land, 1997; Warrant, 1999).

However, it seems strange that especially fast-flying flies living in a nonstationary environment would have a low spatiotemporal vision from an evolutionary perspective. So, it is no surprise that experimental research has discovered different ways the fly eyes have evolved to compensate for some of their visual constraints, especially for overcoming motion blur. These adaptations involve a range of biological mechanisms, such as acute zones and the head/thorax countering body movements (Dietrich, 1909; Collett and Land, 1975; van Hateren and Schilstra, 1999; Schilstra and van Hateren, 1999; Hornstein et al., 2000; Burton, Tatler and Laughlin, 2001; Burton and Laughlin, 2003), with different fly species having their own mechanisms.

In *Drosophila,* for instance, recent research (Juusola et al., 2017) found that photoreceptors contract photomechanically, narrowing their receptive fields. They argued that these photomechanical contractions, with the aid of refractory sampling, enables *Drosophila* to have hyperacute vision, allowing them to see tiny objects moving with fast velocities. This study highlighted the dynamic nature of how the photoreceptors sample visual information and the resulting fly vision, more generally. Additional evidence supporting these ideas (unpublished data) used high-speed video imaging to reveal that the direction of the photoreceptors' photomechanical contractions differed throughout the *Drosophila* eye.

Following on from the Juusola et al. (2017) research, I decided to test whether hyperacuity was also present in the vision of the much faster flying housefly (*Musca domestica*). The main aim was to test if its R1-R6 photoreceptors and L1-L3 LMCs can resolve finer details than its compound eye's interommatidial angle ($\Delta\varphi \approx 0.8°$- $3°$) (Beersma, Stavenga and Kuiper, 1975). As in Juusola et al. (2017), I decided to use the interommatidial angle, instead of the acceptance angle ($\Delta\rho \approx 2.3°$- $3.5°$, the photoreceptor's angular sensitivity half-width), because, theoretically, $\Delta\varphi$ gives the smallest unit the eye can see. So using this value is necessary when determining if hyperacuity begins with photoreceptors.

I was also keen to investigate if, due to the photoreceptors' changing photomechanical movement directions throughout the eye, *Musca* photoreceptors and LMCs would display direction selectivity (to any of the four cardinal directions) when testing with hyperacute objects (dots, bars and narrowing gratings). During these investigations, I studied both male and female flies, separately, to see if there was any evidence for enhanced spatial resolution due to sexual dimorphism; as hyperacute perception could potentially be enhanced in the "love spot" (the male's frontal-dorsal acute zone) (Hardie et al., 1981; Land and Eckert, 1985; Perry and Desplan, 2016). Photoreceptor resolvability has never been studied at this extensive level before. Furthermore, there are no previous physiological studies of LMC resolvability, except for one theoretical simulation (Juusola and French, 1997).

I performed *in vivo* intracellular recordings in houseflies' R1-R6 photoreceptors and L1-L3 LMCs to quantify these cells' resolvability using two separate visual stimulus apparatuses: (i) a 25-point LED array and (ii) a digital light projector. First, I quantified the cells' resolvability using a 25-point LED array (Juusola et al., 2017). The used stimulation was performed by having two bright light dots (dot size: 0.7^o) with different angular distances (0.7^o, 1.4^o and 2.1^o) moving in parallel, with two velocities (84 ^{o}/s and 167 ^{o}/s) front-to-back across each studied cell's receptive field. The moving dots separated by an angular distance of 0.7^o were less than the eye's interommatidial angle ($\Delta\varphi$) and, thus, resolving them would suggest hyperacuity. The results initially suggested that *Musca* R1-R6 could resolve two moving dots separated by less than the interommatidial angle ($\Delta\varphi < 0.8°$) and their resolvability was much higher than in *Drosophila* R1-R6 (Juusola et al., 2017).

However, the used light stimulation was suboptimal, especially when exploring LMCs' resolvability. Additionally, the 25-point LED array did not allow me to study the resolvability of different objects moving in different directions. Thus, further investigation was done using a digital light projector; featuring light dots or light bars, instead of the 25-point LED array. The dark-adapted photoreceptors' and LMCs' resolvability was tested to two bright light dots/bars (dot size/bar width: 0.7º) with different angular distances (0.7º, 1.4º, 2.1º, 2.8º, 3.5º, 4.9º and 6.3º) moving with five velocities (10 º/s, 21 º/s, 42 º/s, 84 º/s and 168 º/s) in four different directions (up ↑, down ↓, front-to-back → and back-to-front ←) across the cell's receptive field. Finally, the impact of light adaptation on the cells' resolvability was tested by using a novel light stimulation: moving bar-grating stimuli that dynamically narrowed in time. The width of the bars narrowed from 5º to 0.33º as seen by the fly. This stimulus was tested with five different velocities (6 º/s, 20 º/s, 40 º/s, 60 º/s and 120 º/s) moving in four cardinal directions across the cell's receptive field.

Although the experiments with the moving bright dots/bars initially indicated that some photoreceptors were able to resolve within the hyperacute range, there was no statistically significant evidence supporting hyperacuity. Additionally, even under light adaptation, photoreceptors, in general, were not hyperacute. It should also be noted, the absence of any strong case for hyperacuity was despite testing at velocities much slower than their full flying range due to limitations with the digital light projector. Research shows us that the full velocity range fast-flying flies exhibit, either during saccadic turns or head/body saccades, can exceed even 4,000 º/s (Wagner, 1986a; Wagner, 1986b; Schilstra and van Hateren, 1999; van Hateren and Schilstra, 1999). Given that there was a decline in resolvability across velocities I was able to test, it is extremely hard to imagine that testing with much faster velocities would have yielded any meaningful results.

Somewhat surprisingly, the male "love spot" did not show any enhancement in the resolvability to moving hyperacute dots/bars/narrowing bar-gratings compared to other parts of the eye and the female eye. As research indicates that this would be the most optimal location for resolving fine details, it appears that neither the part of the eye nor the sex of the fly has much of an impact on hyperacuity.

When testing the LMC resolvability (using one long-lasting stable LMC recording), the cell showed clear hyperacuity to two moving dots but significantly weaker hyperacuity to bars. Furthermore, the tested LMC showed clear direction-selectivity for resolving both dots and bars. These results indicate that the early *Musca domestica* vision cannot encode hyperacute features at the level of photoreceptors, but conclusions cannot be drawn regarding LMCs until more research is done.

4.2 Materials and methods

4.2.1 Fly stocks

Adult, wild-type houseflies (*Musca domestica*) were used in the experiments. The housefly larvae/pupae were ordered from a commercial provider (Blades Biological Ltd, Cowden, Kent, UK). The houseflies, cultured in a standard laboratory incubator (60% humidity) at the Department of Biomedical Science, were fed with liver, and sugar water. The flies were kept at ~22 ^{o}C in a 12:12 h light:dark cycle.

4.2.2 *In vivo* intracellular recordings

In vivo intracellular recordings from R1-R6 photoreceptors and L1-L3 LMCs were performed as described in Chapter 2. In the 25-point LED array experiments, the fly's temperature was kept at 25 ± 1 ^{o}C by a feedback-controlled Peltier device. However, when using the digital light projector for the visual stimuli, a feedback-controlled Peltier device was not used, and instead, the recordings were performed at room temperature warmed by the projector (24 ± 1 ^{o}C). This approach was chosen to minimise 50 Hz harmonic noise from the temperature controller during the recordings.

4.2.3 Visual stimuli

Musca photoreceptors' (R1-R6) and LMCs' spatial resolvability to moving objects *in vivo* was tested separately using two different visual stimulators: (i) a 25-point LED array or (ii) a digital light projector.

4.2.3.1 The 25-point LED array

The 25-point LED (light-emitting diode) array was fixed on a rotatable Cardan-arm system and placed 17 cm away from the fly, subtending a viewing angle of 16.73^{o}. Therefore, each (LED) point subtended an angle of ~0.7^{o} with a 0.7^{o} minimum inter-dot-distance (or angular separation) seen by the fly (**Figure 4-1**). Two DA-converter channels were used to run the system (voltage input range: 0 – 10 V): Channel 0 selected the light point/points for the stimulation, and Channel 1 set the intensity of the light point/points. Dark-adapted photoreceptors' (R1-R6) and LMCs' (L1-L3) resolvability was tested using two bright light dots (dot size: 0.7^{o}) with different angular distances (0.7^{o}, 1.4^{o} and 2.1^{o}) moving with two velocities (84 ^{o}/s and 167 ^{o}/s) front-to-

back across each tested cell's receptive field. Furthermore, the cells' voltage responses to one bright dot (dot size: 0.7°) moving with two velocities (84 °/s and 167 °/s) front-to-back across its receptive field were tested. This control stimulation was done to exclude the possibility of voltage responses to two moving light dots being merely temporal responses instead of spatial. For producing the front-to-back moving bright light dot/dots, Channel 0 was driven with an increasing ramp whilst Channel 1 was driven with a 2 V DC signal. The increasing ramp turned one light point, or two adjacent light points, on and off after each other. This sequence created the movement seen by the fly. Additionally, slower velocities (8 °/s, 16 °/s, 23 °/s and 40 °/s) were tested. However, predictably - as such stimuli moved in a slow step-wise manner - the resulting responses consisted of multiple light-on- and light-off-peaks. Thus, only the responses to the fastest velocities were analysed for resolvability.

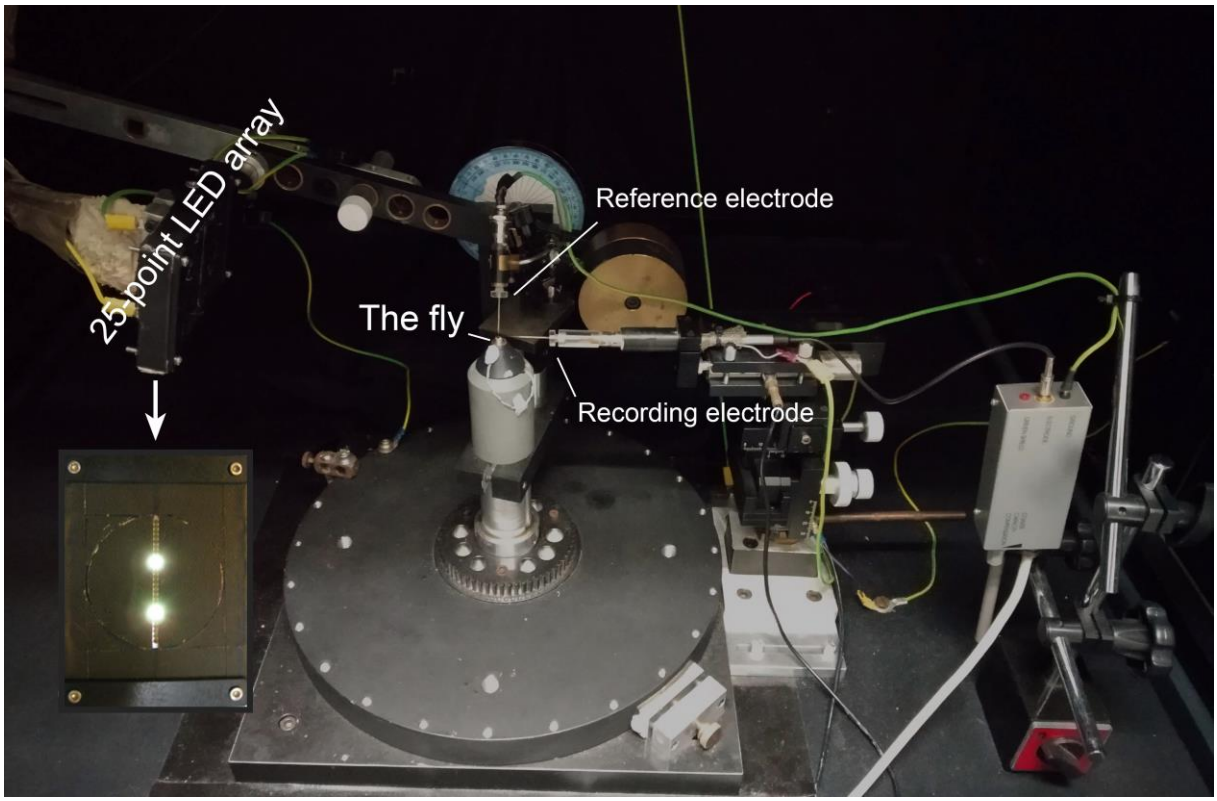

Figure 4-1. *In vivo* intracellular setup using a 25-point LED array for visual stimulation. *Musca* photoreceptors' and LMCs' resolvability to two bright light dots (dot size: 0.7°) with different angular distances (0.7°, 1.4° and 2.1°), moving with two velocities (84 °/s and 167 °/s) front-to-back across its receptive field, was tested using this setup. Additionally, a close-up image (modified from Juusola et al., 2017) from the 25-point LED array showing two bright light dots (moving) 6.8° apart.

A custom-written software system controlled both the stimulus generation and data acquisition, Biosyst in MATLAB (MathWorks, USA) (Juusola and Hardie, 2001a; Juusola and de Polavieja, 2003), with an interface package for National Instruments (Austin, TX) boards (MATDAQ: H. P. C. Robinson, 1997-2005). For more information about the 25-point LED array, see Juusola et al. (2017).

4.2.3.2 The digital light projector

A digital light projector (EKB DLP® LIGHTCRAFTER™ E4500 MKII™, EKB Technologies Ltd, Israel) fixed on a rotatable Cardan-arm system was used for the light stimulation (**Figure 4-2**). The projector had three independent LED sources: UV (385nm), Blue (460nm) and Green (520nm). The 360 Hz UV-stimulation was focused onto a back-projection (diffuser) screen using three close up lenses (ZEIKOS, Japan, model ∅ 68 mm, +10, +5,+1). This system provided a native 912 x 1140 pixel resolution for the fly. The projector can run with 8-bit depth. However, my recordings only required 1-bit depth to turn the pixels on and off. The projector was shielded in copper mesh fabric and grounded to reduce electrical noise contamination during the data acquisition.

The stimuli were produced using the open-access Psychophysics toolbox (http://psychtoolbox.org) in Matlab (MathWorks, USA). A custom-written software system controlled the data acquisition, Biosyst in MATLAB (MathWorks, USA) (Juusola and Hardie, 2001a; Juusola and de Polavieja, 2003), with an interface package for National Instruments (Austin, TX) boards (MATDAQ: H. P. C. Robinson, 1997-2005). Biosyst was synchronised with Lightcrafter (projector software).

Three different visual stimuli were used to test dark-adapted R1-R6 photoreceptors' and L1-L3 LMCs' resolvability: moving dots, bars and narrowing grating stimuli. For the dot stimulation, resolvability was tested using two bright light dots (dot size: 0.7º) with different angular distances (0.7º, 1.4º, 2.1º, 2.8º, 3.5º, 4.9º and 6.3º) moving with five velocities (10 º/s, 21 º/s, 42 º/s, 84 º/s and 168 º/s) across the cell's receptive field. Moreover, to test whether resolvability was affected by the motion direction, the dots were run in four different directions (up ↑, down ↓, front-to-back → and back-to-front ←). The corresponding control recordings used one dot.

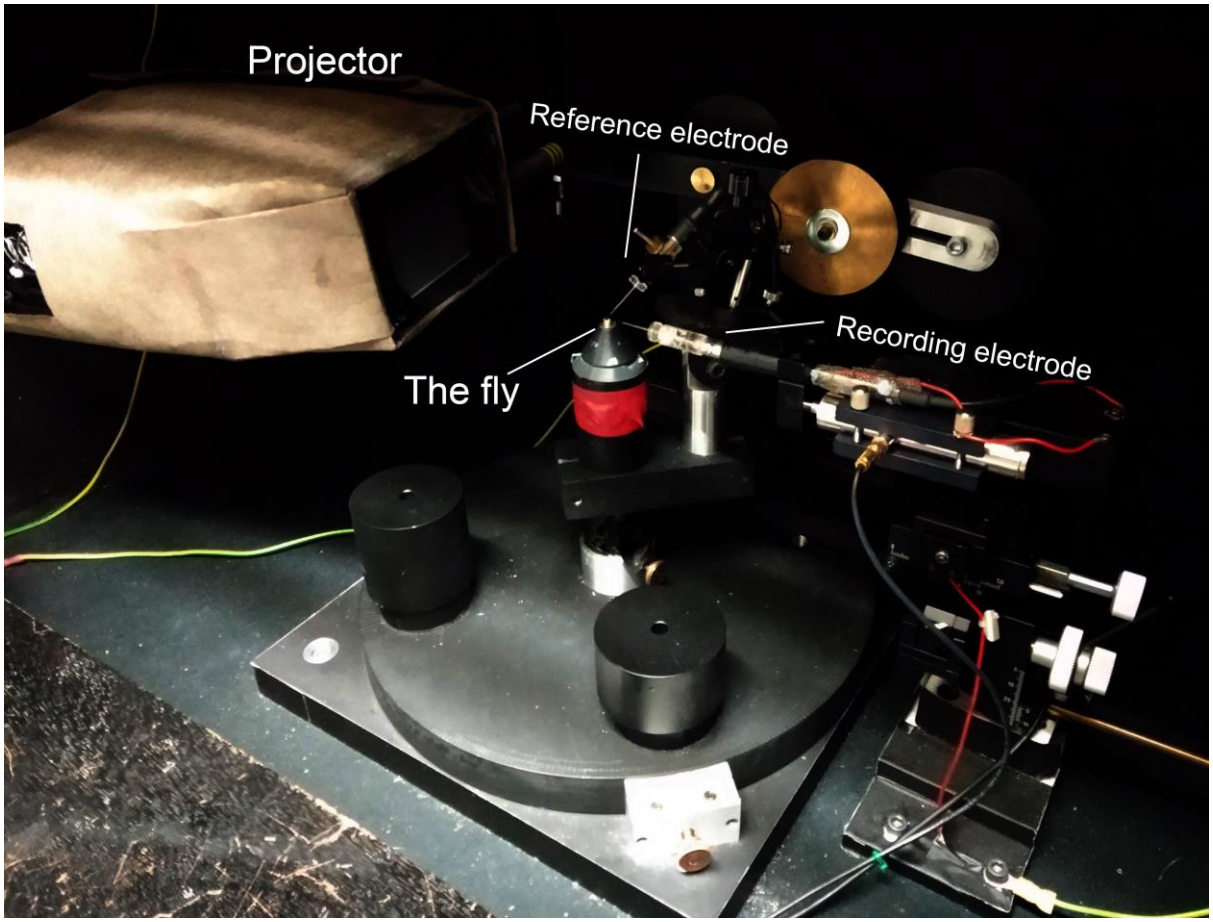

Figure 4-2. *In vivo* intracellular setup using a digital light projector for visual stimulation. *Musca* photoreceptors' and LMCs' resolvability to three different visual stimuli (moving dots, bars and narrowing gratings) were tested using this setup. For dots and bars: two bright light dots/bars (dot size/bar width: 0.7°) with different angular distances (0.7°, 1.4°, 2.1°, 2.8°, 3.5°, 4.9° and 6.3°) moving with five velocities (10 °/s, 21 °/s, 42 °/s, 84 °/s and 168 °/s) across the cell's receptive field. This was tested by stimulus moving in four cardinal directions (up ↑, down ↓, front-to-back → and back-to-front ←). Furthermore, the voltage responses to one moving dot/bar were tested with the same velocities and the four directions mentioned earlier. The impact of light adaptation was investigated using the moving dynamically narrowing grating stimulus that continuously decreased its wavelength (i.e. the two-bar distance) from 5° to 0.33° as seen by the fly. This stimulus was tested for five different velocities (6 °/s, 20 °/s, 40 °/s, 60 °/s and 120 °/s) moving in four cardinal directions (up ↑, down ↓, front-to-back → and back-to-front ←) across the cell's receptive field.

The experiments using the bars were performed the same way as with dots but now having two bright bars (bar width: 0.7°) with different angular distances (0.7°, 1.4°, 2.1°, 2.8°, 3.5°, 4.9° and 6.3°) moving with five velocities (10 °/s, 21 °/s, 42 °/s, 84 °/s and 168 °/s) across the cell's receptive field. Again, the direction selectivity was tested

in four cardinal directions (up ↑, down ↓, front-to-back → and back-to-front ←). Recordings were repeated using the one bar controls.

Moving narrowing bar-grating stimulus was used to test the resolvability under light adaptation, which narrows the photoreceptors' receptive field, enabling higher resolvability (Stavenga, 2004; Juusola et al., 2017). The grating continuously decreased its wavelength (i.e. the inter-bar width) from 5° to 0.33°, as seen by the fly (**Figure 4-3A-C**).

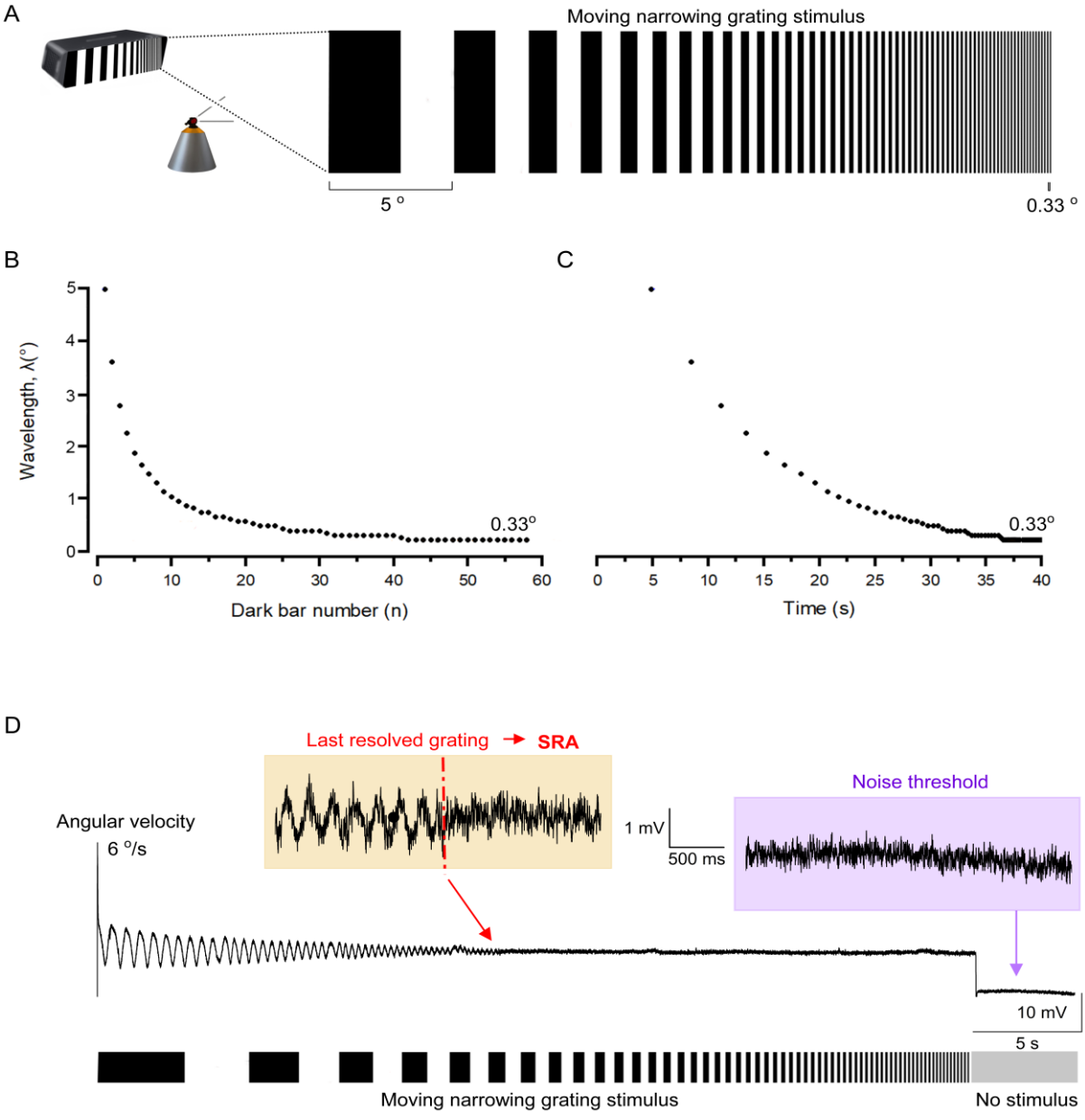

Figure 4-3. The four-parameter bar-grating stimulus for testing photoreceptors' resolvability (smallest resolved angle, SRA). (A) The moving narrowing grating was used to test R1-R6 resolvability under light adaptation. **(B)** The grating (its bar width) continuously decreased from 5° to 0.33°, as seen by the fly. **(C)** The same as in **B**, but shown against the time the stimulus requires to run. **(D)** An example of a photoreceptor's voltage response to a narrowing grating stimulus moving with an angular velocity of 6 °/s. The resolvability was estimated by determining the SRA from the voltage response. One of the main limiting factors for resolvability is the noise level acquired when the projector is on without any stimulus. The cell was deemed not to resolve the grating when its peak amplitudes became smaller than the noise threshold.

The stimulus was programmed by Keivan Razban Haghighi in MATLAB (MathWorks, USA) using a novel four-parameter bar-grating definition. The four parameters were the speed (*s*), motion direction (θ), starting wavelength (λ_0 = 5°) and the last wavelength (λ_1 = 0.33°). The inter-bar wavelength (i.e. the angular distance of the bars) over time followed a geometric sequence:

$$\lambda(t+dt) = \left(\frac{\lambda_1}{\lambda_0}\right)^{1/D} \lambda(t) = \lambda_0 \left(\frac{\lambda_1}{\lambda_0}\right)^{t/D}, \quad (4\text{-}1)$$

where *D* is the duration of the stimulus, each intracellularly recorded cell was simultaneously presented the moving narrowing grating with five different velocities (6 °/s, 20 °/s, 40 °/s, 60 °/s and 120 °/s) in four cardinal directions (up ↑, down ↓, front-to-back → and back-to-front ←) across its receptive field.

4.2.4 Data analysis

4.2.4.1 Resolvability of two moving light points using the 25-point LED array

Each stimulus was repeated 20-30 times. Only the steady-state adapted responses were analysed and, therefore, the first 5-10 responses to the repeated stimulation were discarded. The resolvability (R) for the two moving bright dot recordings was calculated by using the Rayleigh criterion (Born and Wolf, 1999):

$$R = \frac{d}{P}\%, \quad (4\text{-}2)$$

where *P* is the amplitude of the larger peak (most often the first peak) and *d* is the depth of the dip between the two peaks in the voltage response (**Figure 4-4**). Two separate peaks in the voltage response indicated that the dots were resolved neurally. Conversely, if the response had a single peak, the dots were not neurally resolved. Some cells' resolvability changed over time between the stimulus repetitions. So the total resolvability was calculated by averaging each repetition's resolvability (**Figure 4-7**).

4.2.4.2 Resolvability of two moving light dots/bars using the digital light projector

Each recording from photoreceptors and LMCs, using either dots or bars, were repeated only once. The resolvability was calculated using the Rayleigh criterion (Born and Wolf, 1999) (**Equation 4-2** and **Figure 4-4**).

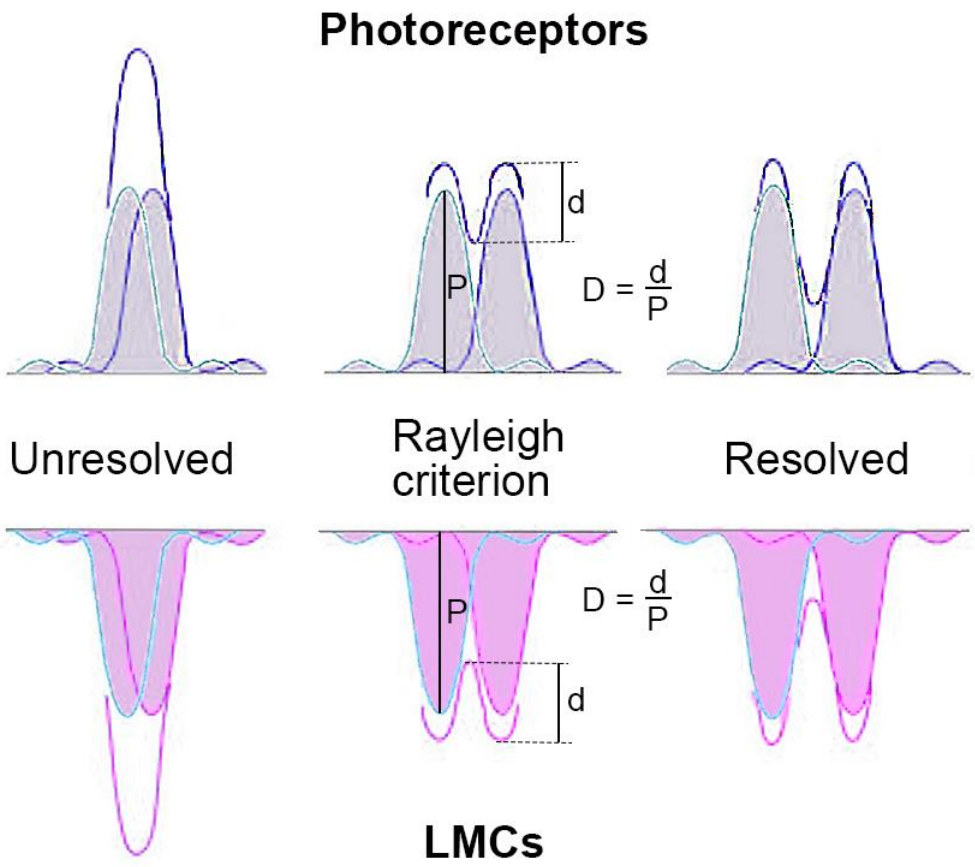

Figure 4-4. Applying the Rayleigh criterion for calculating photoreceptors' and LMCs' resolvability to two moving dots/bars. Photoreceptors depolarise to light increments (two bright dots/bars), whereas LMCs hyperpolarise to the same stimulus. Nonetheless, if the voltage response had just one superimposed peak, the moving two dots/bars were not neurally resolved. However, if the voltage response consisted of two separate peaks, the Rayleigh criterion was used to determine the cell's resolvability.

4.2.4.3 Smallest resolvable angle (SRA) when using moving narrowing bar-grating

For the moving narrowing grating (consisting of bars) stimulus, the resolvability was estimated by determining the smallest resolvable angle (SRA) from the voltage response. This measure was achieved by feeding the voltage response as an input to a six hyperparameter algorithm in Python (written by Keivan Razban Haghighi), which then returned the SRA as the output (**Figure 4-3D**). In the algorithm, the resolvability was calculated using the Rayleigh criterion (Born and Wolf, 1999):

$$R = \frac{P_{min} - T}{P_{max} - T}, \tag{4-3}$$

where T is the trough and P_{min} and P_{max} are the smallest and highest peak, respectively. Two of the six parameters (noise threshold and inter-peak noise threshold) determine the peak detection accuracy from the voltage response. The first requirement for a successful peak detection is that $P_{min} - T >$ noise threshold, otherwise $R = 0$ (the cell does not resolve the grating at that time point). Another requirement is that the inter-peak noise < inter-peak noise threshold, otherwise $R = 0$. Two other parameters are used to detect false negatives, while the remaining two parameters determine the last pair of peaks that are resolved ($R > 0$) and give the SRA as the output.

4.2.5 Statistics

Statistical analyses were carried out in Prism 9 (Graphpad) and MATLAB. The differences between male and female resolvability to two moving bright dots (**Figure 4-6**) and photoreceptors' resolvability to moving dots/bars (**Figure 4-10** and **Figure 4-13**) were compared using either parametric (unpaired or paired two-tailed t-test) or non-parametric tests (Mann-Whitney, Friedman or Wilcoxon signed-rank test)

depending on whether the raw data passed the Kolmogorov-Smirnov normality test. For unpaired t-test, if the two compared data sets had different variances, Welch's correction was applied. When required, power analysis was performed to confirm that the sample sizes were sufficient for the used statistical test.

4.3 Results

4.3.1 Photoreceptors' resolvability using the 25-point LED array

I aimed to test whether *Musca* R1-R6 photoreceptors can resolve small objects moving with different velocities. Specifically, I asked could these cells resolve moving light dots, which were less than the 0.8º interommatidial angle apart? *In vivo* intracellular recordings were performed from individual R1-R6s while exposing the fly to bespoke stimuli, consisting of two bright dots (dot size: 0.7º) with different inter-dot-distances (0.7º, 1.4º and 2.1º), moving with two velocities (84 º/s and 167 º/s) across the tested photoreceptor's receptive field (**Figure 4-5A-B**). Here, only the 0.7º inter-dot-distance stimuli were less than the *Musca* compound eye's interommatidial angle ($\Delta\varphi \approx 0.8^{o} – 3^{o}$). The two moving bright dots were created using the 25-light-point array by rapidly turning each of its light points on and off, one after another, in the front-to-back direction.

Resolvability (R) was calculated using the Rayleigh criterion (**Figure 4-4**). Two peaks in the voltage response showed that the dots were resolved neurally, while a single peak indicated this was not the case.

When testing with the slower velocity (84 º/s), almost all the *Musca* photoreceptors (14 out of 15) resolved the two dots at the hyperacute range (0.7º angular separation) (**Figure 4-5C-D**). However, increasing the stimulus speed to 167 º/s, reduced the resolvability significantly with only 3 out of 15 photoreceptors resolving dots with 0.7º separation (**Figure 4-5E-F**). **Figure 4-5A-B** shows a widespread R1-R6 response to this type of stimuli, but in some cases, the resolvability was extremely good, as shown in **Figure 4-5C** and **E**. Note that due to the limited number of one bright dot (dot size: 0.7º) experiments, it was not possible to perform statistical analysis to rule out that these peaks were merely temporal responses caused by the LEDs going on and off.

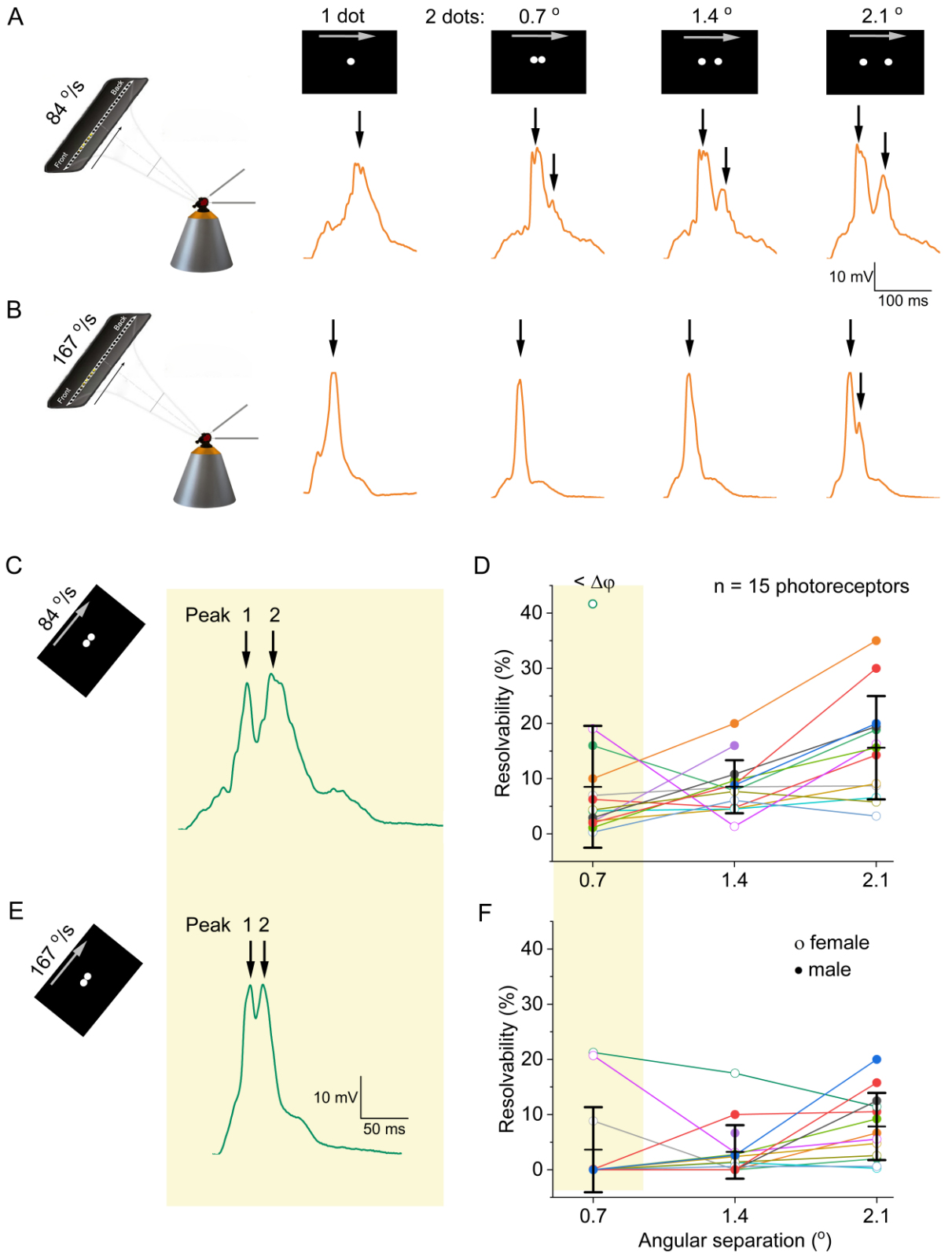

Figure 4-5. *Musca* photoreceptors' resolvability to two moving bright dots using the 25-point LED array. *In vivo* intracellular recordings were performed from R1-R6 while simultaneously showing the fly visual stimuli of two bright dots (dot size: 0.7º) with different inter-dot-distances (0.7º, 1.4º and 2.1º), moving front-to-back **(A)** with a velocity of 84 º/s or **(B)** 167 º/s across its receptive field. Additionally, responses to one bright dot (dot size: 0.7º) were measured using both velocities. Note that

only the dots with 0.7º angular separation was considered hyperacute. **(C)** The resolvability (R) was calculated using the Rayleigh criterion. Two peaks in the voltage response indicate that the dots were resolved neurally, whereas a single peak indicates that the dots were not neurally resolved. Some cells responded exceptionally well to the hyperacute objects moving with 84 º/s speed (showing the best response recorded from one photoreceptor). **(D)** Calculated resolvability (velocity of 84 º/s) of all the recorded photoreceptors (n = 15), mean ± SD. **(E)** Few cells responded exceptionally well to the hyperacute objects moving with 167 º/s (the same photoreceptor as in **C**). **(F)** Calculated resolvability (velocity of 167 º/s) of all the recorded photoreceptors (n = 15 photoreceptors), mean ± SD. The arrows point out the peaks in the voltage response that determine whether the two bright dots were resolved (two peaks = resolved, one peak = not resolved). The photoreceptor coloured orange in **A** and **B** and the photoreceptor coloured dark green in **C** and **E** can be identified using the same colour in figures **D** and **F**. In **C** to **F**, the yellow box indicates the angular separation that is considered hyperacute.

To explore to what extent, if any, sexual dimorphism was responsible for the distinct differences in resolvability, I analysed the data by sex (**Figure 4-6**). I found no differences between the male and female resolvability across both velocities when the angular separation was smaller than the interommatidial angle (< 0.8º). However, when the separation was wider (1.4º and 2.1º), males could resolve significantly better than females (**Figure 4-6B**). This finding was even more pronounced when testing with the slower velocity.

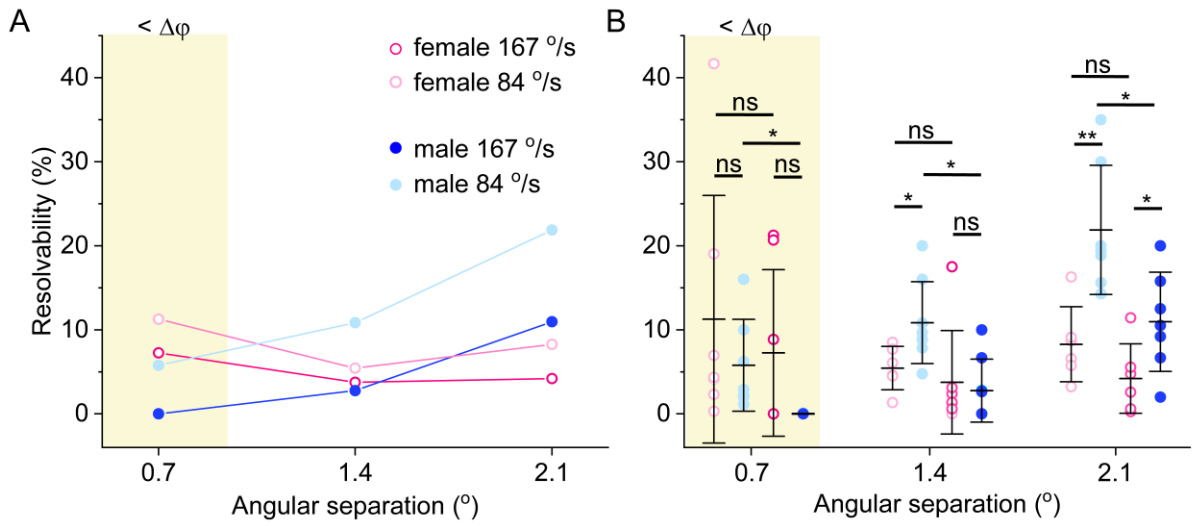

Figure 4-6. Differences between male and female resolvability to two moving bright dots. (A) Male and female average resolvability to two bright dots (dots size: 0.7º) with three different angular separations (0.7º, 1.4º and 2.1º) moving front-to-back with two different velocities (84 º/s and 167 º/s). Only the dots with 0.7º angular separation was considered hyperacute (yellow box). **(B)** There were no significant differences between male and female photoreceptors' resolvability to hyperacute dot

separation. However, males better resolved the dots with larger angular separations (1.4° and 2.1°) when the dots moved slower. Unpaired two-tailed t-test with Welch's correction or Mann-Whitney U test used when comparing the male photoreceptor resolvability to that of the females, mean ± SD, *P < 0.05, **P < 0.01. Paired two-tailed t-test or Wilcoxon signed-rank test used when comparing the same sex at different velocities, mean ± SD, *P < 0.05. Number of recorded photoreceptors: n♀ = 7 and n♂ = 8 for both of the tested velocities.

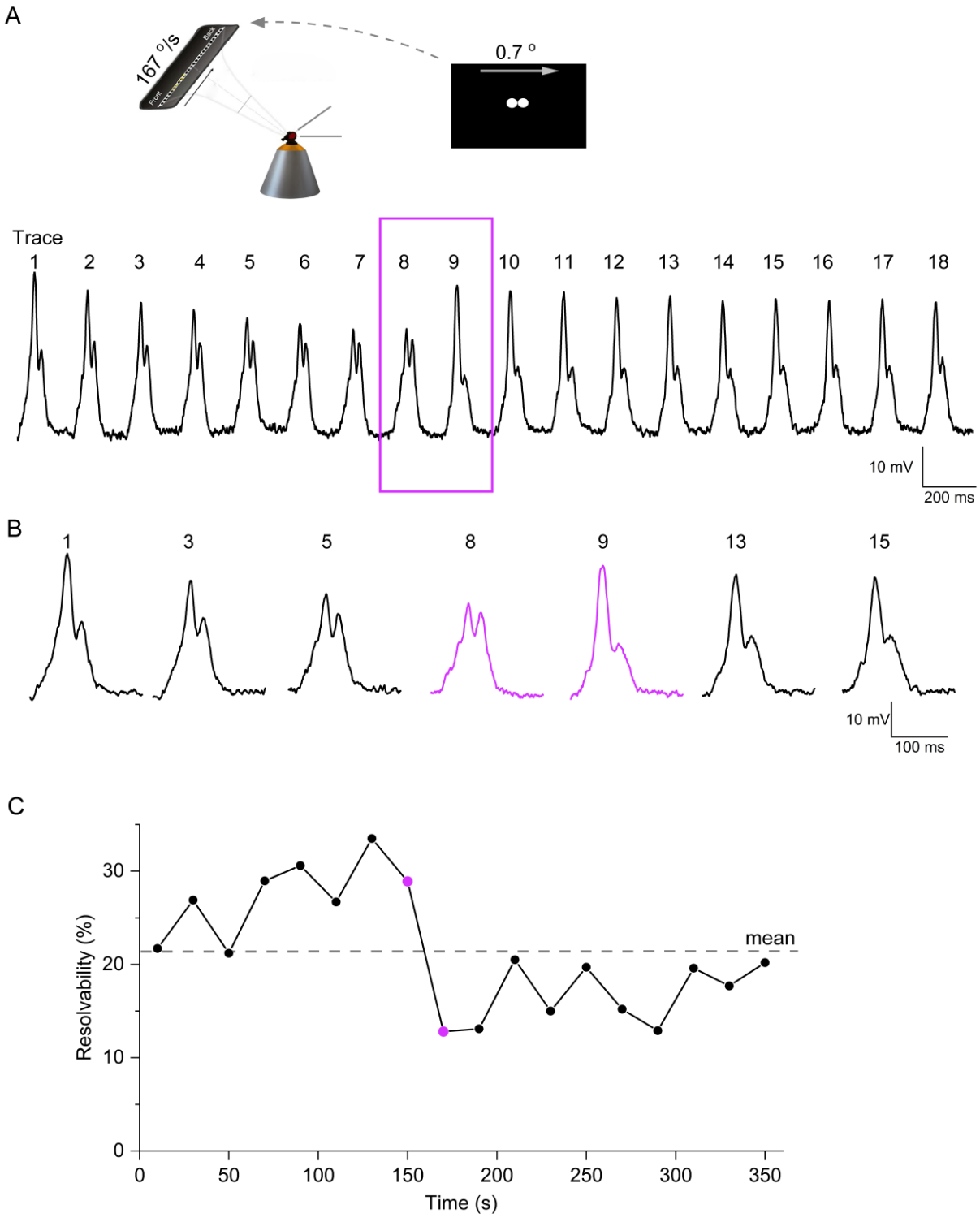

Figure 4-7. Photoreceptor's resolvability changes dynamically in time. (A) R1-R6 photoreceptor's voltage responses to two moving bright dot stimuli (with 167 °/s speed and 0.7° inter-dot-distance) repeated one after another (showing n = 18 traces). **(B)** Some example traces highlighted from **A** show the change in resolvability. **(C)** Calculated resolvability in time for the photoreceptor. The mean resolvability is approximately 21%. However, the response dynamics were highly nonstationary. The same photoreceptor is shown in **Figure 4-6D** and **F** (magenta trace).

It is important to note that some recorded photoreceptors had highly nonstationary response dynamics (**Figure 4-7**), possibly suggesting active vision. Sometimes the photoreceptor's optical axis moved in the middle of the experiments (for the shown cell, between traces 8 and 9), which caused a drop in the resolvability (**Figure 4-7B**). Such changes could result from intrinsic intraocular muscle activity. Nevertheless, the photoreceptor could resolve the dots in all the trials (**Figure 4-7C**), having a mean resolvability of ~21%. Because of such dynamic (intrinsic) modulation, the resolvability was calculated for each repetition separately, and the mean of them was then used to describe the photoreceptor's total resolvability.

4.3.2 LMCs' resolvability using the 25-point LED array

After finding some evidence that photoreceptors could resolve small dots closer than the interommatidial angle, I aimed to explore whether this was also the case for L1-L3 LMCs. LMCs could have better resolvability than photoreceptors to rapidly moving objects because LMCs receive similar input from six outer photoreceptors and, thus, the signal-to-noise ratio could improve up to $\sqrt{6}$ -fold (Braitenberg, 1967; Kirschfeld, 1967; de Ruyter van Steveninck and Laughlin, 1996; Zheng et al., 2006). Besides, lateral inhibition occurs in lamina neurons, narrowing their receptive fields and improving their resolvability (Reichardt and Poggio 1976; Srinivasan et al., 1990).

There has been no prior experimental research on LMC acuity, except a theoretical study from Juusola and French (1997). Using *Calliphora vicina,* they simulated how photoreceptors and LMCs might resolve moving two-point objects with different angular distances in different light conditions. These simulations did not reveal hyperacuity, possibly due to several factors, such as being based upon a low recording temperature (16-18 °C) and not considering lateral inhibition.

While performing *in vivo* intracellular recordings, I tested the LMCs' resolvability to two bright dots with different inter-dot-distances (0.7º, 1.4º and 2.1º), moving with two velocities (84 º/s and 167 º/s) in the front-to-back direction across its receptive field, using the 25-light-point array (**Figure 4-8A-B**). Here, only the 0.7º inter-dot-distance stimuli were finer than the *Musca* compound eye's interommatidial angle ($\Delta\varphi \approx 0.8^{\circ}$ - 3°). Additionally, LMCs' responses to one bright dot (dot size: 0.7º) moving with the same velocities were measured to rule out that these peaks were temporal responses to LEDs turning on and off.

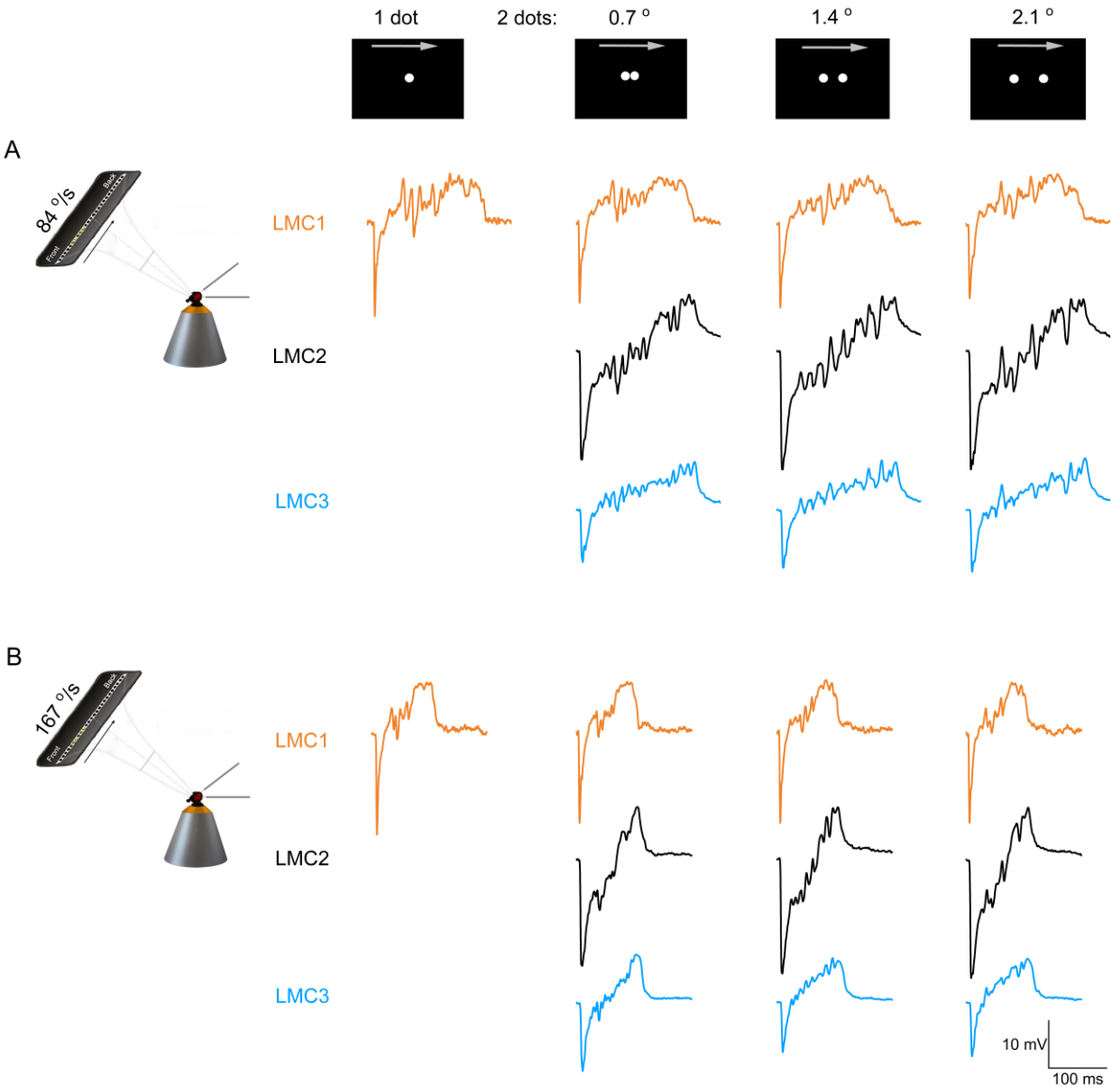

Figure 4-8. *Musca* LMCs' resolvability could not be attained using the 25-point LED array. The LMCs' (n = 3) resolvability was tested using two bright dots with different inter-dot-distances (0.7º, 1.4º and 2.1º), moving with two velocities **(A)** 84 º/s and **(B)** 167 º/s in the front-to-back direction across its

receptive field. Additionally, LMCs' responses to one bright dot (dot size: 0.7º) moving across its receptive field, was tested. Comparing the voltage responses for one dot and two dots suggested that the fluctuations in the responses might be produced by the LEDs turning on and off. Thus, LMCs hyperacuity could not be tested using this type of stimulation.

Unfortunately, this light stimulation was not sufficient to record the resolvability in LMCs. This finding may result from LMCs having faster temporal responses, which meant they likely responded to the LEDs turning on and off (**Figure 4-8**), as suggested by comparing the one-moving-dot LMC responses to the responses evoked by two moving dots. Because of this stimulation method's spatiotemporal and directional limitations, I later began using a digital light projector rather than the 25-point LED array as a more suitable stimulus for LMCs as well photoreceptors.

4.3.3 Photoreceptors' resolvability to moving light dots using a digital light projector

The digital light projector stimulator system enabled more detailed resolvability studies, using different objects (light dots, light bars, narrowing gratings) with a wider variety of angular separations (0.7º, 1.4º, 2.1º, 2.8º, 3.5º, 4.9º and 6.3º) and velocities (10 º/s, 21 º/s, 42 º/s, 84 º/s and 168 º/s) (**Figure 4-9A-E**). Again, only the 0.7º angular separation was considered hyperacute. Additionally, the projector system enabled changing the objects' movement direction (up ↑, down ↓, front-to-back → and back-to-front ←) to test whether *Musca* photoreceptors are direction-selective to the hyperacute features.

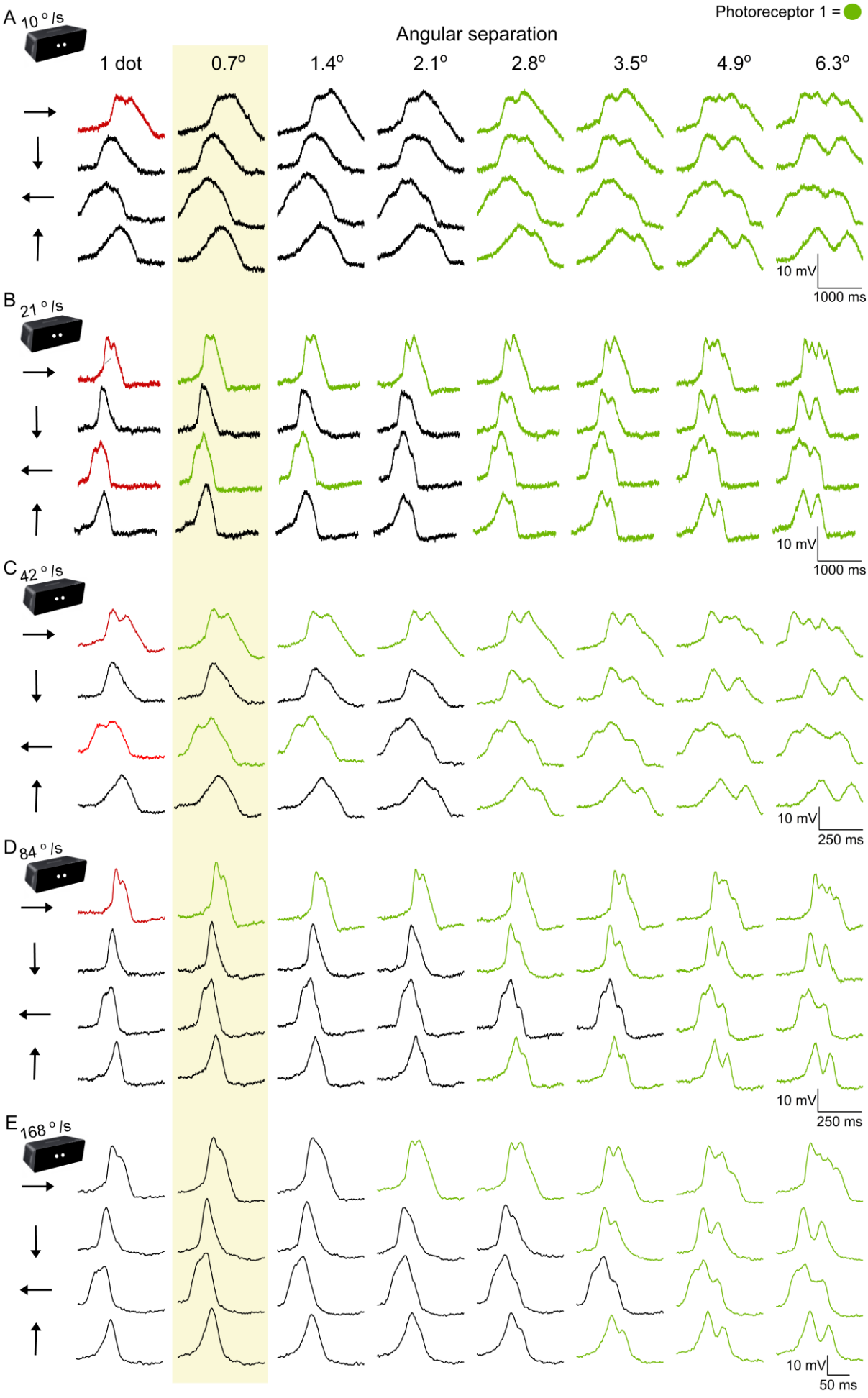
A 10 °/s
B 21 °/s
C 42 °/s
D 84 °/s
E 168 °/s
Photoreceptor 1 =
Angular separation
1 dot
0.7°
1.4°
2.1°
2.8°
3.5°
4.9°
6.3°
10 mV
1000 ms
10 mV
1000 ms
10 mV
250 ms
10 mV
250 ms
10 mV
50 ms

Figure 4-9. Dark-adapted *Musca* photoreceptor's voltage responses to one or two moving bright light dots with a broad range of angular separations and velocities. (A) Photoreceptor's intracellularly recorded voltage responses to one dot or two dots with different angular separations (0.7°, 1.4°, 2.1°, 2.8°, 3.5°, 4.9° and 6.3°) with a velocity of 10 °/s tested in four different directions (up ↑, down ↓, front-to-back → and back-to-front ←). Dot/dots were moving with a velocity of **(B)** 21 °/s, **(C)** 42 °/s, **(D)** 84 °/s and **(E)** 168 °/s. Only the angular separation of 0.7° was considered hyperacute (yellow box). Green traces indicate angular separations, which the photoreceptor was able to separate. Additionally, the red traces indicate the double-peaked voltage response to only one moving dot. The photoreceptor is named photoreceptor #1 and can be identified in **Figure 4-10**. The same photoreceptor's responses to one bar/two bars are shown in **Figure 4-12** and **Figure 4-13**.

The digital light projector was used to examine both photoreceptors' and LMCs' resolvability, but here I will only talk about R1-R6 photoreceptors' responses to bright dots before moving onto bright bars and narrowing gratings. LMC data will be discussed in Chapters 4.3.6 and 4.3.7. Interestingly, with photoreceptors (n = 28), only very few (six photoreceptors at 10 °/s and one at 168 °/s) could resolve two moving dots with a 0.7° angular separation across all the tested velocities (**Figure 4-10A-E**). This should not be viewed as compelling evidence of hyperacuity, however, as photoreceptors' voltage responses also had two peaks to one moving dot (dot size: 0.7°) (**Figure 4-9**, **red traces**). Therefore, to rule out the possibility of the two-peaked responses being merely a result of the biphasic temporal modulation (on-off) to one dot moving across the photoreceptor's receptive field, statistical comparisons (Friedman test with Dunn's multiple comparisons test) looking at the resolvability of each angular separation against the respective one moving dot control were performed. Conclusions from the statistical analysis showed that photoreceptors' resolvability to dots with 0.7° angular separation was not significant and therefore, hyperacuity was not demonstrated for this type of stimulation (**Figure 4-10A-E**). In addition, for all the tested velocities, resolvability to dots with 1.4° angular separation did not significantly differ from the respective one dot resolvability. In general, the resolvability became worse for angular separations < 2.8° as the velocity increased.

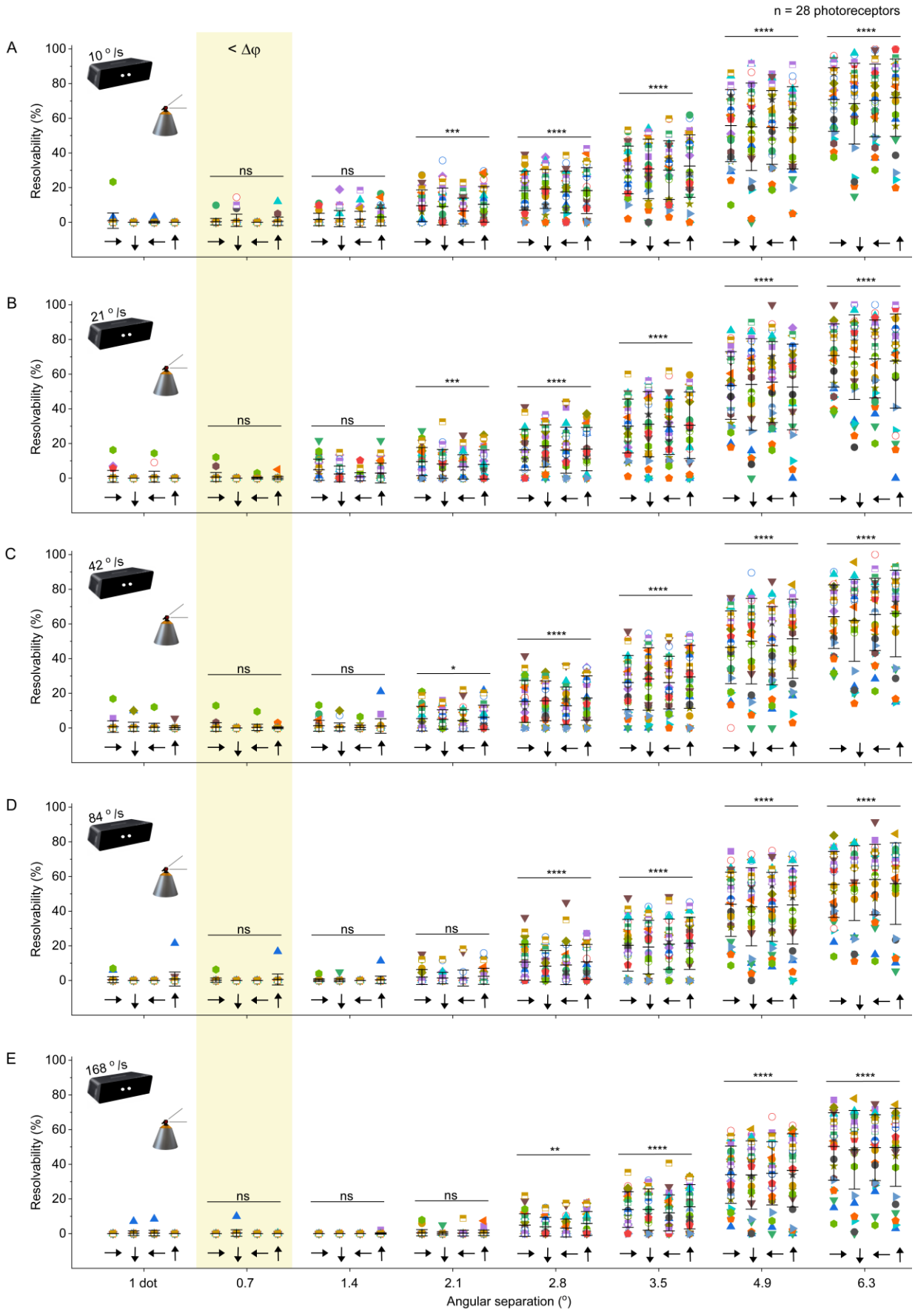
n = 28 photoreceptors
A
10 °/s
< Δφ
B
21 °/s
C
42 °/s
D
84 °/s
E
168 °/s
Resolvability (%)
ns
*
**
***
****
1 dot
0.7
1.4
2.1
2.8
3.5
4.9
6.3
Angular separation (°)

Figure 4-10. Photoreceptors' resolvability to two moving bright light dots. *Musca* photoreceptors' (n = 28) resolvability to one dot/two dots with 0.7º, 1.4º, 2.1º, 2.8º, 3.5º, 4.9º and 6.3º separation moving in four different directions (up ↑, down ↓, front-to-back → and back-to-front ←) with a velocity of **(A)** 10 º/s, **(B)** 21 º/s, **(C)** 42 º/s, **(D)** 84 º/s and **(E)** 168 º/s. Only the angular separation of 0.7º was considered hyperacute (yellow box). Mean ± SD. Statistical comparisons of resolvability to each angular separation were made against the respective one moving dot control: *P < 0.05, **P < 0.01, ***P < 0.001, ****P < 0.0001, Friedman test with Dunn's multiple comparisons test. The same photoreceptor is shown by a unique colour and shape combination throughout this figure and **Figures 4-13** and **4-15**.

As for direction selectivity, those photoreceptors that could resolve did not always do so in all tested directions (only to one or to its reverse direction). For instance, the photoreceptor shown in **Figure 4-9** had better resolvability to front-to-back (→) direction than any other tested. Statistical analysis was performed to find out if the apparent preference for certain directions was of significance. This proved not to be the case when directions at each angular separation were compared to one another.

Going back to hyperacuity, although only a small minority of photoreceptors showed a two-peaked voltage response at 0.7º angular separation, I wanted to investigate whether or not there were any differences between the different parts of the eye. If all the gathered responses did come from the same location (for example, where the interommatidial angle is the smallest) then this would suggest that there is a hyperacute zone within the eye. As such, I performed separate intracellular recordings from the back, middle and front of the eye, doing so for both males and females (**Figure 4-11A**). Note that based on how I chose to divide the eye, the male "love spot" is located in the middle. Dividing the results further by sex enabled me to see any potential influence of sexual dimorphism on the acquired photoreceptors' resolvability.

When looking at males and females separately, there was no significant enhancement across the different locations in the eye, regardless of the velocity the two dots were moving (**Figure 4-11B-F**). Although neither sex showed any location preference, there were some differences between them. None of the tested male photoreceptors could separate the dots beyond 21 º/s, whereas a few female photoreceptors managed to resolve them up to 168 º/s. Given the limited number of photoreceptors being compared, this data should be treated with some caution.

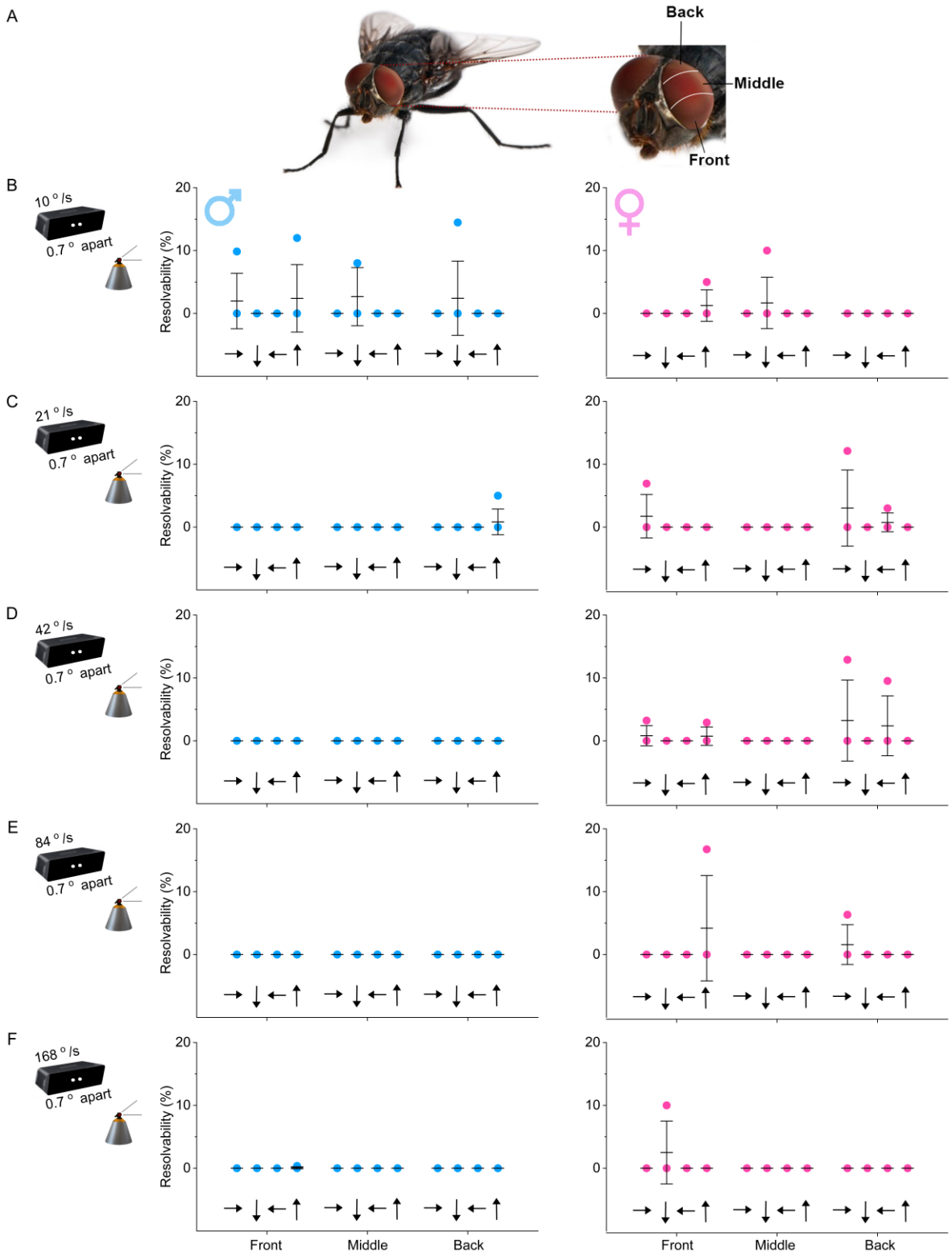

Figure 4-11. Comparing photoreceptors' hyperacute resolvability to two moving bright dots across the whole compound eye between males and females. (A) *In vivo* intracellular recordings were performed from *Musca* photoreceptors from different eye locations (front, middle, back). The male "love spot" is considered to be in the middle section. The resolvability of male (left) and female (right) photoreceptors to two bright light dots with 0.7° angular separation (hyperacute) moving in four cardinal directions with a velocity of **(B)** 10 °/s, **(C)** 21 °/s, **(D)** 42 °/s, **(E)** 84 °/s and **(F)** 168 °/s. Number of recorded

photoreceptors in the n♂(front) = 5, n♂(middle) = 3, n♂(back) = 6, n♀(front) = 4, n♀(middle) = 6 and n♀(back) = 4, mean ± SD.

4.3.4 Photoreceptors' resolvability to moving light bars using a digital light projector

Although hyperacuity was not evident when using light dots, I wanted to test if this remained the case when using another type of stimuli. For this, I used two bright light bars with a range of angular separations (0.7º, 1.4º, 2.1º, 2.8º, 3.5º, 4.9º and 6.3º) with a comprehensive velocity range (10 º/s, 21 º/s, 42 º/s, 84 º/s and 168 º/s) moving across the photoreceptor's receptive field (**Figure 4-12A-E**) with only 0.7º angular separation considered hyperacute. Moreover, direction selectivity was addressed by moving the bars in different directions (up ↑, down ↓, front-to-back → and back-to-front ←).

Initially, there seemed to be some interesting data produced by the light bar stimulus. For example, when using two bars, more photoreceptors could resolve the bars with 0.7º angular separation compared to dots (compare **Figure 4-10** to **Figure 4-13**) across all the tested velocities. The maximum resolvability was attained to two moving bright light bars at 21 º/s, where 12 out of 28 photoreceptors responded to hyperacute bars (**Figure 4-13B**) while the lowest resolvability was seen for the fastest velocity (168 º/s), where only 5 photoreceptors responded to bars with 0.7º angular separation (**Figure 4-13E**).

Despite this, it is crucial to note that more photoreceptors displayed double-peaked voltage responses to one bar (bar width: 0.7º) at all tested velocities (**Figure 4-12A-E**). Due to the results of the one bar control, it was necessary to exclude the possibility that the two-peaked responses were merely a result of the biphasic temporal modulation (on-off) to one bar moving across the photoreceptor's receptive field. This was done by performing statistical analysis (Friedman test with Dunn's multiple comparisons test), which found that, as with dots, the resolvability to two bars with 0.7º angular separation was not statistically significant, so there was no real evidence of hyperacuity in this instance.

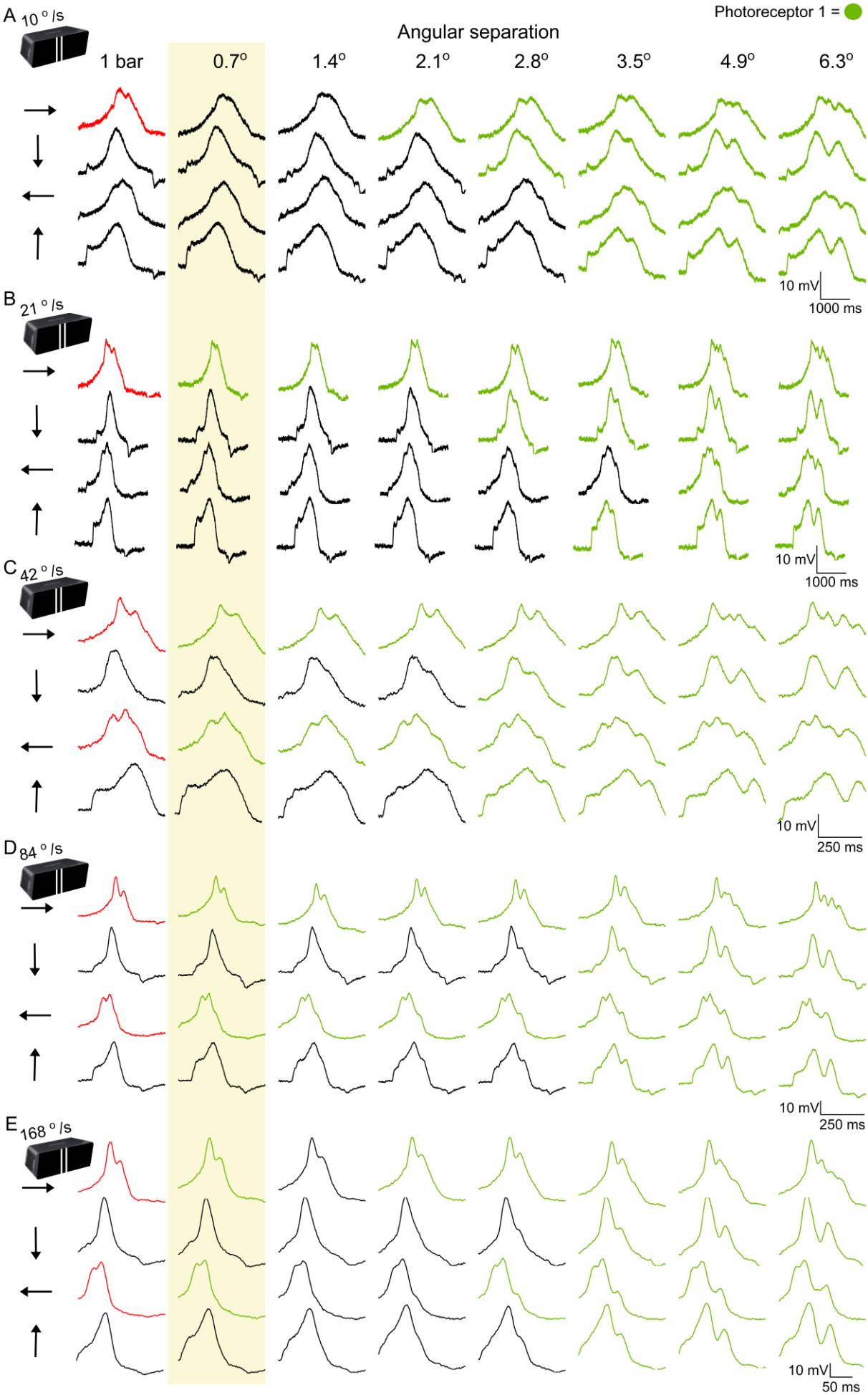
A 10 °/s
B 21 °/s
C 42 °/s
D 84 °/s
E 168 °/s
Photoreceptor 1 =
Angular separation
1 bar
0.7°
1.4°
2.1°
2.8°
3.5°
4.9°
6.3°
10 mV
1000 ms
10 mV
1000 ms
10 mV
250 ms
10 mV
250 ms
10 mV
50 ms

Figure 4-12. Dark-adapted *Musca* photoreceptor's voltage responses to one or two moving bright light bars with a broad range of angular separations and velocities. (A) Photoreceptor's intracellularly recorded voltage responses to one bar (bar width: 0.7°) or two bars with different angular separations (0.7°, 1.4°, 2.1°, 2.8°, 3.5°, 4.9° and 6.3°) with a velocity of 10 °/s tested in four different directions (up ↑, down ↓, front-to-back → and back-to-front ←). Bar/bars were moving at the velocity of **(B)** 21 °/s, **(C)** 42 °/s, **(D)** 84 °/s and **(E)** 168 °/s. Only the angular separation of 0.7° was considered hyperacute (yellow box). Green traces indicate angular separations, which the photoreceptor was able to resolve. The red traces indicate the double-peaked voltage response to only one moving dot. The photoreceptor is named photoreceptor #1 and can be identified in **Figures 4-9**, **4-10** and **4-13**.

Results from wider angular separations (**Figure 4-13**) also support the idea that hyperacuity is not present within the eye. Many tested photoreceptors failed to resolve two bars at angular separations wider (1.4° and 2.1°) than what was considered hyperacute. Most surprisingly there was a significant number of them that failed to resolve two bars with the largest angular separation (6.3°), which is well above the optical limit. To remove the possibility that the order of the stimuli (dots, bars and narrowing gratings) impacted the results, photoreceptors were tested in a pseudorandom order.

As with dots, some photoreceptors initially seemed to have a directional preference when shown moving bars, supporting the possibility that there could be some direction selectivity. The photoreceptor presented in **Figure 4-12**, for instance, showed direction selectivity to front-to-back (→), and with some velocities, to back-to-front (←) as well. The same photoreceptor showed better resolvability to the front-to-back direction when tested with dots (**Figure 4-9**). To investigate how significant this apparent direction preference was, statistical analysis was performed across the photoreceptors. Results of the analysis failed to show that there was any significant evidence of direction selectivity in response to the moving light bars.

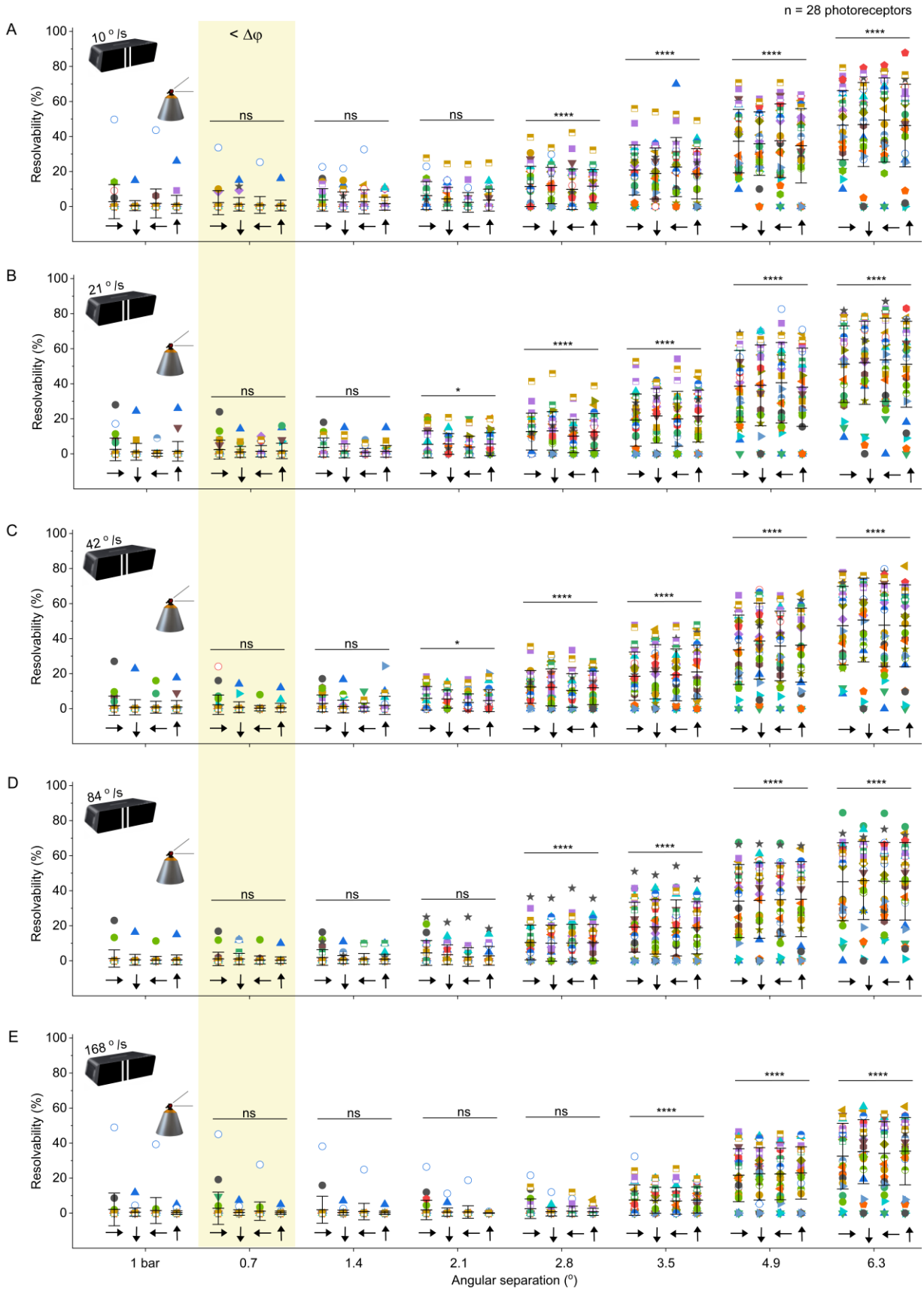

Figure 4-13. Photoreceptors' resolvability to two moving bright light bars. *Musca* photoreceptors' (n = 28) resolvability to one bar/two bars with 0.7º, 1.4º, 2.1º, 2.8º, 3.5º, 4.9º and 6.3º separation moving

in four different directions (up ↑, down ↓, front-to-back → and back-to-front ←) with a velocity of **(A)** 10 °/s, **(B)** 21 °/s, **(C)** 42 °/s, **(D)** 84 °/s and **(E)** 168 °/s. Only the angular separation of 0.7° was considered hyperacute (yellow box). Mean ± SD. Statistical comparisons of resolvability to each angular separation were made against the respective one moving bar control: *P < 0.05, **P < 0.01, ***P < 0.001, ****P < 0.0001, Friedman test with Dunn's multiple comparisons test. The same photoreceptor is shown by a unique colour and shape combination throughout this figure and **Figures 4-10** and **4-15**.

In addition to examining direction selectivity, I also investigated whether or not the location of the eye, or sex of the fly, had any impact on the flies' ability to resolve hyperacute features. Although statistical analysis later showed that the resolvability to two bars at an angular distance of 0.7° was not significant overall, this is not to say this would apply to each location within the eye. To test this, I performed separately *in vivo* intracellular recordings from the back, middle and front of the eye, doing so for both males and females.

My assumption, as with dots, was if there were areas of greater resolvability, it would be found within the "love spot" of the tested males. Again though, this was not the case when looking at the data as a whole (**Figure 4-14A-E**). When using the light bar stimulus there were no major differences when it came to the location of the eye, nor sex of the fly.

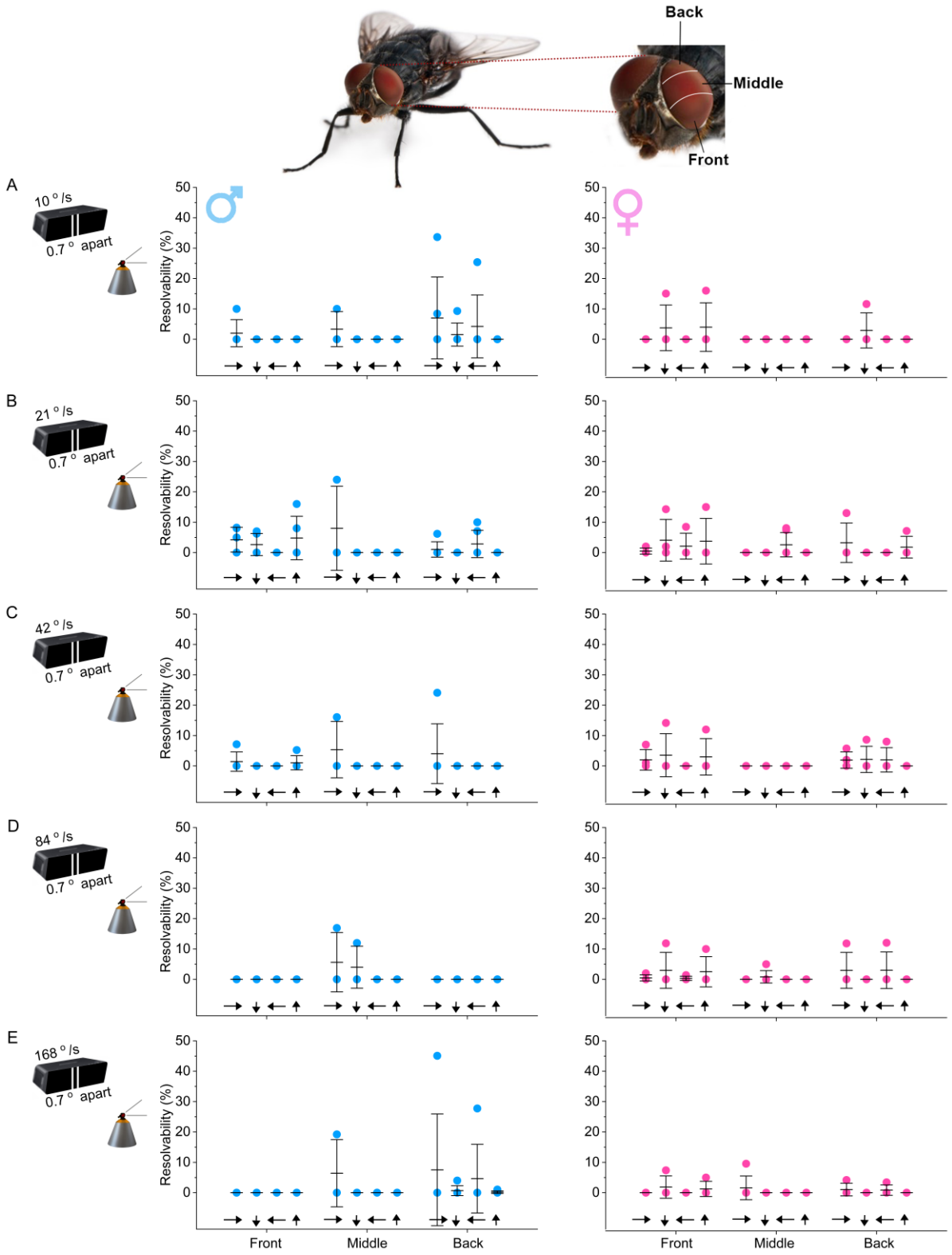

Figure 4-14. Comparing photoreceptors' hyperacute resolvability to two moving bright bars across the whole compound eye between males and females. (A) *In vivo* intracellular recordings were performed from *Musca* photoreceptors from different eye locations (front, middle, back). The male "love spot" is considered to be in the middle section. The resolvability of male (left) and female (right) photoreceptors to two bright light bars with 0.7º angular separation (hyperacute) moving in four cardinal directions with a velocity of **(B)** 10 º/s, **(C)** 21 º/s, **(D)** 42 º/s, **(E)** 84 º/s and **(F)** 168 º/s. Number of

recorded photoreceptors in the n♂(front) = 5, n♂(middle) = 3, n♂(back) = 6, n♀(front) = 4, n♀(middle) = 6 and n♀(back) = 4, mean ± SD.

4.3.5 Photoreceptors' resolvability to moving narrowing bar-grating

The aforementioned moving light dots and bars experiments were both carried out using dark-adapted R1-R6 photoreceptors. However, light adaptation can improve spatial resolution by narrowing the photoreceptor's receptive field (Stavenga, 2004; Juusola et al., 2017). This acuity improvement is achieved through pupil closure: during light adaptation, pigment granules surrounding the eye migrate towards the rhabdomere to reduce the light flux by absorbing and reflecting the incoming photons (Kirschfeld and Franceschini, 1969; Franceschini, 1972; Stavenga, 1975; Howard, Blakeslee and Laughlin, 1987; Roebroek and Stavenga, 1990).

To examine the light-adapted photoreceptors' resolvability, I used a novel moving narrowing bar-grating stimulus. This type of stimulus was chosen over dots/bars because using the digital light projector with either was not feasible for light-adapted experiments. The grating continuously decreased its wavelength (the bar width) from 5^{o} to 0.33^{o,} as seen by the fly (**Figure 4-15A**). *In vivo* intracellular recordings were performed from R1-R6 photoreceptors while presenting the stimulus moving with five different velocities (6 ^{o}/s, 20 ^{o}/s, 40 ^{o}/s, 60 ^{o}/s and 120 ^{o}/s) in four cardinal directions (up ↑, down ↓, front-to-back → and back-to-front ←) across their receptive field (**Figure 4-15B-F**). The resolvability was determined by detecting the narrowest pair of gratings that the photoreceptor could separate using a six hyperparameter algorithm in Python. Rayleigh criterion was applied to calculate the resolvability limit, which was called the smallest resolvable angle (SRA) here.

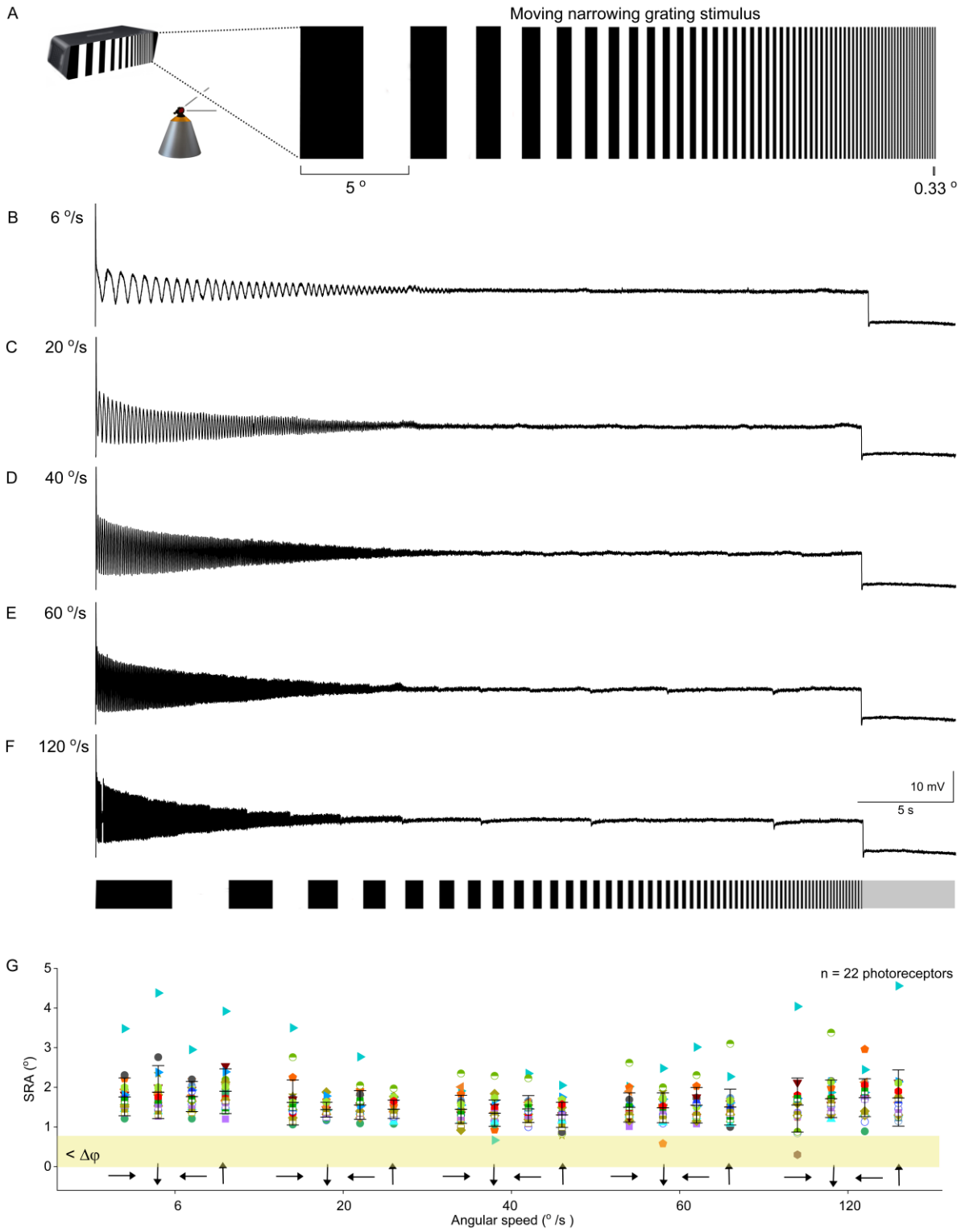

Figure 4-15. Photoreceptors' resolvability (SRA) to moving narrowing bar-grating stimuli. (A) *Musca* photoreceptors' (n = 22) resolvability under light adaptation was tested to moving narrowing bar-grating. The grating wavelength (i.e. bar width) continuously decreased from 5° to 0.33°, as seen by the fly. Showing one photoreceptor's intracellular voltage responses the stimulus moving with a velocity of **(B)** 6 °/s, **(C)** 20 °/s, **(D)** 40 °/s, **(E)** 60 °/s and **(F)** 120 °/s. Additionally, the stimuli were run in four different directions (up ↑, down ↓, front-to-back → and back-to-front ←). Photoreceptors' voltage responses were recorded 5 s after the stimulation while the projector was on without the stimulus. The noise threshold

was acquired from this period. Note the drops in the voltage responses, especially when testing with higher velocities, were due to the photoreceptor detecting the decrement of the bar wavelengths (see **Figure 4-3B-C**). **(G)** The resolvability was estimated by determining the smallest resolvable angle (SRA) from the voltage response. The cell could resolve the gratings until its response peak amplitudes became smaller than the noise threshold. Only when SRA < 0.8^{o} (smaller than $\Delta\varphi$) was the resolvability considered to be hyperacute (yellow box). The same photoreceptor is shown by a unique colour and shape combination throughout this figure and **Figures 4-10** and **4-13**. Mean ± SD.

Only 3 of the 22 photoreceptors tested were able to resolve gratings narrower than the optical limit (< 0.8^{o}) among all the tested velocities (**Figure 4-15G**). This shows that even under light adaptation, when acuity should be improved, still photoreceptors were not able to resolve these gratings that had hyperacute angular separation. This could be influenced by the type of stimulation and analysis, where the noise threshold was the resolvability limit. Although instrumental noise was kept as minimal as possible, some levels are unavoidable, which contaminates the recordings and affects the estimation of the SRA. However, based on the analysis from dots and bars, it seems safer to assume that the results are as they are simply because *Musca* photoreceptors do not appear to be hyperacute, not even when light-adapted. All these recordings were performed in a pseudorandom order; thus, the recording order did not impact these results.

With the moving narrowing gratings, I also looked at how the overall resolvability was distributed throughout the eye, performing *in vivo* intracellular recordings from the back, middle and front of the eye from both males and females (**Figure 4-16**). Although only a few photoreceptors (3 out of 22) could resolve hyperacute gratings, the potential influence of sexual dimorphism and direction selectivity was tested nonetheless. Interestingly, all the three cells that resolved beyond the hyperacute limit were all recorded from the female eye (one front, two back), not from the male “love spot” (**Figure 4-16C-E**). Due to the limited number of cells that responded in the hyperacute range, however, no strong conclusions should be made from this.

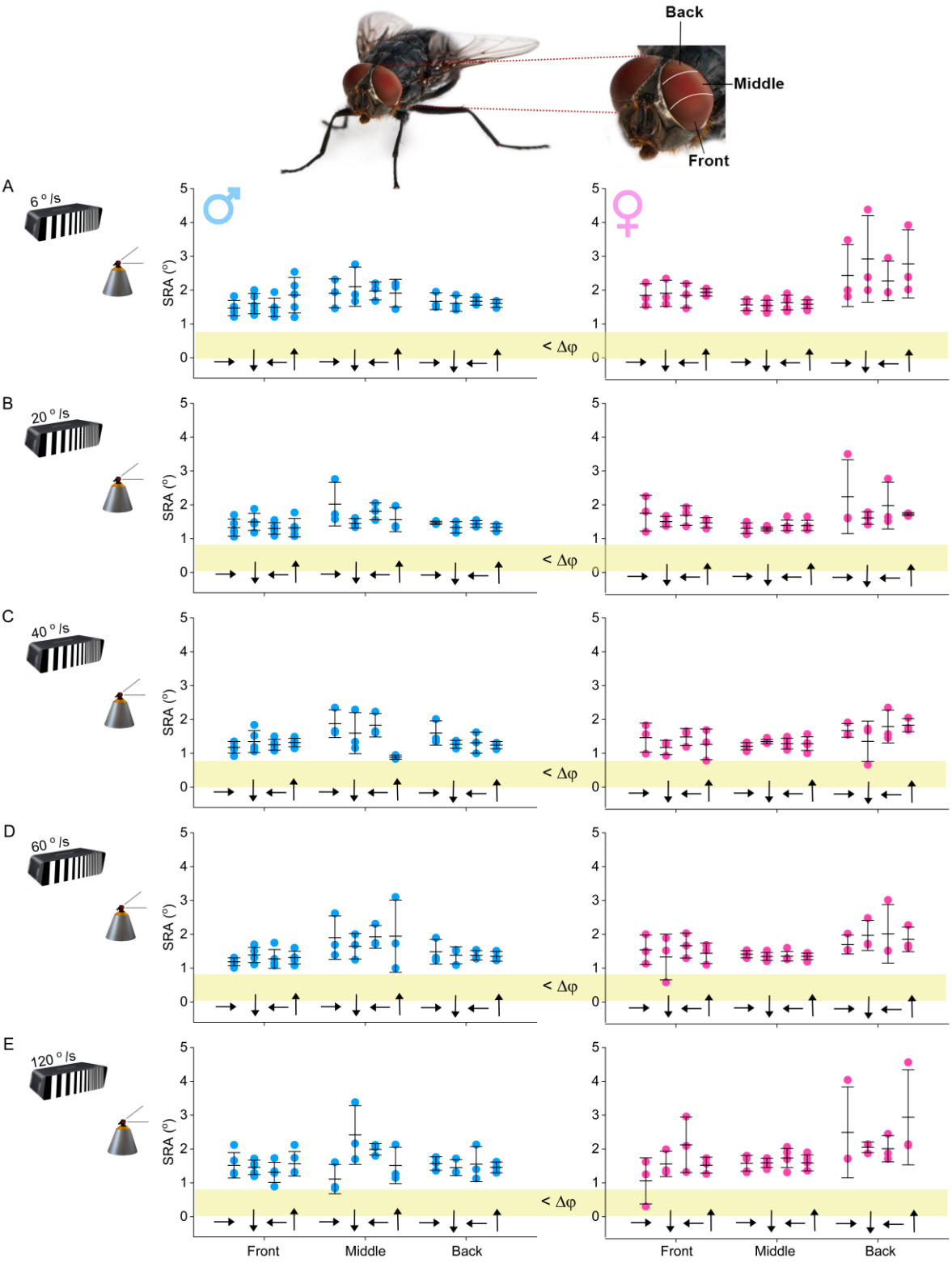

Figure 4-16. Comparing photoreceptors' hyperacute resolvability to moving narrowing bar-grating across the whole compound eye between males and females. *In vivo* intracellular recordings were performed from *Musca* photoreceptors from different eye locations (front, middle, back). The male "love spot" is considered to be in the middle section. The resolvability (SRA) of males (left) and females (right) to the grating narrowing from 5° bar width to 0.33° moving in four cardinal directions with a velocity of **(A)** 6 °/s, **(B)** 20 °/s, **(C)** 40 °/s, **(D)** 60 °/s and **(E)** 120 °/s. Only when SRA

< 0.8º (smaller than ∆φ) was the resolvability considered to be hyperacute (yellow box). n♂(front) = 5, n♂(middle) = 3, n♂(back) = 3, n♀(front) = 3, n♀(middle) = 5 and n♀(back) = 3, mean ± SD.

4.3.6 LMC's resolvability to moving light dots using a digital light projector

To summarise findings from R1-R6 photoreceptors so far, there was no statistically significant evidence of hyperacuity nor direction selectivity to moving bright light dots, bars and narrowing gratings (**Figure 4-9**, **4-10**, **Figure 4-12, Figure 4-13** and **Figure 4-15**). After studying resolvability in photoreceptors, I aimed to test how L1-L3 LMCs resolve similar stimuli (moving light dots and bars). I did not, however, test LMCs' intracellular voltage responses to moving narrowing bar-grating stimulus.

There is no prior experimental research on LMC resolvability, only one theoretical study (Juusola and French, 1997). However, based on the neural structure of the fly compound eye (neural superposition) and the neural connections (lateral inhibition), it is a real possibility that LMCs could resolve even finer details than photoreceptors (Braitenberg, 1967; Kirschfeld, 1967; Reichardt and Poggio 1976; Srinivasan et al. 1990; de Ruyter van Steveninck and Laughlin, 1996; Zheng et al., 2006).

In Chapter 4.3.2, I tested LMCs' resolvability using a 25-point LED array. Unfortunately, this method was not appropriate to test the resolvability in LMCs. After this, I instead studied LMC resolvability to two moving bright light dots, using a digital light projector, with the same angular separations (0.7º, 1.4º, 2.1º, 2.8º, 3.5º, 4.9º and 6.3º) and velocity ranges (10 º/s, 21 º/s, 42 º/s, 84 º/s and 168 º/s) as with photoreceptors (**Figure 4-17A-E**). Only the angular separation of 0.7º was considered hyperacute. Direction selectivity was tested moving the two light dots in four different directions (up ↑, down ↓, front-to-back → and back-to-front ←). As when testing photoreceptors, the responses to one dot moving were also recorded.

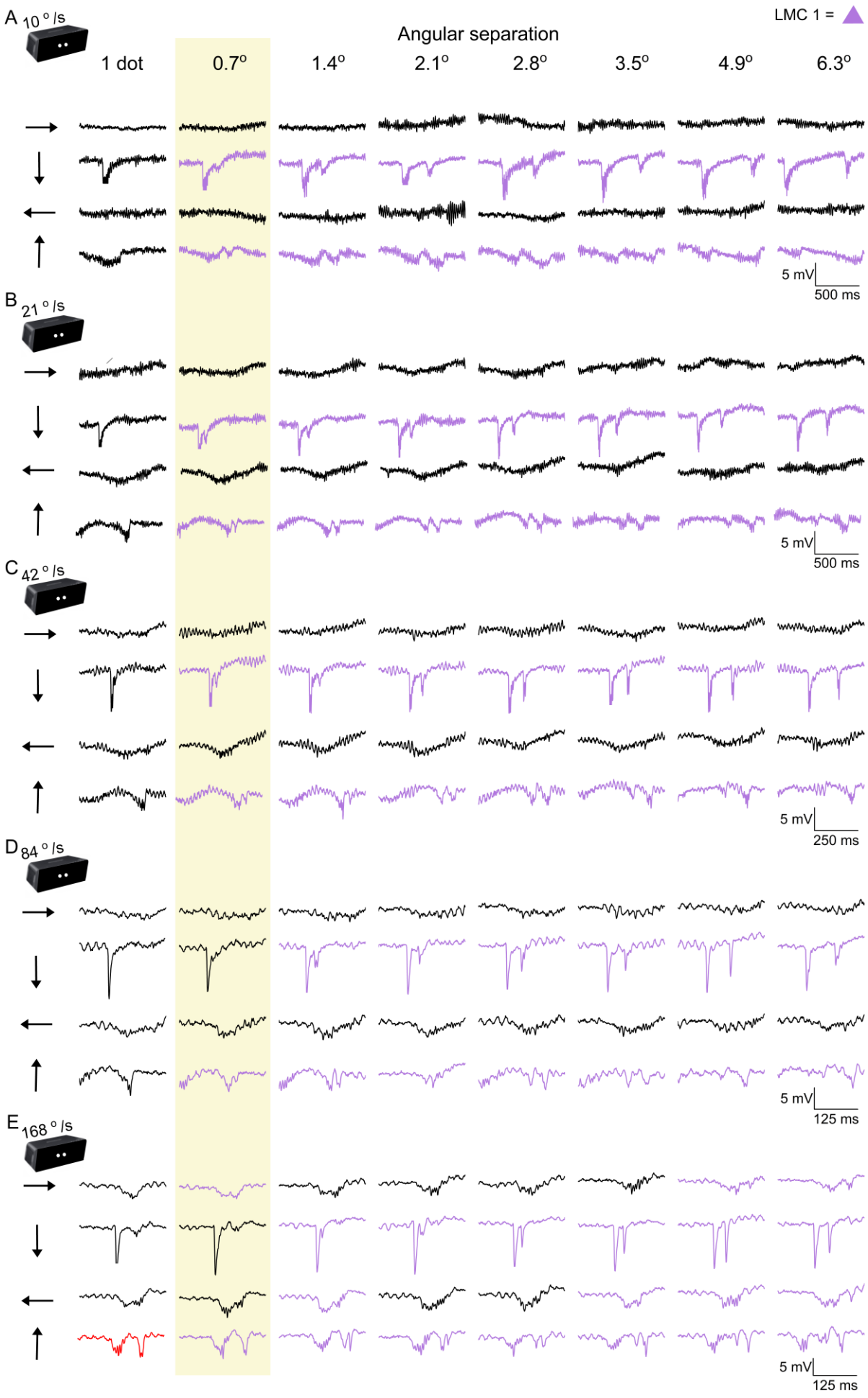
A 10 °/s
B 21 °/s
C 42 °/s
D 84 °/s
E 168 °/s
LMC 1 =
Angular separation
1 dot
0.7°
1.4°
2.1°
2.8°
3.5°
4.9°
6.3°
5 mV
500 ms
5 mV
500 ms
5 mV
250 ms
5 mV
125 ms
5 mV
125 ms

Figure 4-17. *Musca* LMC's voltage responses to one or two moving bright light dots with a broad range of angular separations and velocities. (A) LMC's intracellularly recorded voltage responses to one dot (dot size: 0.7°) or two dots with different angular separations (0.7°, 1.4°, 2.1°, 2.8°, 3.5°, 4.9° and 6.3°) with a velocity of 10 °/s tested in four directions (up ↑, down ↓, front-to-back → and back-to-front ←). Dot/dots were moving at the velocity of **(B)** 21 °/s, **(C)** 42 °/s, **(D)** 84 °/s and **(E)** 168 °/s. Only the angular separation of 0.7° was considered hyperacute (yellow box). Purple traces indicate angular separations, which the photoreceptor was able to resolve. The red traces indicate the double-peaked voltage response to only one moving dot. The photoreceptor is named LMC #1 and can be identified in **Figures 4-18**, **4-19** and **4-20**.

The tested LMC resolved two moving bright light dots with an angular separation of 0.7° across all the tested velocities (**Figure 4-17A-E** and **4-18A-E**). This LMC's hyperacute resolvability was evident and largely velocity-independent (compare **Figure 4-18** and **4-10**). Additionally, the LMC did not produce double-peaked responses to one dot moving across its receptive field (only to up (↑) direction at 168 °/s), whereas this often occurred with photoreceptors (**Figure 4-17**, **red trace**). However, as only one LMC was recorded, compared to 28 photoreceptors, stark conclusions should not be drawn based on this data.

According to the classical EMD model, LMCs are not thought to be direction-selective nor motion-sensitive. It is interesting, therefore, that the recorded LMC resolved two moving light dots in the up (↑) and the down (↓) directions (**Figure 4-17**). In both cases, but especially to down (↓), where the voltage responses were the largest. This finding could indicate that LMCs are direction-selective.

Interestingly, the front-to-back (→) and back-to-front (←) moving dots only produced responses with one peak or no peak (flat response). The limited or null responses to the orthogonal directions give support to the presence of direction-selectivity. It is possible, however, albeit unlikely, that this was because the receptive field was moving off-axis, and thus, the dots would not be crossing the centre of the receptive field.

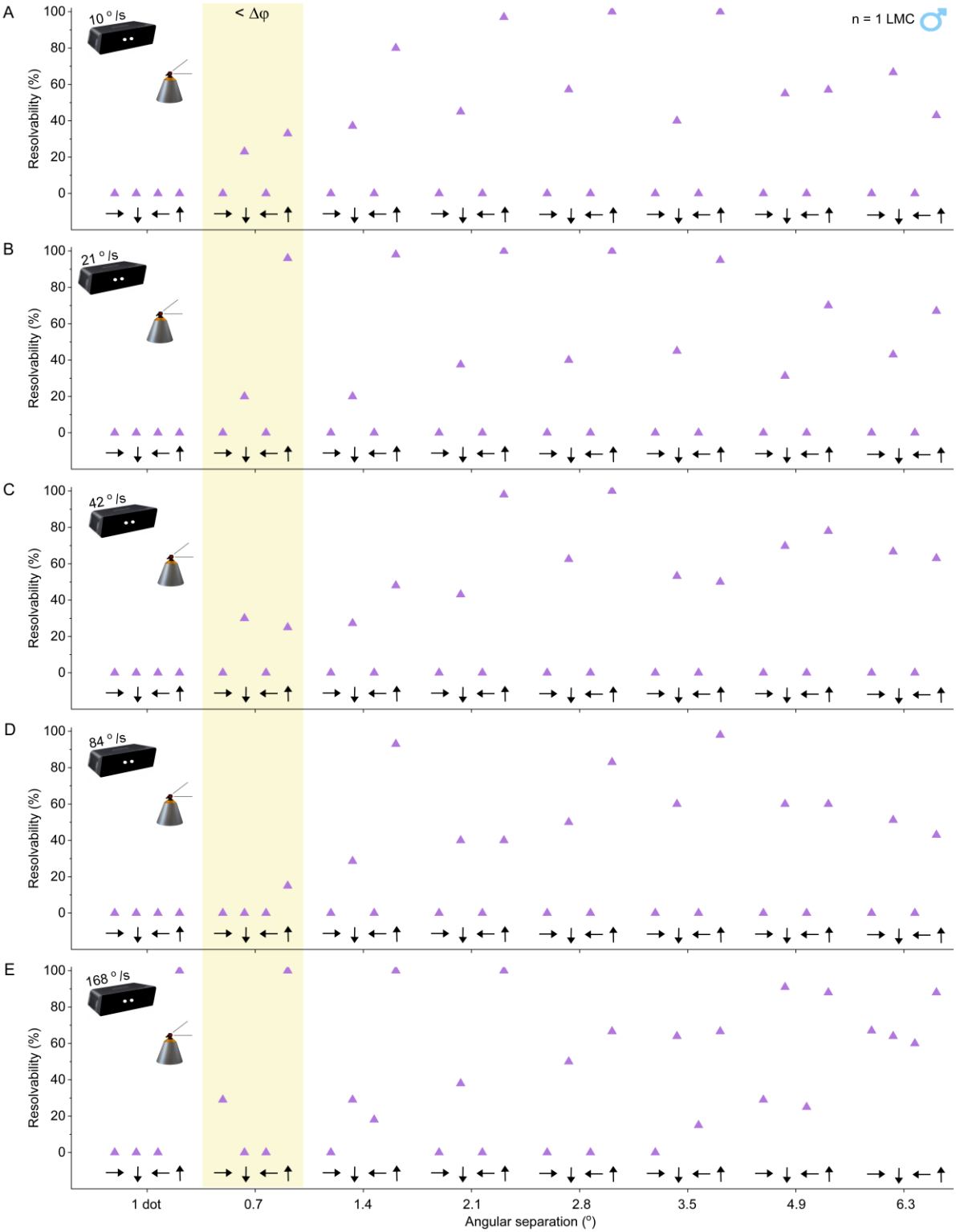

Figure 4-18. LMC's resolvability to two moving bright light dots. *Musca* LMC's (n = 1, male) resolvability to one dot/two dots with 0.7°, 1.4°, 2.1°, 2.8°, 3.5°, 4.9° and 6.3° separation moving in four different directions (up ↑, down ↓, front-to-back → and back-to-front ←) with a velocity of **(A)** 10 °/s, **(B)** 21 °/s, **(C)** 42 °/s, **(D)** 84 °/s and **(E)** 168 °/s. Only the angular separation of 0.7° was considered hyperacute (yellow box). Mean ± SD.

4.3.7 LMC's resolvability to moving light bars using a digital light projector

After testing resolvability to hyperacute light dots, I tested LMC's resolvability to two moving bright light bars with the same angular separations (0.7°, 1.4°, 2.1°, 2.8°, 3.5°, 4.9° and 6.3°) and velocity ranges (10 °/s, 21 °/s, 42 °/s, 84 °/s and 168 °/s) as before (**Figure 4-19A-E**). Again, only the angular separation of 0.7° was considered hyperacute, and direction selectivity was addressed by moving the bars in four different directions (up ↑, down ↓, front-to-back → and back-to-front ←).

Surprisingly, the tested LMC (same as used for moving light dots) struggled to resolve the two bars beyond the optical limit (0.7°) at most tested velocities and failed to do so with the fastest velocity (**Figure 4-19A-E** and **Figure 4-20A-E**). Compared with the dots, the resolvability to two bars with larger angular separations was relatively low. This specific LMC resolving two hyperacute dots, but not bars, could be due to lateral inhibition. Another possibility for the non-resolvability is that the LMC was starting to detach from the electrode, which would lead to the recording being slightly unstable.

As for direction selectivity, when using bars, LMCs displayed a preference to the down (↓) direction only, as opposed to dots, which resolved better both up (↑) and down (↓) directions. While this is another intriguing finding from my research, it is essential not to make any firm conclusions using the data as only one LMC was examined. To fully understand LMC resolvability, direction selectivity and the impact of lateral inhibition, further LMCs need testing with the dots/bars stimuli.

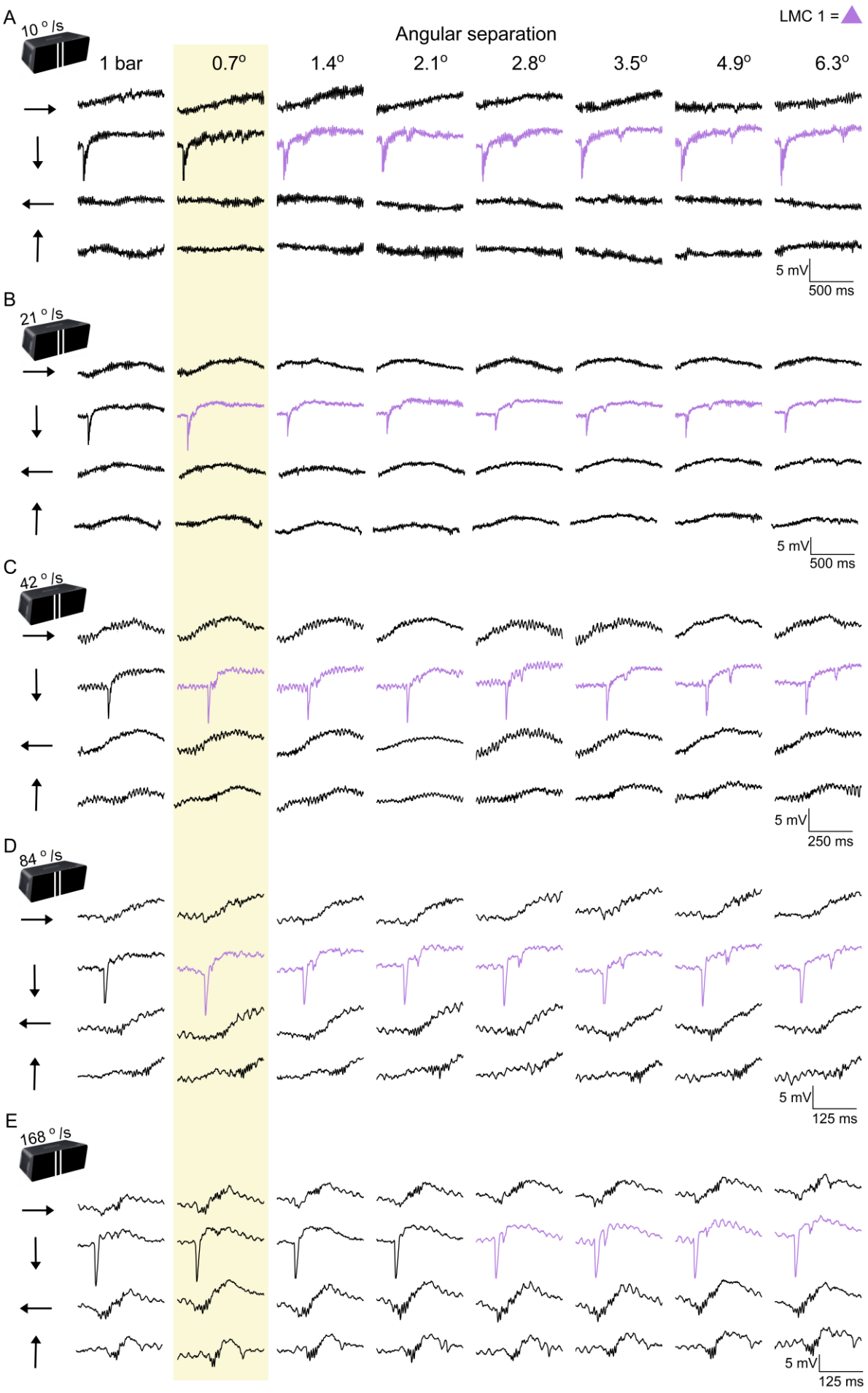
A
10 °/s
1 bar
Angular separation
0.7°
1.4°
2.1°
2.8°
3.5°
4.9°
6.3°
LMC 1 =
5 mV
500 ms
B
21 °/s
5 mV
500 ms
C
42 °/s
5 mV
250 ms
D
84 °/s
5 mV
125 ms
E
168 °/s
5 mV
125 ms

Figure 4-19. *Musca* LMC's voltage responses to one or two moving bright light bars with a broad range of angular separations and velocities. (A) LMC's intracellularly recorded voltage responses to one bar (bar width: 0.7°) or two bars with different angular separations (0.7°, 1.4°, 2.1°, 2.8°, 3.5°, 4.9° and 6.3°) with a velocity of 10 °/s tested in four different directions (up ↑, down ↓, front-to-back → and back-to-front ←). Bar/bars were moving at the velocity of **(B)** 21 °/s, **(C)** 42 °/s, **(D)** 84 °/s and **(E)** 168 °/s. Only the angular separation of 0.7° was considered hyperacute (yellow box). Purple traces indicate angular separations, which the photoreceptor was able to resolve. The LMC is named LMC #1.

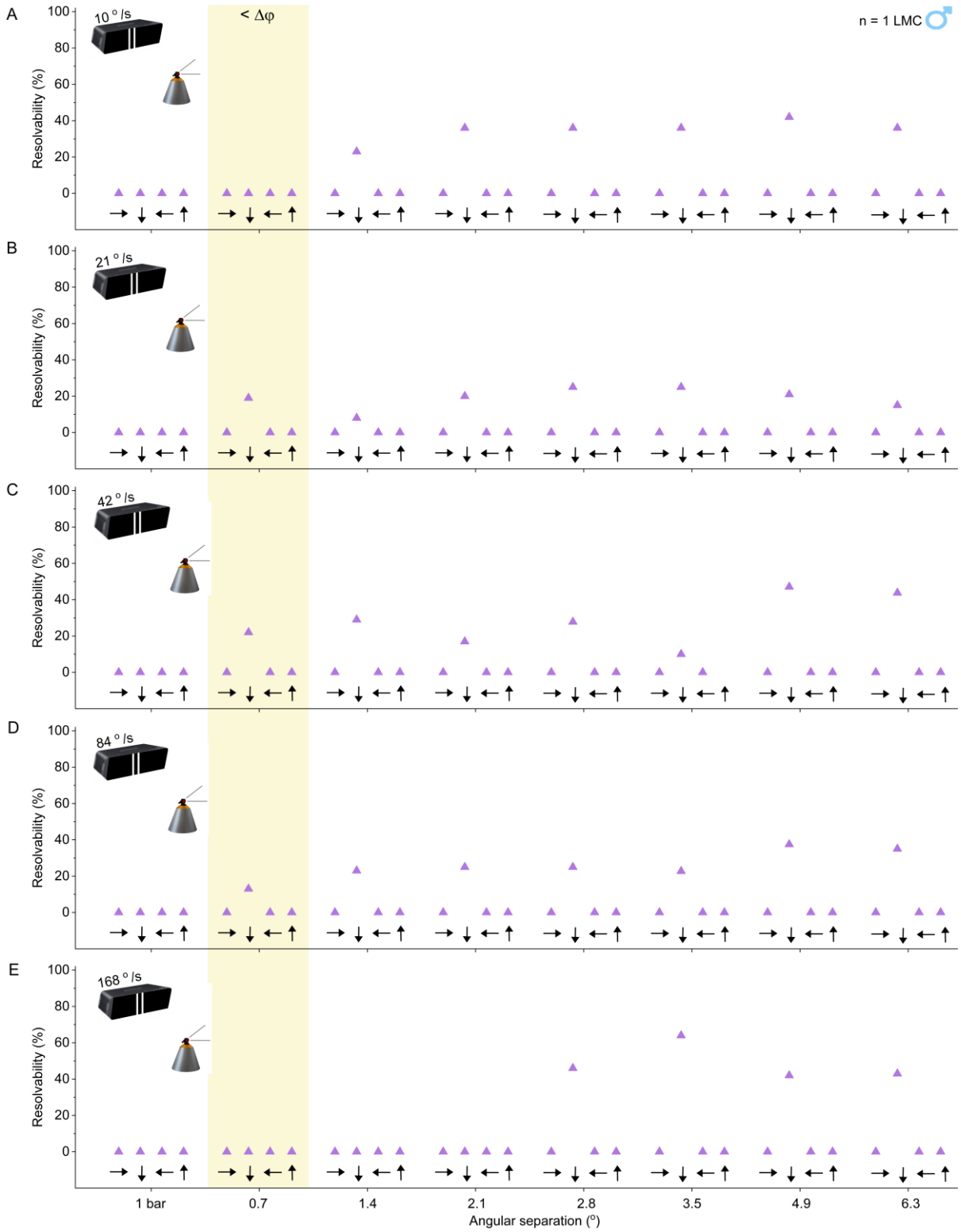

Figure 4-20. LMC's resolvability to two moving bright light bars. *Musca* LMC's (n = 1, male) resolvability to one bar/two bars with 0.7°, 1.4°, 2.1°, 2.8°, 3.5°, 4.9° and 6.3° separation moving in four different directions (up ↑, down ↓, front-to-back → and back-to-front ←) with a velocity of **(A)** 10 °/s, **(B)** 21 °/s, **(C)** 42 °/s, **(D)** 84 °/s and **(E)** 168 °/s. Only the angular separation of 0.7° was considered hyperacute (yellow box). Mean ± SD.

4.4 Discussion

4.4.1 Photoreceptors' hyperacute resolvability

I found no strong evidence of hyperacuity to dots nor bars (**Figure 4-10** and **Figure 4-13**) and even when replicating the experiments using the narrowing bar-grating, to test the impact of light adaptation, the resolvability was surprisingly low (**Figure 4-15G**). The results were largely consistent when looking at different locations within the eye and between sexes (**Figure 4-11**, **Figure 4-14** and **Figure 4-16**), although small discrepancies were noted in a couple of instances. None of these discrepancies indicated that hyperacuity was possible in a specific region of the eye for either males or females.

This is a contrast to the data gathered using the 25-point LED array (used in the Juusola et al., 2017 article as well), which showed a much higher resolvability to hyperacute stimuli (**Figure 4-5**). However, neither myself nor Juusola et al. carried out a substantial amount of one dot control experiments – they performed none while I only performed a limited number as initially I did not even consider the possibility that one moving light point could result in a double-peaked voltage response. Additionally, there were some limitations to the LED setup itself. Firstly, the LEDs had different intensities reaching maximally up to a ~6.5-fold intensity difference (Juusola et al., 2017). Secondly, the movement on the 25-point array was created by turning on one light point, or simultaneously two adjacent light points, on and off after each other, which the fly might not see as smooth movement but rather a sequence of flickering lights. As a final point, I later noticed that when testing with two moving light points, there was a slight delay with the second light point, which should have been triggered simultaneously with the first. Not only did the second light point appear with a small delay but it was also slower than the first light point moving ahead of it. This could have impacted the results using the 25-point LED array in Juusola et al. (2017) as well as mine.

Subsequently, I would suggest that fresh experiments would need to be performed on *Drosophila* to demonstrate if hyperacuity is present. Given that my projector data shows the ability to resolve fine details is unlikely to be a feature of *Musca* vision, this

raises the question of why such a feature would be found in a slower flying *Drosophila* with optically much poorer vision.

As just mentioned, although my data indicates that hyperacuity is highly unlikely to be a feature of *Musca* photoreceptors, there is some evidence from *Drosophila* that photomechanical contractions differ in their direction throughout the eye (unpublished data), and this might be the reason why a minority of photoreceptors were able to resolve the light dots/bars with small angular distances. While this could be a feasible explanation, it needs to be quantified in *Musca* by high-speed imaging of the deep-pseudopupils (Franceschini and Kirschfeld, 1971b; Franceschini, 1972). Specifically, the photoreceptor contractions need to be combined with the direction that produced the biggest resolvability. This approach would require testing, via *in vivo* intracellular recordings, possibly using more angles than the four used in my research, although there is little evidence to suggest testing more directions would unearth something novel. Additionally, to locate the specific photoreceptor being tested, it might be necessary to stain the recorded R1-R6 cells electrophoretically.

As an alternative, it is plausible that some photoreceptors better resolved smaller details due to their differing rhabdomere diameter and subsequent differing acceptance angles (Juusola et al., 2017). This structural difference means that some photoreceptors can resolve smaller details; R2 and R4 rhabdomeres, for example, are smaller than R1, R3 and R6. It is also possible, albeit improbable, that despite R1-R6 being discussed, some R7 and R8 cells were captured during the recordings. If either were recorded, their small rhabdomere diameters would result in enhanced resolvability beyond what R1-R6 can. Given that the digital light projector used UV light for stimulation, R7 cells would respond well because they express Rh3 and Rh4, which are UV-sensitive pigments (Fryxell and Meyerowitz, 1987; Montell et al., 1987; Feiler et al., 1992).

Although I tested a range of velocities across all the stimuli used, I was limited by the digital light projector itself - the projector could only handle velocities up to ~168 ^{o}/s. However, *Musca* males have shown to perform saccadic turns with angular velocities >1,000 ^{o}/s when detecting a target (Wagner, 1986a). By and large, it is not uncommon for *Musca* to move at ~100 ^{o}/s – 1,000 ^{o}/s (Burton and Laughlin, 2003). Even with the

velocities used in my experiments (dots/bars: 10 º/s, 21 º/s, 42 º/s, 84 º/s and 168 º/s; gratings: 6 º/s, 20 º/s, 40 º/s, 60 º/s and 120 º/s) though, hyperacute resolvability weakened, quite significantly, as the velocities increased (**Figure 4-10**, **Figure 4-13** and **Figure 4-15**). Therefore, it is unlikely (but not impossible) that photoreceptors would resolve anything considered hyperacute with considerably faster velocities. To be sure, these velocities could be tested by using a laser galvanometer system (with two mirrors).

Finally, although not shown in my data, I did test several photoreceptors with two moving light dots and bars (dot size/bar width: either 0.18º or 0.4º) with angular separations of 0.18º and 0.4º, but in no instances were these objects resolved.

4.4.2 LMCs' hyperacute resolvability

The LMC recorded for my research showed hyperacuity to dots and a lesser extent to bars (**Figure 4-18** and **Figure 4-20**). Direction selectivity was also shown, but as only one LMC was examined, more data is required before any conclusions can be safely made. In future, it would be interesting to study, ideally through staining electrophoretically, if there are any differences between L1, L2 and L3 cells.

L1 and L2 are the primary inputs for the ON and OFF motion pathway, respectively (Joesch et al., 2010; Clark et al., 2011; Eichner et al., 2011; Joesch et al., 2013; Silies et al., 2013). If further research finds direction selectivity in LMCs and slight differences between L1-L3, it would be interesting to see how this would impact motion vision (possible motion opponency) and upstream visual encoding.

4.4.3 Optomotor responses to hyperacute features

Juusola et al. (2017) showed via open-loop optomotor flight experiments that *Drosophila* responds to hyperacute black-and-white bar panorama. However, when testing with more natural closed-loop flight experiments (magnetic tethering) using a static panorama, Salem et al. (2020) did not show hyperacuity in *Drosophila*. Ideally, further research would examine hyperacuity in even more natural conditions that mimic real-world environments. It is important to see that hyperacute features occur naturally and are not merely induced by specific lab conditions. This reasoning should

also apply to the stimuli used, so rather than solely using full contrast light bars/dots, a more comprehensive range of contrast/objects should be tested.

It would be worthwhile to test both closed-loop flying and walking optomotor responses with *Musca*. However, to match the velocities used in my *in vivo* experiments with the optomotor behaviour, testing walking using a virtual reality (VR) trackball system would be more suitable. I attempted to carry out this myself, but our VR trackball system was initially designed for cockroach (*Periplaneta americana*) use, and thus, it was so large that *Musca* was physically unable to move it. Unfortunately, therefore, I could not proceed with this line of investigation.

5 General discussion

At the end of each thesis chapter, I have thoroughly discussed its specific research, strengths and limitations, and future work ideas. Here, I intend to provide a much more general overview of all the work I undertook while exploring broader points about fly visual research.

I find these general points of discussion fascinating, especially as my thesis covered such a broad range of investigations. Rather than attempting to unravel one single aspect of *Musca* vision, I set out to study multiple aspects using a range of different stimuli and setups. In all cases, what I chose to examine had not been looked at previously in *Musca,* or there was very little relevant work. In total, I ended up examining three different areas, which are briefly summarised below:

1) How much information *Musca* photoreceptors encode when performing body saccades and how much of this information is passed downstream to LMCs. This was tested using light stimuli, which broadly resembled the temporal changes a fly sees while performing head and body saccades.
2) How light adaptation shapes the R1-R6 photoreceptors' and L1-L3 LMCs' response properties, and how this can be explained through the changes occurring at the level of the elementary responses (quantum bumps, QBs).
3) How *Musca* R1-R6 and L1-L3 cells encode hyperacute objects, given the opto-physiological constraints of its compound eye.

Through my research in these three areas, I discovered that *Musca* vision, in some areas, is more advanced and better performing than what was thought previously. For one, I found that *Musca*, especially males, were able to see the world in much finer temporal resolution. This raises the important question as to why it has evolved to such an extent, particularly in males. After all, the better the vision, the more energy it consumes (Niven, Anderson and Laughlin, 2007). Even if vision is the most important sense for fly survival, it has evolved well beyond expectations in this area.

Musca vision did not always manage to impress, however. When attempting to resolve objects closer than their interommatidial angle, most photoreceptors failed to do so regardless of the velocity tested. There is some indication that LMCs can resolve within the hyperacute range but more research is needed before any conclusions can be made.

While discussing my results, an essential point to consider is that all my data was collected in lab conditions drastically different from the flies' natural environment. *Musca* may respond a certain way, when waxed to a cone, to a single light stimulus, but is this something that would be replicated in a more natural environment? It is already known that when behaving (i.e. flying, walking), flies' downstream neurons exhibit changes in their visual processing (Chiappe et al., 2010; Maimon, Straw and Dickinson, 2010; Jung, Borst and Haag, 2011; Suver, Mamiya and Dickinson, 2012; Strother et al., 2018). Although these changes are thought to be mostly octopamine mediated, enhancements could still happen in photoreceptors. Ideally, this could be tested in the virtual reality (VR) system by performing simultaneous *in vivo* intracellular recordings while the fly is in motion (tethered walking or flying).

To better understand how flies explore their natural environment, their visual neurons need to be tested by more than one kind of light stimuli. For *in vivo* intracellular recordings, a single stimulus can be highly beneficial, but a fly would seldom see just one moving object in a real-life setting. Among other things, testing with multiple stimuli would allow us to study the selective attention span between hyperacute and non-hyperacute features.

When acquiring *in vivo* intracellular responses, we are limited to one photoreceptor at a time. Thus, simultaneous two-photon imaging of multiple neurons could be combined with these electrophysiological findings to improve our understanding of parallel neural processing. Note that two-photon imaging is often limited by the relatively slow calcium dynamics when using calcium indicators (such as Gcamp6f) or SNR when using voltage indicators (such as ASAP2f or ASAP3) (Yang et al., 2016; Villette et al., 2019).

It would also be valuable to expose flies to other sensory cues beyond vision. Multimodal sensory information in a natural environment could very feasibly enhance fly vision. One assumption is that multisensory integration could heighten photoreceptor encoding and enhance downstream neurons' response properties to visual stimuli even further. The influences of other factors were not something I could consider while concentrating solely on vision.

Overall, my research data should not be considered conclusive due to the lack of 'real-life' testing conditions. It does, however, provide a strong foundation for further research.

References

Agi, E., Langen, M., Altschuler, S.J., Wu, L.F., Zimmermann, T. and Hiesinger, P.R. (2014). The Evolution and Development of Neural Superposition. Journal of Neurogenetics, 28(3-4), pp.216–232.

Arendt, D. (2003). Evolution of eyes and photoreceptor cell types. Int. J. Dev. Biol., 47(7-8), pp.563–571.

Arenz, A., Drews, M.S., Richter, F.G., Ammer, G. and Borst, A. (2017). The Temporal Tuning of the *Drosophila* Motion Detectors Is Determined by the Dynamics of Their Input Elements. *Current Biology*, 27(7), pp.929–944.

Autrum, H., Zettler, F. and Järvilehto, M. (1970). Postsynaptic potentials from a single monopolar neuron of the ganglion opticum I of the blowfly *Calliphora*. *Zeitschrift für Vergleichende Physiologie*, 70(4), pp.414–424.

Barlow, H.B. (1953). Summation and inhibition in the frog's retina. *The Journal of Physiology*, 119(1), pp.69–88.

Barlow, H.B. (1961). Possible Principles Underlying the Transformations of Sensory Messages. In: *Sensory Communication*. Cambridge, MA: MIT Press, pp. Ch13, 217–234.

Bausenwein, B., Dittrich, A.P.M. and Fischbach, K.-F. (1992). The optic lobe of *Drosophila melanogaster*. II. Sorting of retinotopic pathways in the medulla. *Cell & Tissue Research*, 267(1), pp.17–28.

Beersma, D.G.M., Stavenga, D.G. and Kuiper, J.W. (1975). Organization of visual axes in the compound eye of the fly *Musca domestica* L. and behavioural consequences. *Journal of Comparative Physiology A*, 102(4), pp.305–320.

Bendat, J.S. and Piersol, A.G. (1971). *Random data: analysis and measurement procedures*. New York: Wiley Interscience, p.

Blaj, G. and van Hateren, J.H. (2004). Saccadic head and thorax movements in freely walking blowflies. *Journal of Comparative Physiology A*, 190(11), pp.861–868.

Bloomquist, B.T., Shortridge, R.D., Schneuwly, S., Perdew, M., Montell, C., Steller, H., Rubin, G. and Pak, W.L. (1988). Isolation of a putative phospholipase c gene of *Drosophila*, norpA, and its role in phototransduction. *Cell*, 54(5), pp.723–733.

Born, M. and Wolf, E. (1999). *Principles of Optics*. Cambridge University Press.

Boschek, G.B. (1971). On the fine structure of the peripheral retina and lamina ganglionaris of the fly, *Musca domestica*. *Zeitschrift für Zellforschung und Mikroskopische Anatomie*, 118(3), pp.369–409.

Braitenberg, V. (1967). Patterns of projection in the visual system of the fly. I. Retina-lamina projections. *Experimental Brain Research*, 3(3).

Braitenberg, V. (1972). Periodic structures and structural gradients in the visual ganglia of the fly. In: WehnerR., ed., *Information processing in the visual systems of arthropods*. Berlin; New York: Springer-Verlag, pp.3–15.

Broglie, L. de (1924). XXXV. A tentative theory of light quanta. *The London, Edinburgh, and Dublin Philosophical Magazine and Journal of Science*, 47(278), pp.446–458.

Buchner, E. (1971). *Dunkelanregung des stationaeren Flugs der Fruchtfliege Drosophila*. Dipl Thesis.

Buchner, E., Buchner, S. and Buelthoff, I. (1984). Deoxyglucose mapping of nervous activity induced in*Drosophila* brain by visual movement. *Journal of Comparative Physiology A*, 155(4), pp.471–483.

Burkhardt, D., de la Motte, I. and Seitz, G. (1966). Physiological optics of the compound eye of the blowfly. In: C.G. Bernhard, ed., *The functional organization of the compound eye*. Oxford, New York, Symposium Publications Division, Pergamon Press, pp.51–62.

Burkhardt, W. and Braitenberg, V. (1976). Some peculiar synaptic complexes in the first visual ganglion of the fly, *Musca domestica*. *Cell and Tissue Research*, 173(3).

Burton, B.G. (2002). Long-term light adaptation in photoreceptors of the housefly, *Musca domestica*. *Journal of Comparative Physiology A*, 188(7), pp.527–538.

Burton, B.G. (2006). Adaptation of single photon responses in photoreceptors of the housefly, *Musca domestica*: A novel spectral analysis. *Vision Research*, 46(5), pp.622–635.

Burton, B.G. and Laughlin, S.B. (2003). Neural images of pursuit targets in the photoreceptor arrays of male and female houseflies *Musca domestica*. *Journal of Experimental Biology*, 206(22), pp.3963–3977.

Burton, B.G., Tatler, B.W. and Laughlin, S.B. (2001). Variations in Photoreceptor Response Dynamics Across the Fly Retina. *Journal of Neurophysiology*, 86(2), pp.950–960.

Cajal, R. y C. and Sanchez, D. (1915). *Contribución al conocimiento de los insectos*. *Trab Lab Invest Biol Uni Madrid*, Madrid: Imprenta de Hijos de Nicolás Moya, pp.1–168.

Campos-Ortega, J.A. and Strausfeld, N.J. (1973). Synaptic connections of intrinsic cells and basket arborizations in the external plexiform layer of the fly's eye. *Brain Research*, 59(), pp.119–136.

Carpenter, R. and Reddi, B. (2012). *Neurophysiology: a conceptual approach*. London: Hodder Arnold.

Chi, C. and Carlson, S.D. (1980). Membrane specializations in the first optic neuropil of the housefly, *Musca domestica* L. I. Junctions between neurons. *Journal of Neurocytology*, 9(4), pp.429–449.

Chiappe, M.E., Seelig, J.D., Reiser, M.B. and Jayaraman, V. (2010). Walking Modulates Speed Sensitivity in *Drosophila* Motion Vision. *Current Biology*, 20(16), pp.1470–1475.

Clark, Damon A., Bursztyn, L., Horowitz, Mark A., Schnitzer, Mark J. and Clandinin, Thomas R. (2011). Defining the Computational Structure of the Motion Detector in *Drosophila*. *Neuron*, 70(6), pp.1165–1177.

Collett, T.S. and Land, M.F. (1975). Visual control of flight behaviour in the hoverfly Syritta pipiens L. *Journal of Comparative Physiology A*, 99(1), pp.1–66.

Coombe, P.E. (1986). The large monopolar cells L1 and L2 are responsible for ERG transients in*Drosophila*. *Journal of Comparative Physiology A*, 159(5), pp.655–665.

Dau, A., Friederich, U., Dongre, S., Li, X., Bollepalli, M.K., Hardie, R.C. and Juusola, M. (2016). Evidence for Dynamic Network Regulation of *Drosophila* Photoreceptor Function from Mutants Lacking the Neurotransmitter Histamine. Frontiers in Neural Circuits, 10.

de Ruyter van Steveninck, R.R. and Laughlin, S.B. (1996). Light adaptation and reliability in blowfly photoreceptors. *International Journal of Neural Systems*, 07(04), pp.437–444.

Dietrich, W. (1909). *Die facettenaugen der dipteren*. *Z Wiss Zool*, Leipzig: W. Engelmann, pp.465–539.

Dodge, F.A., Knight, B.W. and Toyoda, J. (1968). Voltage Noise in Limulus Visual Cells. *Science*, 160(3823), pp.88–90.

Dubs, A. (1981). Non-Linearity and light adaptation in the fly photoreceptor. *Journal of Comparative Physiology A*, 144(1), pp.53–59.

Dubs, A. (1982). The spatial integration of signals in the retina and lamina of the fly compound eye under different conditions of luminance. *Journal of Comparative Physiology*, 146(3), pp.321–343.

Edwards, T.N., Nuschke, A.C., Nern, A. and Meinertzhagen, I.A. (2012). Organization and metamorphosis of glia in the *Drosophila* visual system. *The Journal of Comparative Neurology*, 520(10), pp. Spc1–Spc1.

Eichner, H., Joesch, M., Schnell, B., Reiff, Dierk F. and Borst, A. (2011). Internal Structure of the Fly Elementary Motion Detector. *Neuron*, 70(6), pp.1155–1164.

Fain, G.L., Hardie, R. and Laughlin, S.B. (2010). Phototransduction and the Evolution of Photoreceptors. *Current Biology*, 20(3), pp. R114–R124.

Faivre, O. and Juusola, M. (2008). Visual Coding in Locust Photoreceptors. *PLoS ONE*, 3(5), p.e2173.

Farrow, K., Haag, J. and Borst, A. (2003). Input Organization of Multifunctional Motion-Sensitive Neurons in the Blowfly. *The Journal of Neuroscience*, 23(30), pp.9805–9811.

Feiler, R., Bjornson, R., Kirschfeld, K., Mismer, D., Rubin, G., Smith, D., Socolich, M. and Zuker, C. (1992). Ectopic expression of ultraviolet-rhodopsins in the blue photoreceptor cells of *Drosophila*: visual physiology and photochemistry of transgenic animals. *The Journal of Neuroscience*, 12(10), pp.3862–3868.

Fermi, G. and Richardt, W. (1963). Optomotorische Reaktionen der Fliege *Musca domestica*. *Kybernetik*, 2(1), pp.15–28.

Fischbach, K.-F. and Dittrich, A.P.M. (1989). The optic lobe of *Drosophila melanogaster*. I. A Golgi analysis of wild-type structure. *Cell and Tissue Research*, 258(3).

Franceschini, N. (1972). Pupil and pseudopupil in the compound eye of *Drosophila*. In: R. Wehner, ed., *Information processing in the visual systems of arthropods*. Berlin-Heidelberg New York: Springer, pp.75–82.

Franceschini, N. and Kirschfeld, K. (1971a). Etude optique *in vivo* des éléments photorécepteurs dans l'œil composé de *Drosophila*. *Kybernetik*, 8(1), pp.1–13.

Franceschini, N. and Kirschfeld, K. (1971b). Les phénomènes de pseudopupille dans l'œil composé de*Drosophila*. *Kybernetik*, 9(5), pp.159–182.

Franceschini, N., Münster, A. and Heurkens, G. (1979). Äquatoriales und binokulares Sehen bei der Fliege *Calliphora* erythrocephala. *Verh Dtsch Zool Ges*, p.209.

French, A.S. (1980). Phototransduction in the fly compound eye exhibits temporal resonances and a pure time delay. *Nature*, 283(5743), pp.200–202.

Fryxell, K.J. and Meyerowitz, E.M. (1987). An opsin gene that is expressed only in the R7 photoreceptor cell of *Drosophila*. *The EMBO Journal*, 6(2), pp.443–451.

Fuortes, M.G.F. and Yeandle, S. (1964). Probability of Occurrence of Discrete Potential Waves in the Eye of Limulus. *Journal of General Physiology*, 47(3), pp.443–463.

Gao, S., Takemura, S., Ting, C.-Y., Huang, S., Lu, Z., Luan, H., Rister, J., Thum, A.S., Yang, M., Hong, S.-T., Wang, J.W., Odenwald, W.F., White, B.H., Meinertzhagen, I.A. and Lee, C.-H. (2008). The Neural Substrate of Spectral Preference in *Drosophila*. *Neuron*, 60(2), pp.328–342.

Geurten, B.R.H., Jähde, P., Corthals, K. and Göpfert, M.C. (2014). Saccadic body turns in walking *Drosophila*. *Frontiers in Behavioral Neuroscience*, 8.

Gonzalez-Bellido, P.T., Wardill, T.J. and Juusola, M. (2011). Compound eyes and retinal information processing in miniature dipteran species match their specific ecological demands. *Proceedings of the National Academy of Sciences*, 108(10), pp.4224–4229.

Gu, Y., Oberwinkler, J., Postma, M. and Hardie, R.C. (2005). Mechanisms of Light Adaptation in *Drosophila* Photoreceptors. *Current Biology*, 15(13), pp.1228–1234.

Guy, R.G. and Srinivasan, M.V. (1988). Integrative properties of second-order visual neurons: a study of large monopolar cells in the dronefly Eristalis. *Journal of Comparative Physiology A*, 162(3), pp.317–331.

Hardie, R.C. (1979). Electrophysiological analysis of fly retina. I: Comparative properties of R1-6 and R 7 and 8. *Journal of Comparative Physiology A*, 129(1), pp.19–33.

Hardie, R.C. (1985). Functional organization of the fly retina. In: D. Ottoson, ed., *Progress in sensory physiology*. Berlin, Heidelberg, New York: Springer, pp.1–79.

Hardie, R.C. (1987). Is histamine a neurotransmitter in insect photoreceptors? *Journal of Comparative Physiology A*, 161(2), pp.201–213.

Hardie, R.C. (1989). A histamine-activated chloride channel involved in neurotransmission at a photoreceptor synapse. *Nature*, 339(6227), pp.704–706.

Hardie, R.C. (1991). Voltage-sensitive potassium channels in *Drosophila* photoreceptors. *The Journal of Neuroscience*, 11(10), pp.3079–3095.

Hardie, R.C. (2011). Phototransduction mechanisms in *Drosophila* microvillar photoreceptors. *Wiley Interdisciplinary Reviews: Membrane Transport and Signaling*, 1(2), pp.162–187.

Hardie, R.C., Franceschini, N., Ribi, W. and Kirschfeld, K. (1981). Distribution and properties of sex-specific photoreceptors in the fly *Musca domestica*. *Journal of Comparative Physiology A*, 145(2), pp.139–152.

Hardie, R.C. and Juusola, M. (2015). Phototransduction in *Drosophila*. *Current Opinion in Neurobiology*, 34, pp.37–45.

Hardie, R.C., Peretz, A., Suss-Toby, E., Rom-Glas, A., Bishop, S.A., Selinger, Z. and Minke, B. (1993). Protein kinase C is required for light adaptation in *Drosophila* photoreceptors. *Nature*, 363(6430), pp.634–637.

Hardie, R.C. and Postma, M. (2008). Phototransduction in microvillar photoreceptors of *Drosophila* and other invertebrates. *The Senses - A Comprehensive Reference*, 1(), pp.77–130.

Hardie, R.C. and Raghu, P. (2001). Visual transduction in *Drosophila*. *Nature*, 413(6852), pp.186–193.

Hardie, R.C., Voss, D., Pongs, O. and Laughlin, S.B. (1991). Novel potassium channels encoded by the Shaker locus in *Drosophila* photoreceptors. *Neuron*, 6(3), pp.477–486.

Hardie, R.C. and Weckström, M. (1990). Three classes of potassium channels in large monopolar cells of the blowfly *Calliphora vicina*. *Journal of Comparative Physiology A*, 167(6).

Hartline, H.K. (1949). Inhibition of activity of visual receptors by illuminating nearby retinal elements in the Limulus eye. *Fed. Proc.*, 8(69).

Hassenstein, B. and Reichardt, W. (1956). Systemtheoretische Analyse der Zeit-, Reihenfolgen- und Vorzeichenauswertung bei der Bewegungsperzeption des Rüsselkäfers Chlorophanus. *Zeitschrift für Naturforschung B*, 11(9-10), pp.513–524.

van Hateren, J.H. (1986). Electrical coupling of neuro-ommatidial photoreceptor cells in the blowfly. *Journal of Comparative Physiology A*, 158(6), pp.795–811.

van Hateren, J.H. (1989). Photoreceptor Optics, Theory and Practice. In: D.G. Stavenga and R.C. Hardie, eds., *Facets of vision*. Berlin: Springer -Verlag.

van Hateren, J.H. (1992a). A theory of maximizing sensory information. *Biological Cybernetics*, 68(1), pp.23–29.

van Hateren, J.H. (1992b). Theoretical predictions of spatiotemporal receptive fields of fly LMCs, and experimental validation. *Journal of Comparative Physiology A*, 171(2), pp.157–170.

van Hateren, J.H. (1997). Processing of Natural Time Series of Intensities in the Early Visual System of the Blowfly. *Perception*, 26(1_suppl), pp.24–24.

van Hateren, J.H. and Laughlin, S.B. (1990). Membrane parameters, signal transmission, and the design of a graded potential neuron. *Journal of Comparative Physiology A*, 166(4), pp.437–448.

van Hateren, J.H. and Schilstra, C. (1999). Blowfly flight and optic flow. II. Head movements during flight. *Journal of Experimental Biology*, 202, pp.1491–1500.

van Hateren, J.H. and Snippe, H.P. (2001). Information theoretical evaluation of parametric models of gain control in blowfly photoreceptor cells. *Vision Research*, 41(14), pp.1851–1865.

Hauser-Holschuh, H. (1975). *Vergleichend quantitative Untersuchungen an den Sehganglien der Fliegen Musca domestica und Drosophila melanogaster*. PhD thesis. Eberhard-Karls-Universität zu Tübingen, Tübingen, Germany.

Heisenberg, M. (1971). Separation of Receptor and Lamina Potentials in the Electroretinogram of Normal and Mutant *Drosophila*. *Journal of Experimental Biology*, 55(1), pp.85–100.

Heisenberg, M. and Buchner, E. (1977). The role of retinula cell types in visual behavior of *Drosophila melanogaster*. *Journal of Comparative Physiology A*, 117(2), pp.127–162.

Henderson, S.R., Reuss, H. and Hardie, R.C. (2000). Single photon responses in *Drosophila* photoreceptors and their regulation by Ca2+. *The Journal of Physiology*, 524(1), pp.179–194.

Hochstrate, P. and Hamdorf, K. (1990). Microvillar components of light adaptation in blowflies. *The Journal of General Physiology*, 95(5), pp.891–910.

Hornstein, E.P., O'Carroll, D.C., Anderson, J.C. and Laughlin, S.B. (2000). Sexual dimorphism matches photoreceptor performance to behavioural requirements. *Proceedings of the Royal Society of London. Series B: Biological Sciences*, 267(1457), pp.2111–2117.

Horridge, G.A. (1977). The Compound Eye of Insects. *Scientific American*, 237(1), pp.108–120.

Horridge, G.A., Mimura, K. and Hardie, R.C. (1976). Fly photoreceptors. III. Angular sensitivity as a function of wavelength and the limits of resolution. *Proceedings of the Royal Society of London. Series B. Biological Sciences*, 194(1115), pp.151–177.

Howard, J., Blakeslee, B. and Laughlin, S. (1987). The intracellular pupil mechanism and photoreceptor signal: noise ratios in the fly Lucilia cuprina. *Proceedings of the Royal Society of London. Series B. Biological Sciences*, 231(1265), pp.415–435.

Huber, A., Smith, D.P., Zuker, C.S. and Paulsen, R. (1990). Opsin of *Calliphora* peripheral photoreceptors R1-6. Homology with *Drosophila* Rh1 and posttranslational processing. *Journal of Biological Chemistry*, 265(29), pp.17906–17910.

Jansonius, N.M. (1990). Properties of the sodium pump in the blowfly photoreceptor cell. *Journal of Comparative Physiology A*, 167(4).

Järvilehto, M. and Zettler, F. (1971). Localized intracellular potentials from pre- and postsynaptic components in the external plexiform layer of an insect retina. *Zeitschrift für vergleichende Physiologie*, 75(4), pp.422–440.

Joesch, M., Plett, J., Borst, A. and Reiff, D.F. (2008). Response Properties of Motion-Sensitive Visual Interneurons in the Lobula Plate of *Drosophila melanogaster*. *Current Biology*, 18(5), pp.368–374.

Joesch, M., Schnell, B., Raghu, S.V., Reiff, D.F. and Borst, A. (2010). ON and OFF pathways in *Drosophila* motion vision. *Nature*, 468(7321), pp.300–304.

Joesch, M., Weber, F., Eichner, H. and Borst, A. (2013). Functional Specialization of Parallel Motion Detection Circuits in the Fly. *Journal of Neuroscience*, 33(3), pp.902–905.

Johnson, E.C. and Pak, W.L. (1986). Electrophysiological study of *Drosophila* rhodopsin mutants. *Journal of General Physiology*, 88(5), pp.651–673.

Jung, S.N., Borst, A. and Haag, J. (2011). Flight Activity Alters Velocity Tuning of Fly Motion-Sensitive Neurons. *Journal of Neuroscience*, 31(25), pp.9231–9237.

Juusola, M. (1993). Linear and non-linear contrast coding in light-adapted blowfly photoreceptors. *Journal of Comparative Physiology A*, 172(4), pp.511–521.

Juusola, M., Dau, A., Song, Z., Solanki, N., Rien, D., Jaciuch, D., Dongre, S.A., Blanchard, F., de Polavieja, G.G., Hardie, R.C. and Takalo, J. (2017). Microsaccadic sampling of moving image information provides *Drosophila* hyperacute vision. *Elife*, 6(),

Juusola, M., Dau, A., Zheng, L. and Rien, D. (2016). Electrophysiological Method for Recording Intracellular Voltage Responses of *Drosophila* Photoreceptors and Interneurons to Light Stimuli *In vivo*. *Journal of Visualized Experiments*, (112).

Juusola, M. and de Polavieja, G.G. (2003). The Rate of Information Transfer of Naturalistic Stimulation by Graded Potentials. *Journal of General Physiology*, 122(2), pp.191–206.

Juusola, M. and French, A.S. (1997). Visual Acuity for Moving Objects in First- and Second-Order Neurons of the Fly Compound Eye. *Journal of Neurophysiology*, 77(3), pp.1487–1495.

Juusola, M. and Hardie, R.C. (2001a). Light Adaptation in *Drosophila* Photoreceptors: I. Response Dynamics and Signalling Efficiency at 25oC. *Journal of General Physiology*, 117(1), pp.3–25.

Juusola, M. and Hardie, R.C. (2001b). Light Adaptation in *Drosophila* Photoreceptors: II. Rising temperature increases the bandwidth of reliable signaling. *Journal of General Physiology*, 117(1), pp.27–42.

Juusola, M., Kouvalainen, E., Järvilehto, M. and Weckström, M. (1994). Contrast gain, signal-to-noise ratio, and linearity in light-adapted blowfly photoreceptors. *The Journal of General Physiology*, 104(3), pp.593–621.

Juusola, M. and Song, Z. (2017). How a fly photoreceptor samples light information in time. *The Journal of Physiology*, 595(16), pp.5427–5437.

Juusola, M., Song, Z. and Hardie, R.C. (2015). Biophysics of insect phototransduction. *Encyclopedia of Computational Neuroscience*, pp.2359–2376.

Juusola, M., Uusitalo, R.O. and Weckström, M. (1995). Transfer of graded potentials at the photoreceptor-interneuron synapse. *The Journal of General Physiology*, 105(1), pp.117–148.

Juusola, M., Weckstrom, M., Uusitalo, R.O., Korenberg, M.J. and French, A.S. (1995). Nonlinear models of the first synapse in the light-adapted fly retina. *Journal of Neurophysiology*, 74(6), pp.2538–2547.

K. Kirschfeld, K. (1966). Discrete and graded receptor potentials in the compound eye of the fly (*Musca*). In: C.G. Bernhard, ed., *The functional organization of the compound eye*. Oxford, New York, Pergamon Press, pp.291–307.

Kirschfeld, K. (1967). Die projektion der optischen umwelt auf das raster der rhabdomere im komplexauge von *Musca*. *Experimental Brain Research*, 3(3).

Kirschfeld, K. and Franceschini, N. (1969). Ein Mechanismus zur Steuerung des Lichtflusses in den Rhabdomeren des Komplexauges von *Musca*. *Kybernetik*, 6(1), pp.13–22.

Kirschfeld, K., Franceschini, N. and Minke, B. (1977). Evidence for a sensitising pigment in fly photoreceptors. *Nature*, 269(5627), pp.386–390.

Kirschfeld, K. and Vogt, K. (1980). Calcium ions and pigment migration in fly photoreceptors. *Naturwissenschaften*, 67(10), pp.516–517.

Kuiper, J.W. (1966). The functional organization of the compound eye. In: C.G. Bernhard, ed., *on the image formation in a single ommatidium of the compound eye in diptera.* Oxford, New York, Symposium Publications Division, Pergamon Press.

Land, M.F. (1997). Visual acuity in insects. *Annual Review of Entomology*, 42(1), pp.147–177.

Land, M.F. (1999). Motion and vision: why animals move their eyes. *Journal of Comparative Physiology A: Sensory, Neural, and Behavioral Physiology*, 185(4), pp.341–352.

Land, M.F. and Collett, T.S. (1974). Chasing behaviour of houseflies (Fannia canicularis). *Journal of Comparative Physiology*, 89(4), pp.331–357.

Land, M.F. and Eckert, H. (1985). Maps of the acute zones of fly eyes. *Journal of Comparative Physiology A*, 156(4), pp.525–538.

Laughlin, S.B. (1973). Neural integration in the first optic neuropile of dragonflies. I. Signal amplification in dark-adapted second order neurons. *Journal of Comparative Physiology*, 84(4), pp.335–355.

Laughlin, S.B. (1981a). A Simple Coding Procedure Enhances a Neuron’s Information Capacity. *Zeitschrift für Naturforschung C*, 36(9-10), pp.910–912.

Laughlin, S.B. (1981b). Neural principles in the peripheral visual systems of invertebrates. *Handbook of sensory physiology*, 7/6b, p.

Laughlin, S.B. (1987). Form and function in retinal processing. *Trends in Neurosciences*, 10(11), pp.478–483.

Laughlin, S.B. (1989). The role of sensory adaptation in the retina. *J Exp Biol*, 146, pp.39–62.

Laughlin, S.B. and Hardie, R.C. (1978). Common strategies for light adaptation in the peripheral visual systems of fly and dragonfly. *Journal of Comparative Physiology A*, 128(4), pp.319–340.

Laughlin, S.B., Howard, J. and Blakeslee, B. (1987). Synaptic limitations to contrast coding in the retina of the blowfly *Calliphora*. *Proceedings of the Royal Society of London. Series B. Biological Sciences*, 231(1265), pp.437–467.

Laughlin, S.B. and Lillywhite, P.G. (1982). Intrinsic noise in locust photoreceptors. *The Journal of Physiology*, 332(1), pp.25–45.

Laughlin, S.B. and Osorio, D. (1989). Mechanisms for neural signal enhancement in the blowfly compound eye. *J. Exp. Biol*, 144, pp.113–146.

Laughlin, S.B. and Weckström, M. (1993). Fast and slow photoreceptors - a comparative study of the functional diversity of coding and conductances in the Diptera. *Journal of Comparative Physiology A*, 172(5), pp.593–609.

Li, X. (2011). *Information Processing and Distribution in the Fly Early Visual system*. PhD thesis.

Li, X., Abou Tayoun, A., Song, Z., Dau, A., Rien, D., Jaciuch, D., Dongre, S., Blanchard, F., Nikolaev, A., Zheng, L., Bollepalli, M.K., Chu, B., Hardie, R.C., Dolph, P.J. and Juusola, M. (2019). Ca2+-Activated K+ Channels Reduce Network Excitability, Improving Adaptability and Energetics for Transmitting and Perceiving Sensory Information. *The Journal of Neuroscience*, 39(36), pp.7132–7154.

Lillywhite, P.G. (1977). Single photon signals and transduction in an insect eye. *Journal of Comparative Physiology*, 122(2), pp.189–200.

Lillywhite, P.G. and Laughlin, S.B. (1979). Transducer noise in a photoreceptor. *Nature*, 277(5697), pp.569–572.

Liu, C.-H., Chen, Z., Oliva, M.K., Luo, J., Collier, S., Montell, C. and Hardie, R.C. (2020). Rapid Release of Ca2+ from Endoplasmic Reticulum Mediated by Na+/Ca2+ Exchange. *The Journal of Neuroscience*, 40(16), pp.3152–3164.

Maimon, G., Straw, A.D. and Dickinson, M.H. (2010). Active flight increases the gain of visual motion processing in *Drosophila*. *Nature Neuroscience*, 13(3), pp.393–399.

Maisak, M.S., Haag, J., Ammer, G., Serbe, E., Meier, M., Leonhardt, A., Schilling, T., Bahl, A., Rubin, G.M., Nern, A., Dickson, B.J., Reiff, D.F., Hopp, E. and Borst, A. (2013). A directional tuning map of *Drosophila* elementary motion detectors. *Nature*, 500(7461), pp.212–216.

Mallock, A. (1894). I. Insect sight and the defining power of composite eyes. *Proceedings of the Royal Society of London*, 55(331-335), pp.85–90.

Marmarelis, P.Z. and Marmarelis, V.Z. (1978). *Analysis of physiological systems: the white-noise approach*. London: Plenum Press.

Mauss, A.S., Pankova, K., Arenz, A., Nern, A., Rubin, G.M. and Borst, A. (2015). Neural Circuit to Integrate Opposing Motions in the Visual Field. *Cell*, 162(2), pp.351–362.

Meinertzhagen, I.A. and O'Neil, S.D. (1991). Synaptic organization of columnar elements in the lamina of the wild type in *Drosophila melanogaster*. *The Journal of Comparative Neurology*, 305(2), pp.232–263.

Melamed, J. and Trujillo-Cenóz, O. (1967). The fine structure of the central cells in the ommatidia of dipterans. *Journal of Ultrastructure Research*, 21(3-4), pp.313–334.

Mongeau, J.-M. and Frye, M.A. (2017). *Drosophila* Spatiotemporally Integrates Visual Signals to Control Saccades. *Current Biology*, 27(19), pp.2901-2914.e2.

Montell, C. (1989). Molecular genetics of *Drosophila* vision. *BioEssays*, 11(2-3), pp.43–48.

Montell, C. (2012). *Drosophila* visual transduction. *Trends in Neurosciences*, 35(6), pp.356–363.

Montell, C., Jones, K., Zuker, C. and Rubin, G. (1987). A second opsin gene expressed in the ultraviolet-sensitive R7 photoreceptor cells of *Drosophila melanogaster*. *The Journal of Neuroscience*, 7(5), pp.1558–1566.

Nicol, D. and Meinertzhagen, I.A. (1982). An analysis of the number and composition of the synaptic populations formed by photoreceptors of the fly. *The Journal of Comparative Neurology*, 207(1), pp.29–44.

Niemeyer, B.A., Suzuki, E., Scott, K., Jalink, K. and Zuker, C.S. (1996). The *Drosophila* Light-Activated Conductance Is Composed of the Two Channels TRP and TRPL. *Cell*, 85(5), pp.651–659.

Nikolaev, A., Zheng, L., Wardill, T.J., O'Kane, C.J., de Polavieja, G.G. and Juusola, M. (2009). Network Adaptation Improves Temporal Representation of Naturalistic Stimuli in *Drosophila* Eye: II Mechanisms. *PLoS ONE*, 4(1), p.e4306.

Niven, J.E., Anderson, J.C. and Laughlin, S.B. (2007). Fly Photoreceptors Demonstrate Energy-Information Trade-Offs in Neural Coding. *PLoS Biology*, 5(4), p.e116.

Niven, J.E., Vähäsöyrinki, M., Kauranen, M., Hardie, R.C., Juusola, M. and Weckström, M. (2003). The contribution of Shaker K+ channels to the information capacity of *Drosophila* photoreceptors. *Nature*, 421(6923), pp.630–634.

O'Tousa, J.E., Baehr, W., Martin, R.L., Hirsh, J., Pak, W.L. and Applebury, M.L. (1985). The *Drosophila* ninaE gene encodes an opsin. *Cell*, 40(4), pp.839–850.

Osorio, D. (2007). Spam and the evolution of the fly's eye. *BioEssays*, 29(2), pp.111–115.

Pak, W., Istrit, S., Deland, M. and Wu, C. (1976). Photoreceptor mutant of *Drosophila*: is protein involved in intermediate steps of phototransduction? *Science*, 194(4268), pp.956–959.

Pak, W.L., Grossfield, J. and Arnold, K.S. (1970). Mutants of the Visual Pathway of *Drosophila melanogaster*. *Nature*, 227(5257), pp.518–520.

Pantazis, A., Segaran, A., Liu, C.-H., Nikolaev, A., Rister, J., Thum, A.S., Roeder, T., Semenov, E., Juusola, M. and Hardie, R.C. (2008). Distinct Roles for Two Histamine Receptors (hclA and hclB) at the *Drosophila* Photoreceptor Synapse. *Journal of Neuroscience*, 28(29), pp.7250–7259.

Perry, M.W. and Desplan, C. (2016). Love spots. *Current Biology*, 26(12), pp. R484–R485.

Pick, B. (1977). Specific misalignments of rhabdomere visual axes in the neural superposition eye of dipteran flies. *Biological Cybernetics*, 26(4), pp.215–224.

Raghu, S.V. and Borst, A. (2011). Candidate Glutamatergic Neurons in the Visual System of *Drosophila*. *PLoS ONE*, 6(5), p.e19472.

Ramos-Traslosheros, G., Henning, M. and Silies, M. (2018). Motion detection: cells, circuits and algorithms. *Neuroforum*, 24(2), pp. A61–A72.

Ranganathan, R., Malicki, D.M. and Zuker, C.S. (1995). Signal Transduction in *Drosophila* Photoreceptors. *Annual Review of Neuroscience*, 18(1), pp.283–317.

Reichardt, W. (1961). Autocorrelation, a principle for the evaluation of sensory information by the central nervous system. In: W.A. Rosenblith, ed., *Sensory Communication*. MIT Press, pp.303–317.

Reuss, H., Mojet, M.H., Chyb, S. and Hardie, R.C. (1997). *In vivo* analysis of the *Drosophila* light-sensitive channels, TRP and TRPL. *Neuron*, 19(6), pp.1249–59.

Ribi, WilliA. (1978). Gap junctions coupling photoreceptor axons in the first optic ganglion of the fly. *Cell and Tissue Research*, 195(2).

Rice, S.O. (1944). Mathematical Analysis of Random Noise. *Bell System Technical Journal*, 23(3), pp.282–332.

Rister, J., Pauls, D., Schnell, B., Ting, C.-Y., Lee, C.-H., Sinakevitch, I., Morante, J., Strausfeld, N.J., Ito, K. and Heisenberg, M. (2007). Dissection of the Peripheral Motion Channel in the Visual System of *Drosophila melanogaster*. *Neuron*, 56(1), pp.155–170.

Rivera-Alba, M., Vitaladevuni, Shiv N., Mishchenko, Y., Lu, Z., Takemura, S., Scheffer, L., Meinertzhagen, Ian A., Chklovskii, Dmitri B. and de Polavieja, Gonzalo G. (2011). Wiring Economy and Volume Exclusion Determine Neuronal Placement in the *Drosophila* Brain. *Current Biology*, 22(2), p.172.

Roebroek, J.G.H. and Stavenga, D.G. (1990). On the effective optical density of the pupil mechanism in fly photoreceptors. *Vision Research*, 30(8), pp.1235–1242.

Roebroek, J.G.H., van Tjonger, M. and Stavenga, D.G. (1990). Temperature dependence of receptor potential and noise in fly (*Calliphora* erythrocephala) photoreceptor cells. *Journal of Insect Physiology*, 36(7), pp.499–505.

Rusanen, J. and Weckström, M. (2016). Frequency-selective transmission of graded signals in large monopolar neurons of blowfly *Calliphora vicina* compound eye. *Journal of Neurophysiology*, 115(4), pp.2052–2064.

Salem, W., Cellini, B., Frye, M.A. and Mongeau, J.-M. (2020). Fly eyes are not still: a motion illusion in *Drosophila* flight supports parallel visual processing. *The Journal of Experimental Biology*, 223(10), p.jeb212316.

Sarthy, P.V. (1991). Histamine: A Neurotransmitter Candidate for *Drosophila* Photoreceptors. *Journal of Neurochemistry*, 57(5), pp.1757–1768.

Sato, M., Suzuki, T. and Nakai, Y. (2013). Waves of differentiation in the fly visual system. *Developmental Biology*, 380(1), pp.1–11.

Sayeed, O. and Benzer, S. (1996). Behavioral genetics of thermosensation and hygrosensation in *Drosophila*. *Proceedings of the National Academy of Sciences*, 93(12), pp.6079–6084.

Schilstra, C. and van Hateren, J.H. (1999). Blowfly flight and optic flow. I. Thorax kinematics and flight dynamics. *J Exp Biol*, 202, pp.1481–1490.

Schneider, J., Murali, N., Taylor, G.W. and Levine, J.D. (2018). Can *Drosophila melanogaster* tell who's who? *PLOS ONE*, 13(10), p.e0205043.

Schnell, B., Joesch, M., Forstner, F., Raghu, S.V., Otsuna, H., Ito, K., Borst, A. and Reiff, D.F. (2010). Processing of Horizontal Optic Flow in Three Visual Interneurons of the *Drosophila* Brain. *Journal of Neurophysiology*, 103(3), pp.1646–1657.

Schnell, B., Raghu, S.V., Nern, A. and Borst, A. (2012). Columnar cells necessary for motion responses of wide-field visual interneurons in *Drosophila*. *Journal of Comparative Physiology A*, 198(5), pp.389–395.

Scholes, J. (1969). The electrical responses of the retinal receptors and the lamina in the visual system of the fly *Musca*. *Kybernetik*, 6(4), pp.149–162.

Scott, E.K., Raabe, T. and Luo, L. (2002). Structure of the vertical and horizontal system neurons of the lobula plate in *Drosophila*. *The Journal of Comparative Neurology*, 454(4), pp.470–481.

Scott, K., Becker, A., Sun, Y., Hardy, R. and Zuker, C. (1995). Gqα protein function *in vivo*: Genetic dissection of its role in photoreceptor cell physiology. *Neuron*, 15(4), pp.919–927.

Scott, K. and Zuker, C.S. (1998). Assembly of the *Drosophila* phototransduction cascade into a signalling complex shapes elementary responses. *Nature*, 395(6704), pp.805–808.

Shannon, C.E. (1948). The Mathematical Theory of Communication. *Bell Syst. Tech. J.*, 27(), pp.623–656.

Shannon, C.E. and Weaver, W. (1949). The Mathematical Theory of Communication. *University of Illinois Press*.

Shapley, R. and Enroth-Cugell, C. (1984). Chapter 9 Visual adaptation and retinal gain controls. *Progress in Retinal Research*, 3, pp.263–346.

Shaw, S. (1984). Early visual processing in insects. *J Exp Biol*, 112(), pp.225–251.

Shaw, S. (1988). The retina-Lamina pathway in insects, particularly Diptera, viewed from an evolutionary perspective. In: D. Stavenga and R. Hardie, eds., *Facets of vision*. Springer-Verlag.

Shaw, S. and Stowe, S. (1982). Freeze-fracture evidence for gap-junctions connecting the axon terminals of dipteran photoreceptors. *Journal of Cell Science*, 53(), pp.115–141.

Shaw, S.R. (1981). Anatomy and physiology of identified non-spiking cells in the photoreceptor-lamina complex of the compound eye of insects, especially Diptera. In: A. Roberts and B.M.H. Bush, eds., *Neurons without impulses*. Cambridge University Press, pp.61–116.

Shaw, S.R., Fröhlich, A. and Meinertzhagen, I.A. (1989). Direct connections between the R7/8 and R1?6 photoreceptor subsystems in the dipteran visual system. *Cell and Tissue Research*, 257(2), pp.295–302.

Shinomiya, K., Huang, G., Lu, Z., Parag, T., Xu, C.S., Aniceto, R., Ansari, N., Cheatham, N., Lauchie, S., Neace, E., Ogundeyi, O., Ordish, C., Peel, D., Shinomiya, A., Smith, C., Takemura, S., Talebi, I., Rivlin, P.K., Nern, A. and Scheffer, L.K. (2019). Comparisons between the ON- and OFF-edge motion pathways in the *Drosophila* brain. *eLife*, 8.

Shinomiya, K., Karuppudurai, T., Lin, T.-Y., Lu, Z., Lee, C.-H. and Meinertzhagen, Ian A. (2014). Candidate Neural Substrates for Off-Edge Motion Detection in *Drosophila*. *Current Biology*, 24(10), pp.1062–1070.

Silies, M., Gohl, Daryl M., Fisher, Yvette E., Freifeld, L., Clark, Damon A. and Clandinin, Thomas R. (2013). Modular Use of Peripheral Input Channels Tunes Motion-Detecting Circuitry. *Neuron*, 79(1), pp.111–127.

Skingsley, D.R., Laughlin, S.B. and Hardie, R.C. (1995). Properties of histamine-activated chloride channels in the large monopolar cells of the dipteran compound eye: a comparative study. *Journal of Comparative Physiology A*, 176(5), pp.611–623.

Smakman, J.G.J., van Hateren, J.H. and Stavenga, D.G. (1984). Angular sensitivity of blowfly photoreceptors: intracellular measurements and wave-optical predictions. *Journal of Comparative Physiology A*, 155(2), pp.239–247.

Smith, D.P., Stamnes, M.A. and Zuker, C.S. (1991). Signal Transduction in the Visual System of *Drosophila*. *Annual Review of Cell Biology*, 7(1), pp.161–190.

Snyder, A.W. (1975). Photoreceptor optics - theoretical principles. In: A.W. Snyder and R. Menzel, eds., *Photoreceptor optics*. Berlin; New York: Springer-Verlag, pp.38–55.

Snyder, A.W. (1977). Acuity of compound eyes: Physical limitations and design. *Journal of Comparative Physiology A*, 116(2), pp.161–182.

Snyder, A.W., Menzel, R. and Laughlin, S.B. (1973). Structure and function of the fused rhabdom. *Journal of Comparative Physiology*, 87(2), pp.99–135.

Song, Z. and Juusola, M. (2014). Refractory Sampling Links Efficiency and Costs of Sensory Encoding to Stimulus Statistics. *Journal of Neuroscience*, 34(21), pp.7216–7237.

Song, Z. and Juusola, M. (2017). A biomimetic fly photoreceptor model elucidates how stochastic adaptive quantal sampling provides a large dynamic range. *The Journal of Physiology*, 595(16), pp.5439–5456.

Song, Z., Postma, M., Billings, Stephen A., Coca, D., Hardie, Roger C. and Juusola, M. (2012). Stochastic, Adaptive Sampling of Information by Microvilli in Fly Photoreceptors. *Current Biology*, 22(15), pp.1371–1380.

Song, Z., Zhou, Y. and Juusola, M. (2016). Random Photon Absorption Model Elucidates How Early Gain Control in Fly Photoreceptors Arises from Quantal Sampling. *Frontiers in Computational Neuroscience*, 10.

Srinivasan, M.V. and Bernard, G.D. (1975). The effect of motion on visual acuity of the compound eye: A theoretical analysis. *Vision Research*, 15(4), pp.515–525.

Srinivasan, M.V., Laughlin, S.B. and Dubs, A. (1982). Predictive coding: a fresh view of inhibition in the retina. *Proceedings of the Royal Society of London. Series B. Biological Sciences*, 216(1205), pp.427–459.

Stavenga, D.G. (1975). Visual adaptation in butterflies. *Nature*, 254(5499), pp.435–437.

Stavenga, D.G. (1989). Pigments in Compound Eyes. In: D.G. Stavenga and R.C. Hardie, eds., *Facets of vision*. Berlin: Springer -Verlag.

Stavenga, D.G. (2004). Angular and spectral sensitivity of fly photoreceptors. III. Dependence on the pupil mechanism in the blowfly *Calliphora*. *Journal of Comparative Physiology A: Sensory, Neural, and Behavioral Physiology*, 190(2), pp.115–129.

Stavenga, D.G., Kruizinga, R. and Leertouwer, H.L. (1990). Dioptrics of the facet lenses of male blowflies *Calliphora* and Chrysomyia. *Journal of Comparative Physiology A*, 166(3).

Strausfeld, N. (1976). *Atlas of an insect brain*. Berlin: Springer.

Strausfeld, N. (1970). Golgi studies on insects Part II. The optic lobes of Diptera. *Philosophical Transactions of the Royal Society of London. B, Biological Sciences*, 258(820), pp.135–223.

Strausfeld, N.J. and Campos-Ortega, J.A. (1973). The L4 monopolar neurone: a substrate for lateral interaction in the visual system of the fly *Musca domestica* (L). *Brain Research*, 59, pp.97–117.

Strausfeld, NicholasJ. (1991). Structural organization of male-specific visual neurons in calliphorid optic lobes. *Journal of Comparative Physiology A*, 169(4).

Strother, J.A., Wu, S.-T., Rogers, E.M., Eliason, J.L.M., Wong, A.M., Nern, A. and Reiser, M.B. (2018). Behavioral state modulates the ON visual motion pathway of *Drosophila*. *Proceedings of the National Academy of Sciences*, 115(1), pp. E102–E111.

Sukontason, K.L., Chaiwong, T., Piangjai, S., Upakut, S., Moophayak, K. and Sukontason, K. (2008). Ommatidia of blow fly, house fly, and flesh fly: implication of their vision efficiency. *Parasitology Research*, 103(1), pp.123–131.

Suss-Toby, E., Selinger, Z. and Minke, B. (1991). Lanthanum reduces the excitation efficiency in fly photoreceptors. *Journal of General Physiology*, 98(4), pp.849–868.

Suver, Marie P., Mamiya, A. and Dickinson, Michael H. (2012). Octopamine Neurons Mediate Flight-Induced Modulation of Visual Processing in *Drosophila*. *Current Biology*, 22(24), pp.2294–2302.

Takemura, S., Bharioke, A., Lu, Z., Nern, A., Vitaladevuni, S., Rivlin, P.K., Katz, W.T., Olbris, D.J., Plaza, S.M., Winston, P., Zhao, T., Horne, J.A., Fetter, R.D., Takemura, S., Blazek, K., Chang, L.-A., Ogundeyi, O., Saunders, M.A., Shapiro, V. and Sigmund, C. (2013). A visual motion detection circuit suggested by *Drosophila* connectomics. *Nature*, 500(7461), pp.175–181.

Takemura, S., Karuppudurai, T., Ting, C.-Y., Lu, Z., Lee, C.-H. and Meinertzhagen, Ian A. (2011). Cholinergic Circuits Integrate Neighboring Visual Signals in a *Drosophila* Motion Detection Pathway. *Current Biology*, 21(24), pp.2077–2084.

Takemura, S., Nern, A., Chklovskii, D.B., Scheffer, L.K., Rubin, G.M. and Meinertzhagen, I.A. (2017). The comprehensive connectome of a neural substrate for “ON” motion detection in *Drosophila*. *eLife*, 6.

Trujillo-Cenóz, O. (1965). Some aspects of the structural organization of the intermediate retina of dipterans. *Journal of Ultrastructure Research*, 13(1-2), pp.1–33.

Tuthill, John C., Nern, A., Holtz, Stephen L., Rubin, Gerald M. and Reiser, Michael B. (2013). Contributions of the 12 Neuron Classes in the Fly Lamina to Motion Vision. *Neuron*, 79(1), pp.128–140.

Uusitalo, R.O., Juusola, M., Kouvalainen, E. and Weckström, M. (1995). Tonic transmitter release in a graded potential synapse. *Journal of Neurophysiology*, 74(1), pp.470–473.

Uusitalo, R.O., Juusola, M. and Weckström, M. (1995). Graded responses and spiking properties of identified first-order visual interneurons of the fly compound eye. *Journal of Neurophysiology*, 73(5), pp.1782–1792.

Villette, V., Chavarha, M., Dimov, I.K., Bradley, J., Pradhan, L., Mathieu, B., Evans, S.W., Chamberland, S., Shi, D., Yang, R., Kim, B.B., Ayon, A., Jalil, A., St-Pierre, F., Schnitzer, M.J., Bi, G., Toth, K., Ding, J., Dieudonné, S. and Lin, M.Z. (2019). Ultrafast Two-Photon Imaging of a High-Gain Voltage Indicator in Awake Behaving Mice. *Cell*, 179(7), pp.1590-1608.e23.

Vogt, K., Kirschfeld, K. and Stavenga, D.G. (1982). Spectral effects of the pupil in fly photoreceptors. *Journal of Comparative Physiology A*, 146(2), pp.145–152.

Vähäsöyrinki, M., Niven, J., Hardie, R., Weckström, M. and Juusola, M. (2006). Robustness of Neural Coding in *Drosophila* Photoreceptors in the Absence of Slow Delayed Rectifier K+ Channels. *Journal of Neuroscience*, 26(10), pp.2652–2660.

Wada, S. (1974). Spezielle randzonale ommatidien von *Calliphora* Erythrocephala meig. (diptera calliphoridae): Architektur der zentralen rhabdomeren-kolumne und topographie im komplexauge. *International Journal of Insect Morphology and Embryology*, 3(3-4), pp.397–424.

Wagner, H. (1986a). Flight performance and visual control of flight of the free-flying housefly (*Musca domestica* L.) I. Organization of the flight motor. *Philosophical Transactions of the Royal Society of London. B, Biological Sciences*, 312(1158), pp.527–551.

Wagner, H. (1986b). Flight performance and visual control of flight of the free-flying housefly (*Musca domestica* L.) II. Pursuit of targets. *Philosophical Transactions of the Royal Society of London. B, Biological Sciences*, 312(1158), pp.553–579.

Wang, T., Xu, H., Oberwinkler, J., Gu, Y., Hardie, R.C. and Montell, C. (2005). Light Activation, Adaptation, and Cell Survival Functions of the Na+/Ca2+ Exchanger CalX. *Neuron*, 45(3), pp.367–378.

Wardill, T.J., List, O., Li, X., Dongre, S., McCulloch, M., Ting, C.-Y., O'Kane, C.J., Tang, S., Lee, C.-H., Hardie, R.C. and Juusola, M. (2012). Multiple Spectral Inputs Improve Motion Discrimination in the *Drosophila* Visual System. *Science*, 336(6083), pp.925–931.

Warrant, E.J. (1999). Seeing better at night: life style, eye design and the optimum strategy of spatial and temporal summation. *Vision Research*, 39(9), pp.1611–1630.

Warrant, E.J. (2001). The design of compound eyes and the illumination of natural habitats. In: F.G. Barth and A. Schmid, eds., *Ecology of sensing*. Berlin; New York: Springer-Verlag, pp.187–213.

Warrant, E.J. (2016). Sensory matched filters. *Current Biology*, 26(20), pp. R976–R980.

Warrant, E.J. and McIntyre, P.D. (1992). The trade-off between resolution and sensitivity in compound eyes. In: *Nonlinear vision: determination of neural receptive fields, function, and networks*. Boca Raton, Fl; London; Tokyo: Crc Press.

Washizu, Y., Burkhardt, D. and Streck, P. (1964). Visual field of single retinula cells and interommatidial inclination in the compound eye of the blowfly *Calliphora* erythrocephala. *Zeitschrift für Vergleichende Physiologie*, 48(4), pp.413–428.

Weckström, M., Hardie, R.C. and Laughlin, S.B. (1991). Voltage-activated potassium channels in blowfly photoreceptors and their role in light adaptation. *The Journal of Physiology*, 440(1), pp.635–657.

Weckström, M., Kouvalainen, E. and Järvilehto, M. (1988). Non-linearities in response properties of insect visual cells: An analysis in time and frequency domain. *Acta Physiologica Scandinavica*, 132(1), pp.103–113.

Weckström, M. and Laughlin, S.B. (1995). Visual ecology and voltage-gated ion channels in insect photoreceptors. *Trends in Neurosciences*, 18(1), pp.17–21.

Wehrhahn, C. (1979). Sex-specific differences in the chasing behaviour of houseflies (*Musca*). *Biological Cybernetics*, 32(4), pp.239–241.

Wehrhahn, C., Poggio, T. and Bülthoff, H. (1982). Tracking and chasing in houseflies (*Musca*). *Biological Cybernetics*, 45(2), pp.123–130.

Wernet, M.F., Mazzoni, E.O., Çelik, A., Duncan, D.M., Duncan, I. and Desplan, C. (2006). Stochastic spineless expression creates the retinal mosaic for colour vision. *Nature*, 440(7081), pp.174–180.

Wernet, Mathias F., Velez, Mariel M., Clark, Damon A., Baumann-Klausener, F., Brown, Julian R., Klovstad, M., Labhart, T. and Clandinin, Thomas R. (2012). Genetic Dissection Reveals Two Separate Retinal Substrates for Polarization Vision in *Drosophila*. *Current Biology*, 22(1), pp.12–20.

Wolff, T. and Ready, D.F. (1993). Pattern formation in the *Drosophila* retina. In: *The development of Drosophila melanogaster*. New York: Cold Spring Harbor Laboratory Press.

Wong, F. and Knight, B.W. (1980). Adapting-bump model for eccentric cells of Limulus. *Journal of General Physiology*, 76(5), pp.539–557.

Wong, F., Knight, B.W. and Dodge, F.A. (1980). Dispersion of latencies in photoreceptors of Limulus and the adapting-bump model. *Journal of General Physiology*, 76(5), pp.517–537.

Wu, C.F. and Pak, W.L. (1975). Quantal basis of photoreceptor spectral sensitivity of *Drosophila melanogaster*. *The Journal of General Physiology*, 66(2), pp.149–168.

Wu, C.F. and Pak, W.L. (1978). Light-induced voltage noise in the photoreceptor of *Drosophila melanogaster*. *Journal of General Physiology*, 71(3), pp.249–268.

Yang, Helen H., St-Pierre, F., Sun, X., Ding, X., Lin, Michael Z. and Clandinin, Thomas R. (2016). Subcellular Imaging of Voltage and Calcium Signals Reveals Neural Processing *In vivo*. *Cell*, 166(1), pp.245–257.

Yoshioka, T., Inoue, H. and Hotta, Y. (1985). Absence of Phosphatidylinositol Phosphodiesterase in the Head of a *Drosophila* Visual Mutant, norpA (no receptor potential A)1. *The Journal of Biochemistry*, 97(4), pp.1251–1254.

Zelhof, A.C., Hardy, R.W., Becker, A. and Zuker, C.S. (2006). Transforming the architecture of compound eyes. *Nature*, 443(7112), pp.696–699.

Zettler, F. (1969). Die Abhangigkeit des Ubertragungsverhaltens von Frequenz und Adaptationszustand; gemessen am einzelnen Lichtrezeptor von *Calliphora* erythrocephala. *Zeitschrift für Vergleichende Physiologie*, 64(4), pp.432–449.

Zettler, F. and Järvilehto, M. (1972). Lateral inhibition in an insect eye. *Zeitschrift für Vergleichende Physiologie*, 76(3), pp.233–244.

Zheng, L., de Polavieja, G.G., Wolfram, V., Asyali, M.H., Hardie, R.C. and Juusola, M. (2006). Feedback Network Controls Photoreceptor Output at the Layer of First Visual Synapses in *Drosophila*. *Journal of General Physiology*, 127(5), pp.495–510.

Zheng, L., Nikolaev, A., Wardill, T.J., O'Kane, C.J., de Polavieja, G.G. and Juusola, M. (2009). Network Adaptation Improves Temporal Representation of Naturalistic Stimuli in *Drosophila* Eye: I Dynamics. *PLoS ONE*, 4(1), p.e4307.

Zuker, C.S., Cowman, A.F. and Rubin, G.M. (1985). Isolation and structure of a rhodopsin gene from D. melanogaster. *Cell*, 40(4), pp.851–858.